

**SORPTION OF ANTIBIOTICS BY BLACK CARBON SORBENTS AND ITS IMPACT
TO TRANSPORT OF ANTIBIOTICS IN SOILS**

By

CHENG-HUA LIU

A DISSERTATION

Submitted to
Michigan State University
in partial fulfillment of the requirements
for the degree of

Crop and Soil Sciences–Doctor of Philosophy

2018

ABSTRACT

SORPTION OF ANTIBIOTICS BY BLACK CARBON SORBENTS AND ITS IMPACT TO TRANSPORT OF ANTIBIOTICS IN SOILS

By

CHENG-HUA LIU

Antibiotics are extensively used in human health care and livestock industry, resulting in rapid increases in their environmental concentrations. These anthropogenic antibiotics are considered emerging contaminants, and their increased concentrations in the environment have raised serious concerns on the proliferation of antibiotic resistant bacteria and associated impacts to human and ecosystem health. Therefore, innovative management strategies are needed to manage the risks of antibiotic resistance. Engineered black carbon (BC) materials (e.g., biochars and activated carbon) may be used as sorbents to sequester antibiotics from contaminated soils and waters *in situ*, thus decreasing the mobility and bioavailability of antibiotics in the environment. To this end, a better understanding of mechanisms controlling the sorption of antibiotics to BC (specifically biochars) is critically needed for developing scientifically-sound mitigation strategies.

The first research topic aimed to investigate sorption of lincomycin (one class of antibiotics) to manure-based biochars and their potentials for the long-term lincomycin immobilization. Lincomycin sorption to biochars was greater at solution pH (6.0–7.5) below the pKa of lincomycin (7.6) than at pH (9.9–10.4) above its pKa. The enhanced lincomycin sorption at lower pH likely resulted from electrostatic attraction between the positively charged lincomycin and the negatively charged biochar surfaces. This was corroborated by the observation that lincomycin sorption decreased with increasing ionic strength at lower pH (6.7) but remained constant at higher pH (10). Long-term lincomycin sorption was characterized by two-stage kinetics

with fast sorption reaching quasi-equilibrium in the first two days, followed by slow sorption over the long term. The fast sorption was primarily attributed to surface adsorption, whereas the long-term slow sorption was controlled by slow pore diffusion. Specially, lower-temperature (300°C) biochars had higher sorption capacity and faster sorption kinetics than higher-temperature (400–600°C) biochars. The continuous release of dissolved organic carbon (DOC) from the lower-temperature biochars may enhance the lincomycin sorption by decreasing biochar particle size and/or increasing the accessibility of sorption sites initially blocked by DOC. This study further quantified and characterized the DOC extracted by deionized water, 0.1 M HCl, and 0.1 M NaOH from 46 biochars produced from diverse feedstocks and pyrolysis conditions. A quick, easy and robust UV-vis spectrometric method was developed to measure the DOC concentrations in diverse biochar samples. Our findings highlight that biochars may have the potential to be used as soil amendment to immobilize antibiotics in situ over the long term.

The second research topic was to understand the unintended consequence of BC nanoparticles on the transport of antibiotics in soils. BC nanoparticles are ubiquitous in nature, and may act as carriers to facilitate the transport of antibiotics. Hence, we investigated the facilitated transport of three veterinary antibiotics (lincomycin, oxytetracycline, and sulfamethoxazole) by BC nanoparticles in saturated sand columns at solution pH of 7, and ionic strength of 0.1, 1, or 10 mM. The total transport of antibiotics was enhanced in the presence of BC nanoparticles in low-salinity water, but decreased at high-salinity water, implying that the facilitated transport of antibiotics may occur under rainfall or irrigation that can decrease soil salinity.

Copyright by
CHENG-HUA LIU
2018

This dissertation is dedicated to my supportive parents, Shao-Chih Liu and Sung-Ying Chung, and parents-in-law, Shuang-Jung Chuang and Su-Mei Peng, my brother, Cheng-Wen Liu, my love, Ya-Hui Chuang, and our beloved daughter, Emma Liu. I love you all!

ACKNOWLEDGEMENTS

My dissertation research would not have been possible without the support of numerous people. First and foremost, I am extremely thankful to my academic advisor Professor Wei Zhang for his guidance, prudent advice and mentorship throughout my doctoral study. Without him taking me as one of his graduate students, I cannot fulfill one of my goals today; and without his support, professional experience and endless patience, this dissertation would not have been possible or completed. I also express my profound appreciation to my academic committee members, Professor Stephen A. Boyd, Professor Hui Li, and Professor Jay P. Zarnetske, for generously offering their time, recommendations, and suggestions to improve this dissertation research.

I would like to extend my acknowledgment to all my wonderful lab group members, colleagues, and friends at Michigan State University: Drs. Yingjie Zhang, Yuan Tian, Haiyan Wang, Shen Qu, Sangho Jeon, Zeyou Chen, Thaisa Pegoraro, J. Brett Sallach, and Yuanbo Li, as well as Mark Bezdek, Sicao Wang, Feng Gao, Gemini D. Bhalsod, Xiaohang Yu, Anping Peng, Jianzhou He, Yike Shen, Yu Zhang, and many others. I am greatly appreciated for their help, support, brainstorming ideas, friendship, and collaborations.

Last but not least, I would like to express my deepest gratitude to my parents Shao-Chih Liu and Sung-Ying Chung, my parents-in-law, Shuang-Jung Chuang and Su-Mei Peng, and my brother, Cheng-Wen Liu, for their love, encouragement, and spiritual support in all aspects of my life. My greatest appreciation is to my wife, Ya-Hui Chuang for her love, support, and collaboration as well as always being with me throughout my research journey. To my beloved daughter, Emma Liu, in particular, thank you for always being such a sweet and wonderful girl!

TABLE OF CONTENTS

LIST OF TABLES	x
LIST OF FIGURES	xii
CHAPTER I INTRODUCTION AND OBJECTIVES	1
INTRODUCTION	2
OBJECTIVES	6
CHAPTER II SORPTION OF LINCOMYCIN BY MANURE-DERIVED BIOCHARS FROM WATER	8
ABSTRACT.....	9
INTRODUCTION	10
MATERIALS AND METHODS	12
Biochar Samples and Characterization	12
Sorption Experiments.....	14
Chemicals and Experimental Setup	14
Sorption Kinetics	15
Effects of Biochar Particle Size and Solid-Water Ratio	18
Effects of Solution pH and Ionic Strength	18
LC-MS/MS Analytical Procedure.....	19
Mathematical Modeling	19
RESULTS AND DISCUSSION	20
Properties of Manure-Derived Biochars	20
Two-phase Sorption Kinetics.....	24
Effects of Biochar Particle Size and Solid-Water Ratio	29
Effect of Solution pH and Ionic Strength.....	31
Implications.....	36
CHAPTER III QUANTIFICATION AND CHARACTERIZATION OF DISSOLVED ORGANIC CARBON FROM BIOCHARS	38
ABSTRACT.....	39
INTRODUCTION	40
MATERIALS AND METHODS	43
Biochars	43
Extraction of Biochar-DOC	48
Fractionation of Biochar-DOC.....	49
TOC and UV-vis Analyses of Biochar-DOC.....	49
Solid-state ¹³ C NMR Analyses.....	50
Estimation of Biochar-DOC Concentrations	53
RESULTS AND DISCUSSION	54
DOC Concentrations in Biochars.....	54
Fractionation of Biochar-DOC.....	57
UV-vis Absorption Spectra Characterization	60
Advanced Solid-state ¹³ C NMR	65
Factors Influencing Biochar-DOC	71
Quick and Easy Method to Estimate DOC Concentrations	75

Implications.....	86
CHAPTER IV LONG-TERM SORPTION OF LINCOMYCIN TO BIOCHARS: THE INTERTWINED ROLES OF PORE DIFFUSION AND DISSOLVED ORGANIC CARBON	
ABSTRACT.....	87
INTRODUCTION	88
MATERIALS AND METHODS	89
Chemicals.....	92
Sorbents	92
Sorbent Characterization.....	93
Sorption Experiments.....	94
Effects of DOC on Lincomycin Sorption	97
Extraction of Sorbed-lincomycin from Biochars	99
Analytical Methods	100
Mathematical Modeling	101
RESULTS AND DISCUSSION	102
Characterization of Biochars.....	102
Long-term Sorption Kinetics	107
Long-term Sorption Isotherms	115
Effects of DOC on Sorption.....	120
Desorption Hysteresis	128
Implications.....	130
CHAPTER V BLACK CARBON NANOPARTICLES FACILITATED TRANSPORT OF ANTIBIOTICS IN SATURATED SAND	
ABSTRACT.....	131
INTRODUCTION	132
MATERIALS AND METHODS	133
Chemicals.....	136
BC Nanoparticles	137
Porous Medium.....	139
Batch Sorption Experiments	139
Column Transport Experiments	141
Analytical Methods	144
Mathematical Modeling	146
XDLVO and α_{theory} Calculations	149
RESULTS AND DISCUSSION	151
Characterization of the BC nanoparticles and Sand.....	151
Sorption Isotherms	153
Transport of BC nanoparticles	156
Transport of Antibiotics	159
Implications.....	164
CHAPTER VI CONCLUSIONS AND FUTURE WORK	
CONCLUSIONS.....	165
FUTURE WORK.....	166
APPENDICES	
Appendix A: Sorption Isotherms Data	168
	169

Appendix B: Sorption Kinetics Data	175
Appendix C: Column Breakthrough Experiments Data.....	180
REFERENCES	188

LIST OF TABLES

Table 2.1. Chemical and physical properties of lincomycin [†]	14
Table 2.2. Selected physical and chemical properties of manure-derived biochars [†]	21
Table 2.3. Fitted parameters of pseudo-first-order, pseudo-second-order, and intraparticle diffusion models for long-term sorption kinetics of lincomycin on manure-derived biochars. ...	27
Table 2.4. Fitted parameters of Langmuir and Freundlich equations for lincomycin sorption on manure-derived biochars.....	31
Table 3.1. Feedstock and production details of biochar samples.....	45
Table 3.2. Selected properties of biochar samples.	47
Table 3.3 Extractable DOC concentration of biochar samples.	56
Table 3.4. UV-vis spectral parameters of AEOC, WEOC, BEOC, BEOC-AS, and BEOC-AP.	63
Table 3.5. Functional groups of the biochars and DOC estimated by quantitative ¹³ C multiCP/MAS spectra. ^a	70
Table 3.6. Variation across pyrolysis temperature and feedstock of the WEOC of 20 tested biochars. ^a	72
Table 3.7. The correlation coefficient (r) between WEOC and biochar properties (* and ns denote significant at $p < 0.05$ and not significant, respectively).	73
Table 4.1. Physicochemical properties of lincomycin.	92
Table 4.2. Selected properties of biochar and graphite samples.	104
Table 4.3. Fitted parameters of the intraparticle diffusion model for the long-term sorption kinetics of lincomycin by the biochars. ^a	108
Table 4.4. Fitted parameters of the Freundlich model for quasi-equilibrium sorption isotherms of lincomycin on the biochars at 1, 7, 30, and 365 days. ^a	116
Table 4.5. Fitted parameters of the intraparticle diffusion model for the sorption kinetics of lincomycin by woodchip waste biochar. ^a	121
Table 4.6. Fitted parameters of the intraparticle diffusion model for the sorption kinetics of lincomycin by raw-, DI-water-washed, and 0.01M-NaOH-washed biochars. ^a	122

Table 5.1. Physicochemical properties of lincomycin, oxytetracycline, and sulfamethoxazole.	137
Table 5.2. Surface energy components and Hamaker constants used in XDLVO calculations.	151
Table 5.3. Properties for BC nanoparticles and sand colloids. ^a	152
Table 5.4. Fitted parameters of the Freundlich model for sorption isotherms of LCM, OTC, or SMX on BC nanoparticles and sand under ionic strength (IS) of 0.1, 1, or 10 mM and pH of 7.0. ^a	155
Table 5.5. Fitted transport parameters for breakthrough curves of BC nanoparticles with and without LCM, OTC or SMX in saturated sand column. ^a	158
Table 5.6. Effluent mass recovery calculations of breakthrough curves for LCM, OTC, and SMX in the antibiotic-only and co-transport experiments.	162
Table 5.7. Fitted transport parameters of breakthrough curves for LCM, OTC, and SMX in the antibiotic-only and co-transport experiments. ^a	162

LIST OF FIGURES

Figure 2.1. Lincomycin concentration versus time for lincomycin sorption kinetics experiments. Control was the biochar-free lincomycin solution.....	16
Figure 2.2. Precursor ion scan spectra of (a) Control (freshly prepared), (b) Control (180 days), (c) BM600 (180 days), (d) DM600 (180 days), (e) AM600 (180 days), and (f) PM600 (180days). Control was the biochar-free lincomycin solution. No degradation candidates of lincomycin was detected in long-term kinetics samples (b, d, f).	17
Figure 2.3. Zeta potential of manure-derived biochars as a function of solution pH.	22
Figure 2.4. SEM images of manure-derived biochars: (a) BM600, (b) DM600, (c) AM600, and (d) PM600, prepared from biochar suspensions of 1-day water exposure.	23
Figure 2.5. (a) Short-term and (b) long-term lincomycin sorption kinetics on manure-derived biochars. The solid lines were fitted with the intraparticle diffusion model.	26
Figure. 2.6. SEM images of manure-derived biochars after 1-day and 180-day water exposure: (a, b) BM600, (c, d) DM600, (e, f) AM600, and (g, h) PM600.....	28
Figure. 2.7. Sorption of lincomycin on manure-derived biochars with varying (a) particle sizes and (b) solid-water ratios.	30
Figure. 2.8. Observed and fitted sorption isotherms of lincomycin on biochars at solution pH 6.0–7.3 and pH 9.9–10.4. The solid lines were fitted with the Langmuir model, and the dashed lines with the Freundlich model.....	34
Figure. 2.9. Sorption of lincomycin on manure-derived biochars at solution pH of 6.1–7.5 and 10–10.3 under varying ionic strength.	35
Figure 3.1. Dissolved organic carbon (DOC) concentrations (a) and illustrative solution colors (b) of acid-extractable DOC (AEOC), water-extractable DOC (WEOC), and base-extractable DOC (BEOC) from 46 tested biochars (FP: fast pyrolysis; SP: slow pyrolysis; n/a: not available).	55
Figure 3.2. Fractionation of WEOC and BEOC extracted from biochars.	58
Figure 3.3. Effects of the extraction methods (a), pyrolysis conditions (b), and feedstocks(c) on the acid-soluble (AS) and acid-precipitated (AP) fraction ratio of biochar-DOC. (AEOC: acid-extractable DOC; WEOC: water-extractable DOC; BEOC: base-extractable DOC; FP: fast pyrolysis at 500 °C; SP300-400: slow pyrolysis at 300 to 400 °C; SP450-600: slow pyrolysis at 450 to 600 °C).....	59

Figure 3.4. UV-vis spectra of DOC solutions (bull manure biochar as examples): (a) AEOC, (b) WEOC, (c) BEOC, and (d) the As and AP fractions of BEOC (BM300). 61

Figure 3.5. Box plots of UV-vis spectroscopic analyses of DOC in biochars: (a) $E_2:E_3$ ratio and (b) $S_{275-295}$. The box plots showed the first quartile, median, mean, and third quartile of the samples, and the whiskers showed the range of minimum and maximum. The symbols on the left side of box plots showed the distribution of sample values. Detailed data are provided in Table 3.4. (FP: fast pyrolysis; SP: slow pyrolysis; n/a: not available) 62

Figure 3.6. Solid-state ^{13}C multiCP/MAS NMR spectra (block black line) and multiCP/MAS after dipolar dephasing (thin red line) of biochar-Raw ((a) to (e)), biochar-DI ((f) and (g)), biochar-NaOH ((h) to (l)), BEOC (m) and dBEOC ((n) to (q)) samples. 69

Figure 3.7. Box-whisker plot of WEOC concentrations vs pyrolysis temperature (a), pyrolysis type (b) and feedstocks (c). The box plots showed the first quartile, median, mean, and third quartile of the samples, and the whiskers showed the 1.5 times interquartile range. The column charts by the right side of the box plots showed the sample sets for box plots. 74

Figure 3.8. Linear regressions between decadic absorption coefficient at 254 nm and biochar DOC concentrations in solution for (a) AEOC, WEOC, and BEOC, and (b) BEOC-AS and BEOC-AP. The dilution factor for AEOC and WEOC was 10 and for BEOC, BEOC-AS, and BEOC-AP was 50. For AEOC, 11 samples with serve matrix interference were excluded. For WEOC, SB500 and SG500 skewed the correlation because of the distinct compositional difference with other 44 samples (Figure 3.2), and thus were excluded. For BEOC-AS and BEOC-AP, only 27 fractionable BEOC samples were included. 82

Figure 3.9. (a) Experimental data for BM300 as example, (b) boxplot of the E_2/E_3 ratios of 27 fractionable BEOC samples, and (c) Fitting E_2/E_3 vs f data with the rational function model. ... 83

Figure 3.10. Measured versus modeled water-extractable DOC (WEOC) by E_2/E_3 ratio and a_{254} . Dashed line represents the 1:1 relationship. Dilution was made by 10-folds for the WEOC samples. 84

Figure 3.11. Measured versus modeled DOC for (a) AEOC and (b) BEOC by E_2/E_3 ratio and a_{254} . Dashed line represents the 1:1 relationship. Dilution was made by 10- and 50-folds for the AEOC and BEOC samples, respectively. 85

Figure 4.1. Lincomycin concentrations in solution over time in the kinetic sorption experiments for the 17 tested biochars. Control was the biochar-free lincomycin solution. 96

Figure 4.2. The relationship of (a) total carbon, (b) fixed carbon, (c) volatile matter, and (d) ash contents versus CO_2 -BET specific surface area for biochars. 105

Figure 4.3. Scanning electron microscopy images of raw biochars: (a) BM300 (bull manure biochar produced at 300 °C) and (b) BM600 (bull manure biochar produced at 600 °C). 106

Figure 4.4. Long-term kinetics of lincomycin sorption by biochars. The sorption data were fitted by the intraparticle diffusion model (solid line), and the hollow data were excluded from the fitting because of reaching sorption saturation.	111
Figure 4.5. Sorption kinetics (a) and isotherms (b) of lincomycin to graphite. The solid lines were fitted by the pseudo-second-order model and the Freundlich model, respectively.....	112
Figure 4.6. The relationship of (a) intraparticle diffusion rate constant (k_{id}), (b) initial sorption (C_{id}), and (c) interparticle diffusion factor (R_{id}) versus pyrolysis temperature for 17 biochars.	113
Figure 4.7. Long-term release of dissolved organic carbon from biochars.	114
Figure 4.8. Quasi-equilibrium sorption isotherms of lincomycin by bull manure-based biochars produced at different temperature: (a)BM300, (b) BM400, (c) BM500, and (d) BM600. K_F ($\mu\text{g}^{1-N} \text{g}^{-1} \text{L}^N$) is the Freundlich sorption coefficient, and N (dimensionless) is the Freundlich nonlinearity factor.	117
Figure 4.9. Quasi-equilibrium sorption isotherms of lincomycin to biochars: (a) DM300, (b) DM400, (c) DM600, (d) PM300, (e) PM400, (f) PM500, (g) PM600, (h) RDM500, (i) DDM500, (j) DDM600, (k) CDM500, (l) CDMW500, and (m) WW500. The solid lines were fitted with the Freundlich isotherm model.	118
Figure 4.10. The relationship of Freundlich sorption coefficient (K_F) and Freundlich nonlinearity factor (N) versus pyrolysis temperature for biochars.....	119
Figure 4.11. The effect of DOC as co-solutes on sorption kinetics of lincomycin by WW500 biochar (WW500+DI was the control of absence DOC).	123
Figure 4.12. Long-term kinetics of lincomycin sorption by raw and DOC-washed biochars. The sorption data were fitted by intraparticle diffusion model (solid line).	124
Figure 4.13. Long-term kinetics of lincomycin sorption by raw and DOC-washed biochars. The sorption data were fitted by the intraparticle diffusion model (solid line) and the hollow data were excluded because of approaching sorption saturation.....	125
Figure 4.14. Scanning electron microscopy images of bull manure biochar pyrolyzed at 300°C (BM300): (a) raw BM300 without treatment, (b) BM300 after 1-d background solution exposure, (c) BM300 after 365-d background solution exposure, and (d) BM300 after 1-d 0.1M NaOH solution exposure. Background solution contained 1000 $\mu\text{g L}^{-1}$ lincomycin, 6.7 mM NaCl, 2.5 mM Na_2CO_3 , 2.5 mM NaHCO_3 , and 200 mg L^{-1} NaN_3	126
Figure 4.15. Particles size distribution of (a) bull manure biochar pyrolyzed at 300°C (BM300) and (b) bull manure biochar pyrolyzed at 600°C (BM600) suspended in 0.1 M NaCl (upper panel) or in 0.1 M NaOH (lower panel) after one-day exposure.	127

Figure 4.16. (a) Extraction efficiency of 240 d-sorbed lincomycin in the biochars and (b) the relationship of intraparticle diffusion rate constant (K_{id}) versus lincomycin extraction efficiency for biochars.	129
Figure 5.1. Scanning electron microscopy images of BC nanoparticles prepared from stock suspensions.	138
Figure 5.2. Sorption kinetics of LCM (a and d), OTC (b and e), SMX (c and f) on BC nanoparticles and sands under ionic strength (IS) of 0.1, 1 or 10 mM and solution pH of 7.0. .	141
Figure 5.3. Linear regressions between UV-vis absorbance at 550 nm and BC nanoparticle concentrations in suspension.....	144
Figure 5.4. Measured and fitted breakthrough curve of the bromide tracer through saturated sand column. Symbols are experimental data and lines are fitted result.....	148
Figure 5.5. Aggregation kinetics of BC nanoparticles dispersed in the KCl solution with ionic strength (IS) of 0.1, 1, or 10 mM at pH 7.0.	153
Figure 5.6 Sorption isotherm of LCM (a and d), OTC (b and e), SMX (c and f) on black carbon (BC) nanoparticles and sands under ionic strength (IS) of 0.1, 1 or 10 mM and pH of 7.0.	155
Figure 5.7. Measured and fitted breakthrough curves of black carbon nanoparticles (BCN) without (a) and with (b, c and d) of lincomycin (LCM), oxytetracycline (OTC) or sulfamethoxazole (SMX) in saturated sand columns at solution pH of 7 and ionic strength (IS) of 0.1, 1, or 10 mM KCl.	157
Figure 5.8. XDLVO surface energy profiles for black carbon (BC) nanoparticles interacting with sand surfaces with the energy barrier (a) and the secondary minima (b).	158
Figure 5.9. Measured and fitted breakthrough curves of lincomycin (LCM), oxytetracycline (OTC) and sulfamethoxazole (SMX) without black carbon nanoparticles (BCN) (a, b and c) and the BCN-associated LCM, OTC and SMX (d, e and f) in saturated sand columns at solution pH of 7 and ionic strengths of 0.1, 1, or 10 mM KCl	161
Figure 5.10. Breakthrough curves of LCM (a), OTC (b), and SMX (c) in the presence of black carbon (BC) nanoparticles in saturated sand columns at solution pH of 7 and ionic strengths of 0.1, 1, or 10 mM KCl. The inserts (d, e, and f) showed the x-axis range of 0.0 to 0.1 to better view the released antibiotics in solution.	163

CHAPTER I
INTRODUCTION AND OBJECTIVES

INTRODUCTION

Anthropogenic antibiotics have been recognized as emerging contaminants, and increasing environmental concentrations of antibiotics warrants more attention. Antibiotics are widely used in human and veterinary medicine for disease treatment. In addition to their therapeutic use, antibiotics are also widely used in food animal production for disease prevention and growth promotion.¹⁻³ Because of the extensive use of antibiotics, they are frequently detected in soils, sediments, wastewater, surface water, and groundwater.⁴ A nationwide survey on US water resources indicated that 15 different antibiotics were found in 50% of the 139 tested streams.⁵ Although the concentrations of antibiotics in environmental waters are generally low (ng L^{-1} to $\mu\text{g L}^{-1}$), their potential impact on human and ecosystem health has raised serious concerns.⁶ The prevalence of antibiotics in the environment may increase selective pressure on bacteria and thus facilitate the development of antibiotic resistance in natural systems.^{1, 7} Moreover, exposure to antibiotics may elicit acute toxicity to aquatic organisms (algae, invertebrate, fish, and plant) or unknown long-term impact to human and ecosystem health.^{8, 9}

Antibiotics can enter the environment via land application of animal manure and sewage sludge, as well as discharge of wastewater treatment plant (WWTP) effluents. Manure application has been considered a major source of anthropogenic antibiotics in the environment.⁴ In the US, an estimated 11.2 million kg of antibiotics are used each year as nontherapeutic additives in animal feeding operations, accounting about 70% of total annual use of antibiotics.¹⁰ A large percentage of administered antibiotics are not fully metabolized within animal bodies, and are thus excreted into manure.¹¹ Manure is typically land-applied for waste disposal and fertilizer use. Consequently, manure-borne antibiotics are introduced into soils through manure application, and are further transported into surface water and groundwater via surface runoff and leaching, respectively.^{12, 13}

Additionally, conventional WWTPs are not specifically designed for the effective removal of antibiotics from wastewaters. Thus, antibiotics may be left in the WWTP effluents and sewage sludge, and then introduced into soils through land application of sewage sludge and crop irrigation using WWTP effluents (i.e., reclaimed water).^{5, 14} Because increasing environmental concentrations of antibiotics could promote antibiotic resistant bacteria population and the abundance of antibiotic resistance genes,^{15, 16} best management practices are critically needed to manage the antibiotics in the environment and mitigate environmental risks associated with antibiotic resistance. When assessing environmental risks of antibiotics, one needs to evaluate the mobility and bioavailability of antibiotics rather than their total concentrations. Since soil can be a significant sink for many antibiotics, soil amendment with geosorbents (such as black carbon or biochars, BC) may prove to be a novel management strategy by sequestering antibiotics *in-situ* in soils and thus reducing their environmental risks.

BC includes a variety of pyrogenic carbonaceous materials produced from incomplete fuel combustion or thermal decomposition of biomass under oxygen-free or -limited conditions (i.e., pyrolysis).^{17, 18} BC is ubiquitous in the environment and can originate from wild and managed fires, and burning of fossil fuels.¹⁸⁻²⁰ Recently, a particular form of BC (biochars) has been purposely produced (often as a co-product of syngas and bio-oil production in biomass pyrolysis) and used as a soil amendment for agronomic and environmental benefits, including improving soil fertility, carbon sequestration, and immobilization of contaminants.²¹⁻²⁶ Biochars can have vastly different chemical and physical properties, depending on the feedstock biomass and pyrolysis temperature.^{24, 26, 27} A numbers of feedstocks could be used, including crop residues, woody biomass, manure, and sewage sludge. In general, biochars produced from crop residues and woody biomass has higher carbon content and lower ash content, whereas biochars produced from manure

and sewage sludge has lower carbon content and higher ash content²⁸. Pyrolysis temperature also plays an important role in determining the biochar properties. Typically, surface area increases with increasing pyrolysis temperature, whereas surface functional group density decreases with increasing pyrolysis temperature.²⁹ Lower-temperature biochars are characterized by a relatively small number of aromatic rings, mostly with polar functional groups. With increasing pyrolysis temperature, the percentage of polar functional group and the oxygen/carbon ratio of biochars decrease, with a concomitant increase in aromaticity and graphitic structure.²⁴

Recent intense interest on soil amendment with biochars is partially due to their potential to immobilize environmental contaminants.³⁰ Sorption of contaminants in soils is an important process affecting the contaminant fate and transport in the environment.³¹⁻³⁴ Biochars with porous structure may be desirable for soil remediation due to their large capacity to immobilize environmental contaminants.^{29, 33, 35} Previous studies have reported that biochars have strong sorption ability for many organic contaminants including antibiotics.^{29, 33, 35-40} The knowledge on the sorption of antibiotics to biochars is still insufficient. Compared to other environmental containments, fewer studies have investigated the sorption of antibiotics to biochars, and the underlying sorption mechanisms still remain unclear.⁴¹⁻⁴⁷ Hydrophobic partitioning, electrostatic interaction, hydrogen bonding, pore filling, van der Waals forces, and π - π electro-donor-acceptor (EDA) interactions have been proposed as mechanisms responsible for the sorption of antibiotics to biochars.^{29, 35-37, 48} The sorption of antibiotics to biochars also depends on physicochemical properties of biochars, such as surface area and surface functional group. In addition, the sorption characteristics of antibiotics to biochars can be also influenced by chemical properties of antibiotics (such as polarity, hydrophobicity, and ionization) and environmental conditions (solution pH, ionic strength, temperature, and co-solutes).^{29, 33, 35, 49, 50} Most antibiotics are

ionizable hydrophilic compounds and the speciation of antibiotics highly depends on solution pH. Liao et al. (2013) investigated the sorption of tetracycline and chloramphenicol to bamboo biochar, proposing π - π EDA and hydrogen bonding interactions as the main sorption mechanisms for tetracycline and chloramphenicol.⁴³ They also reported that hydrophobic interaction and electrostatic interaction were thought to have a minor contribution to tetracycline and chloramphenicol sorption.⁴³ Ji et al. found that the sorption of sulfamethoxazole to biochars was controlled by micropore filling, whereas the tetracycline sorption was controlled by surface complexation and/or cation exchange.⁴¹ Wu et al. reported the sorption of sulfamethoxazole to BC increased with increasing pyrolysis temperature, but no significant trend was observed for the sorption of ofloxacin and norfloxacin to biochars.⁴⁵ Jia et al. reported that the sorption of oxytetracycline to biochars was enhanced by the coexistence of Cu^{2+} and Pb^{2+} ,⁴⁴ probably due to cation bridging. According to the previous studies, strong sorption of many antibiotics to biochars indicates that biochars have the potential to effectively immobilize antibiotics in the environment. However, due to the complexity and variability of both biochars and antibiotics, the sorption mechanisms of antibiotics to biochars are still not fully understood, which hinders our ability to design cost-effective mitigation strategies.

Recent studies raised a revived interest on dissolved organic carbon (DOC) originated from biochars because of their important role in soil and water environments.⁵¹⁻⁵⁶ DOC is often operationally defined as the fraction passed through a threshold pore size of filter membrane (e.g., 0.45 or 0.70 μm),¹⁷ thus including both truly dissolved molecules or submicron-sized BC particles (i.e., BC nanoparticles). The DOC released from BC has been reported to play a significant role in the fate and transport of soil contaminants,^{34, 57} microbial activity in soil and aquatic environments,^{55, 58} and plant growth.⁵⁹ Furthermore, the DOC fraction in BC is of importance to

assessing the carbon turnover, because the DOC fraction is more labile and is more susceptible to photo- and bio-degradation than bulk BC.^{56, 60} In addition, the DOC leached from BC could be rapidly transported from soils into nearby surface and ground waters via surface runoff and infiltration,⁶¹ which is also critical to soil carbon loss and the mobility of other contaminants in soils. Thus, knowledge regarding both qualitative and quantitative characteristics of DOC released from biochars would be essential for better accessing the quality of biochars and their impact on agroecosystems. Developing a quick, simple, and robust method for characterizing and quantifying the DOC from the biochars is key to the quality control of biochar production and application. To do so, a thorough study on both quantification and characterization of DOC in the biochars with different feedstock and pyrolysis condition should be conducted. In addition, the DOC may initially fill up the biochar pores during production, or coated on the biochar surface, thus blocking the sorption sites for antibiotics. The release of DOC from biochars may therefore enhance the sorption of antibiotics to BC. However, the effects of DOC release from biochars on their sorption affinity to antibiotics have not been well studied. Finally, the potential for the co-transport of antibiotics and BC nanoparticles should not be overlooked. Intentional addition and accidental release of BC particles due to wild and managed fires, crop residue burning, fossil fuel combustion, and carbon black production increased the abundance of BC particles in nature. BC particles that are mobile may facilitate the transport of sorbed antibiotics, especially for BC nanoparticles that are more mobile in soil profiles than micron-sized and bulk BC particles.^{62, 63} Therefore, a better understanding of the facilitated transport of antibiotics with BC nanoparticles is essential, but again has not been fully investigated.

OBJECTIVES

To fill the knowledge gaps identified above, this dissertation research aimed to:

1. Elucidate the sorption mechanisms of antibiotics to BC (specifically biochars).
2. Quantify and characterize the DOC released from biochars as influenced by feedstock type, pyrolysis condition, and extraction procedures; and develop a quick, easy and robust method to characterize and quantify the DOC from biochars.
3. To study the long-term sequestration of antibiotics by biochars and the potential effect of the long-term DOC release from biochars on the sorption of antibiotics.
4. To examine the facilitated transport of antibiotics by BC nanoparticles in saturated sand as influenced by solution ionic strength.

The following chapters address the four objectives of this research. Objective 1 is addressed in Chapter II and IV, Objective 2 in Chapter III, Objective 3 in Chapter IV, and Objective 4 in Chapter V. The dissertation ends with Chapter VI that concludes the findings of this research and provides future research directions.

CHAPTER II

SORPTION OF LINCOMYCIN BY MANURE-DERIVED BIOCHARS FROM WATER

ABSTRACT

The presence of antibiotics in agroecosystems raises serious concerns about the proliferation of antibiotic resistant bacteria and potential adverse effects to human health. Soil amendment with biochars pyrolyzed from manures may be a win-win strategy for novel manure management and antibiotics abatement. In this study, lincomycin sorption by manure-derived biochars was examined using batch sorption experiments. Lincomycin sorption was characterized by two-stage kinetics with fast sorption reaching quasi-equilibrium in the first two days, followed by slow sorption over 180 days. The fast sorption was primarily attributed to surface adsorption, whereas the long-term slow sorption was controlled by slow diffusion of lincomycin into biochar pore structures. Two-day sorption experiments were performed to explore effects of biochar particle size, solid-water ratio, solution pH, and ionic strength. Lincomycin sorption to biochars was greater at solution pH (6.0–7.5) below the pKa of lincomycin (7.6) than at pH (9.9–10.4) above its pKa. The enhanced lincomycin sorption at lower pH likely resulted from electrostatic attraction between the positively charged lincomycin and the negatively charged biochar surfaces. This was corroborated by the observation that lincomycin sorption decreased with increasing ionic strength at lower pH (e.g., 6.7), but remained constant at higher pH (e.g., 10). Nonetheless, the long-term lincomycin sequestration by biochars was largely due to pore diffusion plausibly independent of solution pH and ionic composition. Therefore, manure-derived biochars had lasting lincomycin sequestration capacity, implying that biochar soil amendment could significantly impact the distribution, transport and bioavailability of lincomycin in agroecosystems.

INTRODUCTION

Antibiotics are considered contaminants of emerging concerns, and increasing concentrations of antibiotics in agroecosystems could lead to the proliferation of antibiotic resistant bacteria and potential adverse impacts on human health.^{1, 7, 8} The ubiquitous existence of antibiotics in agroecosystems has been linked to the widespread and imprudent use of veterinary antibiotics in animal feeding operations as nontherapeutic feed additives¹. After administration to food animals, a large percentage of veterinary antibiotics are excreted into manure as parent compounds or bioactive metabolites, and then released to the environment through manure land applications.^{4, 12, 13} Thus, animal manure has been considered a major source of antibiotics in agroecosystems, and manure-borne antibiotics will likely increase selective pressure on bacteria and facilitate the development of antibiotic resistance.^{1, 7}

Lincomycin and combination antibiotics containing lincomycin are widely used in food animals for treatment and control of diseases (e.g., dysentery and porcine proliferative enteropathies in pigs, necrotic enteritis in chicken, acute mastitis in dairy cattle, and contagious foot-rot in sheep), as well as for growth promotion.⁶⁴ Resultant antibiotic-resistant bacteria often possess macrolide–lincosamide–streptogramin B (MLSB) cross-resistance.⁶⁴ This type of multi-drug resistance poses enormous threat to human and ecosystem health. Therefore, it is essential to reduce the release of lincomycin and other antibiotics to, and their mobility and bioavailability in the environment. However, lincomycin is frequently detected in the environment as a result of veterinary overuse, manure land application, and limited degradation of lincomycin.^{5, 65-67} Lissemore et al. found lincomycin concentrations of 0.2 to 355 ng L⁻¹ in 92% of 125 water samples collected from the Grand River in Canada, and agricultural husbandry was considered the major source.⁶⁸ Kuchta and Cessna reported lincomycin concentrations of 0.08 to 0.84 ng L⁻¹ in

snowmelt runoff samples from agricultural land receiving liquid swine manure containing lincomycin concentrations of 2.5 to 240 $\mu\text{g L}^{-1}$.¹² Although soil is an important filter media and sink for antibiotics, Watanabe et al. have indicated the high mobility of manure-borne lincomycin from soil to groundwater.⁶⁶ Therefore, novel soil amendment is needed for enhancing sequestration of lincomycin and other antibiotics in agricultural soils and thus reducing their environmental risks.

Biochar as a soil amendment has received increasing attention because of its potential agronomical and environmental benefits such as improving soil quality, carbon sequestration, contaminant immobilization, as well as agricultural waste management.^{24, 26, 33} Biochars are carbon-rich porous materials typically produced from a variety of feedstock (e.g., manure, woody biomass, crop residues, and sewage sludge) under limited oxygen condition and temperatures less than 700 °C.²⁴ Depending on feedstock type and pyrolysis temperature, biochars can have vastly different chemical and physical properties.^{26, 28, 69} Previous studies have shown that biochars typically have strong sorption ability for organic contaminants.^{33, 36-38} Because sorption of contaminants in soil often decreases their mobility and bioavailability,^{31, 34, 70} the addition of biochars to soils may play an important role in controlling transport and bioavailability of antibiotics in agroecosystems.

In this study, we proposed an innovative win-win strategy for novel manure management and antibiotics abatement by land application of biochars produced from pyrolysis of manures. Using manure as feedstock to produce biochars could have a number of potential benefits such as inactivation of microbial pathogens and degradation of antibiotics in manure from the thermal treatment (i.e. 300 to 700 °C). Then the manure-derived biochars could be either directly applied to the land or mixed with manures before spreading to reduce the mobility and bioavailability of

antibiotics. To develop better strategies of biochar soil amendment for antibiotics sequestration, it is important to understand the behaviors and underlying mechanisms of antibiotics sorption by manure-derived biochars. Therefore, the aim of this study was to assess the potential of biochar soil amendment for *in-situ* sequestration of antibiotics in agroecosystems through sorption studies. Lincomycin was chosen as a model compound to investigate the sorption of antibiotics by manure-derived biochars from water, due to its prevalence, high mobility, and limited degradation in the environment. The sorption kinetics and quasi-equilibrium sorption of lincomycin were evaluated to elucidate the underlying lincomycin sorption mechanisms by biochars.

MATERIALS AND METHODS

Biochar Samples and Characterization

Biochar samples used in this study were produced by slow pyrolysis of oven-dried manure feedstock at a temperature of 600 °C (Daisy Reactor, Best Energies Inc., Cashton, WI, USA). A detailed description of the biochar production can be found in Enders et al.²⁸ and Rajkovich et al.⁷¹ The produced biochars were ground and passed through sieves to obtain the fractions of 150–850, 75–150, and < 75 µm, and then stored in glass vials prior to use. Hereafter these biochars were designated according to feedstock type and pyrolysis temperature as BM600 (bull manure with sawdust), DM600 (dairy manure with rice hulls), PM600 (poultry manure with sawdust), and AM600 (anaerobically digested dairy manure).

The four manure-derived biochars have previously been well characterized.^{28, 71} Volatile matter, fixed carbon, and ash content of biochar samples were determined by the modified ASTM D1762-84 method. Carbon and nitrogen content were determined by a PDZ Europa ANCA-GSL elemental analyzer interfaced to a PDZ Europa 20–20 isotope ratio mass spectrometer (Sercon Ltd., Cheshire, UK). Hydrogen content was determined by a Hekatech HT Oxygen Analyzer

interfaced to a PDZ Europa 20–20 isotope ratio mass spectrometer (Sercon Ltd., Cheshire, UK). Oxygen content was calculated by subtracting C, N, H, and ash content from total mass. Cation exchange capacity (CEC) and exchangeable cation concentrations were determined by the ammonium acetate exchange method. More detailed biochar characterization can be found in Enders et al.²⁸ and Rajkovich et al.⁷¹

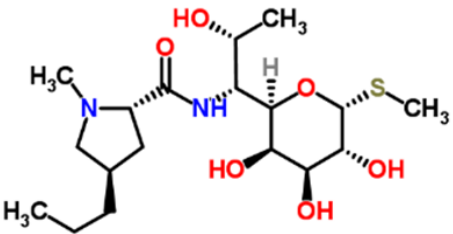
Additionally, specific surface area (SSA) of biochar samples was determined from 5-point CO₂ adsorption isotherms using the Brunauer–Emmett–Teller (BET) method by a Micromeritics Tristar 3020 analyzer (Micromeritics, USA) at Pacific Surface Science Inc. (Port Hueneme, CA). Zeta potential of the biochars was measured by Malvern Zetasizer Nano-ZS equipped with a MPT-2 autotitrator (Malvern Instruments, Worcestershire, UK). The isoelectric point (pH_{IEP}) of biochars was determined by measuring the zeta potential of biochars as a function of solution pH. To generate biochar colloid suspension for isoelectric point (pH_{IEP}) measurement, 10 mg biochar (particle size < 75 µm) was mixed with 50 mL DI water in a polyethylene centrifuge tube and then sonicated for 30 min. After sonication, top 10 mL of biochar suspension was withdrawn and then titrated with 0.1 M HCl or NaOH titrant from pH 10 to 2 using the autotitrator, and the corresponding zeta potential at each pH was measured by the Zetasizer Nano-ZS. The pH_{IEP} value was determined at the pH where the zeta potential is zero. Additionally, zeta potential for biochar suspensions of 1-day or 180-day water exposure was also determined by the zetasizer. In order to monitor the change of surface properties and surface morphology of biochar particles, zeta potential measurement and scanning electron microscopy (SEM, JEOL JSM-7500F, Japan) were performed for biochar samples of 75–150 µm, prepared from biochar suspensions of 1-day and 180-day water exposure.

Sorption Experiments

Chemicals and Experimental Setup

Lincomycin hydrochloride (purity $\geq 90\%$) was purchased from Sigma-Aldrich. The chemical structure and properties of lincomycin are summarized in Table 2.1. Deionized (DI) water was used for all the solution preparations. Amber borosilicate glass vials covered with aluminum foils were used in the experiments to prevent photodegradation of lincomycin. Batch sorption experiments were conducted in duplicate at room temperature (23 ± 1 °C). Prior to the sorption experiments, lincomycin solution was pre-adjusted to pH of 3 or 10 by 0.1 M HCl or NaOH. Solution pH was not controlled during the sorption experiments, but the final solution pH was recorded. To prevent competitive effect of other salts during lincomycin sorption, no electrolyte was added to control ionic strength unless otherwise noted. The biochar fraction of 75–150 μm and the solid-water ratio of 1 g L⁻¹ were used, unless mentioned otherwise, to achieve the removal efficiency of lincomycin at about 20% after two-day equilibration in order to better study sorption kinetics over a longer period. More details of the experimental protocols are given below.

Table 2.1. Chemical and physical properties of lincomycin[†]

Properties	Lincomycin
Molecular structure [‡]	
Molecular Formula [§]	C ₁₈ H ₃₄ N ₂ O ₆ S
Molecular weight [§]	406.54
pKa [§]	7.6
log K _{ow} [§]	0.20
Water solubility [§]	927 mg L ⁻¹ at 25 °C

[†] pKa: dissociation constant, K_{ow}: octanol/water partition coefficient; [‡] Data from ChemSpider (<http://www.chemspider.com/>); [§] Data from TOXNET (<http://www.toxnet.nlm.nih.gov/>)

Sorption Kinetics

Sorption kinetics experiments were performed to evaluate kinetic sorption rates and the equilibration time required for the subsequent sorption isotherm experiments. Additionally, sorption kinetics can be used to probe underlying sorption mechanisms,³⁸ and are highly complementary to equilibrium sorption isotherm data. Eight mg of each biochar with particle size of 75–150 μm were added into amber borosilicate glass vials containing 8 mL lincomycin of 1000 $\mu\text{g L}^{-1}$ at pH 10. The vials were placed on an end-over-end shaker (Glas-Col, USA) and shaken at 30 rpm for duration of 1 hour to 180 days. At pre-determined times, a sub-set of the sample vials were withdrawn, and the suspensions in the vials were filtered through a 0.45- μm syringe filter with mixed cellulose esters membrane (Millipore, USA). During filtration, the first 1 mL of filtrate was discarded and the following 1 mL of filtrate was collected so as to avoid the loss of lincomycin to the filter. Lincomycin concentrations in the filtrate were determined by a Shimadzu Prominence high-performance liquid chromatograph coupled to an Applied Biosystems Sciex 3200 triple quadrupole mass spectrometer (LC-MS/MS). More details of the LC-MS/MS analytical procedure are given below. The data from the biochar-free control experiments indicated a negligible loss of lincomycin via degradation throughout the experiments (Figure 2.1). In addition, the filtrates in the 180-day samples were also examined using the precursor ion scan mode by LC-MS/MS. Based on Calza et al. (2012),⁷² no degradation candidates of lincomycin were detected (Figure 2.2), suggesting that the disappearance of lincomycin from the aqueous phase was caused by sorption onto biochars instead of degradation. Therefore, the sorbed lincomycin concentration on the biochars was determined by the difference between initial and final lincomycin concentrations in the aqueous phase.

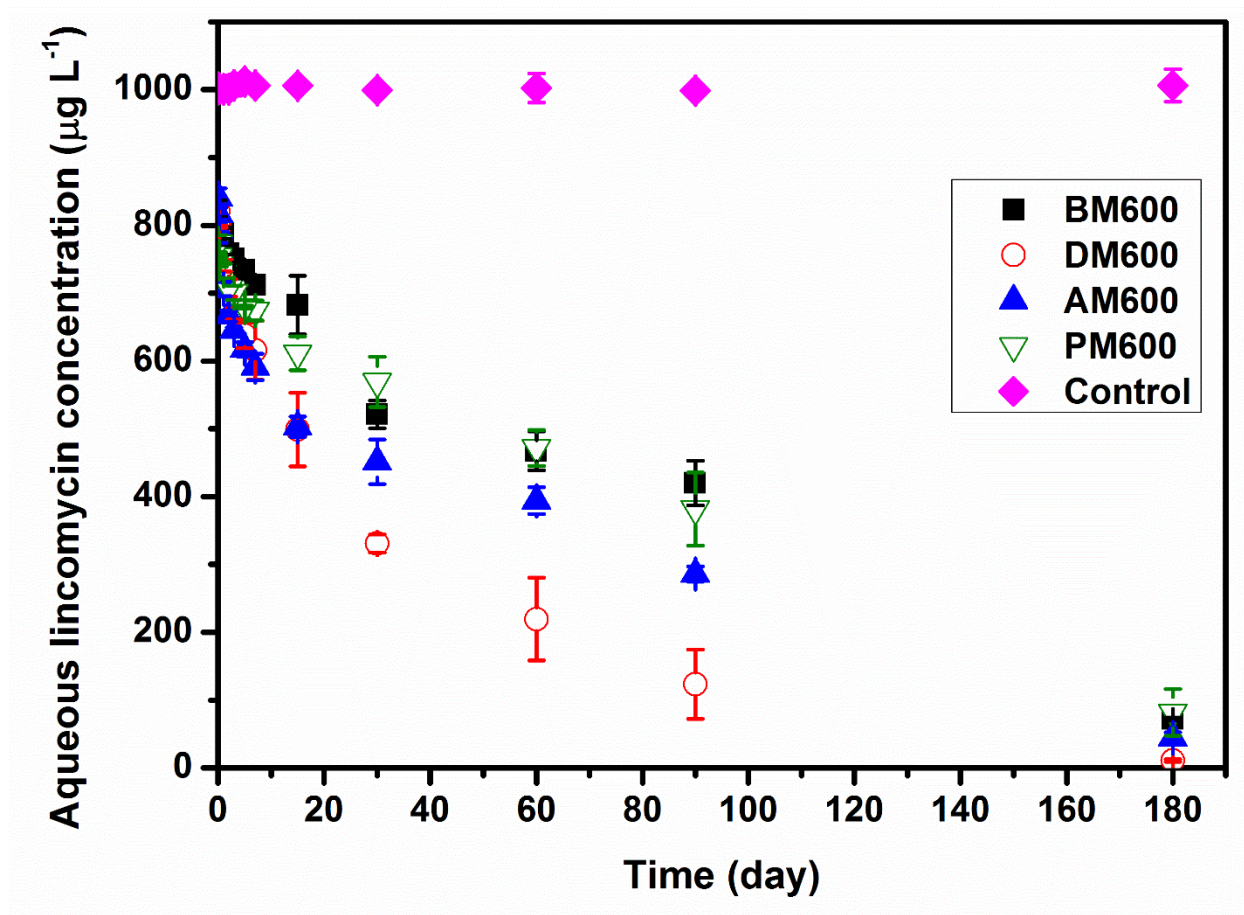


Figure 2.1. Lincomycin concentration versus time for lincomycin sorption kinetics experiments. Control was the biochar-free lincomycin solution.

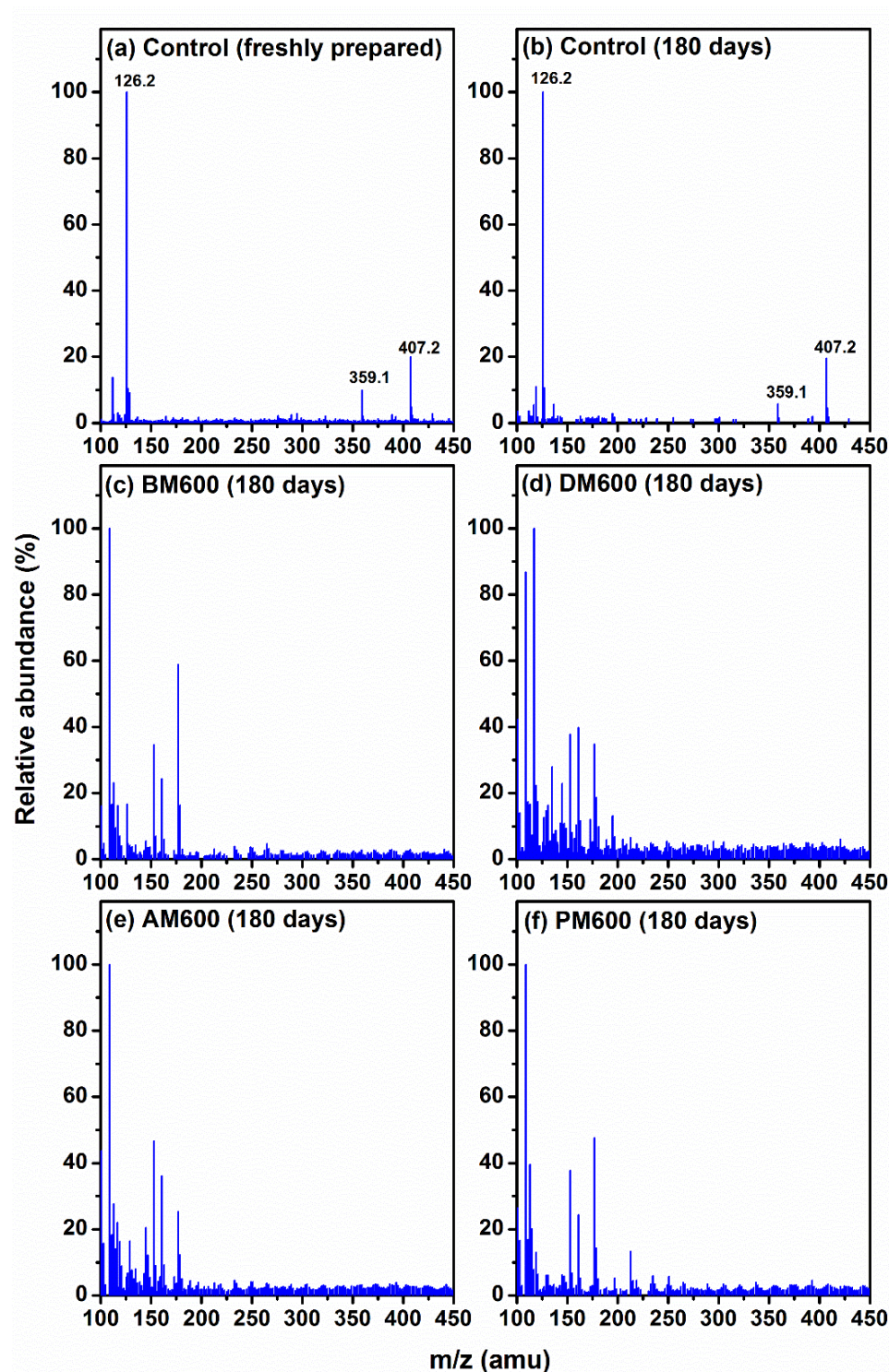


Figure 2.2. Precursor ion scan spectra of (a) Control (freshly prepared), (b) Control (180 days), (c) BM600 (180 days), (d) DM600 (180 days), (e) AM600 (180 days), and (f) PM600 (180days). Control was the biochar-free lincomycin solution. No degradation candidates of lincomycin was detected in long-term kinetics samples (b, d, f).

Effects of Biochar Particle Size and Solid-Water Ratio

We investigated the effects of biochar particle size and solid-water ratio to determine desired experimental conditions for the sorption isotherm experiments. To examine the effect of solid-water ratio, 4, 8, 40, and 80 mg of biochar samples were added to 8 mL lincomycin of $1000\ \mu\text{g L}^{-1}$ at pH 10 to achieve the solid-water ratio of 0.5, 1, 5, and $10\ \text{g L}^{-1}$. Additionally, to examine the effect of biochar particle size, 8 mg of biochars with particle size of either < 75 , 75–150, and 150–850 μm were mixed with 8 mL lincomycin of $1000\ \mu\text{g L}^{-1}$ at pH 10. The suspensions were then shaken at 30 rpm for 2 days, filtered, and the lincomycin concentration in the filtrate determined. The other sorption experimental procedures were identical to the protocols previously described.

Effects of Solution pH and Ionic Strength

We investigated lincomycin sorption mechanisms for the tested biochars through manipulating the interactions between lincomycin and biochar surfaces by changing solution pH and ionic strength. To determine the sorption isotherm, 8 mg of biochars were mixed with 8 mL lincomycin working solution at initial concentration of 100, 250, 500, 750, or $1000\ \mu\text{g L}^{-1}$ in the absence of NaCl addition. Conversely, to examine ionic strength effects, 8 mg of biochars were mixed with 8 mL of lincomycin working solution of $1000\ \mu\text{g L}^{-1}$ with the addition of 0, 0.01, 0.05, or 0.1 M NaCl. These experiments were conducted at initial solution pH of 3 and 10. Due to the alkalinity of the biochar samples, the final pH often increased to about 6.7 ± 0.5 for the lower pH tests, and remained unchanged for the higher pH tests (about 10.0 ± 0.2). The other procedures were similar to those previously described.

LC-MS/MS Analytical Procedure

Lincomycin concentrations in the solution were determined by a Shimadzu Prominence high-performance liquid chromatograph coupled to an Applied Biosystems Sciex 3200 triple quadrupole mass spectrometer (LC-MS/MS). A Gemini 5u C18 110A 50×2.00 mm 5 µm column was used. The mobile phase consisted of water (A) and 1:1 (v/v) acetonitrile-methanol mixture (B) with A and B both containing 0.3% formic acid. Gradient conditions were 0 % to 40 % B in 0 to 1 minute, 40 % to 70% B in 1 to 2 minutes, 70 % – 80 % B in 2 to 3 minutes, 80 % to 100 % B in 3 to 3.5 minutes, and held for 0.5 minutes at a flow rate of 0.35 mL/min. Injection volume was 10 µL. The tandem quadrupole MS was used with an electrospray ionization (ESI) and positive ion mode. Lincomycin was detected and quantified using a multiple reaction monitoring mode with a precursor/product transition of 407.2/126.2. The retention time and instrument detection limit of lincomycin was 2.37 min and 0.2 pg.

Mathematical Modeling

The linear forms of pseudo-first-order (Eq. 2.1), pseudo-second-order (Eq. 2.2), and intraparticle diffusion (Eq. 2.3) kinetic models^{73, 74} given below were used to fit the experimental data:

$$\ln(q_t - q_e) = \ln q_e - k_1 t \quad (2.1)$$

$$\frac{t}{q_t} = \frac{1}{q_e} t + \frac{1}{k_2 q_e^2} \quad (2.2)$$

$$q_t = k_i t^{0.5} + C \quad (2.3)$$

where q_e (µg g⁻¹) is the sorbed lincomycin concentration in the solid phase at equilibrium, q_t (µg g⁻¹) is the sorbed lincomycin concentration at time t , k_1 (day⁻¹) is the pseudo-first-order rate constant, k_2 (g µg⁻¹ day⁻¹) is the pseudo-second-order rate constant, k_i (µg g⁻¹ day^{-0.5}) is the intraparticle diffusion rate constant, and C (µg g⁻¹) reflects the boundary layer effect.

The Langmuir (Eq. 2.4) and Freundlich (Eq. 2.5) isotherm models below were fitted to the experimental data:

$$\frac{C_e}{q_e} = \frac{1}{q_{\max}} C_e + \frac{1}{K_L q_{\max}} \quad (2.4)$$

$$\ln q_e = \frac{1}{n} \ln C_e + \ln K_F \quad (2.5)$$

where C_e ($\mu\text{g L}^{-1}$) is the equilibrium lincomycin concentration in the solution, q_{\max} ($\mu\text{g g}^{-1}$) is the maximum lincomycin sorption capacity, K_L ($\text{L } \mu\text{g}^{-1}$) is the Langmuir constant, and K_F ($\mu\text{g}^{(1-1/n)} \text{g}^{-1} \text{L}^{1/n}$) and $1/n$ are the Freundlich constants. The goodness of fit to the models was evaluated by root mean squared error (RMSE) and coefficient of determination (R^2).

RESULTS AND DISCUSSION

Properties of Manure-Derived Biochars

Physicochemical properties of four manure-derived biochars are shown in Table 2.2. BM600, DM600, and AM600 had high carbon contents (62.8–76.0%), while PM600 had a relatively lower carbon content (28.7%). Conversely, BM600, DM600, and AM600 had relatively lower ash content (10.6–18.8%), while PM600 had a greater ash content (55.8%). The low atomic ratio of H/C, O/C, and (O+N)/C indicate that the biochars were highly carbonized, less hydrophilic, and low in polar surface functional group content.³⁸ The specific surface area (SSA) of BM600, DM600, and AM600 ($183\text{--}237 \text{ m}^2 \text{ g}^{-1}$) was higher than that of PM600 ($47 \text{ m}^2 \text{ g}^{-1}$), and was positively related to the carbon content ($R^2 = 0.996$), suggesting that the CO_2 -SSA of these biochars was mainly a result of the carbon matrix.³⁰

Zeta potential measurements indicate that the manure-derived biochars carried net negative surface charge within a wide pH range (Figure 2.3). The negative zeta potential remained nearly constant between pH 6 and 10. Within this pH range, the zeta potential of BM600, DM600, and AM600 was around $-56\text{--}64 \text{ mV}$, which was more negative than that of PM600 (i.e., about -36

mV). Below pH 6, the zeta potential became progressively less negative with decreasing pH, and the p_{HIEP} was found approximately at 1.9–2.2. Finally, a complex porous structure of the biochars was revealed by the SEM images, and the pore size spanned widely from nanometer level to micrometer level (Figure 2.4). The macroporous structure was likely preserved from the original feedstock structure, and the nanoporous structure was possibly formed during pyrolysis.²⁴

Table 2.2. Selected physical and chemical properties of manure-derived biochars[†]

Properties	BM600	DM600	AM600	PM600
<u>Proximate analyses (%)</u> [‡]				
Volatile matter	30.0	30.7	39.4	44.2
Fixed carbon	59.4	56.6	41.7	0
Ash	10.6	12.6	18.8	55.8
<u>Elemental analyses (%)</u> [‡]				
C	76.0	75.2	62.8	28.7
H	1.8	2.0	nd	0.4
O	14.3	11.6	nd	14.3
N	0.80	1.3	2.2	0.9
H/C	0.28	0.32	nd	0.17
O/C	0.14	0.12	nd	0.37
(O+N)/C	0.15	0.13	nd	0.40
CEC (mmolc kg ⁻¹) [‡]	336	97	151	59
<u>Exchangeable cation (mmolc kg⁻¹)</u> [‡]				
Ca	88.3	90.2	291	1098
Mg	67.7	15.6	164	126
K	464	60.5	413	464
Na	54.4	62.8	257	71.8
<u>SSA (m² g⁻¹)</u>				
<75 µm	nd	nd	nd	nd
75–150 µm	237	221	187	47
150–850 µm	250	229	187	37
p _{HIEP}	1.9	2.0	2.0	2.2
<u>Zeta potential (mV)</u>				
1-day	-60.4 ± 1.5	-64.1 ± 0.4	-55.6 ± 3.5	-36.3 ± 2.5
180-day	-61.5 ± 3.1	-60.8 ± 0.9	-56.4 ± 1.2	-35.0 ± 1.0

[†] H/C = atomic ratio of H to C, O/C = atomic ratio of O to C, (O+N)/C = atomic ratio of the sum of O and N to C, CEC = cation exchange capacity, SSA = specific surface area, p_{HIEP} = isoelectric point, Zeta potential was measured at pH 10, nd = not determined. [‡] Data from Enders et al.²⁸ and Rajkovich et al.⁷¹

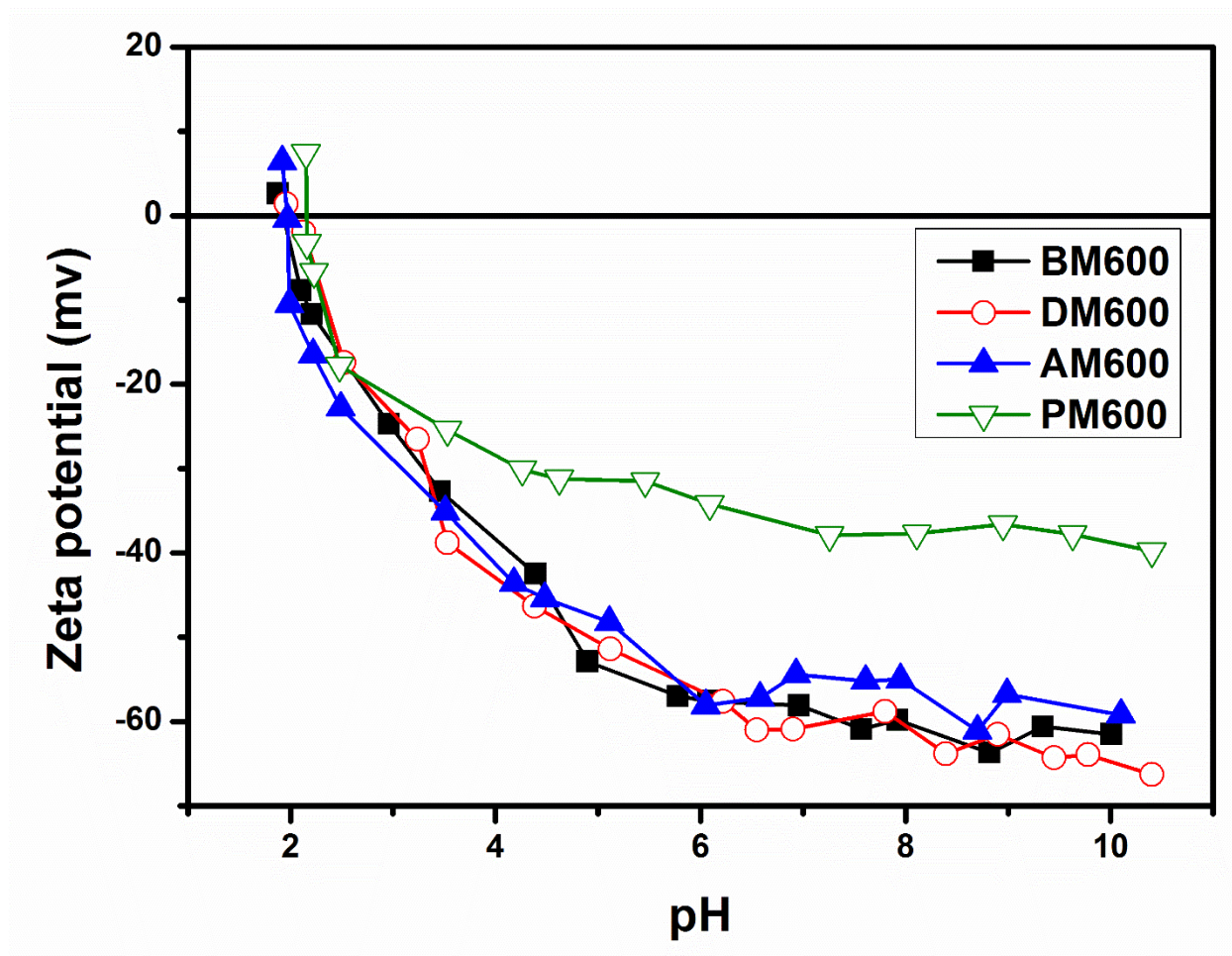


Figure 2.3. Zeta potential of manure-derived biochars as a function of solution pH.

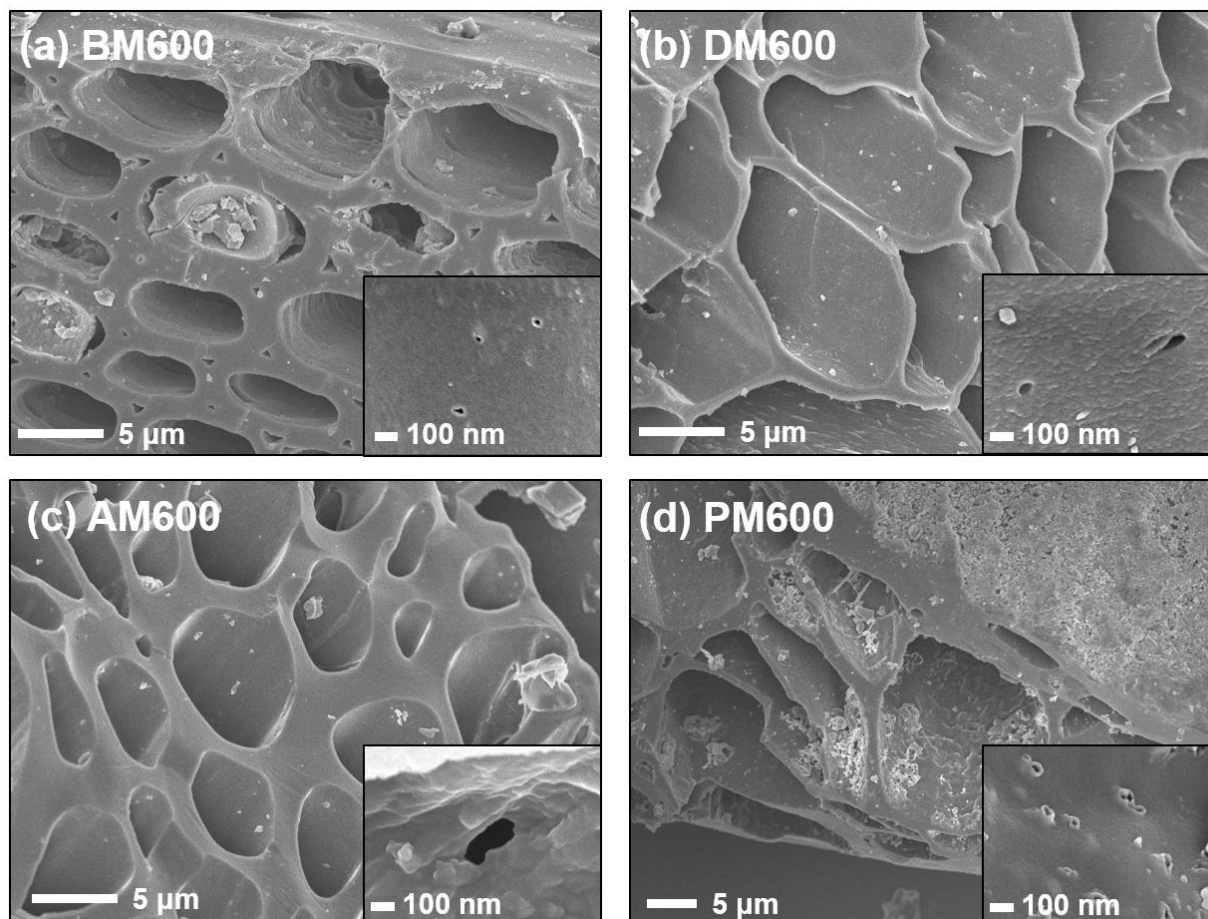


Figure 2.4. SEM images of manure-derived biochars: (a) BM600, (b) DM600, (c) AM600, and (d) PM600, prepared from biochar suspensions of 1-day water exposure.

Two-phase Sorption Kinetics

Sorption of lincomycin by the biochars was characterized as a two-phase sorption kinetics (Figure 2.5). Although the physicochemical properties varied greatly among the four biochars, the sorption kinetics showed similar patterns. In the initial sorption phase, the sorbed lincomycin concentration on the biochars increased rapidly during the first several hours of the first day, and then gradually reached a first-stage sorption plateau after 2 days (Figure 2.5a). In the longer-term sorption phase, the sorbed lincomycin concentration continuously increased and did not reach equilibrium by the end of the experimental period (i.e., 180 days) (Figure 2.5b). Typically, the initial fast sorption phase primarily results from surface adsorption between sorbate and sorbent surfaces that often occurs almost instantaneously or at a rapid rate, whereas the second slow sorption phase was caused by diffusion of sorbate into sorbent pore structures that occurs at a much slower rate (i.e., pore-diffusion process).³² Since the biochars have abundant surface sorption sites and pore structures, we therefore believed that lincomycin sorption by the biochars was governed by both processes, fast surface adsorption followed by slow pore diffusion. In addition, only 25–34 % of the applied lincomycin was removed from solution after 2 days, but 92–99% of that was removed after 180 days. This result indicated the large lincomycin sequestration potential of biochars and the predominant role of the pore diffusion process in lincomycin sorption over the long-term. Indeed, the intraparticle diffusion model fitted the sorption kinetic data well, whereas the pseudo-first-order and pseudo-second-order kinetic models were less satisfactory in fitting the sorption kinetics indicated by greater RMSE values (Table 2.3). This kind of two-phase sorption kinetics is consistent with the sorption of other organic compounds by biochars.^{38, 75} For example, Kasozi et al. (2010) studied the sorption of catechol on biochars and showed a similar sorption

kinetics trend, in which around 59% of total sorption occurred within the first few days and then reached sorption equilibrium after 14 days.

Since lincomycin sorption continued to increase over 180 days, it is important to evaluate the potential change of surface properties and surface morphology of biochar particles due to long-term water exposure. There was no significant difference in zeta potentials of biochars upon exposure to water for 1 day and 180 days (Table 2.2), implying surface functional groups of biochar particles on average did not change significantly during the length of the experiment. However, a close examination of biochar SEM images revealed that biochar surfaces became more eroded and cracked over time (Figure 2.6). The results implied that fine biochar fragments, minerals such as silica, and soluble elements were potentially detached or dissolved from biochar particle surface after long-term water exposure.⁷⁶⁻⁷⁸ In addition, biochar surface roughness might have increased with subsequent changes to its pore structure.

Based on the kinetic sorption results, the short-term (i.e., 2-day) sorption experiments could be used to characterize lincomycin adsorption to the external surfaces of biochars, whereas the long-term (i.e., 180-day) sorption experiments could be used to characterize lincomycin sorption to biochar interior spaces only accessible via pore diffusion. Because the underlying mechanisms during short-term surface adsorption have not been previously elucidated, two-day sorption experiments were performed to better understand interactions between lincomycin and biochar external surfaces.

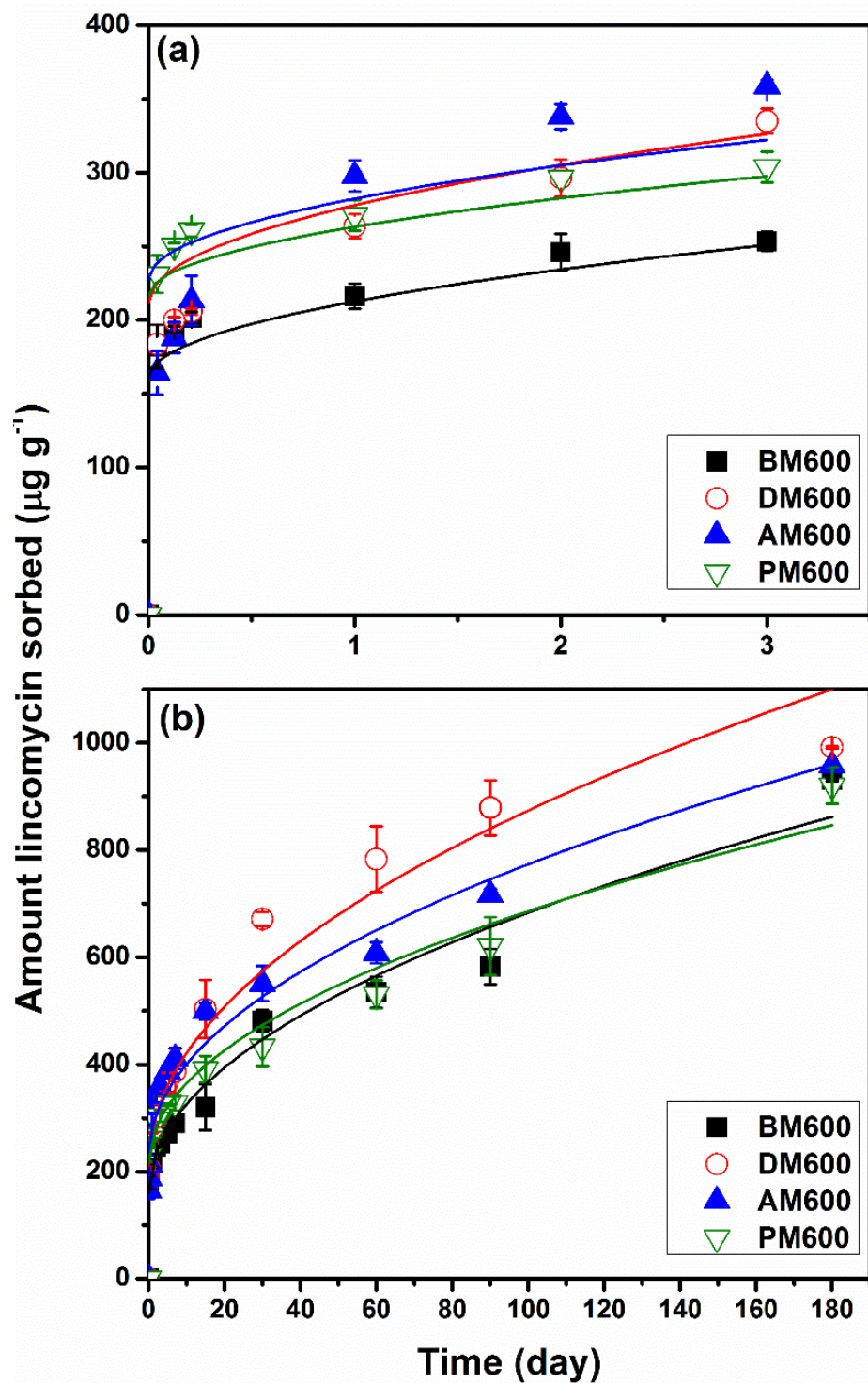


Figure 2.5. (a) Short-term and (b) long-term lincomycin sorption kinetics on manure-derived biochars. The solid lines were fitted with the intraparticle diffusion model.

Table 2.3. Fitted parameters of pseudo-first-order, pseudo-second-order, and intraparticle diffusion models for long-term sorption kinetics of lincomycin on manure-derived biochars.

Biochar	Pseudo-first-order			
	q_e ($\mu\text{g}\cdot\text{g}^{-1}$)	k_1 (day^{-1})	R^2	RMSE
BM600	937	3.11×10^{-2}	0.837	175
DM600	855	3.37×10^{-2}	0.951	187
AM600	851	3.13×10^{-2}	0.867	203
PM600	860	3.07×10^{-2}	0.837	197
	Pseudo-second-order			
	q_e ($\mu\text{g g}^{-1}$)	k_2 ($\mu\text{g g}^{-1} \text{day}^{-1}$)	R^2	RMSE
BM600	856	9.91×10^{-5}	0.916	144
DM600	990	1.46×10^{-4}	0.987	124
AM600	907	1.40×10^{-4}	0.959	142
PM600	852	1.13×10^{-4}	0.927	169
	Intraparticle diffusion			
	C ($\mu\text{g}\cdot\text{g}^{-1}$)	k_i ($\mu\text{g g}^{-0.5} \text{day}^{-0.5}$)	R^2	RMSE
BM600	160	52.3	0.973	34.0
DM600	212	66.2	0.965	49.7
AM600	228	54.6	0.963	42.1
PM600	216	47.0	0.972	31.2

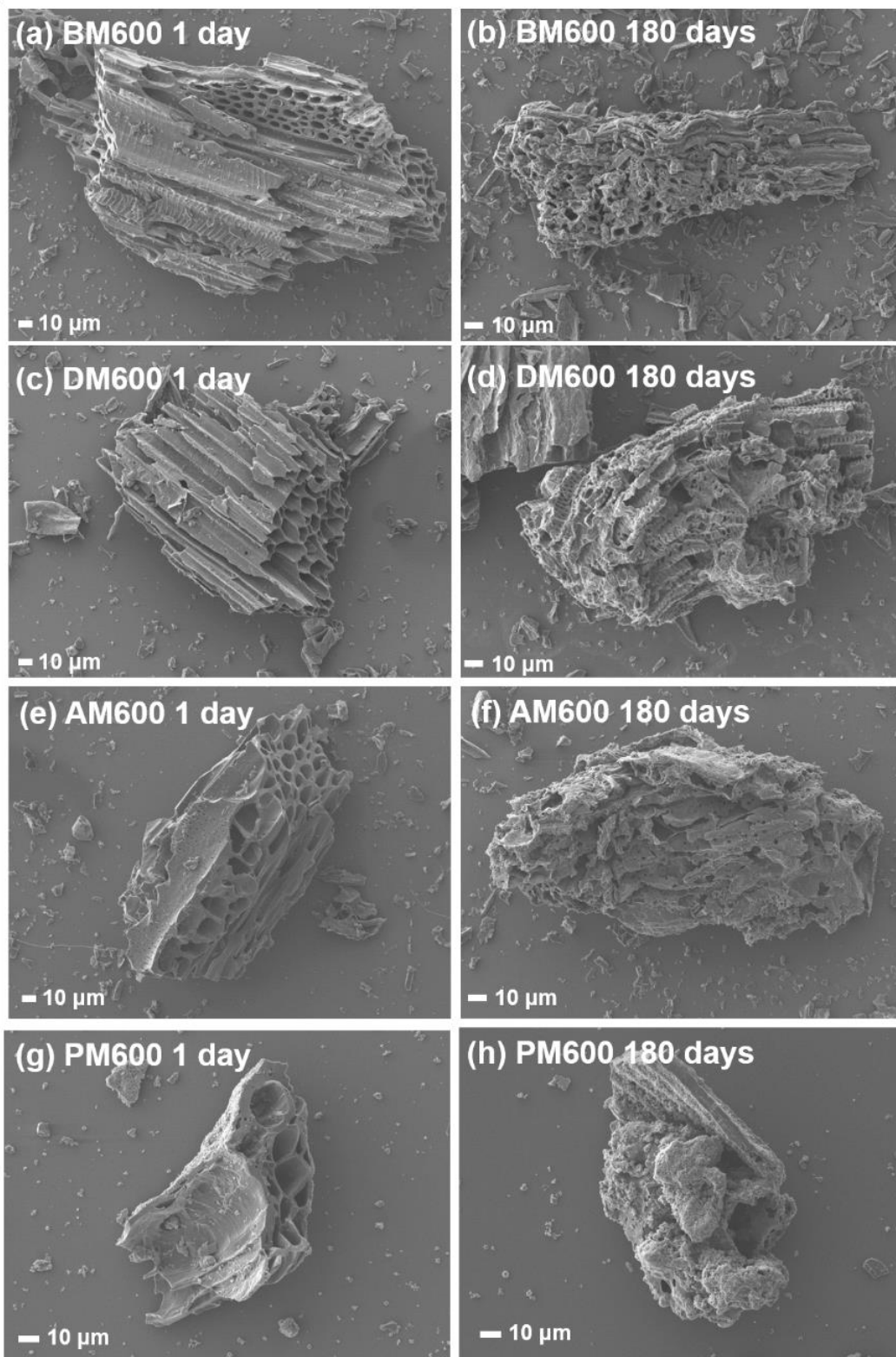


Figure. 2.6. SEM images of manure-derived biochars after 1-day and 180-day water exposure: (a, b) BM600, (c, d) DM600, (e, f) AM600, and (g, h) PM600.

Effects of Biochar Particle Size and Solid-Water Ratio

Biochar particle size and solid-water ratio significantly affected lincomycin sorption processes. As shown in Figure 2.7a, when the biochar particle size decreased from 150–850 μm to $< 75 \mu\text{m}$, the sorbed lincomycin concentration increased from 182–291 $\mu\text{g g}^{-1}$ to 403–463 $\mu\text{g g}^{-1}$. The increased 2-day sorption with smaller biochar particle sizes was likely due to increased external biochar surfaces easily accessible by lincomycin at smaller particle sizes. As the SSA values for biochars of larger and smaller particle size were similar (Table 2.2), the BET-SSA might not be an accurate index for biochar external surface areas. As expected, with increasing solid-water ratio, the lincomycin removal efficiencies increased from 16.8–24.0 to 89.7–92.8 %, but the sorbed lincomycin concentration decreased from 348–497 to 92.8–95.8 $\mu\text{g g}^{-1}$ (Figure 2.7b). These results are in accordance with the sorption of other organic contaminants by carbonaceous materials including biochars.⁷⁹⁻⁸¹ For example, Zheng et al. (2010) reported that the sorption of atrazine and simazine on biochars were greater and faster at smaller particle size. In addition, they also observed increased removal efficiency and decreased sorption capacity of biochars for both pesticides with increasing solid-water ratio.⁸⁰

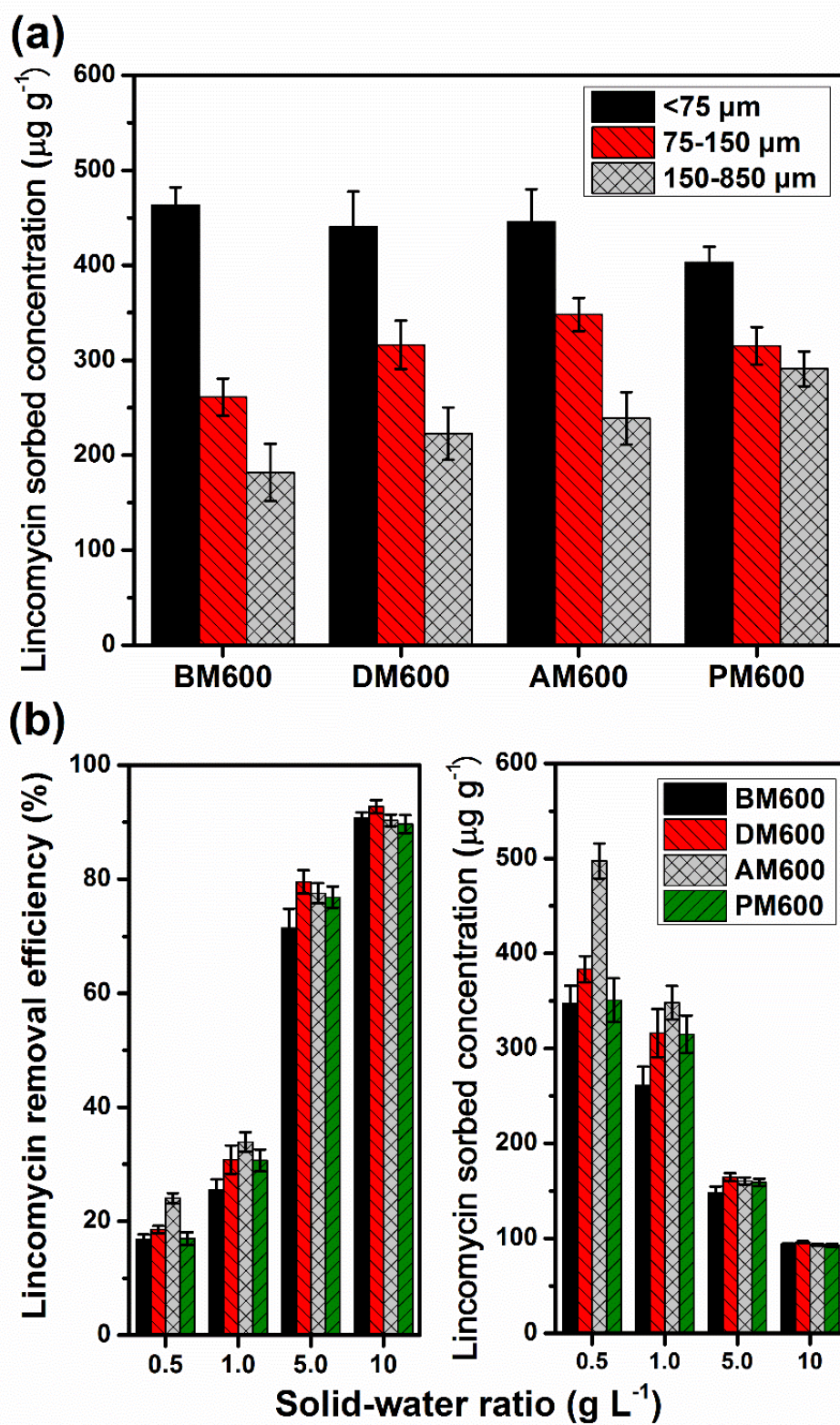


Figure. 2.7. Sorption of lincomycin on manure-derived biochars with varying (a) particle sizes and (b) solid-water ratios.

Effect of Solution pH and Ionic Strength

Two-day sorption isotherms of lincomycin on the biochars at two different pH values are shown in Figure 2.8. A nonlinear concave-downward (L-type) shape was observed for all sorption isotherms. Since surface adsorption is considered the dominant process within two days, a nonlinear sorption isotherm was expected because the availability of active surface sorption sites were limited and thus the sorption became progressively suppressed with increasing lincomycin loading. The fitted isotherm parameters for the Langmuir and Freundlich models are shown in Table 2.4. The isotherm data were better fitted to the Langmuir model, supported by the lower RMSE values, than to the Freundlich model. However, given the heterogeneous nature of biochar surfaces, the Langmuir model can only be considered as an empirical fitting equation carrying no mechanistic meaning. In fact, the Langmuir model has been frequently used in studying sorption of environmental contaminants by natural geosorbents because it provides the empirical maximum sorption capacities that allow for evaluating the contaminant sequestration potential of the natural geosorbents such as soils.⁸²

Table 2.4. Fitted parameters of Langmuir and Freundlich equations for lincomycin sorption on manure-derived biochars.

Biochar	Langmuir					Freundlich		
	q_{\max} ($\mu\text{g g}^{-1}$)	K_L ($\text{L } \mu\text{g}^{-1}$)	R^2	RMSE	n^{-1}	K_F ($\mu\text{g}^{(1-1/n)} \text{g}^{-1} \text{L}^{1/n}$)	R^2	RMSE
BM600 pH 6.6	555	1.29×10^{-2}	0.99	15	0.47	28.5	0.98	34
BM600 pH 9.9	299	7.87×10^{-3}	1.00	5.2	0.44	15.4	0.96	18
DM600 pH 6.5	605	1.40×10^{-2}	0.99	19	0.48	30.7	0.97	38
DM600 pH 10.0	372	5.68×10^{-3}	0.97	17	0.48	13.4	0.97	13
AM600 pH 6.9	697	6.18×10^{-3}	1.00	9.3	0.61	13.7	0.99	29
AM600 pH 10.0	436	4.58×10^{-3}	0.97	18	0.55	10.1	0.95	19
PM600 pH 7.3	576	2.68×10^{-3}	0.96	15	0.71	4.29	0.96	29
PM600 pH 10.4	424	3.41×10^{-3}	0.98	12	0.59	6.83	0.98	11

The dissociation constant (pKa) of lincomycin is 7.6 (Table 2.1). Hence, the lincomycin in aqueous solution would exist predominantly as cationic species at pH values much lower than 7.6 and as neutral species at pH much greater than 7.6. As shown in Figure 2.8, the lincomycin sorption of all four biochars was greater at pH 6.0–7.3 than that at pH 9.9–10.4. As biochar particles were negatively charged at these two pH levels (Figure 2.3), the enhanced lincomycin sorption at lower pH likely resulted from electrostatic attraction between positively charged lincomycin and negatively charged biochar surfaces,³⁵ similar to the observations for the sorption of tetracycline.⁴³ To further investigate the possibility of electrostatic interactions (i.e., cation exchange and cation- π bonding) as lincomycin sorption mechanisms, the sorption experiments were conducted under different ionic strength at two pH levels, i.e., below and above 7.6.

The effects of solution pH and ionic strength were interactive as shown in Figure 2.9. With increasing ionic strength, the lincomycin sorption decreased by 10.5–23.3% at lower solution pH (6.1–7.5), but remained essentially unchanged at higher solution pH (9.9–10.3). Likely, sorption competition occurred between the background electrolytes of Na^+ and positively charged lincomycin at lower solution pH ($\text{pH} < \text{pKa}$); conversely, this competition effect would not occur between Na^+ and neutral species of lincomycin at higher solution pH ($\text{pH} \gg \text{pKa}$). Although the four biochars had the same trend for pH and ionic strength effects, the lincomycin sorption capacity of PM600 was lower. This may be due to the less negative surface charge of PM600 (Figure 2.3) and the less cationic fraction of lincomycin at the final solution pH (7.3 or 7.5) of PM600 close to the pKa (7.6).

The abovementioned observations suggest that electrostatic interaction was involved in lincomycin sorption on biochar when solution pH was below the pKa of lincomycin. Nonetheless, an appreciable amount of lincomycin could still be adsorbed on the biochars at high solution pH.

The Langmuir maximum sorption capacity (q_{max}) at pH 9.9–10.4 was 54–74% of that at pH 6.5–7.3 for the four biochars (Table 2.5). For the higher pH at which lincomycin exists as neutral species, electrostatic interaction was unlikely to play a role. Therefore, non-electrostatic interactions were also involved in lincomycin sorption on biochars. Some of the non-electrostatic interactions proposed in the past include hydrophobic partition, π – π electron donor–acceptor (EDA) interaction, hydrogen bonding, and van der Waals forces.^{41, 43, 83} Due to the high water solubility and low log K_{ow} value of lincomycin (Table 2.1), the hydrophobic partition should not be significant in this study. Moreover, due to the lack of aromatic ring structures and π -electron-acceptor functional groups of lincomycin, the π – π EDA interaction between the lincomycin and the graphite-like biochar surface should not exist. Hence, considering the functional groups, molecular size, and molecular structure of lincomycin, it seems reasonable to infer that the non-electrostatic interactions may include hydrogen bonding and van der Waals forces. Nonetheless, the proposed mechanisms need to be validated by direct evidences in future studies.

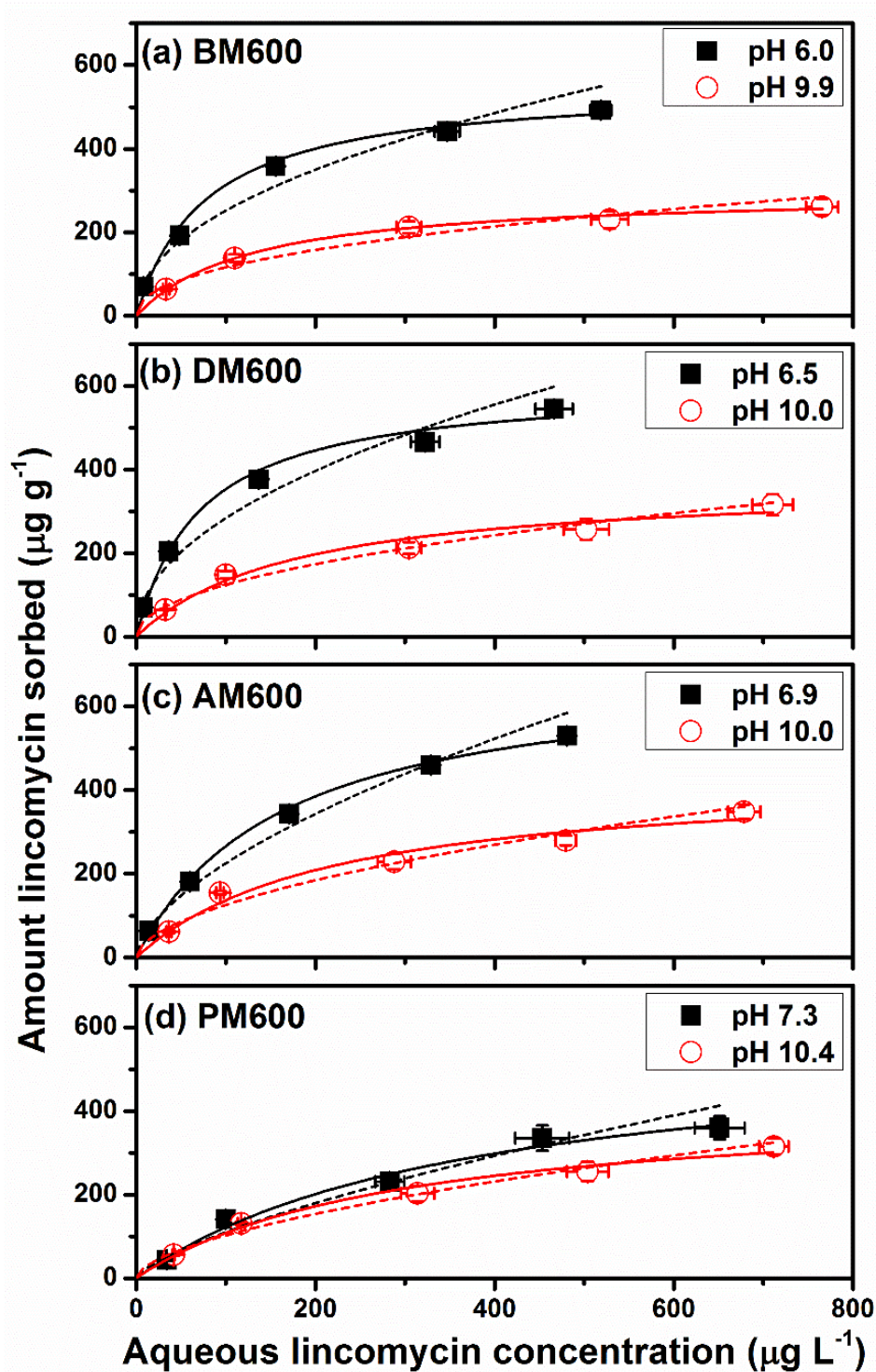


Figure. 2.8. Observed and fitted sorption isotherms of lincomycin on biochars at solution pH 6.0–7.3 and pH 9.9–10.4. The solid lines were fitted with the Langmuir model, and the dashed lines with the Freundlich model.

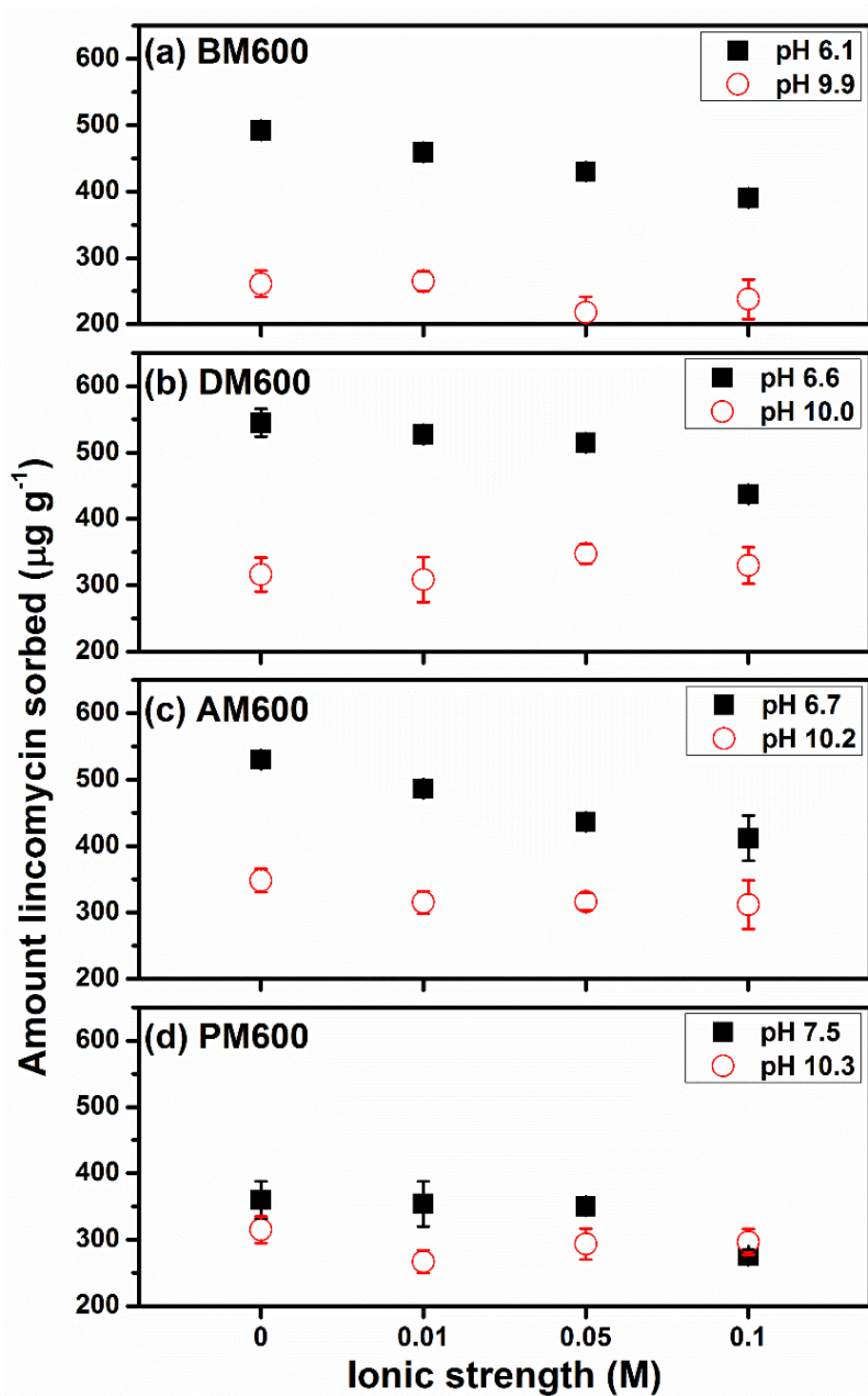


Figure. 2.9. Sorption of lincomycin on manure-derived biochars at solution pH of 6.1–7.5 and 10–10.3 under varying ionic strength.

Implications

These findings have interesting implications in the application of biochars for sequestration of antibiotics in soils. While natural soils rarely have pH values at 10, the results of lincomycin sorption at higher pH was useful to estimating the contribution of non-electrostatic sorption expected to be operative at all pH ranges. As the electrostatic interaction at lower pH is prone to competition and inhibition from other cations present in soil water,^{84, 85} non-electrostatic sorption appears to be a more useful index of antibiotics sequestration capacity of biochars, independent of solution pH and ionic strength effect. Moreover, given that lincomycin sorption only decreased by 10.5–23.3 % at the maximum when ionic strength increased to 0.1 M NaCl (Figure 2.9) representing the higher end of typical ionic strength in soil water (2×10^{-4} –0.18 M),⁸⁶ the competition from monovalent electrolytes in soil water would be limited. It is noted that the effect of divalent cations such as Ca^{2+} and Mg^{2+} should be further studied. Nonetheless, the presence of Ca^{2+} and Mg^{2+} in the background solution is expected due to dissolution from the unwashed biochars, as suggested by the exchangeable cation concentrations of the biochars (Table 2.2). Competition with these divalent cations should be manifested to certain extent by the sorption results at lower pH. In any case, the decrease in lincomycin sorption due to potential competition with other cations should be less than 26–46% for the four biochars, assuming an unlikely case of complete suppression of electrostatic interaction. The remaining lincomycin sorption would be due to the non-electrostatic interactions such as hydrogen bonding and van der Waals force.

Finally, the above discussion was based on the short-term sorption results, excluding the long-term pore diffusion. Over the long-term, the pore diffusion could result in 2.8–3.8 times greater lincomycin sorption than that over the short-term (Figure 2.5). We hypothesize that the pore diffusion would be minimally influenced by solution pH and ionic composition of soil water.

Nonetheless, future studies should examine the potential effects of organic molecules competing for the filling of biochar pores. It was noted that biochars had lower lincomycin sorption than humic acids and smectite clays.^{84, 87} However, lincomycin sorption to humic acids and smectite clays could be severely affected by solution pH and ionic composition, and pore diffusion might not be important,^{84, 87} Moreover, biochars had much greater lincomycin sorption than whole soils.⁸⁵ Therefore, manure-derived biochars may be attractive geosorbents used for *in-situ* long-term sequestration of antibiotics via soil amendment. After applied to agricultural soils, biochars may provide not only quick immobilization of antibiotics in the short-term by surface adsorption, but also a lasting antibiotics sequestration over the long-term through pore diffusion, thus decreasing bioavailability and mobility of antibiotics in agroecosystems.

CHAPTER III
QUANTIFICATION AND CHARACTERIZATION OF DISSOLVED ORGANIC
CARBON FROM BIOCHARS

ABSTRACT

Dissolved organic carbon (DOC) in biochars is critical to carbon (C) dynamics and contaminant transport in soils. However, a robust and easy method to extract and determine the DOC concentrations in biochars has yet to be developed. This study quantified and characterized the DOC extracted by deionized water, 0.1 M HCl, and 0.1 M NaOH (named water-extractable DOC (WEOC), acid-extractable DOC (AEOC), and base-extractable DOC (BEOC), respectively) from 46 biochars produced from diverse feedstocks and pyrolysis conditions. BEOC concentrations were the highest (2.3–139 mg-C/g-biochar), followed by WEOC (0.5–40 mg-C/g-biochar) and AEOC (0.2–23 mg-C/g-biochar). In general, fast-pyrolysis biochars had higher DOC concentrations than slow-pyrolysis biochars. DOC concentrations in slow-pyrolysis biochars decreased exponentially with increasing pyrolysis temperature from 300 to 600 °C. As revealed by solid-state ^{13}C NMR, biochar-DOC had abundant small fused-ring aromatics, aliphatic C, and carboxyl C. Biochar-DOC included an acid-precipitated (AP) fraction of higher molecular weight and aromaticity and an acid-soluble (AS) fraction of lower molecular weight and aromaticity. BEOC generally had a greater AP fraction than WEOC and AEOC. Both molecular weight and aromaticity of AEOC and BEOC differed from that of the more environmentally-relevant WEOC, suggesting that the acid- and base/alkali-extraction may not produce the DOC released under realistic soil conditions. Finally, a quick, easy and robust UV-vis spectrometric method was developed to measure the WEOC concentrations in diverse biochar samples ($R^2 = 0.96$ and $n = 46$).

INTRODUCTION

Biochars are carbonaceous porous materials co-produced with syngas and bio-oil from pyrolysis of biomass, and have been promoted as soil amendments for agronomic and environmental benefits.^{24, 88-91} The potential benefits of soil biochar amendment include increased soil carbon (C) storage, improved soil characteristics (e.g., improving soil structure, reducing bulk density, and enhancing water and nutrient retention), decreased greenhouse gas emission, and *in-situ* immobilization of contaminants such as excess nutrients, organic pollutants, and trace metals.^{29, 33, 91-93} During the last several years, dissolved organic C (DOC) in biochars has sparked strong research interest,⁵¹⁻⁵⁶ because it plays an important role in controlling biochar persistence and mobility,^{56, 60, 94, 95} contaminant fate and transport,^{34, 57, 96} microbial activities,^{55, 58} and plant growth⁹⁷ in agroecosystems. Once applied in the field, biochars could release DOC into soil water, and directly alter physicochemical properties of soil DOC.^{98, 99} The released DOC from the biochars (hereafter termed as biochar-DOC) could be rapidly transported from soils into receiving surface and ground waters via surface runoff and leaching,^{61, 100, 101} thus contributing to soil C loss and the transport of DOC-associated contaminants. More broadly, the release of DOC from pyrogenic C contributes approximately 10% of total DOC in surface water globally.⁹⁵ Furthermore, the DOC fraction in the biochars is labile and more susceptible to photo- and bio-degradation than bulk biochars.^{56, 60} Thus, both qualitative and quantitative characteristics of biochar-DOC are needed for better assessing the qualities of biochars and their impact on agroecosystems.

DOC is often operationally defined as the organic C fraction smaller than the pores of filter membranes (e.g., 0.45 or 0.75 μm).⁹⁴ The biochar-DOC thus includes both truly dissolved molecules and sub-micron sized biochar particles.^{54, 100-102} Water-soluble organic compounds can

be formed by re-condensation and entrapment of volatile organic compounds into the biochar pore structure during pyrolysis, which can be later released as DOC.¹⁰³⁻¹⁰⁵ In addition, sub-micron biochar particles may initially be present or later produced from physicochemical disintegration of bulk biochars.^{54, 102}

Biochar-DOC is often extracted by either water or strong alkaline (i.e., sodium hydroxide (NaOH) or potassium hydroxide (KOH)) solutions.^{51, 52, 54, 55} The alkaline extraction is adapted from the method of organic matter extraction from soils.¹⁰⁶⁻¹⁰⁸ The extracted soil organic matter (SOM) has been traditionally perceived as primarily humic substances, i.e., stable macromolecules formed by a humification process that are resistant to microbial degradation. However, it is increasingly recognized that the humification process may not actually occur in soils, and SOM is primarily formed through microbial decomposition, biosynthesis, as well as physical protection by sorption on mineral surfaces and sequestration in soil aggregates.¹⁰⁸⁻¹¹⁰ Furthermore, the alkali-extractable SOM may not truly represent organic matter released into soil water because natural soils rarely reach the extreme alkaline and high pH conditions used in the alkaline extraction.¹⁰⁸ Similarly, the alkali-extractable biochar-DOC may not reflect the amount and properties of DOC released into soil water from the added biochars. Indeed, Chen et al.¹¹¹ found that the amount of DOC released from biochars increased with increasing solution pH (2–11). Thus, water extraction may produce more representative DOC released from biochars under natural soil conditions.¹⁰⁸ Additionally, acid washing is commonly used for de-ashing biochars before analysis^{30, 112} and would presumably extract certain fractions of biochar-DOC. However, studies on the difference in the quantity and characteristics of biochar-DOC extracted by water, strong acid solution, and strong base solution are rare.

A number of recent studies have characterized biochar-DOC via advanced spectroscopic and mass spectrometry techniques. About 300–2400 unique molecular formulas could be assigned in the spectra of the biochar-DOC (200–800 m/z) detected by Fourier transform ion cyclotron resonance mass spectrometry (FTICR-MS).⁵⁵ Many small organic compounds in the mass range of 45–500 m/z belonged to phenolic compounds, acids, and bio-oil-like compounds, as revealed by 2D gas chromatography coupled with time of flight mass spectrometer (GC×GC-TOFMS).⁵⁵ Qu et al.⁵⁴ reported that biochar-DOC was composed primarily of small aromatic clusters rich in carboxyl functional groups, based on Fourier transform infrared spectroscopy (FT-IR) and solid-state ^{13}C nuclear magnetic resonance (NMR). Using liquid chromatography-organic C detection (LC-OCD) analysis⁵¹ and fluorescence excitation-emission spectrophotometry with parallel factor analysis (EEM-PARAFAC),^{52, 53} biochar-DOC could be characterized by several components (e.g., low-molecular-weight acids and neutrals, and high-molecular-weight compounds) differing in their individual mean molecular weight (M_w) and fluorescence features. Because these components can have distinct environmental persistence and mobility, their proportion may be used to characterize the biochar-DOC.

Many of the aforementioned methods are costly and not routinely available in many laboratories, thus hampering their wide use in quality assessment during biochar production and application. Therefore, developing a quick, easy and robust method for characterizing and quantifying the biochar-DOC is critically needed. Ultraviolet–visible (UV-vis) absorption spectroscopy is commonly available and has been successfully used to characterize the biochar-DOC.^{53, 56} It was thus selected for developing the new method here.

Therefore, this study aimed to: (1) investigate whether the base/alkali- or acid-extractable DOC from biochars is different with the more environmentally-relevant water-extractable DOC in

terms of their quantities and qualities; and (2) develop a quick, easy and robust method for quantifying the biochar-DOC. To do so, we thoroughly quantify and characterize the DOC extracted with deionized (DI) water, 0.1 M hydrochloric acid (HCl), and 0.1 M NaOH from 46 biochars pyrolyzed from diverse feedstocks and pyrolysis conditions. As the quantities and qualities of biochar-DOC highly depend on pyrolysis temperature,^{51-53, 55, 113} and feedstock type,^{51, 52, 113} the relative importance of these factors in determining the biochar-DOC concentrations was also explored here. Additionally, advanced solid-state ¹³C NMR spectroscopy was used to provide detailed quantitative structural information of DOC and the structure change of bulk biochars after the extraction treatment. Finally, a quick, easy and robust method was developed to quantify the biochar-DOC by only using the commonly available UV-vis absorption spectroscopy.

MATERIALS AND METHODS

Biochars

Details on the feedstocks and production conditions of 46 biochars used in this study are provided in Table 3.1.^{28, 71, 114} Briefly, the feedstocks were: (1) animal manures including bull manure with sawdust bedding (BM), dairy manure with rice hulls bedding (DM), poultry manure with sawdust bedding (PM), raw dairy manure with sawdust bedding (RDM), digested dairy manure (DDM), composted digested dairy manure (CDM), and composted digested dairy manure mixed with woodchips (CDMW) (note that RDM, DDM, CDM, and CDMW were from the same manure source with various pretreatments prior to pyrolysis); (2) woody biomass including oak wood (OW), pine wood (PW), mixed woodchips (WC), mixed hardwood (HW), mixed softwood (SW), Chinese bamboo (CB), and Brazilian pepperwood (BP); (3) herbaceous residues including corn stover (CS), soybean (SB), switchgrass (SG), sugarcane bagasse (BG), and yard leaves (YL); and (4) urban wastes including food waste (FW) and paper mill waste (PMW). The feedstocks

were pyrolyzed via fast pyrolysis at 500 °C or slow pyrolysis at 300–600 °C. Here fast pyrolysis had a residence time of < 30 s, whereas slow pyrolysis had a residence time > 15 min. The produced biochars were ground and passed through a 74- μ m sieve, and stored in glass vials prior to use. This particle size fraction was selected to represent finer biochars that may have greater potential to release DOC once applied to soils. Hereafter, the biochar samples were named by feedstock and pyrolysis temperature (e.g., “BM300” for bull manure pyrolyzed at 300 °C). These selected different biochars have previously been characterized, and their selected physicochemical properties are summarized in Table 3.2.^{28, 71, 114}

Table 3.1. Feedstock and production details of biochar samples.

Biochar ID	Feedstock full name and origin	Pyrolysis temp. (°C)	Pyrolysis condition
SB500	Soybean. Collected in Pennsylvania.	500	Fast pyrolysis in a fluidized bed reactor under N ₂ atmosphere. The residence time was 0.11 second. ¹¹⁵⁻¹¹⁷
SG500	Switchgrass. Collected in Pennsylvania.	500	
HW500	Mixed hardwood. Collected from Dynamotive (Canada).	500	Fast pyrolysis in a bubbling fluidized bed reactor (Dynamotive, Canada). The residence time was less than 5 seconds. ²⁸
SW500	Mixed softwood. Collected from Dynamotive (Canada).	500	
SG(2)500	Switchgrass. Collected from Texas A&M University (College Station, TX)	500	Fast pyrolysis in an auger reactor. The residence time was 15–30 seconds. ²⁸
PW(2)500	Pine wood. Collected from Texas A&M University (College Station, TX)	500	
BM300, BM400, BM500, BM600	Bull manure with sawdust bedding. Collected in Wisconsin	300, 400, 500, 600	Slow pyrolysis in the Daisy Reactor (Best Energies, Cashton, WI) under N ₂ atmosphere. The heating rate was less than 10 °C per minute and the residence time was 15–20 minutes. ^{28, 71}
DM300, DM400, DM600	Dairy manure with rice husks bedding. Collected in Wisconsin	300, 400, 600	
PM300, PM400, PM500, PM600	Poultry manure with sawdust bedding. Collected in Wisconsin	300, 400, 500, 600	
RDM500	Raw dairy manure. Collected from AA Dairy (Candor, NY). Raw dairy manure (with sawdust bedding) did not receive any anaerobic digestion or composting pretreatment prior to pyrolysis.	500	
DDM500, DDM600	Digested dairy manure. Collected from AA Dairy (Candor, NY). The dairy manure with sawdust bedding was anaerobically digested, and the screw-press-dried solid manure product was collected for pyrolysis.	500, 600	
CDM500	Composted digested dairy manure. Collected from AA Dairy (Candor, NY). The above anaerobically digested, screw-press-dried solid manure product was further composted and then collected for pyrolysis.	500	
CDMW500	Composted digested dairy manure mixed with woodchips. The composted digested dairy manure (CDM) was mixed with woodchips in 1:1 ratio just prior to pyrolysis.	500	
OW300, OW400, OW600	Oak wood. Collected in Wisconsin	300,400, 600	

Table 3.1(cont'd)

Biochar ID	Feedstock full name and origin	Pyrolysis temp. (°C)	Pyrolysis condition
PW300, PW400, PW600	Pine wood. Collected in Wisconsin	300,400, 600	Slow pyrolysis in the Daisy Reactor (Best Energies, Cashton, WI) under N ₂ atmosphere. The heating rate was less than 10 °C per minute and the residence time was 15–20 minutes. ^{28, 71}
WC500	Mixed woodchips. Collected from Cornell University (Ithaca, NY).	500	
CS300, CS400, CS600	Corn stover. Collected in Wisconsin	300,400, 600	
YL500	Yard leaves. Collected in Ithaca, NY in fall.	500	
FW500, FW600	Food waste. Collected from Cornell University dining hall (Ithaca, NY).	500, 600	
PMW500, PMW600	Paper mill waste. Collected from Mohawk Paper Company (Waterford, NY).	500, 600	
BG300, BG450, BG600	Sugarcane bagasse. Collected from University of Florida (Gainesville, FL)	300, 450, 600	Slow pyrolysis in a furnace reactor under N ₂ atmosphere. The heating rate was 10 °C per minute and the residence time was 120 minutes. ^{114, 118}
BP300, BP450, BM600	Brazilian pepperwood. Collected from University of Florida (Gainesville, FL)	300, 450, 600	
CS(2)600	Corn stover. Collected from Best Energies Australia (Australia)	600	
SM450	Softwood mixture. Spruce, pine, and fir wood waste mixture. Other details not available	450	Slow pyrolysis, other details not available
CB500	Chinese Bamboo. Other details not available	500	Details not available

Table 3.2. Selected properties of biochar samples.

Biochar ID	Proximate analysis (% w/w)			Ultimate analysis (% w/w)				Atomic ratios		
	VM ^a	Ash	FC ^b	C	O	H	N	H/C	O/C	(O+N)/C
SB500	47.0	15.2	37.8	60.4 ^c	n/a ^d	n/a	0.7 ^c	n/a	n/a	n/a
SG500	35.1	41.2	23.7	44.2 ^c	n/a	n/a	1.3 ^c	n/a	n/a	n/a
HW500	56.8	4.3	38.9	73.5 ^c	n/a	n/a	0.3 ^c	n/a	n/a	n/a
SW500	45.5	5.6	48.9	84.4 ^c	n/a	n/a	0.0 ^c	n/a	n/a	n/a
SG(2)500	27.7	16.5	55.8	69.9 ^c	n/a	n/a	0.5 ^c	n/a	n/a	n/a
PW(2)500	46.8	46.7	6.5	31.9	16.9	2.2	2.3	0.83	0.40	0.46
CS300	51.9	10.7	37.4	59.9	24.8	4.5	1.1	0.90	0.31	0.33
CS400	44.7	12.9	42.4	65.2	20.1	3.3	1.1	0.61	0.23	0.25
CS600	23.5	16.7	59.8	70.7	9.3	2.3	1.1	0.39	0.10	0.11
YL500	40.3	14.5	45.2	60.7	n/a	n/a	1.1	n/a	n/a	n/a
BM300	55.5	7.7	36.8	60.6	26.6	4.9	1.3	0.97	0.33	0.35
BM400	37.0	9.4	53.7	68.5	17.4	3.5	1.2	0.61	0.19	0.21
BM500	30.5	10.4	59.2	74.1	17.4	2.6	1.1	0.42	0.18	0.19
BM600	30.0	10.6	59.4	76.0	14.3	1.8	0.8	0.28	0.14	0.15
DM300	45.4	10.1	44.5	61.5	22.6	4.5	1.6	0.88	0.28	0.30
DM400	39.1	11.5	49.5	67.1	16.8	3.3	1.4	0.59	0.19	0.21
DM600	30.7	12.6	56.6	75.2	11.6	2.0	1.3	0.32	0.12	0.13
PM300	46.8	46.7	6.5	31.9	16.9	2.2	2.3	0.83	0.40	0.46
PM400	43.8	51.7	4.5	32.1	14.3	0.7	1.2	0.26	0.33	0.37
PM500	43.2	52.6	4.2	27.8	17.9	0.5	1.1	0.22	0.48	0.52
PM600	44.2	55.8	0.0	28.7	14.3	0.4	0.9	0.17	0.37	0.40
RDM500	33.0	32.0	35.0	51.2	n/a	n/a	2.1	n/a	n/a	n/a
DDM500	42.7	14.7	42.6	59.4	n/a	n/a	2.6	n/a	n/a	n/a
DDM600	39.4	18.8	41.7	62.8	n/a	n/a	2.2	n/a	n/a	n/a
CDM500	33.0	50.1	16.9	37.8	n/a	n/a	2.0	n/a	n/a	n/a
CDMW500	25.7	58.5	15.8	74.0	n/a	n/a	0.6	n/a	n/a	n/a
OW300	61.1	0.3	38.5	63.9	30.8	4.8	0.1	0.90	0.36	0.36
OW400	40.9	0.8	58.3	78.8	17.1	3.2	0.2	0.49	0.16	0.16
OW600	27.5	1.3	71.2	87.6	8.5	2.5	0.2	0.34	0.07	0.07
PW300	55.3	1.5	43.2	67.2	31.5	4.9	0.1	0.88	0.35	0.35
PW400	45.5	1.1	53.5	76.3	20.8	3.7	0.1	0.58	0.20	0.21
PW600	27.7	1.1	71.2	91.1	9.5	2.3	0.1	0.30	0.08	0.08
WC500	26.9	10.9	62.1	85.9	n/a	n/a	0.4	n/a	n/a	n/a
FW500	33.7	52.7	13.6	42.0	n/a	n/a	2.8	n/a	n/a	n/a
FW600	34.5	52.0	13.6	32.0	n/a	n/a	1.2	n/a	n/a	n/a
PMW500	42.5	57.5	0.0	19.2	22.7	0.5	0.2	0.31	0.89	0.90
PMW600	40.0	59.1	0.0	19.2	21.2	0.4	0.1	0.25	0.83	0.83
BP300	n/a	n/a	n/a	59.3	34.1	5.2	0.3	1.05	0.43	0.44
BP450	n/a	n/a	n/a	75.6	17.2	3.6	0.3	0.57	0.17	0.17
BP600	n/a	n/a	n/a	77.0	17.7	2.2	0.1	0.34	0.17	0.17
BG300	n/a	n/a	n/a	69.5	24.5	4.2	0.9	0.73	0.26	0.28
BG450	n/a	n/a	n/a	78.6	15.5	3.5	0.9	0.53	0.15	0.16
BG600	n/a	n/a	n/a	76.5	18.3	2.9	0.8	0.45	0.18	0.19
SM450	n/a	n/a	n/a	55.5 ^c	n/a	n/a	0.2 ^c	n/a	n/a	n/a
CS(2)600	25.7	64.2	10.1	29.1	n/a	n/a	0.3	n/a	n/a	n/a
CB500	n/a	n/a	n/a	62.9 ^c	n/a	n/a	0.5 ^c	n/a	n/a	n/a

^a VM: Volatile Matter; ^b FC: Fixed Carbon; ^c Analyzed by a Costech ECS 4010 elemental analyzer (Costech, USA) in this manuscript; ^d n/a: not available.

Extraction of Biochar-DOC

Chemicals of analytical grade and deionized (DI) water (Milli-Q water system, Millipore) were used in all experiments. The dissolved organic carbon (DOC) was extracted with three extraction agents respectively, including DI water, 0.1 M hydrochloric acid (HCl, Merck KGaA), and 0.1 M sodium hydroxide (NaOH, J.T. Baker). The DOC extracted by DI water, 0.1 M HCl solution, and 0.1 M NaOH solution was denoted as water-extractable DOC (WEOC), acid-extractable DOC (AEOC), and base-extractable DOC (BEOC), respectively. Briefly, 100 mg of the biochars were first mixed with 10 mL of each extraction agent in polypropylene centrifuge tubes. The tubes were tightly closed, sealed with parafilm, and then shaken on an end-over-end shaker (Glas-Col, USA) at 30 rpm for 7 days at room temperature (23 ± 1 °C). The tubes were wrapped with aluminum foil to prevent light exposure. Afterwards the suspensions in the tubes were vacuum-filtered through a 0.45- μ m mixed cellulose esters membrane (Millipore, USA) that was pre-washed with 50 mL DI water. Since the 0.45- μ m filtrates still contained some nano- or colloidal-sized biochar particles, they were further centrifuged at $10,000 \times g$ for 10 min to minimize the amount of colloidal biochar particles, and the supernatant were then carefully collected. The colloidal biochar particles remained in the supernatant, if there was any, should be less than 80 nm, estimated by the Stokes' law (assuming 1.96 g cm^{-3} as biochar particle density¹¹⁹). The final extracts that passed through a 0.45- μ m filter and remained in the supernatant after the centrifugation at $10,000 \times g$ for 10 min (size limit of 80 nm) are operationally defined as DOC in this study. Thus, the biochar-DOC includes the truly dissolved fraction and the nanoparticle fraction, which represent the most mobile and chemically/biologically reactive components of biochars. The final pH of WEOC solutions of 46 biochars was 8.3 ± 0.5 , ranging from 7.2 to 9.5. The final pH of AEOC and BEOC solutions were not determined, but could be estimated to be

about a pH of 1 and 13, respectively, based on our preliminary test. The collected DOC samples were stored in the dark in a refrigerator until use. In addition, biochar-free blank experiments were also conducted using the same protocol and used for background correction in total organic C (TOC) and UV-vis spectroscopy analyses. The batch DOC extraction experiments were conducted in duplicate.

Fractionation of Biochar-DOC

One aliquot of each WEOC and BEOC samples was further fractionated into an acid-soluble (AS) fraction and an acid-precipitated (AP) fraction by acidification. After acidification, most high-molecular-weight organic compounds rich in oxygenic functional groups should theoretically be protonated and precipitated, which allowed for separating biochar-DOC into the AS and AP fractions. First, 2 mL of the WEOC or BEOC sample was acidified to about a pH of 1 by adding 35 or 70 μL of 6 M HCl, respectively, and then allowed to stand in dark for 16 h. The acidified WEOC and BEOC samples were then centrifuged at $10,000 \times g$ for 10 min to obtain the dark-brown precipitates of the AP fraction and the light-yellow supernatant of the AS fraction. After carefully withdrawing the AS fraction (i.e., the supernatant), the AP fraction (i.e., the pellets) was re-dissolved with 2 mL of 0.1 M NaOH and then collected for TOC and UV-vis analyses. The AEOC sample was originally extracted by 0.1 M HCl and was thus assumed to be 100% of the AS fraction. Additionally, the WEOC and BEOC samples free of AP fraction were verified by no change of the UV-vis spectra before and after acidification, and were operationally assumed to contain 100% of the AS fraction.

TOC and UV-vis Analyses of Biochar-DOC

Prior to the TOC and UV-vis analyses, all the DOC samples were diluted 10-fold with DI water to obtain enough sample volume for TOC analysis, and additional 5-fold dilution (total of

50-fold) were made for some samples of BEOC, the AS fraction, and the AP fraction that still had concentrations too high to perform a reliable UV-vis analysis. The DOC concentrations were measured by a Shimadzu TOC-V_{CPN} TOC analyzer (Shimadzu, Japan) after subtracting the inorganic carbon from the total carbon. The DOC concentrations of each sample were further corrected by the background concentrations in the blank samples (i.e., 0.95 to 1.04 mg-C L⁻¹). The UV-vis absorbance spectra were acquired between 200 to 800 nm with a Varian Cary 50 Bio UV-visible spectrophotometer (Varian, USA) in a 1-cm quartz cuvette with DI water as the reference blank. There was no further correction of the UV-vis absorbance spectra since the blank samples showed a negligible UV-vis absorbance above a wavelength of 230 nm. For the UV-vis analysis, there was severe matrix interference for AEOC samples in 11 biochars with high ash content (but not for WEOC and BEOC), presumably due to the dissolution of ash. The UV-vis results of these samples were thus excluded. The spectral absorption ratio of 254 to 365 nm (E_2/E_3 ratio) and spectral slope coefficient between 275 and 295 nm ($S_{275-295}$) were further used to characterize the aromaticity and M_w of DOC. The E_2/E_3 ratio was calculated as the ratio of decadic absorption coefficient (a , cm⁻¹) at 254 nm and 365 nm. The a was calculated by $a = A/l$, where A is the UV-vis absorbance and l is the path length of 1 cm. The spectral slope coefficients between 275–295 nm ($S_{275-295}$) were determined by the slope of natural logarithm of Napierian absorption coefficient against wavelength of 275 to 295 nm.¹²⁰ The Napierian absorption coefficient was calculated by $2.303 \times A/l$.

Solid-state ¹³C NMR Analyses

Advanced quantitative ¹³C multiple cross polarization/magic angle spinning (multiCP/MAS) and multiCP/MAS with dipolar dephasing (multiCP/MAS/DD) solid-state NMR techniques were used to further investigate the chemical compositions of DOC and the alteration

in biochar compositions after water and base extraction treatments. Five selected biochars and their extracted DOC samples were prepared for the solid-state ^{13}C nuclear magnetic resonance (NMR) analysis. These biochars included three slow-pyrolysis biochars (BM300, BM600, and DDM500) and two fast-pyrolysis biochars (SB500 and SG500). BM300, DDM500, SB500 and SG500 were chosen to represent the biochars with a high DOC concentration. As a comparison, BM600 was selected to represent the biochar with a low DOC concentration. However, we were unable to collect the NMR spectrum for the DOC samples of BM600 because of its low extractable DOC concentration. For the same reason, we did not conduct the NMR analysis for all other samples because of the difficulty to collect enough amount of DOC from our limited amount of biochar samples.

The batch extractions were conducted similarly as described above, but at a higher biochar-water ratio in order to collect enough DOC samples for the NMR analysis. Briefly, one gram of the biochars were mixed with 20 mL of DI water or 0.1 M NaOH and then shaken on the rotary shaker at 30 rpm for 7 days at room temperature in dark. The extraction with 0.1 M HCl was not performed due to the low extractable DOC insufficient for the NMR analysis. The suspensions were then centrifuged at $10,000 \times g$ for 10 min and carefully separated to the extracted DOC (i.e., the supernatant) and the treated biochars (i.e., the pellets) for further treatment. The biochar precipitates were re-dispersed with 50 mL DI water and re-centrifuged for five times to remove excess salt for reducing sample conductivity, and then freeze-dried. The DOC extracts were vacuum-filtered through a 0.45- μm membrane and centrifuged at $10,000 \times g$ for 10 min to removal any remaining colloidal biochar particles. The filtered and centrifuged DOC supernatants were directly freeze-dried. However, near all collected WEOC and BEOC samples were sticky tar-like substances unsuitable for the NMR analysis. The NMR spectrum was only acquired for the BEOC

sample of SB500 because it was the least sticky and more powder-like sample. The phenomenal of sticky freeze-dried DOC samples was also observed by Smith et al.,⁵⁵ suggesting that the stickiness resulted from the presence of some bio-oil-like substances. Therefore, another batch extraction for BM300, DDM500, SB500 and SG500 were conducted by the same protocol, and additional dialysis treatment was included. The filtered and centrifuged DOC supernatants were washed via dialysis (MWCO 100-500 Da, Spectrum Labs, USA) against DI water in dark for two days, and the DI water was replaced at 2, 4, 18, and 24 hr. We noted that the DOC compounds with molecular weight below 500 Da would be washed out during dialysis. Afterward the DOC samples were freeze-dried. The post-dialysis freeze-dried samples were powder-like substances, but only enough amount of BEOC samples were collected for the NMR analysis. The raw, water-extracted and base-extracted biochars, base-extractable DOC, and dialyzed base-extractable DOC were denoted as biochar-Raw, biochar-DI, biochar-NaOH, BEOC, and dBEOC, respectively. The prepared biochar and DOC samples were then analyzed by ^{13}C multiCP/MAS and multiCP/MAS/DD techniques.^{121, 122}

Quantitative ^{13}C multiCP/MAS and multiCP/MAS/DD NMR spectra were acquired on a Bruker Avance III 400 spectrometer (Bruker, USA), equipped with a 4-mm double-resonance probe head, at a ^{13}C frequency of 100 MHz, a spinning frequency of 14 kHz, and a 90° pulse length of 4 μs . Chemical shifts were calibrated to tetramethylsilane. The number of scans for NMR spectra was 1024. Nonprotonated and mobile carbon fractions of multiCP/MAS spectra were determined by its corresponding multiCP/MAS/DD spectra with a dipolar dephasing time of 68 μs . The NMR data processing and functional groups quantitation were performed using the TopSpin software (version 3.5pl5). The ^{13}C multiCP/MAS NMR spectra included all carbon (C) signals and could be divided into following assigned regions:¹²³⁻¹²⁵ 0–50 ppm to nonpolar alkyl C;

50–65 ppm to O/N-alkyl C; 65–95 ppm to O-alkyl C; 95–145 ppm to aromatic C–C/C–H; 145–165 ppm to aromatic C–O; 165–190 ppm to carboxyl/amide C (COO/N–C=O); and 190–220 ppm to carbonyl C (C=O) in ketone/aldehyde. The multiCP/MAS/DD spectra further identified the signals of mobile and nonprotonated carbon moieties, such as CCH₃, $-(CH_2)_n-$, OCH₃, nonprotonated aromatic C–C, aromatic C–O, COO/N–C=O, and ketone. We noted that the proportion of anomeric C overlapped with the right shoulder of aromatic C in the 95–110 ppm range, and thus could not be determined in this study. Consequently, the proportion of assigned aromatic C was slightly overestimated by about 1 to 3%, assuming a 1:1 ratio of anomeric and aromatic C in this overlapped range.¹²⁶ Because most DOC-enriched biochars and their extractable DOC samples have relatively large fraction of alkyl C and carboxyl C, the estimation of average aromatic cluster sizes based on the fraction of aromatic edge carbons was not reliable. Alternatively, the ratio of nonprotonated aromatic C fraction to total aromatic C fraction (F_{aN}/F_a) was used as a proxy of the condensation of aromatic rings. The F_{aN}/F_a ratio has been suggested to increase with increasing average cluster size of fused aromatic rings.^{122, 124, 127}

Estimation of Biochar-DOC Concentrations

The decadic absorption coefficient at 254 nm (a_{254}) was linearly correlated with the concentrations of AEOC, WEOC, BEOC, BEOC-AS, and BEOC-AP to generated linear equations. In addition, based on a_{254} , DOC concentrations, and E_2/E_3 ratio of BEOC-AS and BEOC-AP, we further developed a more universal method to first predict the proportions of AS and AP fractions by measuring E_2/E_3 ratios and then to estimate DOC concentrations by a_{254} . Detailed derivation of the governing equations is described in the Results and Discussion section.

RESULTS AND DISCUSSION

DOC Concentrations in Biochars

DOC was a significant fraction of the biochars (Figure 3.1a and Table 3.3), and was up to 5.7%, 6.6%, and 23% of total C in the biochars for the AEOC, WEOC, and BEOC, respectively (Table 3.3). The biochar-DOC concentrations generally increased in the order of AEOC (0.2 to 23 mg-C/g-biochar) < WEOC (0.5 to 40 mg-C/g-biochar) < BEOC (2.3 to 139 mg-C/g-biochar). In addition, the biochars from fast pyrolysis (FP) and slow pyrolysis (SP) at lower temperatures of 300–400 °C (SP300–400) generally had higher DOC concentrations than the biochars from slow pyrolysis at higher temperatures of 450–600 °C (SP450–600), except for DDM500 (Figure 3.1a and Table 3.3). For most biochars from FP and SP300–400, the AEOC solutions had clear to light-yellow colors, the WEOC solutions had light-yellow to light-brown colors, and the BEOC solutions had brown to dark-brown colors (Figure 3.1b). However, for most biochars from SP450–600, the AEOC and WEOC solutions were generally colorless, and only the BEOC solutions had light-yellow colors. The visual appearances of the extracted DOC solutions generally agreed with the DOC measurements. The BEOC solutions had higher DOC concentrations and darker colors than those of AEOC and WEOC, presumably because more light-absorbing organic compounds were extracted under strong alkaline conditions due to the dissociation of surface functional groups (e.g., carboxyl and phenyl groups) or the cleavage of ester bonds, which promotes the solubility of larger molecules.^{106, 111} Conversely, strong acidic conditions would inhibit the extraction of DOC because most surface functional groups in the biochars would remain non-ionized,¹¹¹ resulting in lower AEOC concentrations. While most WEOC samples had deeper color than that of AEOC, for some biochars the WEOC concentrations were similar or even lower than the AEOC concentrations, especially for the biochars slowly-pyrolyzed at 300 °C (Figure 3.1a and Table 3.3).

This inconsistency was presumably due to acidic hydrolysis of the labile C fraction in the biochars (i.e., pyrolysis intermediates and partly pyrolyzed biomass residues) into weak light-absorbing small organic compounds (e.g., monosaccharides).¹²⁸⁻¹³⁰ These results implied that the amount and chemical composition of AEOC, WEOC, and BEOC were different, which were further corroborated by the DOC fractionation and UV-vis analysis below.

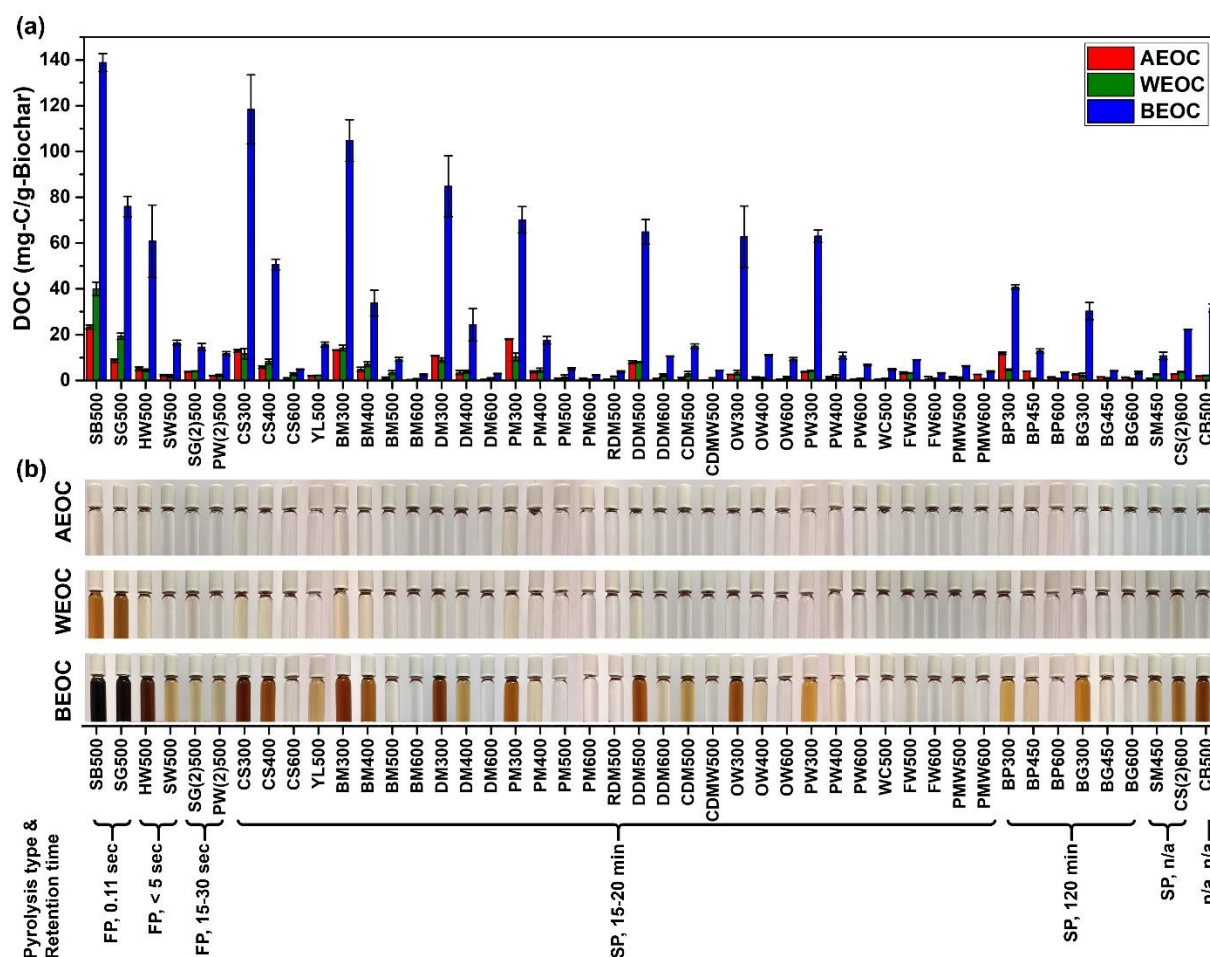


Figure 3.1. Dissolved organic carbon (DOC) concentrations (a) and illustrative solution colors (b) of acid-extractable DOC (AEOC), water-extractable DOC (WEOC), and base-extractable DOC (BEOC) from 46 tested biochars (FP: fast pyrolysis; SP: slow pyrolysis; n/a: not available).

Table 3.3 Extractable DOC concentration of biochar samples.

Biochar ID	Extractable DOC concentration in solution (mg-C/L)			Extractable DOC, total mass based (mg-C/g-Biochar)			Extractable DOC, total carbon based (g-C/g-Biochar-C, %)		
	AEOC	WEOC	BEOC	AEOC	WEOC	BEOC	AEOC	WEOC	BEOC
SB500	252.6	419.2	1501.9	23.4	40.0	138.9	3.9	6.6	23.0
SG500	95.7	210.8	841.8	8.6	19.3	76.0	2.0	4.4	17.2
HW500	52.1	48.9	617.7	5.1	4.4	60.8	0.7	0.6	8.3
SW500	23.4	20.4	173.1	2.2	1.9	16.5	0.3	0.2	2.0
SG(2)500	38.4	44.7	147.8	3.8	4.1	14.6	0.5	0.6	2.1
PW(2)500	22.3	24.8	127.8	2.1	2.3	11.8	0.6	0.7	3.7
CS300	137.3	123.7	1253.8	12.9	11.6	118.4	2.2	1.9	19.8
CS400	60.4	89.0	523.5	5.8	8.3	50.6	0.9	1.3	7.8
CS600	5.8	30.1	50.7	0.6	2.8	4.8	0.1	0.4	0.7
YL500	21.3	24.7	166.5	2.0	2.3	15.7	0.3	0.4	2.6
BM300	138.0	142.8	1087.5	13.3	14.2	104.7	2.2	2.3	17.3
BM400	50.8	77.5	357.8	4.8	7.1	33.8	0.7	1.0	4.9
BM500	10.8	37.2	97.4	1.0	3.5	9.2	0.1	0.5	1.2
BM600	2.6	7.2	24.7	0.3	0.7	2.4	0.0	0.1	0.3
DM300	113.0	96.9	889.4	10.7	8.9	84.8	1.7	1.4	13.8
DM400	35.3	40.0	249.9	3.4	3.8	24.3	0.5	0.6	3.6
DM600	2.1	9.3	31.2	0.2	0.9	2.9	0.0	0.1	0.4
PM300	186.9	112.2	727.1	18.0	10.4	70.1	5.7	3.3	22.0
PM400	39.4	48.0	183.1	3.8	4.5	17.6	1.2	1.4	5.5
PM500	6.4	17.6	53.6	0.6	1.6	5.0	0.2	0.6	1.8
PM600	5.5	6.6	24.3	0.5	0.6	2.3	0.2	0.2	0.8
RDM500	4.1	17.9	39.1	0.4	1.7	3.7	0.1	0.3	0.7
DDM500	82.6	84.4	668.9	8.0	8.0	64.9	1.3	1.3	10.9
DDM600	4.8	24.5	112.6	0.5	2.2	10.6	0.1	0.3	1.7
CDM500	7.8	29.8	158.3	0.7	2.9	15.0	0.2	0.8	4.0
CDMW500	1.9	12.5	46.7	0.2	1.1	4.4	0.0	0.2	0.6
OW300	27.0	36.5	654.2	2.6	3.5	62.7	0.4	0.5	9.8
OW400	10.5	12.0	123.4	0.9	1.1	11.1	0.1	0.1	1.4
OW600	3.3	13.1	99.2	0.3	1.2	9.3	0.0	0.1	1.1
PW300	39.3	44.9	662.0	3.7	4.2	63.0	0.6	0.6	9.4
PW400	12.9	16.7	111.7	1.2	1.5	10.8	0.2	0.2	1.4
PW600	4.2	10.2	76.2	0.4	0.9	6.8	0.0	0.1	0.7
WC500	3.4	5.7	48.9	0.3	0.5	4.8	0.0	0.1	0.6
FW500	35.2	34.0	95.7	3.3	3.2	9.0	0.8	0.8	2.1
FW600	8.9	10.2	33.9	0.8	0.9	3.2	0.3	0.3	1.0
PMW500	11.0	12.4	63.8	1.1	1.1	6.3	0.6	0.6	3.3
PMW600	27.1	7.2	39.3	2.6	0.7	3.8	1.4	0.4	2.0
BP300	130.8	50.1	451.5	11.9	4.7	40.9	2.0	0.8	6.9
BP450	43.6	10.5	138.6	4.0	1.0	12.8	0.5	0.1	1.7
BP600	14.1	9.7	38.4	1.3	0.9	3.6	0.2	0.1	0.5
BG300	25.0	23.2	299.3	2.5	2.3	30.2	0.4	0.3	4.3
BG450	16.1	11.5	43.9	1.5	1.1	4.2	0.2	0.1	0.5
BG600	13.9	8.0	35.0	1.3	0.8	3.3	0.2	0.1	0.4
SM450	4.4	27.1	113.1	0.4	2.6	10.7	0.1	0.5	1.9
CS(2)600	30.4	37.6	245.5	2.8	3.7	22.3	0.9	1.3	7.7
CB500	21.3	23.3	345.7	1.9	2.2	31.6	0.3	0.3	5.0

Fractionation of Biochar-DOC

The acidification of the initially dark-colored BEOC samples from 27 tested biochars resulted in light-yellow colored AS fraction (34.3–79.5%) and dark-brown colored AP fraction (20.5–65.7%) (Figure 3.2). The AP fraction in the light-colored BEOC samples of the other 19 biochars, if any, was too low to form precipitates, which was verified by the UV-vis spectra before and after the acidification. Thus, the AP fraction of these biochars was operationally assumed as 0%. Of the WEOCs, only SB500 and SG500 had observable AP fractions (14.5% and 45.4%, respectively), whereas the AP fraction in the WEOC of other biochars was again too low to be detected and operationally defined as 0%. Clearly, biochar-DOC could be considered as a mixture of the AS and AP fractions that varied with the extraction methods, pyrolysis conditions, and feedstocks, as shown in Figure 3.2 and 3.3. More AP components could be extracted by 0.1 M NaOH than by DI water or 0.1 M HCl (Figure 3.3a), likely due to enhanced ionization of oxygenic functional groups in the biochars at higher pH, which in turn increased the solubility and extraction of the AP fraction. The AP fraction generally decreased with increasing pyrolysis temperature and residence time (Figure 3.3b). As the pyrolysis temperature and residence time increased, more biopolymers and pyrolysis intermediates were transformed into the condensed aromatic structures or cracked into low M_w compounds and syngas. Therefore, less AP fraction characterized by larger M_w (see next section) could be extracted from the high-temperature biochars. Finally, the DOC from herbaceous and manure biochars generally contained more AP fractions than that from woody biochars (Figure 3.3c), presumably due to greater abundance of more pyrolyzable cellulose and hemicellulose in their feedstocks.

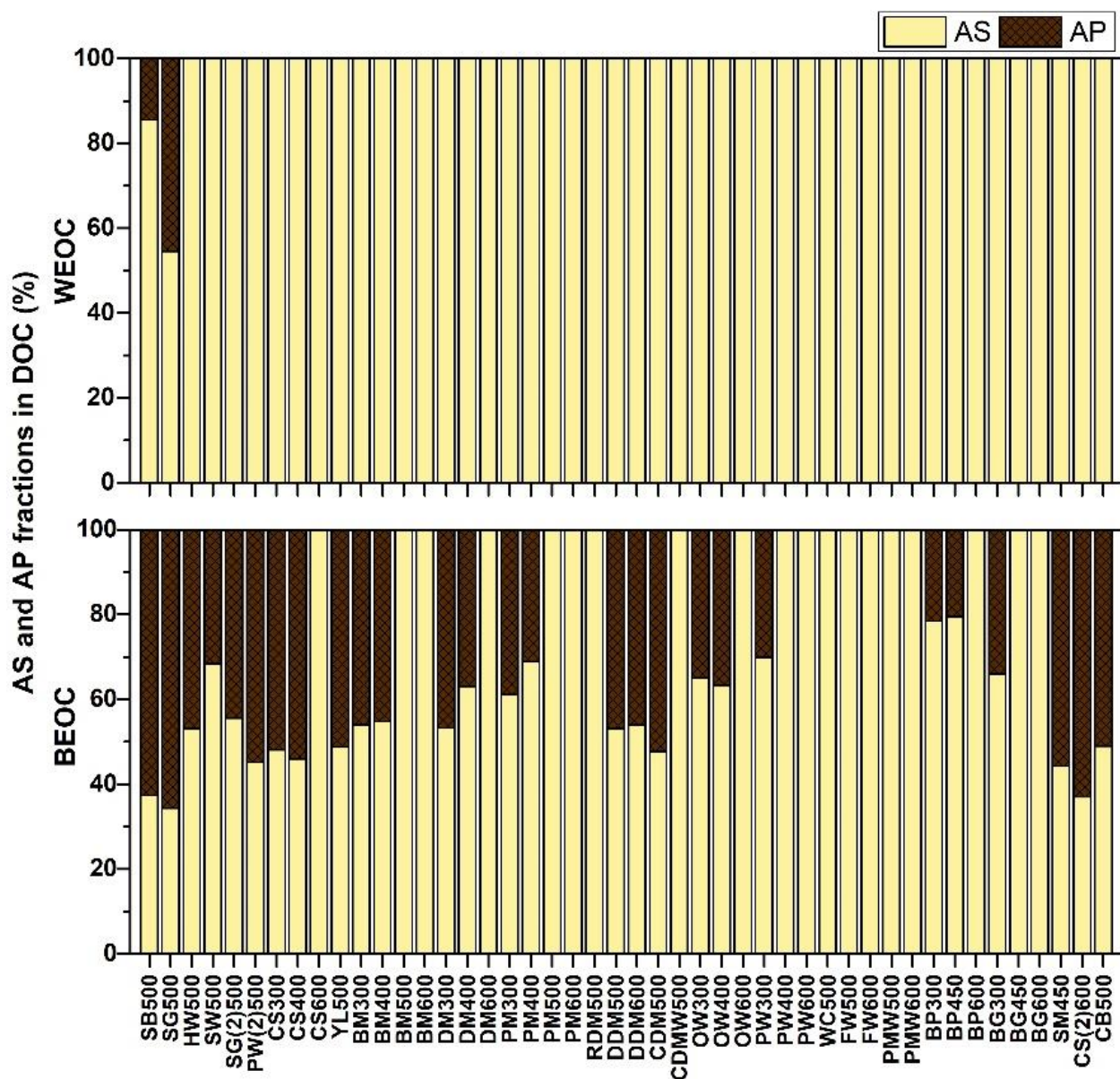


Figure 3.2. Fractionation of WEOC and BEOC extracted from biochars.

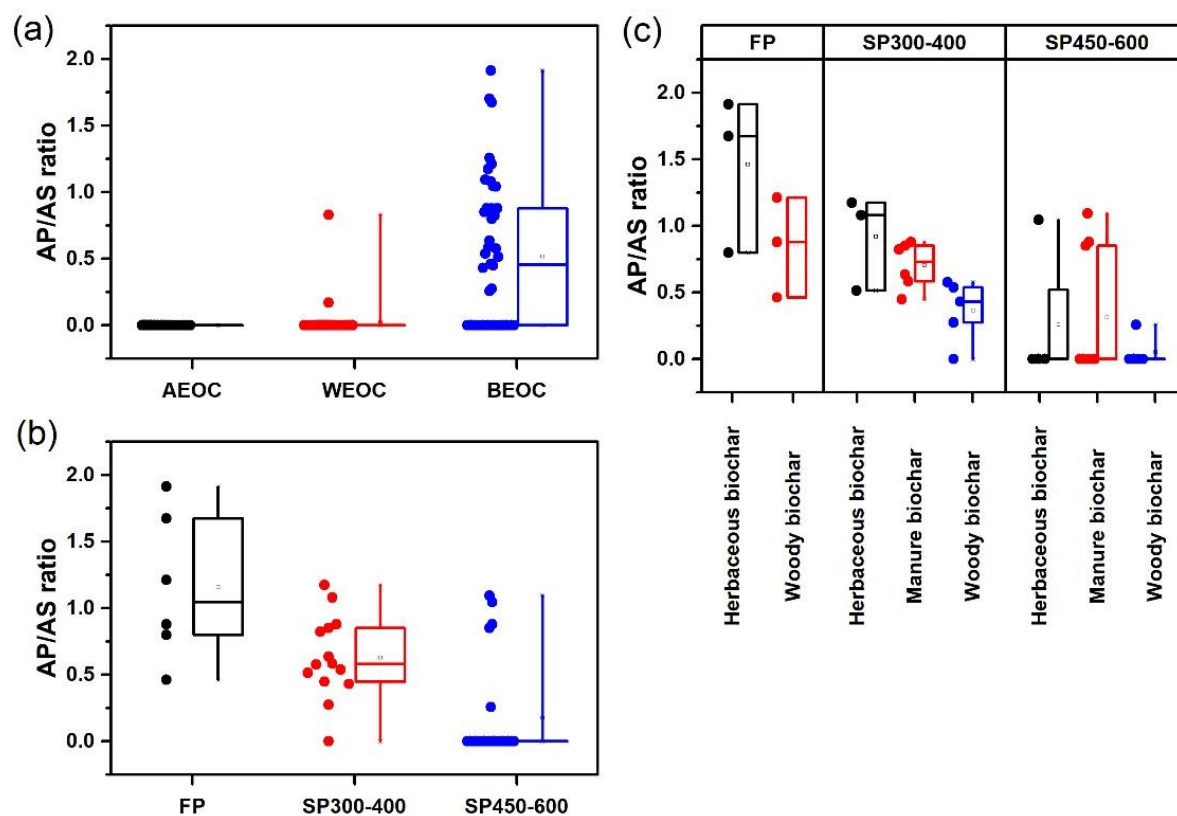


Figure 3.3. Effects of the extraction methods (a), pyrolysis conditions (b), and feedstocks(c) on the acid-soluble (AS) and acid-precipitated (AP) fraction ratio of biochar-DOC. (AEOC: acid-extractable DOC; WEOC: water-extractable DOC; BEOC: base-extractable DOC; FP: fast pyrolysis at 500 °C; SP300-400: slow pyrolysis at 300 to 400 °C; SP450-600: slow pyrolysis at 450 to 600 °C).

UV-vis Absorption Spectra Characterization

The UV-vis absorption spectra of biochar-DOC samples were generally broad and featureless (Figure 3.4), presumably due to the overlapping absorption bands of the multiple chromophores.^{54, 131, 132} The mean E_2/E_3 ratios were 11.3 ± 1.9 , 6.55 ± 1.91 , 4.92 ± 2.00 , 7.47 ± 1.02 , and 2.48 ± 0.25 , and the mean $S_{275-295}$ values were 0.0305 ± 0.0106 , 0.0203 ± 0.0079 , 0.0143 ± 0.0045 , 0.0182 ± 0.0025 , and 0.0078 ± 0.0011 for the AEOC, WEOC, BEOC, AS fraction of BEOC (BEOC-AS), and AP fraction of BEOC (BEOC-AP), respectively (Figure 3.5 and Table 3.4). It is known that the E_2/E_3 ratio is inversely proportional to the aromaticity and M_w of DOC, and the $S_{275-295}$ values has an inverse relationship with M_w of DOC.^{120, 132, 133} Therefore, the aromaticity and M_w decreased in the order of BEOC > WEOC > AEOC. The WEOC and BEOC of the biochars from FP and SP300–400 generally had lower E_2/E_3 ratios and $S_{275-295}$ values (or higher aromaticity and M_w) than the biochars from SP450–600. The AEOC had very low aromaticity and M_w , regardless of the biochar types. The lower E_2/E_3 ratios and $S_{275-295}$ values of BEOC-AP indicated higher aromaticity and M_w than those of BEOC-AS (Figure 3.5). Therefore, the DOCs with greater AP fractions tended to have higher aromaticity and mean M_w , e.g., the BEOC extracted from the biochars produced by FP and SP300–400. Although all AEOC, nearly all of the WEOC (44 of 46 biochars), and the BEOC-AS were composed of 100% AS fraction (Figure 3.5), the E_2/E_3 ratios and $S_{275-295}$ values of the AEOC were significantly larger than those of WEOC and BEOC-AS ($p < 0.05$, one-way ANOVA with post-hoc Tukey test), presumably again because of hydrolysis under acidic conditions (thus generation of smaller molecules). Interestingly, the relatively small variation in the E_2/E_3 ratios and $S_{275-295}$ values of the BEOC-AS and BEOC-AP suggested that aromaticity and M_w could be similar for the AS or AP fraction from diverse biochars. It is expected that the AS fraction with relatively higher water solubility, and

lower aromaticity and M_w may be more susceptible to loss through abiotic and biotic degradation, and off-site transport than the AP fraction, suggesting their differential contribution to the biochar stability.

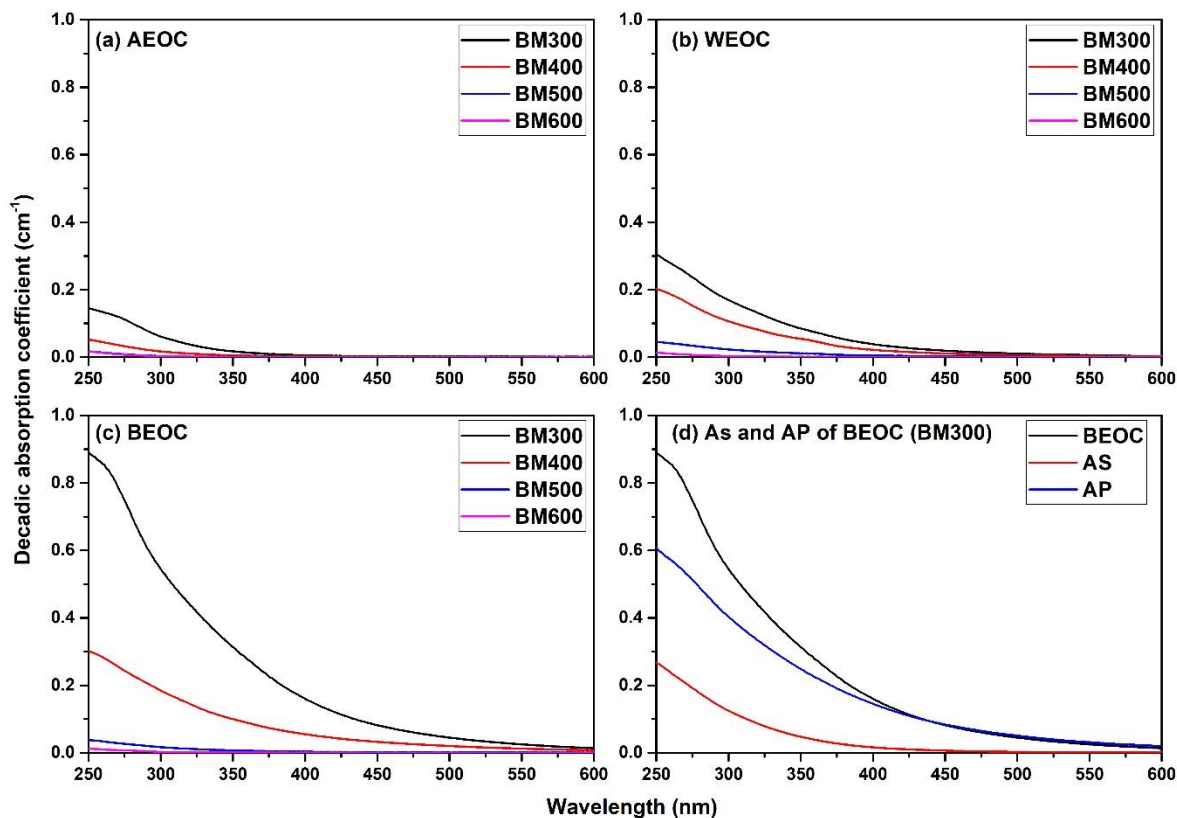


Figure 3.4. UV-vis spectra of DOC solutions (bull manure biochar as examples): (a) AEOC, (b) WEOC, (c) BEOC, and (d) the As and AP fractions of BEOC (BM300).

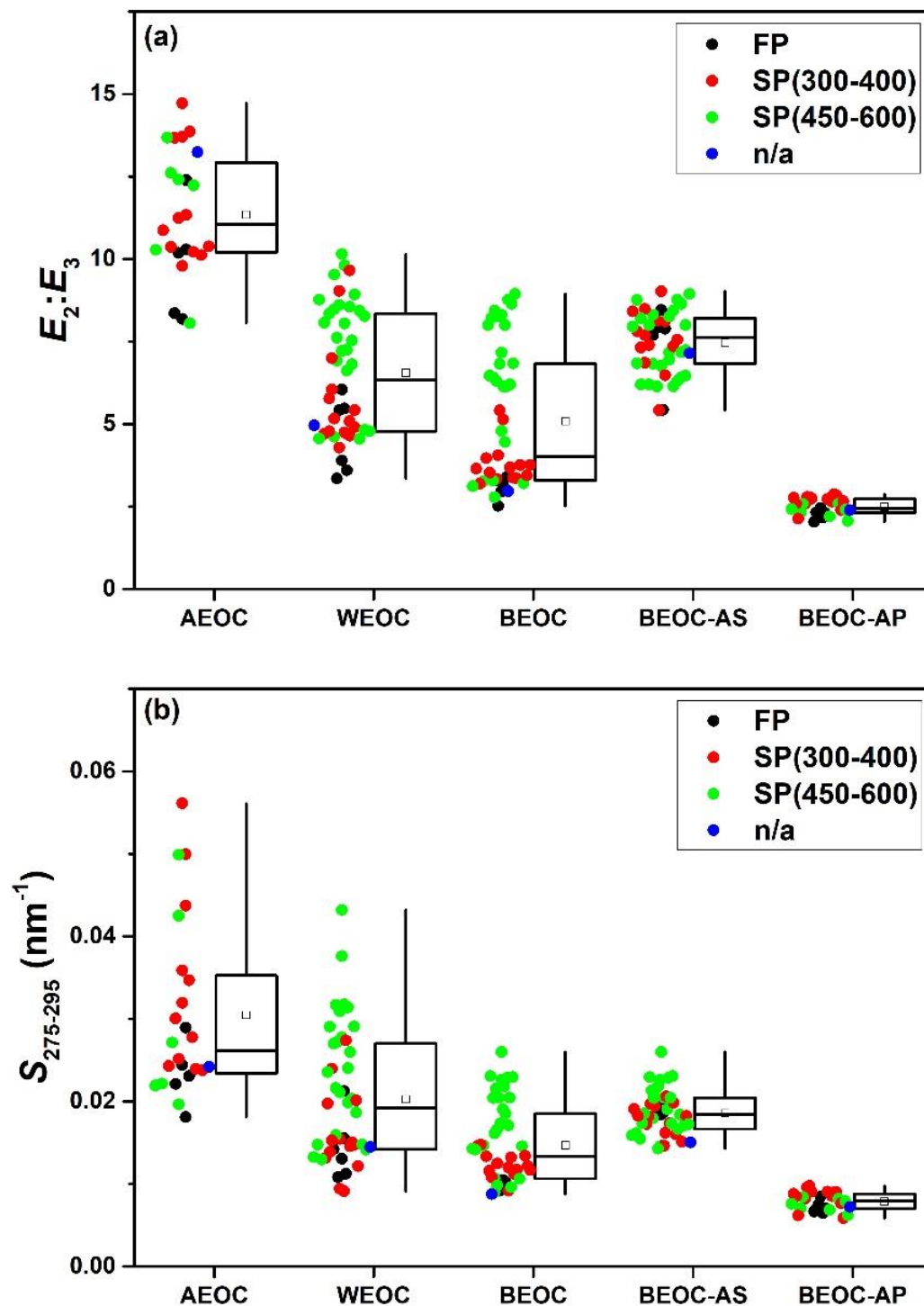


Figure 3.5. Box plots of UV-vis spectroscopic analyses of DOC in biochars: (a) $E_2:E_3$ ratio and (b) $S_{275-295}$. The box plots showed the first quartile, median, mean, and third quartile of the samples, and the whiskers showed the range of minimum and maximum. The symbols on the left side of box plots showed the distribution of sample values. Detailed data are provided in Table 3.4. (FP: fast pyrolysis; SP: slow pyrolysis; n/a: not available)

Table 3.4. UV-vis spectral parameters of AEOC, WEOC, BEOC, BEOC-AS, and BEOC-AP.

Biochar ID	AEOC		WEOC		BEOC		BEOC-AS		BEOC-AP	
	$E_2:E_3$	$S_{275-295}$	$E_2:E_3$	$S_{275-295}$	$E_2:E_3$	$S_{275-295}$	$E_2:E_3$	$S_{275-295}$	$E_2:E_3$	$S_{275-295}$
SB500	10.3	0.0181	3.90	0.0130	3.15	0.0104	7.93	0.0184	2.45	0.0085
SG500	12.4	0.0244	3.35	0.0108	2.97	0.0096	7.99	0.0185	2.33	0.0075
HW500	ud ^a	ud	3.60	0.0112	2.52	0.0092	5.43	0.0146	2.16	0.0065
SW500	10.2	0.0289	5.47	0.0212	3.26	0.0103	7.89	0.0186	2.32	0.0070
SG(2)500	8.18	0.0221	5.43	0.0142	3.39	0.0102	8.45	0.0203	2.31	0.0070
PW(2)500	8.36	0.0231	6.05	0.0155	2.98	0.0097	7.70	0.0191	2.04	0.0066
CS300	10.2	0.0243	4.75	0.0146	3.33	0.0125	8.13	0.0162	2.73	0.0091
CS400	9.79	0.0239	5.09	0.0155	3.68	0.0120	8.11	0.0194	2.74	0.0090
CS600	ud	ud	8.05	0.0211	7.17	0.0190	7.17	0.0190	n/a ^c	n/a
YL500	8.06	0.0221	6.92	0.0199	3.29	0.0107	6.76	0.0180	2.20	0.0069
BM300	11.3	0.0238	4.29	0.0138	3.37	0.0132	7.39	0.0173	2.78	0.0098
BM400	11.2	0.0251	4.64	0.0147	3.53	0.0108	7.36	0.0197	2.64	0.0085
BM500	bd ^b	bd	4.62	0.0159	6.15	0.0173	6.15	0.0173	n/a	n/a
BM600	bd	bd	8.61	0.0278	8.31	0.0226	8.31	0.0226	n/a	n/a
DM300	13.7	0.0278	5.17	0.0150	3.35	0.0112	7.70	0.0182	2.79	0.0096
DM400	13.7	0.0319	4.90	0.0153	3.96	0.0116	7.56	0.0198	2.88	0.0089
DM600	bd	bd	10.2	0.0240	8.26	0.0205	8.26	0.0205	n/a	n/a
PM300	ud	ud	5.43	0.0132	3.76	0.0117	7.32	0.0172	2.58	0.0082
PM400	ud	ud	4.78	0.0122	5.13	0.0133	6.48	0.0160	2.84	0.0090
PM500	bd	bd	8.55	0.0216	8.00	0.0185	8.00	0.0185	n/a	n/a
PM600	bd	bd	9.81	0.0317	8.44	0.0218	8.44	0.0218	n/a	n/a
RDM500	ud	ud	8.48	0.0203	6.83	0.0167	6.83	0.0167	n/a	n/a
DDM500	12.4	0.0271	4.55	0.0130	3.25	0.0106	7.18	0.0173	2.58	0.0084
DDM600	ud	ud	7.21	0.0187	4.79	0.0147	6.95	0.0184	2.59	0.0082
CDM500	ud	ud	6.61	0.0148	3.21	0.0098	6.20	0.0154	2.31	0.0070
CDMW500	ud	ud	8.92	0.0272	6.14	0.0146	6.14	0.0146	n/a	n/a
OW300	10.4	0.0301	4.70	0.0091	3.19	0.0147	6.86	0.0151	2.39	0.0077
OW400	10.1	0.0499	9.03	0.0094	4.05	0.0134	8.49	0.0206	2.14	0.0062
OW600	bd	bd	8.35	0.0309	8.76	0.0260	8.76	0.0260	n/a	n/a
PW300	13.9	0.0437	6.05	0.0240	3.44	0.0092	9.03	0.0182	2.66	0.0058
PW400	10.9	0.0561	9.66	0.0274	5.42	0.0146	5.42	0.0146	n/a	n/a
PW600	bd	bd	8.43	0.0432	8.21	0.0216	8.21	0.0216	n/a	n/a
WC500	ud	ud	8.07	0.0314	6.30	0.0171	6.30	0.0171	n/a	n/a
FW500	12.2	0.0196	4.82	0.0147	6.20	0.0161	6.20	0.0161	n/a	n/a
FW600	ud	ud	7.61	0.0270	8.64	0.0228	8.64	0.0228	n/a	n/a
PMW500	bd	bd	7.25	0.0317	6.41	0.0204	6.41	0.0204	n/a	n/a
PMW600	bd	bd	9.53	0.0376	6.84	0.0204	6.84	0.0204	n/a	n/a

Table 3.4. (cont'd)

Biochar ID	AEOC		WEOC		BEOC		BEOC-AS		BEOC-AP	
	$E_2:E_3$	$S_{275-295}$	$E_2:E_3$	$S_{275-295}$	$E_2:E_3$	$S_{275-295}$	$E_2:E_3$	$S_{275-295}$	$E_2:E_3$	$S_{275-295}$
BP300	14.7	0.0359	5.78	0.0198	3.65	0.0122	7.81	0.0182	2.58	0.0085
BP450	12.6	0.0499	6.82	0.0260	4.45	0.0141	8.76	0.0213	2.41	0.0079
BP600	bd	bd	8.27	0.0291	8.00	0.0231	8.00	0.0231	n/a	n/a
BG300	10.4	0.0347	7.00	0.0201	3.76	0.0117	8.42	0.0191	2.77	0.0088
BG450	10.3	0.0425	7.54	0.0236	6.47	0.0143	6.47	0.0143	n/a	n/a
BG600	bd	bd	8.77	0.0291	8.95	0.0230	8.95	0.0230	n/a	n/a
SM450	ud	ud	4.56	0.0141	2.78	0.0090	7.24	0.0173	2.06	0.0062
CS(2)600	13.7	0.0219	4.78	0.0132	3.12	0.0096	7.96	0.0159	2.43	0.0076
CB500	13.2	0.0242	4.96	0.0145	2.97	0.0088	7.15	0.0150	2.39	0.0072

^a ud: unable to determine due to matrix interference; ^b bd: a_{365} below the detection limit; ^c n/a: not available.

Advanced Solid-state ^{13}C NMR

Figure 3.6 presents the multiCP/MAS and multiCP/MAS/DD spectra and Table 3.5 summarizes the quantitative composition of functional groups for the biochar and DOC samples. Several recognizable peaks could be observed in the ^{13}C NMR spectra of biochar and DOC samples (Figure 3.6). The peaks at 15, 18, 23, and 25 ppm were assigned to methyl group ($-\text{CH}_3$), the peaks at 30 ppm to poly(methylene) group ($-\text{CH}_2$), and the peaks at 35 and 42 ppm to nitrogen-bonded methylene C ($\text{N}-\text{CH}_2$) and/or quaternary C (C_q) groups. These peaks reflected the contributions of various short- and long-chain alkyl groups in biochar and DOC samples. The peak at 56 ppm was associated with both the OCH_3 group in lignin residues and the NCH group in peptides residues. The peak at 74 ppm (OCH) and the shoulder peaks at 62 ppm (OCH_2), 83 ppm (OCH), and 105 ppm (anomeric C, OCO) were attributed to the presence of cellulose residues or pyrolytic sugar. The strong peak at 129 ppm indicated the dominant presence of aromatic C in both biochar and DOC samples. The shoulder peak of aromatic $\text{C}-\text{O}$ at 148 ppm was associated with the phenolic groups in lignin residues or pyrolytic lignin. The peaks at 172, 174, 177, and 181 ppm were assigned to carboxyl group (COO) bonded to alky C or aromatic C as well as partially associated with amide group ($\text{N}-\text{C}=\text{O}$) in peptide residues. The spectra signals in the region of 190–220 ppm were relatively weak and small, suggesting a low abundance of ketone/aldehyde in both biochar and DOC samples.

The BM300-biochar-Raw sample showed the typical NMR characteristics of a biochar with a low degree of carbonization.^{124, 134} The BM300 biochar-Raw sample exhibited great abundance of alky C, O/N-alkyl C, O-alkyl C, and aromatic C, as well as the clear features of incompletely pyrolyzed biopolymers (i.e., cellulose at 74 and 105 ppm, lignin at 56, 129, and 146 ppm, and peptide at 56 and 174 ppm) (Figure 3.6a). Compared to BM300-biochar-Raw, DDM500-

, SB500-, and SG500-biochar-Raw showed further enrichment of aromatic C, but decreased alkyl C, O/N-alkyl C, and O-alkyl C (Figure 3.6b, c and d), indicating a higher degree of carbonization. The characteristic peaks of cellulose and lignin were still recognizable in the spectra of DDM500, indicating that some cellulose and lignin residues were still preserved in DDM500. Conversely, the characteristic peaks of cellulose and lignin were almost non-recognizable in the spectra of SB500 and SG500, suggesting most O/N-alkyl C and O-alkyl C in the fast-pyrolysis biochars were attributed to pyrolytic sugar. The NMR spectrum of BM600-biochar-Raw showed a single well-defined aromatic C signal at 129 ppm with complete depletion of the biopolymer features (Figure 3.6e), indicating the highest degree of carbonization among these five biochars. On the other hand, the quantitative NMR spectra indicated that the major components in DOC samples were aromatic C, followed by alkyl C and carboxyl/amide C (Figure 3.6m to q). The DOC samples exhibited more abundance of alkyl C and carboxyl/amide C than the biochar samples. These results indicated that the biochars with higher extractable DOC content generally also contained considerable amounts of alkyl C and carboxyl/amide C.

In addition, the observation of biopolymer residues, especially for cellulose, in DDM500 was rare for this high degree of pyrolysis temperature. Typically, the most oxygen-containing functional groups and cellulose features should be eliminated at pyrolysis temperature of 500 °C,^{124, 135, 136} and the NMR spectra would be quite similar to BM600 with one dominant aromatic C peak only. The abundance of functional groups and preservation of biopolymer residues in DDM500 indicated that the thermal conversion of DDM biomass was somehow limited during the pyrolysis. While the exact cause was not clear, the NMR spectra of DDM500 corroborated with its high DOC concentrations.

The relative abundance of functional groups in the biochars was altered by the extraction treatment (Figure 3.6 and Table 3.5). Because higher DOC amounts were extracted with 0.1 M NaOH, the changes were more substantial for biochar-NaOH than for biochar-DI. After DOC extraction, the DDM500 (Figure 3.6d and k), SB500 (Figure 3.6a, f and h), and SG500 (Figure 3.6b and i) each showed decreased proportions of alkyl C (0–50 ppm) and carboxyl/amide C (165–190 ppm), but increased proportions of both nonprotonated aromatic C and total aromatic C (95–165 ppm) (Table 3.5). Specifically, because fused aromatic rings increase in average cluster size with higher F_{aN}/F_a ratio and vice versa,^{122, 124, 127} increased F_{aN}/F_a ratio of the biochars (i.e., from 0.67, 0.53, and 0.53 to 0.72, 0.68, and 0.60 for DDM500, SB500, and SG500 biochars, respectively) after the alkaline extraction suggests increased average cluster size of fused aromatic rings in the residual bulk biochar. Because further aromatic condensation was unlikely to occur during the extraction, the increase of average aromatic cluster size may be attributed to the enrichment of highly condensed aromatic C in the biochars by the DOC release. Conversely, for BM300 (Figure 3.6c, g, and j), the relative proportions of alkyl C, aromatic C, and carboxyl/amide C slightly decreased, and the proportion of O-alkyl C slightly increased after DOC extraction. The characteristic peaks of lignin in BM300 were reduced in intensity at 56 and 146 ppm, together with a decrease of aromatic C signal at 129 ppm. Interestingly, in contrast to the decrease of lignin signals, the characteristic peaks of cellulose were markedly enhanced in intensity at 62, 74, 83, and 105 ppm. This observation was presumably because cellulose residues in the biochars have relatively lower solubility in DI water and 0.1 M NaOH compared with lignin,^{130, 137} and thus these non-extractable cellulose residues would be more enriched after the DOC extraction. Furthermore, the enrichment of nonprotonated aromatic C in the DI- and NaOH-extracted biochar was not observed for BM300, presumably because both biochar and DOC in BM300 were composed of

smaller fused aromatic rings due to the insufficient pyrolysis. Finally, the NMR spectra of BM600 (Figure 3.6e and l) acquired before and after the DOC extraction appeared almost identical due to the low DOC concentration.

For DOC samples, the SB500-BEOC exhibited prominent sharp alkyl C, aromatic C, and carboxyl/amide C (Figure 3.6m). Specifically, the majority of aromatic C in SB500-BEOC was protonated, suggesting that the average cluster size of fused aromatic ring structures of SB500-BEOC is very small (F_{aN}/F_a ratio = 0.30).^{122, 124, 127} Compared with SB500-BEOC, the SB500-dBEOC (Figure 3.6n) showed a substantial decrease of alkyl C and carboxyl/amide C, but further enrichment of its aromatic C, especially for the nonprotonated aromatic C (F_{aN}/F_a ratio = 0.56), suggesting that dissolved organic compounds with relatively large aromatic clusters were concentrated in SB500-dBEOC after the removal of the low- M_w compounds (< 500 Da) via dialysis. In fact, this observation was in line with the UV-vis data in that the biochar-DOC could be separated into the AS fraction with lower aromaticity and M_w and the AP fraction with higher aromaticity and M_w . Furthermore, the freeze-dried BEOC samples were generally sticky tar-like substances, in contrast to the powder-like dBEOC samples, implying the sticky texture was due to the low- M_w compounds that were removed during dialysis. Indeed, the markedly reduced spectral signals of alkyl C at 25, 35, and 42 ppm, aromatic C–H at 129 ppm, and COO/N–C=O at 172 and 181 ppm could be attributed to the removal of low- M_w compounds (Figure 3.6m and n). Based on these observations, the low- M_w compounds were presumably bio-oil like compounds, such as organic acids (e.g., acetic and formic acids), small-ring polycyclic aromatic hydrocarbons (PAHs), and fatty acids or fatty acid esters.^{55, 105, 138} Similar with SB500-dBEOC, BM300-, DDM500-, and SG500-dBEOC also contained greater abundance of alkyl C, aromatic C, and carboxyl/amide C (Figure 3.6n–q). Moreover, clear characteristic peaks of cellulose, lignin, and peptides were

present in BM300- and DDM500-dBEOC samples, but not in SB500- and SG500-dBEOC samples, indicating the biopolymer residues were one of the major DOC sources in the slow-pyrolysis biochars.

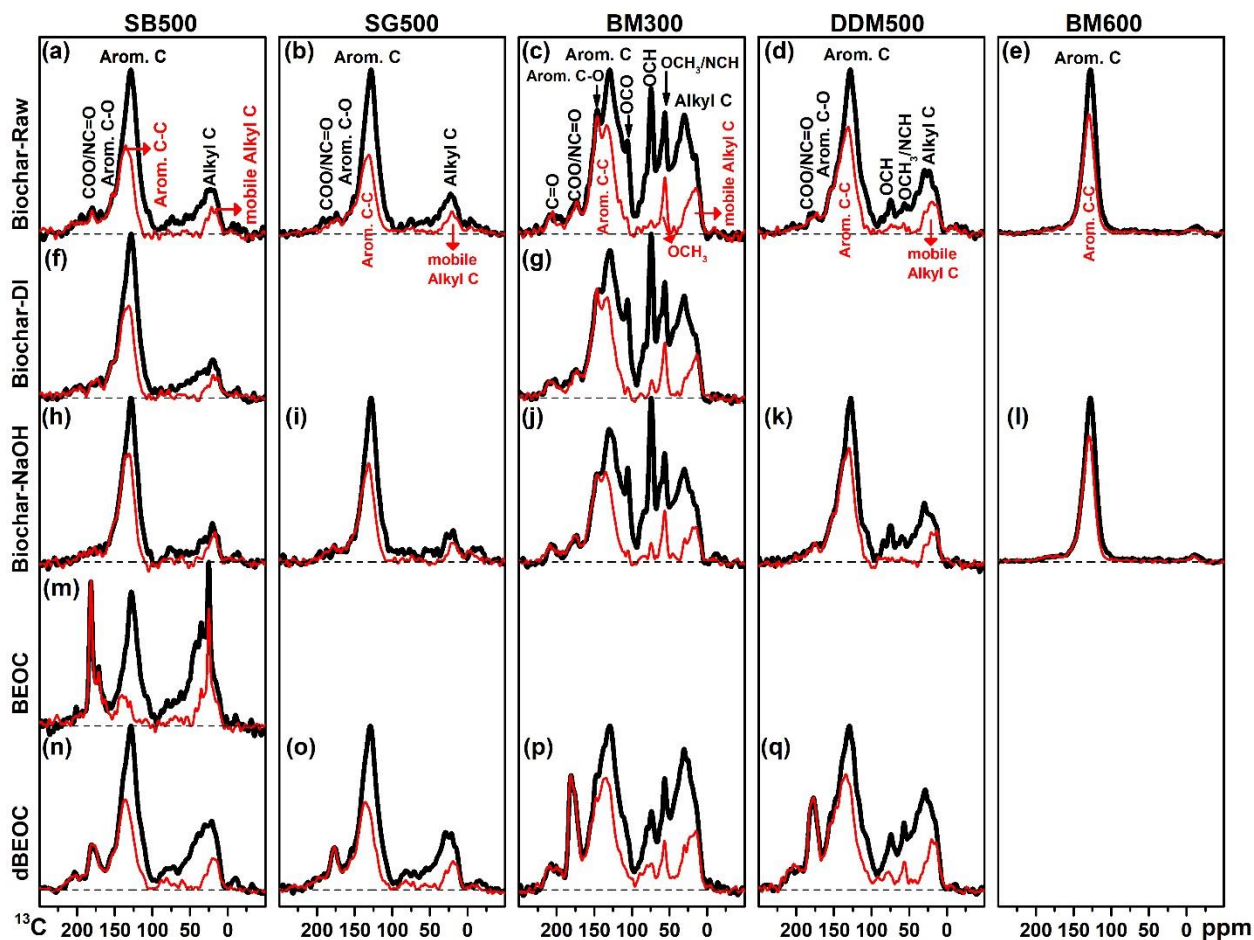


Figure 3.6. Solid-state ^{13}C multiCP/MAS NMR spectra (block black line) and multiCP/MAS after dipolar dephasing (thin red line) of biochar-Raw ((a) to (e)), biochar-DI ((f) and (g)), biochar-NaOH ((h) to (l)), BEOC (m) and dBEOC ((n) to (q)) samples.

Table 3.5. Functional groups of the biochars and DOC estimated by quantitative ^{13}C multiCP/MAS spectra.^a

Biochar ID		ppm										Structural parameters	
		220–190	190–165	165–145	145–95		95–65	65–50		50–0			
					Arom. C-O	Arom. C-C		Arom. C-H	O-alkyl	OCH ₃	NCH ₃		
		C=O	COO/N-C=O									<i>F_a</i> (%)	<i>F_{aN}</i> / <i>F_a</i>
SB500	Biochar-Raw	3.7	6.7	7.0	26.8	30.0	4.1	0.3	2.6	12.9	5.9	63.7	0.53
	Biochar-DI	3.7	5.1	7.4	31.7	28.3	3.4	0.5	2.7	10.7	6.5	67.4	0.58
	Biochar-NaOH	1.7	4.7	7.5	42.0	23.3	3.4	0.1	2.2	6.6	8.4	72.8	0.68
	BEOC	3.0	15.2	5.0	6.0	25.8	5.8	0.9	4.6	20.1	13.7	36.8	0.30
	dBEOC	3.5	8.5	7.7	21.3	23.1	6.1	0.8	3.7	18.3	7.0	52.1	0.56
SG500	Biochar-Raw	2.6	5.6	6.5	29.1	31.6	4.1	0.6	2.3	10.6	7.0	67.3	0.53
	Biochar-NaOH	1.4	4.5	5.6	38.0	29.6	4.9	0.2	2.0	7.6	6.0	73.2	0.60
	dBEOC	3.2	8.5	9.3	24.5	24.7	5.4	0.7	2.7	13.7	7.3	58.5	0.58
BM300	Biochar-Raw	2.0	3.0	8.1	14.7	21.9	13.6	2.5	7.1	21.7	5.3	44.7	0.51
	Biochar-DI	1.4	2.5	7.2	14.9	22.2	15.2	2.9	7.2	21.4	5.1	44.3	0.50
	Biochar-NaOH	1.4	2.6	6.7	14.8	21.4	16.6	2.9	7.5	20.9	5.3	42.9	0.50
	dBEOC	3.5	10.6	9.1	18.4	13.4	9.4	2.8	5.0	18.1	9.7	40.8	0.67
DDM500	Biochar-Raw	2.2	4.5	7.4	32.6	19.4	6.8	1.2	3.3	13.5	9.1	59.4	0.67
	Biochar-NaOH	1.7	4.8	7.7	36.5	17.6	7.1	0.4	3.6	13.2	7.5	61.8	0.72
	dBEOC	3.9	11.5	10.3	22.7	14.1	7.8	1.9	4.1	15.1	8.6	47.1	0.70
BM600	Biochar-Raw	1.3	3.4	4.8	60.6	24.4	2.5	0.4	0.4	1.7	0.6	89.8	0.73
	Biochar-NaOH	1.2	3.4	4.6	62.6	23.0	2.2	0.1	0.7	1.5	0.8	90.1	0.75

^a Arom. C–O: oxygenated aromatic C; Arom. C–C: nonprotonated aromatic C; Arom. C–H: protonated aromatic C; F_a : total aromatic C (165–95 ppm); F_{aN}/F_a : ratio of total nonprotonated aromatic C to total aromatic C, $F_{aN}/F_a = (\text{Arom. C–O} + \text{Arom. C–C})/F_a$

Factors Influencing Biochar-DOC.

Because the WEOC of biochars is considered more environmentally-meaningful,¹⁰⁸ we further compared the WEOC concentrations across a range of pyrolysis conditions and feedstocks. Clearly, the WEOC concentrations in the slow-pyrolysis biochars decreased exponentially with increasing pyrolysis temperature from 300 to 600 °C (Figure 3.7a), likely due to increased degree of carbonization at higher temperature, in agreement with previous studies.^{52, 55} At pyrolysis temperature of 500 and 600 °C, the biochar-DOC concentrations decreased substantially as the pyrolysis residence time increased from 0.11 s to 120 min (Figure 3.7b). During fast pyrolysis, the high heating rate and short residence time facilitate the production of condensable vapors,¹³⁹ which could be easily condensed into biochar pore structure during cyclonic separation, thus forming bio-oil-like substances¹³⁸ that can later be released as DOC. In contrast, during slow pyrolysis, the condensable vapors would have enough time to escape as gases, or the trapped condensable vapors could be further decomposed into syngas or re-polymerized into the biochar structure by the secondary reaction.¹⁰³ Therefore, the fast-pyrolysis biochars had higher DOC concentrations than the slow-pyrolysis biochars at the same pyrolysis temperature. Additionally, woody biochars produced lower DOC concentrations than herbaceous and manure biochars (Figure 3.7c). Compared with the herbaceous and manure feedstocks, woody feedstocks generally have more lignin that is more thermally stable than hemicellulose and cellulose.¹⁴⁰ Thus, they are more favorable for forming biochars instead of bio-oils, resulting in lower DOC concentrations from woody biochars.

Following Zhao et al.,¹⁴¹ standard deviation (SD) and coefficient of variation (CV) of WEOC for the slow-pyrolysis biochars produced in the same facility were calculated (Table 3.6). The temperature-dependent CV of the WEOC ($T\text{-CV} = 0.59$ to 1.0) were generally greater than

the feedstock-dependent CV (F-CV = 0.48 to 0.68) (Table 3.6). Thus, pyrolysis temperature was generally a more important determinant of the DOC concentrations than feedstocks. Additionally, the temperature-dependent SD of WEOC in the herbaceous and manure biochars (T-SD = 4.0 to 5.8 mg-C g⁻¹) were greater than that in the woody biochar (T-SD = 1.3 to 1.8 mg-C g⁻¹), presumably again because of their higher hemicellulose and cellulose content as described above. Furthermore, the SD of the WEOC in the biochars produced from various feedstocks decreased from 4.2 to 0.8 mg-C g⁻¹ when pyrolysis temperature increased from 300 to 600 °C, indicating that the effect of feedstocks diminished at higher temperatures (500 and 600 °C).

Table 3.6. Variation across pyrolysis temperature and feedstock of the WEOC of 20 tested biochars.^a

Feedstock	Pyrolysis temperature (°C)				T-SD	T-CV
	300	400	500	600		
	WEOC (mg-C/g-Biochar)					
CS	11.6	8.27	-	2.76	4.49	0.59
BM	14.2	7.08	3.50	0.69	5.83	0.92
DM	8.89	3.84	-	0.90	4.04	0.89
PM	10.4	4.53	1.61	0.60	4.40	1.03
OW	3.47	1.11	-	1.23	1.33	0.69
PW	4.20	1.46	-	0.89	1.77	0.81
F-SD	4.22	2.89	1.34	0.80		
F-CV	0.48	0.66	0.52	0.68		

^a T-SD: temperature-dependent standard deviation; T-CV: temperature-dependent coefficient of variation; F-SD: feedstock-dependent standard deviation; F-CV: feedstock-dependent coefficient of variation.

Finally, the WEOC concentrations had significantly ($p < 0.05$) positive correlations with oxygen (O) content ($r = 0.39$), hydrogen (H) content ($r = 0.48$), and H/C atomic ratio ($r = 0.67$) (Table 3.7). Thus, it seems that DOC resulted mainly from the biochar labile fraction enriched with oxygenic functional groups. As a higher H/C atomic ratio of biochars indicates a lower degree

of carbonization,³⁶ the biochars with higher H/C atomic ratios tend to produce larger DOC concentrations. The International Biochar Initiative proposed to predict the biochar stability based on the H to organic C (C_{org}) molar ratio,^{142, 143} and the biochars with the H/C_{org} value of less 0.4 or 0.4–0.7 are considered “highly stable” or “stable”, respectively. Compared with bulk biochars, the biochar-DOC is more labile and thus more susceptible to loss through abiotic and biotic decomposition and/or transport. Consequently, the inclusion of DOC in calculating the H/C_{org} atomic ratio may overestimate the biochar stability. Therefore, the biochar-DOC may need to be subtracted from C_{org} when calculating the H/C_{org} atomic ratio. On the contrary, the inclusion of DOC mineralization in calculating the overall biochar mineralization may underestimate the stability of bulk biochars.

Table 3.7. The correlation coefficient (r) between WEOC and biochar properties (* and ns denote significant at $p < 0.05$ and not significant, respectively).

Biochar properties	WEOC	
	r	n
Volatile Matter	0.30 ^{ns, a}	38
Ash	-0.11 ^{ns}	38
Fixed Carbon	-0.02 ^{ns}	38
C	-0.09 ^{ns}	46
O	0.39*	29
H	0.48*	29
N	0.15 ^{ns}	46
H/C	0.67*	29
O/C	0.05 ^{ns}	29
(O+N)/C	0.08 ^{ns}	29

^a High WEOC content of fast pyrolysis biochar (SB500 and SG500) skewed the correlation, and the r can reach 0.48 ($p < 0.05$) if excludes SB500 and SG500.

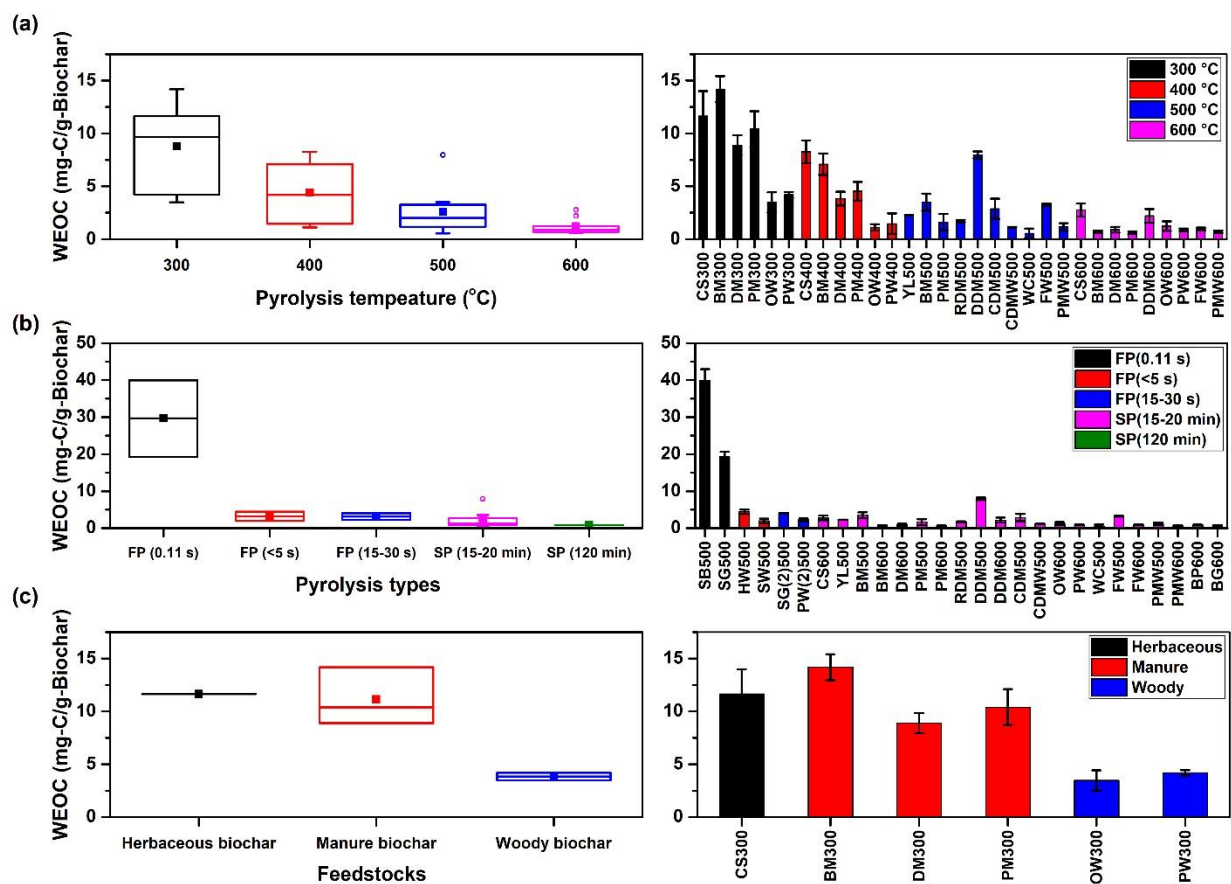


Figure 3.7. Box-whisker plot of WEOC concentrations vs pyrolysis temperature (a), pyrolysis type (b) and feedstocks (c). The box plots showed the first quartile, median, mean, and third quartile of the samples, and the whiskers showed the 1.5 times interquartile range. The column charts by the right side of the box plots showed the sample sets for box plots.

Quick and Easy Method to Estimate DOC Concentrations

Predictive models for the biochar-DOC concentrations based on feedstocks and pyrolysis conditions have yet to be developed. Direct extraction and measurement of biochar-DOC are often needed. The most common method to measure the extracted DOC from biochars is to use a TOC analyzer, but this method is often time-consuming, requires a relatively larger sample volume, and cannot reveal any chemical characteristics of DOC. Alternatively, using UV-vis absorption spectroscopy to estimate biochar-DOC concentrations could be a quicker method that can overcome the above limitations. However, there are no suitable chemicals that can be used as standards for biochar-DOC due to its highly complex composition. Therefore, establishing an appropriate relationship between the UV-vis absorbance and biochar-DOC concentrations would be critical to developing a quick, easy, and robust UV-vis spectrometric method for determining biochar-DOC concentrations.

We first developed the UV-vis spectrometric method for estimating the biochar-DOC concentrations based on the linear regressions between a_{254} and measured TOC concentrations of AEOC, WEOC, and BEOC in 46 tested biochar samples (Figure 3.8). The generated linear regression equation of AEOC, WEOC, and BEOC were shown as follow:

$$\text{DOC}_{\text{AEOC}} = 77.59 \times \alpha_{254} (R^2 = 0.838) \quad (3.1)$$

$$\text{DOC}_{\text{WEOC}} = 48.90 \times \alpha_{254} (R^2 = 0.871) \quad (3.2)$$

$$\text{DOC}_{\text{BEOC}} = 22.29 \times \alpha_{254} (R^2 = 0.941) \quad (3.3)$$

where DOC (mg-C L^{-1}) is the concentration measured by the TOC analyzer and a_{254} (cm^{-1}) is the decadic absorption coefficient at 254 nm measured by the UV-vis spectroscopy. In line with the DOC fractionation and UV-vis characterization, the varying linear correlation slopes of AEOC, WEOC and BEOC suggested their different molecular composition (i.e., different AS and AP

fractions). In practice, the DOC concentration can be simply estimated by measuring a_{254} and then substituted it in to Eq. 3.1, 3.2, or 3.3 according to the extraction agent used (i.e., 0.1 M HCl, DI water, or 0.1 M NaOH). Considering the extracted DOC components (i.e., the AS and AP substances) would vary substantially with the extraction agent (Figure 3.1), these equations are only recommended for determining the concentrations of DOC extracted with the same extraction agents described above (i.e., 0.1 M HCl, DI water, or 0.1 M NaOH). A more universal method independent of the extraction procedure is desirable.

For this purpose, we further developed a method that allows for estimating the proportion of the AS fraction based on the E_2/E_3 ratio and then more accurately determining the DOC concentrations from the AS fraction and a_{254} . We consider the whole DOC concentration (DOC_t) as the sum of the DOC concentrations of the AS fraction (DOC_{AS}) and the AP fraction (DOC_{AP}). Assuming the proportion of the AS fraction in the DOC as f ($0 \leq f \leq 1$), f can be represented as:

$$f = \frac{DOC_{AS}}{DOC_t} = \frac{DOC_t - DOC_{AP}}{DOC_t} \quad (3.4)$$

Hence, DOC_{AS} and DOC_{AP} can be written as:

$$DOC_{AS} = DOC_t f \quad (3.5)$$

$$DOC_{AP} = DOC_t (1 - f) \quad (3.6)$$

The experimental UV-vis spectra of whole DOC, the AS fraction, and the AP fraction were showed in Figure 3.3d, using BM300 as an example, and Figure 3.9a. When the spectra of the AS and AP fractions were added to produce a new spectrum denoted as AS+AP, the spectrum of AP+AS almost overlapped with the spectra of whole DOC in the wavelength of 250 to 450 nm (Figure 3.9a). Therefore, we can assume that the a of whole DOC equals to the sum of the a of the AS and AP fractions. Thus, the a at 254 nm (a_{254}) and a at 365 nm (a_{365}) for the whole DOC can be represented as:

$$a_{254,t} = a_{254,AS} + a_{254,AP} \quad (3.7)$$

$$a_{365,t} = a_{365,AS} + a_{365,AP} \quad (3.8)$$

where $a_{254,t}$, $a_{254,AS}$, and $a_{254,AP}$ are the a value at 254 nm for the whole DOC, the AS fraction, and the AP fraction, respectively, and $a_{365,t}$, $a_{365,AS}$, and $a_{365,AP}$ are the a value at 365 nm for the whole DOC, the AS fraction, and the AP fraction, respectively.

Therefore, the E_2/E_3 ratio of the whole DOC, denoted as r , can be expressed as:

$$r = \frac{E_{2t}}{E_{3t}} = \frac{a_{254,t}}{a_{365,t}} = \frac{a_{254,AS} + a_{254,AP}}{a_{365,AS} + a_{365,AP}} \quad (3.9)$$

According to the Beer-Lambert law ($A = \epsilon l C$), a can be expressed as:

$$a = \frac{A}{l} = \epsilon C \quad (3.10)$$

where A is the absorbance, l is the light path length (cm), ϵ is the extinction coefficient ($L \text{ mg}^{-1} \text{ cm}^{-1}$), and C is the concentration (mg L^{-1}). Therefore, the $a_{254,AS}$, $a_{254,AP}$, $a_{365,AS}$, and $a_{365,AP}$ can be written as follows:

$$a_{254,AS} = \epsilon_{254,AS} \text{DOC}_{AS} \quad (3.11)$$

$$a_{254,AP} = \epsilon_{254,AP} \text{DOC}_{AP} \quad (3.12)$$

$$a_{365,AS} = \epsilon_{365,AS} \text{DOC}_{AS} \quad (3.13)$$

$$a_{365,AP} = \epsilon_{365,AP} \text{DOC}_{AP} \quad (3.14)$$

where $\epsilon_{254,AS}$, and $\epsilon_{254,AP}$ are the ϵ at 254 nm, and $\epsilon_{365,AS}$, and $\epsilon_{365,AP}$ are the ϵ at 365 nm for the AS and AP, respectively. Assuming that the E_2/E_3 ratio of the AS fraction is r_{AS} and the E_2/E_3 ratio of the AP fraction is r_{AP} , r_{AS} and r_{AP} can then be expressed as:

$$r_{AS} = \frac{E_{2AS}}{E_{3AS}} = \frac{a_{254,AS}}{a_{365,AS}} = \frac{\epsilon_{254,AS} \text{DOC}_{AS}}{\epsilon_{365,AS} \text{DOC}_{AS}} \quad (3.15)$$

$$r_{AP} = \frac{E_{2AP}}{E_{3AP}} = \frac{a_{254,AP}}{a_{365,AP}} = \frac{\epsilon_{254,AP} \text{DOC}_{AP}}{\epsilon_{365,AP} \text{DOC}_{AP}} \quad (3.16)$$

Rearranging Eqs. 3.15 and 3.16 to obtain:

$$\varepsilon_{365,AS} = \frac{\varepsilon_{254,AS}}{r_{AS}} \quad (3.17)$$

$$\varepsilon_{365,AP} = \frac{\varepsilon_{254,AP}}{r_{AP}} \quad (3.18)$$

Substituting Eqs. 3.5, 3.6, 3.17 and 3.18 into Eqs. 3.11–3.14 to obtain:

$$a_{254,AS} = \varepsilon_{254,AS} \text{DOC}_t f \quad (3.19)$$

$$a_{254,AP} = \varepsilon_{254,AP} \text{DOC}_t (1 - f) \quad (3.20)$$

$$a_{365,AS} = \frac{\varepsilon_{254,AS}}{r_{AS}} \text{DOC}_t f \quad (3.21)$$

$$a_{365,AP} = \frac{\varepsilon_{254,AP}}{r_{AP}} \text{DOC}_t (1 - f) \quad (3.22)$$

Substituting Eqs. 3.19–3.22 into Eq. 3.9, and simplifying with the intent of eliminating DOC_t , we can obtain:

$$r = \frac{\varepsilon_{254,AS} f + \varepsilon_{254,AP} (1-f)}{\frac{\varepsilon_{254,AS}}{r_{AS}} f + \frac{\varepsilon_{254,AP}}{r_{AP}} (1-f)} \quad (3.23)$$

Eq. 3.23 is the governing equation relating f and the E_2/E_3 ratio (r) of the whole DOC. To further estimate DOC_t based on $a_{254,t}$ and f , we can substitute Eq. 3.19 and 3.20 into Eq. 3.7 and rearrange to obtain:

$$\text{DOC}_t = \frac{a_{254,t}}{\varepsilon_{254,AS} f + \varepsilon_{254,AP} (1-f)} \quad (3.24)$$

Eq. 3.24 is the governing equation for estimating the whole DOC concentration. However, there are no analytical solutions to Eq. 3.23 and 3.24, and they were solved numerically based on the experimental data of BEOC-AS and BEOC-AP of 27 biochars, as follows. The linear regression between a_{254} and the DOC concentrations of the AS and AP fractions are showed in Figure 3.8b. The generated linear regression equations of the AS and AP fractions and the final equation to estimate total DOC are shown as follows:

$$\text{DOC}_{AS} = 43.14 \times a_{254,AS} (R^2 = 0.920) \quad (3.25)$$

$$\text{DOC}_{\text{AP}} = 15.58 \times a_{254,\text{AP}} (R^2 = 0.977) \quad (3.26)$$

From the linear regression of DOC concentrations and a_{254} for the AS and AP fractions, it is known that:

$$\text{DOC}_{\text{AS}} = \frac{1}{\varepsilon_{254,\text{AS}}} a_{254,\text{AS}} = 43.14 a_{254,\text{AS}} \quad (3.27)$$

$$\text{DOC}_{\text{AP}} = \frac{1}{\varepsilon_{254,\text{AP}}} a_{254,\text{AP}} = 15.58 a_{254,\text{AP}} \quad (3.28)$$

Thus, we will have:

$$\varepsilon_{254,\text{AS}} = \frac{1}{43.14} = 0.0231 \quad (3.29)$$

$$\varepsilon_{254,\text{AP}} = \frac{1}{15.58} = 0.0642 \quad (3.30)$$

In addition, the E_2/E_3 ratios of the AS and AP fractions can be taken from the average of these 27 fractionable samples of BEOC-AS and BEOC-AP as $r_{\text{AS}} = 7.56$ and $r_{\text{AP}} = 2.48$, respectively (Figure 3.9b).

Substituting the above numbers into Eq. 3.23 to have:

$$\frac{E_{2t}}{E_{3t}} = r = \frac{0.0231f + 0.0642(1-f)}{\frac{0.0231}{7.56}f + \frac{0.0642}{2.48}(1-f)} \quad (3.31)$$

Since $0 \leq f \leq 1$, we can set f from 0 to 1 in Eq. 3.26 with a step of 0.005 and calculate its corresponding E_{2t}/E_{3t} ratio (r). Based on this set of data, we can draw a curve in f vs the E_{2t}/E_{3t} ratio (r) as shown in Figure 3.9c. Fitting this curve with the rational function model by using MATLAB R2016a, we can obtain:

$$f = \frac{1.135r - 2.813}{r - 1.797} \quad (3.32)$$

Finally, substituting $\varepsilon_{254,\text{AS}} = 0.0231$ and $\varepsilon_{254,\text{AP}} = 0.0642$ into Eq. 3.24 to derive:

$$\text{DOC}_t = \frac{a_{254,t}}{0.0232f + 0.0642(1-f)} \quad (3.33)$$

Thus, Eqs. 3.32 and 3.33 are the final equations we can use to estimate the f and DOC_t from the UV-vis absorbance measurements at 254 and 365 nm. In practice, the f value and biochar-DOC concentrations can be estimated simply by the E_2/E_3 ratio and a_{254} that can be easily determined from the UV-vis spectra. In addition, the E_2/E_3 ratio could be used as a proxy of aromaticity and M_w of biochar-DOC, as previously discussed. It is noted that Eq. 3.32 estimates the DOC concentrations in the extracted solution (in the unit of mg L^{-1}), from which the DOC concentration per unit of biochar mass can be further calculated.

To validate the model, we substituted experimental UV-vis data of a_{254} and a_{365} of AEOC ($n = 35$), WEOC ($n = 46$), and BEOC ($n = 46$) into Eq. 3.32 and 3.33 to calculate the modeled biochar DOC concentrations, and then compared with experimental biochar DOC concentrations. Performance of this model was further evaluated by the coefficient of determination (R^2) and root-mean-square error (RMSE) between measured and modeled data (Figure 3.10 and Figure 3.11). The modeled DOC was generally in good agreement with measured WEOC ($R^2 = 0.96$, $\text{RMSE} = 2.4 \text{ mg L}^{-1}$) and BEOC ($R^2 = 0.97$, $\text{RMSE} = 1.9 \text{ mg L}^{-1}$). Additionally, two data points deviated from the measured versus modeled 1:1 relationship line at high WEOC concentrations were contributed by SB500 and SG500 (Figure 3.10), presumably due to their distinct composition from that of other 44 samples. For the AEOC ($R^2 = 0.85$, $\text{RMSE} = 3.6 \text{ mg L}^{-1}$), the modeled concentrations were substantially lower than the measured concentrations, likely due to increased DOC concentrations from acidic hydrolysis unaccounted for by the predictive equations developed from the BEOC data. It is noted that the WEOC dataset can be considered independent from the BEOC dataset used to develop Eqs. 3.1 and 3.2 due to their distinct difference in quantity and properties. Thus, the good agreement between the modeled and measured WEOC concentrations demonstrated the validity of this method. More importantly, these results suggest that this model

may be universally applied for quantifying DOC concentrations in biochars produced from diverse feedstocks and pyrolysis conditions. The model can potentially be further improved by including more biochars following the approach described here. As UV-vis spectrophotometers are routinely available in many laboratories, this method has the potential to provide a quick, easy and robust way of measuring DOC concentrations in biochars.

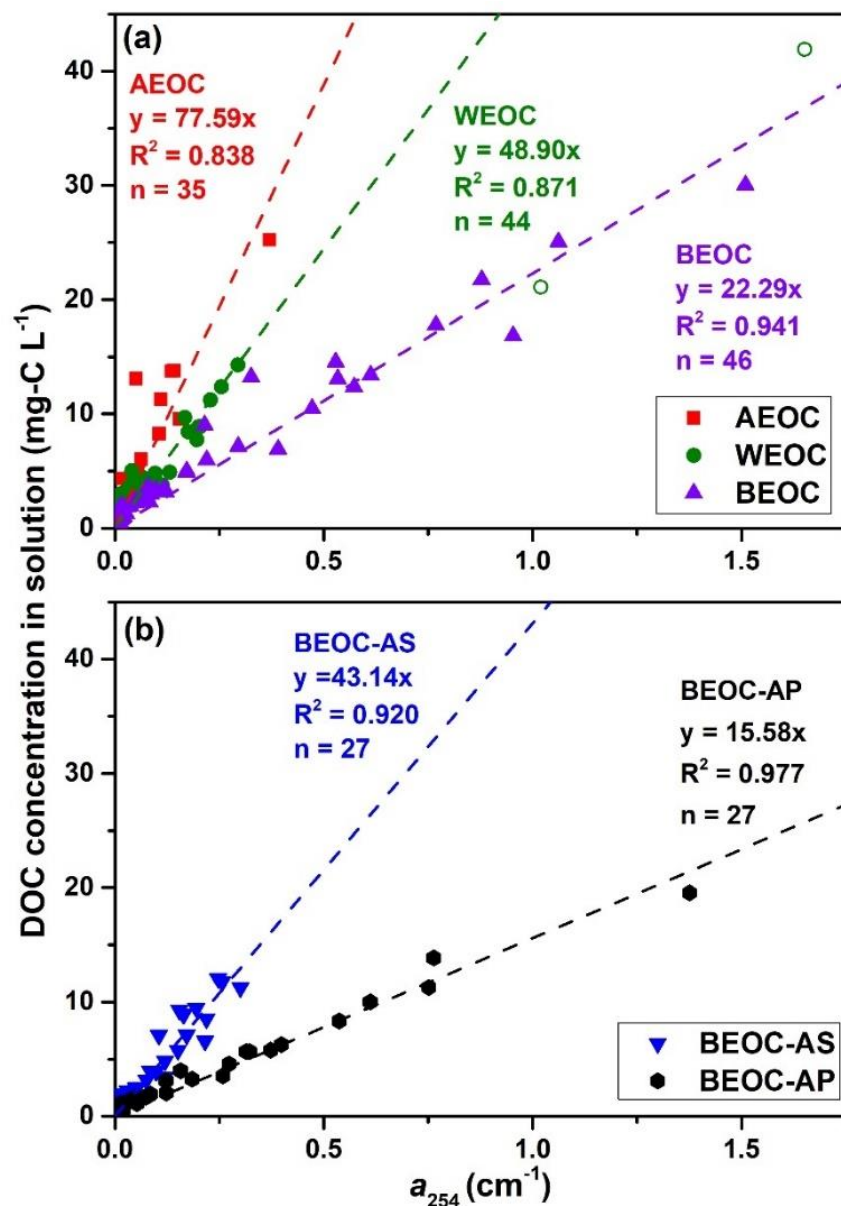


Figure 3.8. Linear regressions between decadic absorption coefficient at 254 nm and biochar DOC concentrations in solution for (a) AEOC, WEOC, and BEOC, and (b) BEOC-AS and BEOC-AP. The dilution factor for AEOC and WEOC was 10 and for BEOC, BEOC-AS, and BEOC-AP was 50. For AEOC, 11 samples with serve matrix interference were excluded. For WEOC, SB500 and SG500 skewed the correlation because of the distinct compositional difference with other 44 samples (Figure 3.2), and thus were excluded. For BEOC-AS and BEOC-AP, only 27 fractionable BEOC samples were included.

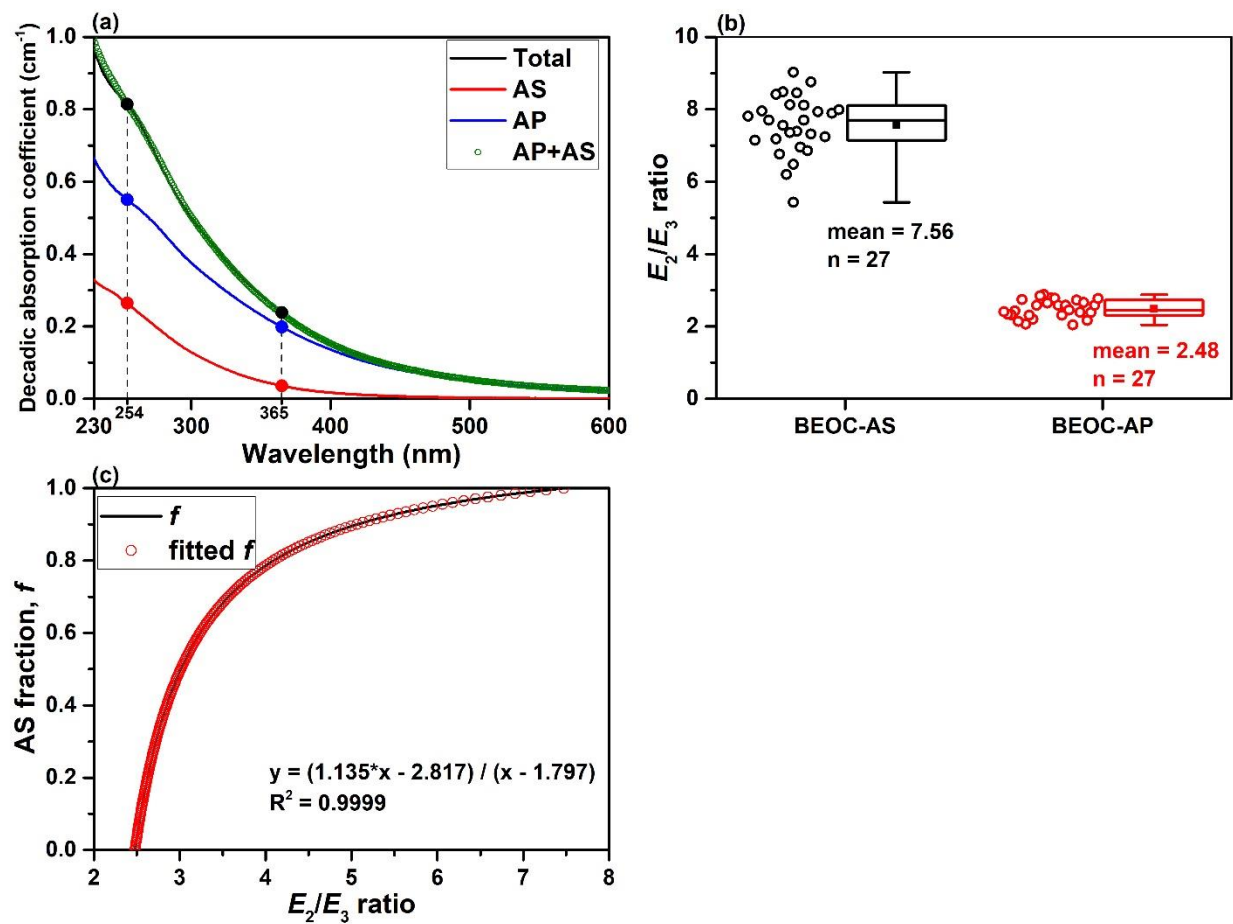


Figure 3.9. (a) Experimental data for BM300 as example, (b) boxplot of the E_2/E_3 ratios of 27 fractionable BEOC samples, and (c) Fitting E_2/E_3 vs f data with the rational function model.

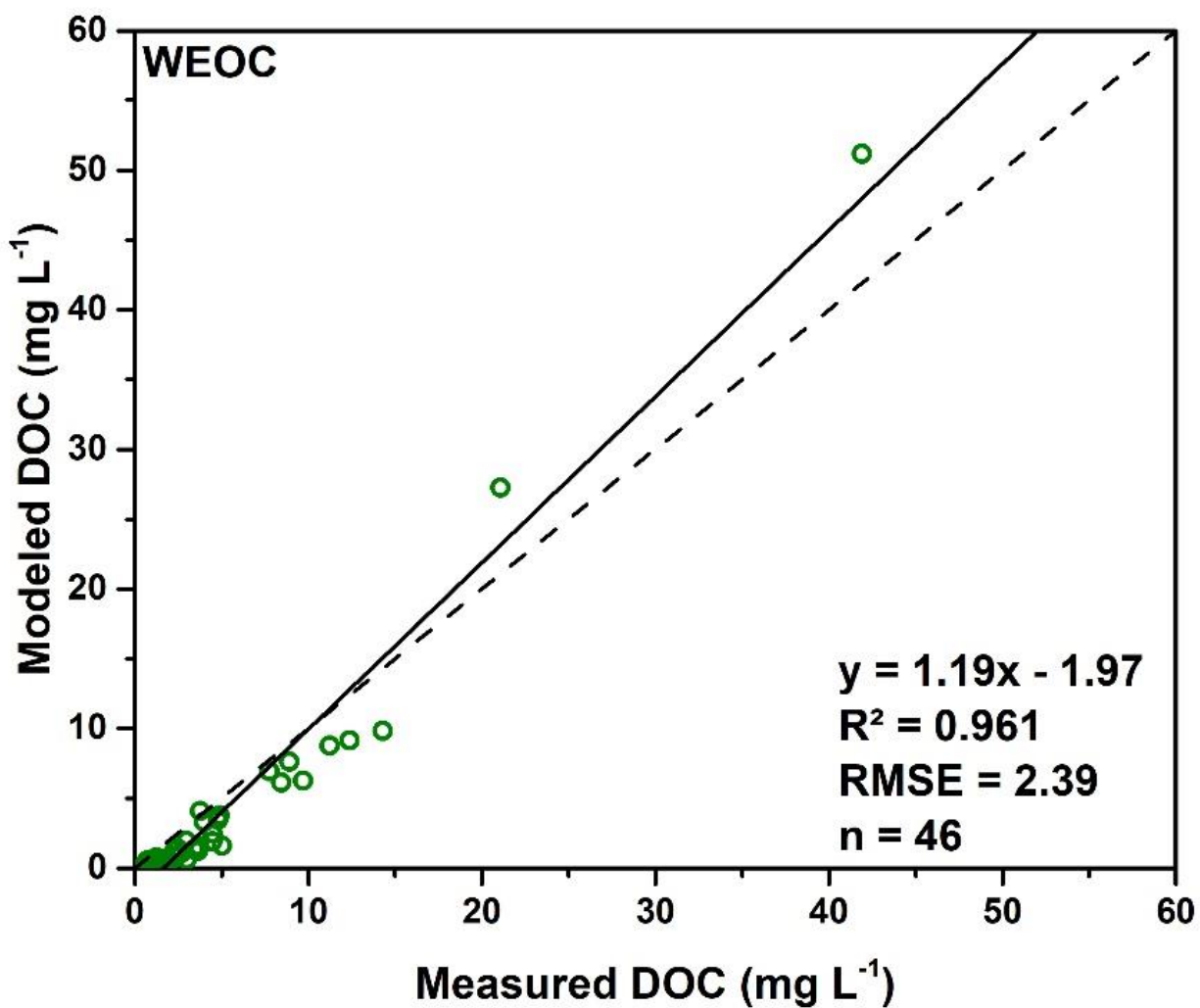


Figure 3.10. Measured versus modeled water-extractable DOC (WEOC) by E_2/E_3 ratio and a_{254} . Dashed line represents the 1:1 relationship. Dilution was made by 10-folds for the WEOC samples.

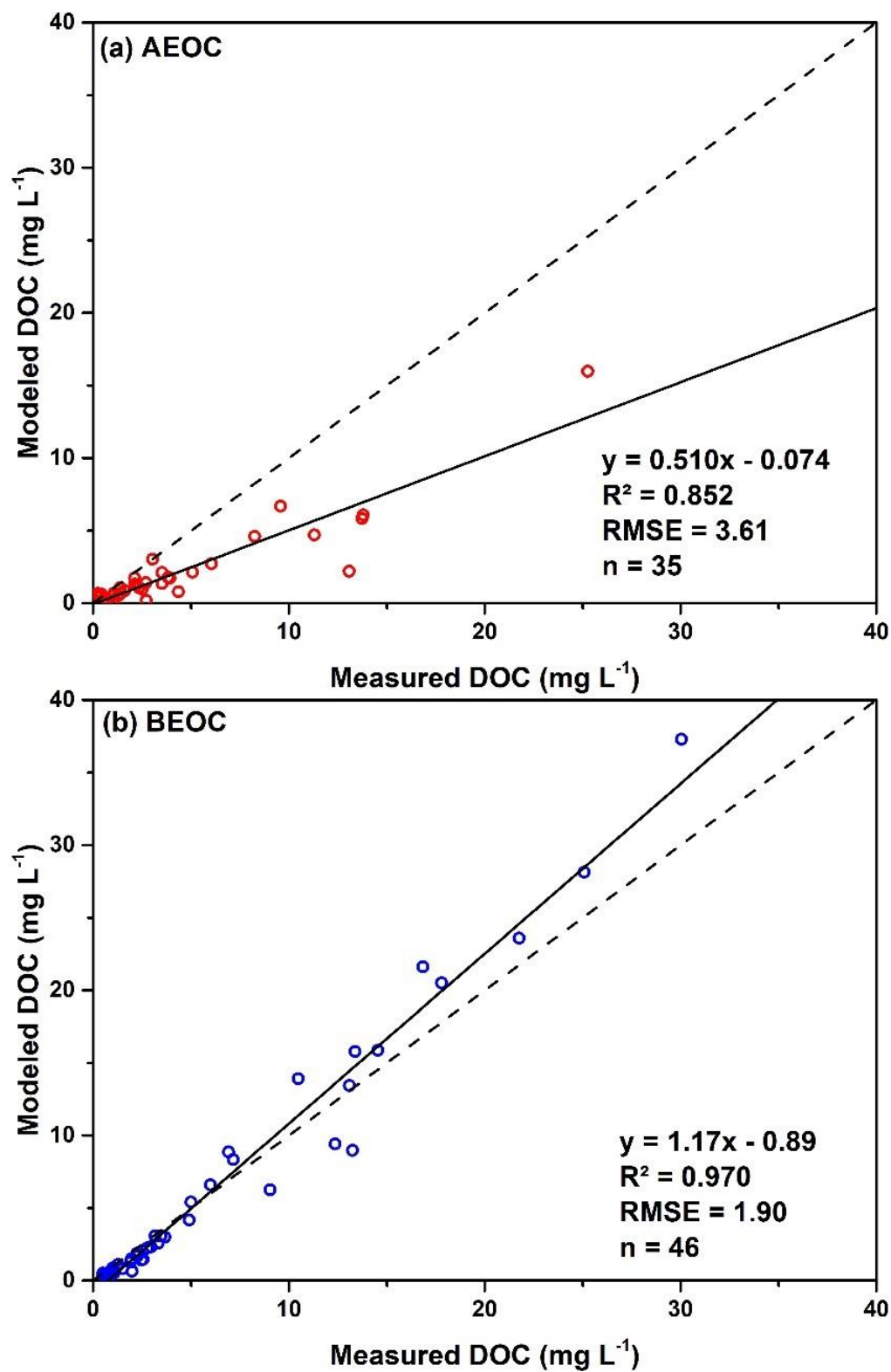


Figure 3.11. Measured versus modeled DOC for (a) AEOC and (b) BEOC by E_2/E_3 ratio and a_{254} . Dashed line represents the 1:1 relationship. Dilution was made by 10- and 50-folds for the AEOC and BEOC samples, respectively.

Implications

Our results may have several important implications to the production and application of biochars for agronomic and environmental uses. Biochar-DOC was shown to be an important fraction of biochars, and its quantity and properties were dependent on feedstocks, pyrolysis conditions (i.e., pyrolysis temperature, and residence time), and the extraction procedure. Thus, biochars may be engineered so that the quantity and characteristics of their DOC can be properly controlled for their intended use. When used for soil C sequestration, the biochars with minimal labile DOC and maximal recalcitrant C content may be desired. If other benefits such as improving soil aggregation, water retention, and microbial health, the release of certain labile DOC may be beneficial. The drastic difference in the amount and chemical composition of BEOC and WEOC suggests that the alkaline extraction cannot be used to produce the environmentally-meaningful DOC measurements, and the water extraction is thus preferred. Accurate measurement of the biochar-DOC is important because the amount of biochar-DOC could significantly influence the biochar stability in soils and the appropriate methods to assess it. Therefore, the developed quick and easy UV-vis method for determining the biochar-DOC concentrations can be a useful tool for biochar production and application.

CHAPTER IV

LONG-TERM SORPTION OF LINCOMYCIN TO BIOCHARS: THE INTERTWINED ROLES OF PORE DIFFUSION AND DISSOLVED ORGANIC CARBON

ABSTRACT

Sequestration of anthropogenic antibiotics by biochars in soils may be a promising strategy to minimize environmental and human health risks of antibiotic resistance. This study investigated the long-term sequestration of lincomycin by 17 slow-pyrolysis biochars using batch sorption experiments during 365 days. Sorption kinetics were well fitted with the Weber-Morris intraparticle diffusion model for all tested biochars with the intraparticle diffusion rate constant (K_{id}) ranging between 25.3–166 $\mu\text{g g}^{-1} \text{day}^{-0.5}$, suggesting that the sorption kinetics were mainly controlled by pore diffusion. The quasi-equilibrium sorption isotherms became more nonlinear with increasing equilibration time at 1, 7, 30, and 365 days, likely due to increasing abundance of heterogeneous sorption sites in biochars over time. Intriguingly, low-temperature (300°C) biochars had higher sorption capacity and faster sorption kinetics than higher-temperature (400–600°C) biochars. The continuous release of dissolved organic carbon (DOC) from the low-temperature biochars may enhance the lincomycin sorption by decreasing biochar particle size and/or increasing the accessibility of sorption sites and pores initially blocked by DOC. Additionally, a large fraction (> 75%) of sorbed lincomycin after 240-day equilibration could not be desorbed by the acetonitrile/methanol extractant from the tested biochars. This observed strong sorption/desorption hysteresis illustrates that there is great potential of biochars as soil amendments to create long-term sequestration of antibiotics in-situ.

INTRODUCTION

Antibiotics are used extensively in livestock industry for therapeutic, preventative, and growth promotion purposes.¹⁻³ The use of antibiotics in animal feeding operations was 14,622 tons in the United States in 2012 and 84,240 tons in China in 2013 (i.e., the two largest users of antibiotics).¹⁴⁴ Globally, the total consumption of antibiotics in livestock industry was about 131,109 tons in 2013 and was projected to increase to 200,235 tons in 2030.¹⁴⁵ Because the administered antibiotics are often poorly absorbed within animals, a large portion of antibiotics are excreted into manure as parent compounds and metabolites, and released into agricultural soils and waters through manure land applications.^{4, 12, 146} The widespread and repeated manure application has increased environmental concentrations of anthropogenic antibiotics, thus raising serious concerns about the proliferation of antibiotic resistant bacteria and associated food safety and human health impacts.^{1, 7, 147, 148} Mitigation strategies to reduce the release, transport, and bioavailability of manure-borne antibiotics in soils are urgently needed to minimize their environmental risks. Enhancing sequestration of antibiotics in soils by biochar amendment may be a promising strategy for this purpose.

Biochars are carbonaceous porous materials produced from the pyrolysis of biomass under oxygen-limited conditions at a typical temperature range of 300–700 °C.¹⁴⁹ Biochars have been promoted as soil amendments for their agronomical and environmental benefits such as increasing soil carbon storage, improving soil structure and quality, and immobilizing environmental contaminants.^{33, 93, 149} Sorption plays an important role in controlling the fate, transport, and bioavailability of contaminants in soils, and the porous nature and heterogeneous surfaces of biochars lead to an excellent sorption ability for many inorganic and organic contaminants^{29, 33, 35} (including antibiotics^{40, 150, 151}). The interactions between antibiotics and biochars may be

controlled by hydrophobic partitioning, van der Waals forces, hydrogen (H) bonding, charge-assisted H bonding (CAHB), electron donor–acceptor (EDA) interaction, electrostatic interaction, and pore filling.^{40, 150, 151} The relative contribution of each sorption mechanism is collectively determined by physicochemical properties of antibiotics (e.g., hydrophobicity, polarity, ionization, and molecular structure) and biochars (e.g., surface area, surface charge, surface functionalization, and pore structure) as well as environmental factors (e.g., pH, ionic strength, and co-solutes).^{40, 151} Thus, the studies on contaminant sorption to biochars have recently focused on clarifying the complexity in sorption processes and controlling factors.

Pyrolysis temperature is one of the key factors determining the physicochemical and sorption properties of biochars.^{29, 33, 35, 39} With increasing pyrolysis temperature, surface area and pore volume of biochars increase, but surface functionalization decreases with a concomitant increase in aromaticity.^{38, 39, 136} As a result, higher-temperature biochars often had stronger sorption affinity to antibiotics (e.g., ciprofloxacin,¹⁵² norfloxacin,¹⁵³ tetracycline,^{154, 155} and sulfamethoxazole^{45, 156, 157}) than lower-temperature biochars, which was attributed to greater surface area and porosity of those biochars. However, a number of studies reported the absence or opposite of such trend with regard to pyrolysis temperature for the sorption of ofloxacin,⁴⁵ norfloxacin,⁴⁵ and sulfamethoxazole¹⁵⁸ to biochars. Clearly, the effect of pyrolysis temperature on the sorption of antibiotics to biochars has yet to be settled.

Additionally, considering the heterogeneous nature of biochar pore structure, the sorption of antibiotics may need longer time to reach the true equilibrium. Kasozi et al. reported that the sorption kinetics of catechol on biochars reached equilibrium after 14 days.⁷⁵ Chen et al. found that the sorption of naphthalene to biochars could take up to 36 days to reach equilibrium, depending on the pyrolysis temperature of biochars.³⁸ Our previous study showed that the

lincomycin sorption to biochars quickly reached a quasi-equilibrium in about 2 days, but did not reach true equilibrium after 180 days.⁹² For most antibiotics that have been studied, the reported sorption equilibration time with biochars was generally several hours or days.^{45, 152-158} Thus, some of those sorption experiments may have only reached quasi-equilibrium during such short equilibration time. Consequently, the contribution of pore diffusion to the overall sorption may be underestimated due to short equilibration time. Furthermore, biochars could release a substantial amount of dissolved organic carbon (DOC, including truly dissolved and colloidal DOC) upon exposure to water,^{51, 54, 55, 76, 159} which may change the biochar surface and pore structure. For example, these water-soluble organic compounds (i.e., DOC) may initially fill up the biochar pores during pyrolysis, or adsorb on the biochar surface, thus blocking the sorptive sites for antibiotics. The release of DOC from biochars may enhance the sorption of antibiotics to biochars.⁹⁶ However, the effects of long-term DOC release from biochars on their sorption capacity for antibiotics have not been well studied.

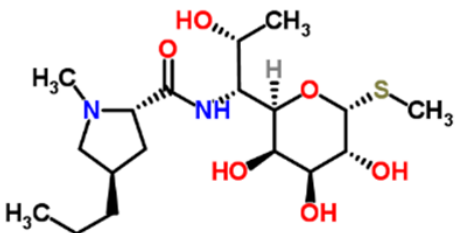
Therefore, this study aimed to examine: (1) the long-term sequestration of antibiotics by biochars and (2) the effect of the long-term DOC release on the sorption of antibiotics to biochars. Lincomycin was selected as a model antibiotic compound because it is one of the antibiotics widely administered to food animals, and is also medically important in human therapy. The long-term sorption kinetics and isotherms of lincomycin by 17 slow-pyrolysis biochars prepared from 7 manure feedstocks at 300–600 °C and one wood feedstock at 500 °C were evaluated to elucidate the underlying sorption mechanisms. For comparison, a commercial graphite powder was selected to represent nonporous carbonaceous sorbents.

MATERIALS AND METHODS

Chemicals

Lincomycin hydrochloride ($\geq 90\%$) and sodium azide (NaN_3 , $\geq 99.5\%$) were purchased from Sigma-Aldrich, and sodium chloride (NaCl), sodium bicarbonate (NaHCO_3), sodium carbonate (NaCO_3) and sodium hydroxide (NaOH) from J.T. Baker. Selected physicochemical properties of lincomycin are listed in the Table 4.1. All chemical reagents used were of analytical grade. Deionized (DI) water from a Milli-Q water system (Millipore, USA) was used for preparing all aqueous solutions.

Table 4.1. Physicochemical properties of lincomycin.

Chemical name	Lincomycin
Molecular structure ^a	
Molecular formula ^b	$\text{C}_{18}\text{H}_{34}\text{N}_2\text{O}_6\text{S}$
Molecular weight ^b	$406.537 \text{ g mol}^{-1}$
Water solubility ^b	927 mg L^{-1} at 25°C
Log octanol-water partition coefficient ($\log K_{ow}$) ^b	0.20
Dissociation constant (pK_a) ^b	7.6

^a Data from ChemSpider (<http://www.chemspider.com/>); ^b Data from TOXNET (<http://www.toxnet.nlm.nih.gov/>)

Sorbents

Sixteen manure-based and one wood-based biochars were produced by the Best Energies Inc. (Daisy Reactor, Cashton, WI). The feedstocks and production conditions of these biochars have been described in detail elsewhere.^{28,71} Briefly, the feedstocks were bull manure with sawdust bedding (BM), dairy manure with rice hull bedding (DM), poultry manure with sawdust bedding (PM), raw dairy manure (RDM), digested dairy manure (DDM), composted digested dairy manure (CDM), composted digested dairy manure mixed with woodchip waste in a 1:1 ratio (CDMW),

and woodchip waste (WW). The same source of dairy manure was used to produce RDM, DDM, CDM, and CDMW with different pretreatments before pyrolysis in a Daisy Reactor at BEST Energies Inc. The feedstocks were slowly pyrolyzed in a N₂ atmosphere at 300, 400, 500 or 600 °C with a heating rate of <10 °C min⁻¹ and a retention time of 15–20 min. The produced biochars were ground and sieved to obtain particles in the 75–150 µm size fraction, and then stored in glass vials prior to use. These biochars were hereafter labeled using feedstock abbreviation and pyrolysis temperature, e.g., BM300 for bull manure with sawdust bedding pyrolyzed at 300 °C. Nonporous graphite powder (< 150 µm, 99.9% C) was purchased from Sigma-Aldrich and used as received.

Sorbent Characterization

The proximate (volatile matter, fixed carbon, and ash) and ultimate (C, H, O, and N) analyses of the biochars have been characterized and reported previously.^{28, 71} Specific surface area (SSA) and micropore volume (V_{mic}) of the biochars were measured by CO₂ adsorption on a Micromeritics Tristar 3020 analyzer (Micromeritics, USA) at Pacific Surface Science Inc. (Oxnard, CA). Zeta potential of the biochar particles was determined by a Zetasizer Nano-ZS (Malvern Instruments, UK). To generate a biochar suspension, 8 mg each biochar was mixed with 8 mL 0.02 M background electrolyte (6.7 mM NaCl, 2.5 mM Na₂CO₃, 2.5 mM NaHCO₃, and 200 mg L⁻¹ NaN₃.) in amber glass vials and then shaken end-over-end for 1 day. Afterwards, the vials were allowed standing for 30 min and then the top 1 mL of the suspension was withdrawn and measured for the zeta potential by the Zetasizer Nano-ZS. The remained suspensions were used to determine solution pH of the suspension (10.0 ± 0.1 for all tested biochars). Additionally, BM300 and BM600 were selected as model biochars (representing poorly- and highly-carbonized biochars, respectively) for further studying the characteristics of biochar particles after water exposure. The shape and surface morphology of BM300 particles before and after 1-d and 365-d

kinetic sorption experiments (described later) and 1-d exposure to 0.1 M NaOH solution were investigated with a scanning electron microscope (SEM) (JEOL JSM-7500F, Japan). To measure the biochar colloid size after the DOC release, biochars were suspended in 0.01M NaCl or 0.01M NaOH solution (1:1 solid/water ratio) and shaken end-over-end for 1 day. After shaking, the vials were allowed standing for 30 min and then the top 1 mL of the biochar suspension was withdrawn and measured for particle size distribution by dynamic light scattering method using the Zetasizer.

Sorption Experiments

Batch sorption experiments were conducted in amber borosilicate glass vials with polytetrafluoroethylene (PTFE) lined screw-caps. All vials were covered with aluminum foils to prevent the potential photodegradation of lincomycin. The lincomycin solutions were freshly prepared in DI water with ionic strength of 0.02 M and pH of 10 using background electrolytes of 6.7 mM NaCl, 2.5 mM Na₂CO₃, and 2.5 mM NaHCO₃. NaN₃ of 200 mg L⁻¹ was included as a biocide to prevent any biodegradation of lincomycin during the long-term sorption experiments. All sorption experiments were performed in duplicate at room temperature (23 ± 1 °C) and a sorbent-water ratio of 1 g L⁻¹. The above experimental condition and setup for the batch sorption studies were followed unless noted otherwise.

For the kinetic sorption experiments, 8 mg of each sorbent were mixed with 8 mL of 1000 µg L⁻¹ lincomycin in 8 mL vials and then agitated on an end-over-end shaker (Glas-Col, USA) at 30 rpm in dark for the duration of 1–365 days. At pre-determined time intervals, two vials for each sorbent were retrieved from the shaker. The vials were centrifuged at 2430 × g for 20 min, and the top 2 mL of supernatants were collected and filtered through a 0.45-µm mixed cellulose esters syringe filter (Millipore, USA). The first 1-mL filtrate was discarded, and the following 1-mL filtrate was collected to minimize the potential loss of lincomycin sorbed by the filter. The

concentrations of lincomycin in the filtrate was determined by a Shimadzu Prominence high-performance liquid chromatograph coupled to an Applied Biosystems Sciex 3200 triple quadrupole mass spectrometer (LC-MS/MS). Since the sorbent-free control experiments showed a negligible loss of lincomycin during the experiments (Figure 4.1), the difference between the initial and final solution concentrations was used to calculate the sorbed lincomycin concentration in the sorbents. In addition, the DOC in the filtrate is operationally defined as biochar-derived DOC in this study. Because the filtrate volume was small, and if diluted, the DOC concentration could be below the detection limit of total organic carbon analyzer, the concentration of DOC in the filtrate was determined by ultraviolet (UV) absorption at 254 and 365 nm on a Varian Cary 50 Bio UV-visible spectrophotometer (Varian, USA), using our recently developed method.¹⁶⁰ Details of the LC-MS/MS and UV analytical protocols are provided in the Analytical Methods section.

To conduct the quasi-equilibrium sorption isotherms, 8 mg of each sorbent were mixed with 8 mL lincomycin solutions with a series of initial concentrations ranging from 100 to 1000 $\mu\text{g L}^{-1}$. The suspensions were shaken end-over-end at 30 rpm in dark. At 1, 7, 30, and 365 days, the vials were retrieved, centrifuged, filtered, and determined for the lincomycin concentration by the LC-MS/MS as described previously.

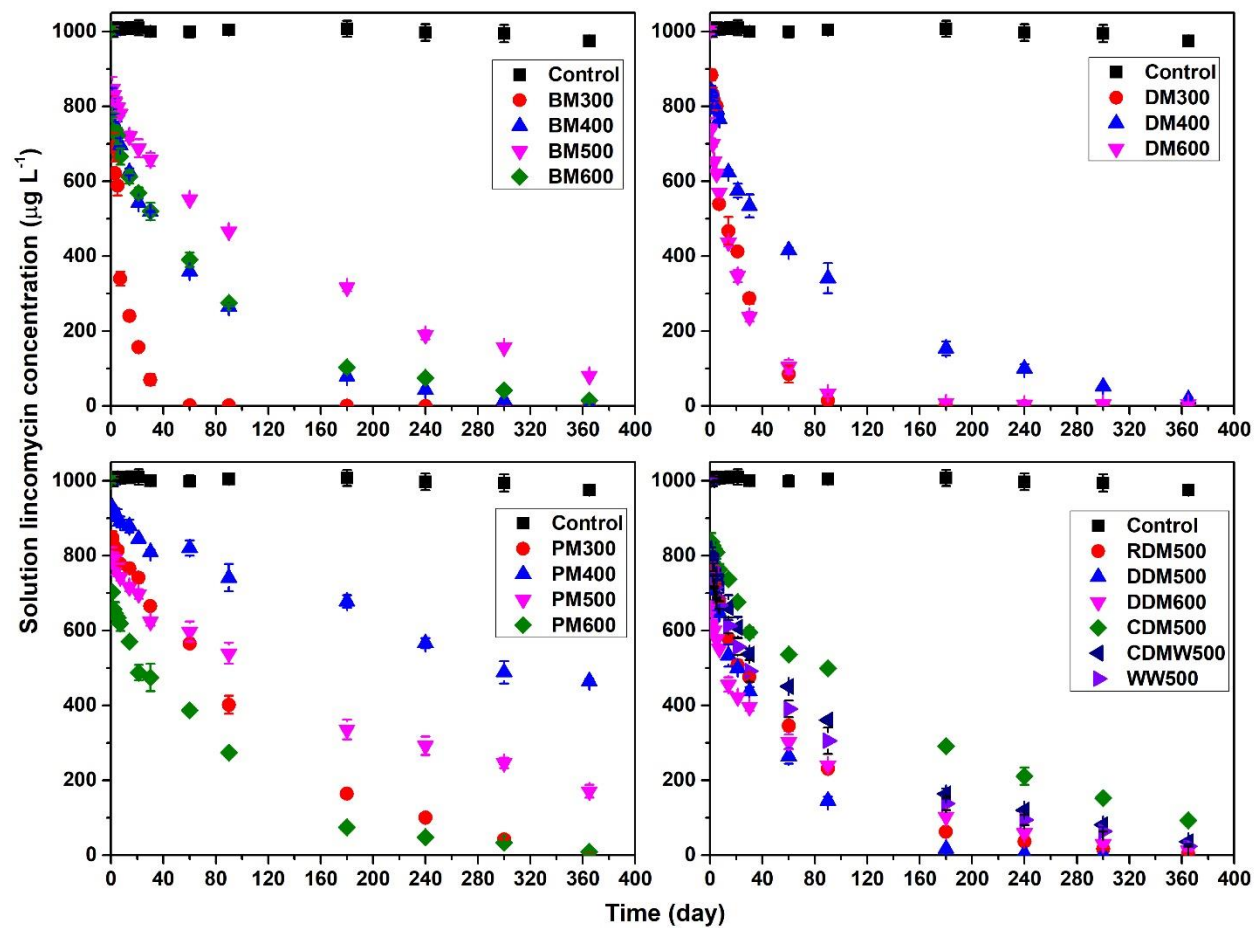


Figure 4.1. Lincomycin concentrations in solution over time in the kinetic sorption experiments for the 17 tested biochars. Control was the biochar-free lincomycin solution.

Effects of DOC on Lincomycin Sorption

To further elucidate the role of DOC on the sorption of lincomycin to biochars, three additional experiments were performed as detailed below. First, the freely dissolved lincomycin and DOC-bound lincomycin in solutions were determined using the solid-phase extraction method.⁸⁷ Briefly, 7.2 mL of each DI-water-extracted DOC solution as described above (40-d extraction) was mixed with 0.8 mL of lincomycin solution (lincomycin concentration of 10,000 $\mu\text{g L}^{-1}$ and ionic strength of 0.2 M background electrolytes) in vials to acquire the lincomycin/DOC mixture solution with the initial lincomycin concentration of 1000 $\mu\text{g L}^{-1}$, ionic strength of 0.02 M, and DOC concentration of 186, 93.8, 97.4, and 89.6 mg-C L^{-1} for BM300-, DM300-, PM300-, and DDM500-DOC, respectively. The vials were then end-over-end shaken at 30 rpm in dark for 1 day. Afterwards, the lincomycin/DOC mixture solution was passed through an Oasis hydrophilic–lipophilic balance (HLB) cartridge (Waters Corporation, USA), which was preconditioned with 3.0 mL of methanol and 3.0 mL of DI water. At this step, the DOC-bound lincomycin in solution could pass through the HLB cartridge and the freely dissolved lincomycin in solution would be retained by the HLB cartridge. The retained freely-dissolved lincomycin was further eluted from the HLB cartridge with 5.0 mL of methanol, and then determined the concentration by LC-MS/MS. Finally, the DOC-bound lincomycin concentration was calculated by the difference between initial applied lincomycin concentration and freely dissolved lincomycin concentration in solutions. Its results could allow us to determine if the enhanced lincomycin sorption over time was due to the binding of lincomycin with DOC.

Second, the lincomycin sorption to a wood biochar (WW500) was measured in the absence and the presence of DOC at 17.2, 7.94, 11.1, and 10.9 mg-C L^{-1} extracted from BM300, DM300, PM300, and DDM500, respectively. To extract the DOC from the biochars, 500 mg of each

selected biochar were mixed with 50 mL of DI water in 50 mL polypropylene (PP) centrifuge tubes, and then shaken end-over-end at 30 rpm in dark for 7 days. Afterwards the tubes were centrifuged at $8,000 \times g$ for 20 min, and the supernatants were then vacuum-filtered through a 0.45- μm membrane (mixed cellulose esters). The final filtrates were collected as the DOC stock solutions, and the DOC concentrations were determined by a Shimadzu TOC-V_{CPN} TOC analyzer (Shimadzu, Japan). Aliquots of each DOC stock solutions were further diluted 10-fold with a lincomycin solution (lincomycin concentration of $1111 \mu\text{g L}^{-1}$ and ionic strength of 0.022 M background electrolytes) to achieve the initial lincomycin concentration of $1000 \mu\text{g L}^{-1}$, ionic strength of 0.02 M, and DOC concentration of 17.2, 7.94, 11.1, and 10.9 mg-C L^{-1} for BM300-, DM300-, PM300-, and DDM500-DOC, respectively. For comparison, a lincomycin solution without DOC was prepared using the same protocol but replacing the DOC stock solution with DI water. The prepared lincomycin solutions with and without DOC were denoted as lincomycin/DOC and lincomycin/DI, respectively. Thereafter, the lincomycin sorption kinetics in the presence of DOC were carried out using WW500 biochar, which was selected because of its low DOC content. Briefly, 8 mL of each lincomycin/DOC and lincomycin/DI solutions were mixed with 8 mg WW500 biochar in vials, and then the vials were shaken end-over-end at 30 rpm in dark for the duration of 1 day to 60 days. The other procedures were same as described in the sorption kinetics section. In addition, the control experiments of lincomycin/DOC solutions without WW500 biochars were also performed using the same protocol, and the lincomycin concentrations in solution had no significant difference regardless of the presence of DOC during 60 days (data not shown). This experiment allowed us to evaluate the effect of free DOC in solution on lincomycin sorption to biochars.

Finally, to evaluate the change in the lincomycin sorption to biochars after the DOC release, BM300, BM600, DM300, PM300, and DDM500 were washed with 0.1 M NaOH (only for BM300, BM600, and DM300) or DI water, respectively. To wash out the DOC, 500 mg of each selected biochar (BM300, BM600, DM300, PM300, and DDM500) were mixed with 50 mL of 0.1 M NaOH (only for BM300, BM600, and DM300) or DI water in vials and then end-over-end shaken at 30 rpm in dark for 1 day or 40 days, respectively. The suspensions were then centrifuged at $8,000 \times g$ for 20 min, and the supernatant was collected. The supernatant was vacuum-filtered through a 0.45- μm membrane and determined for the DOC concentration by the TOC analyzer after appropriate sample dilution. The treated biochar pellets were re-dispersed with 50 mL DI water and re-centrifuged for five times to remove remaining salt and DOC, and then freeze-dried to obtain the DOC-washed biochars. The sorption kinetics of lincomycin on the washed biochars were conducted as previously describe. Briefly, 8 mg of each washed biochar were suspended in 8 mL of $1000 \mu\text{g L}^{-1}$ lincomycin solution, and then end-over-end shaken at 30 rpm in dark for the duration of 1 to 30 days. The rest sampling and analysis procedures were identical as previously described.

Extraction of Sorbed-lincomycin from Biochars

Single-point batch extraction experiments were performed to test the desorption hysteresis of lincomycin on the biochars. Following the sorption kinetics after 240 days, two vials of each biochar in the kinetic sorption experimental set were retrieved. The suspensions in vials were stirred with a PTFE-coated micro stir bar, and 2 mL of each suspension was uniformly withdrawn, filtered, and determined for the lincomycin concentration in filtrates by the LC-MS/MS. In addition, another 1 mL of each suspension was placed into a vial containing 4 mL of acetonitrile/methanol (8/2 in v/v) extraction solvent. The vials were end-over-end shaken at 30

rpm in dark for 7 days and then placed into an ultrasonic bath to sonicate for 60 min at 50 °C. The suspensions were then centrifuged, filtered, and determined for the lincomycin concentration by the LC-MS/MS as described previously. The extraction recovery of lincomycin from biochars were calculated by mass balance.

Analytical Methods

The concentration of lincomycin in solutions were determined by a Shimadzu Prominence high-performance liquid chromatograph coupled to an Applied Biosystems Sciex 3200 triple quadrupole mass spectrometer (LC-MS/MS). The analytical column was an Agilent ZORBAX Eclipse Plus C18 column with 50 mm length \times 2.1 mm diameter and 5 μ m particle size. The mobile phase A consisted of DI water and 0.3% formic acid. The mobile phase B consisted of 1:1 (v/v) acetonitrile-methanol mixture and 0.3% formic acid. Data were acquired using a gradient condition of 0–40 % B in 0–1 min, 40–70% B in 1–2 min, 70–80 % B in 2–3 min, 80–100 % B in 3–3.5 min, and 100% B for 0.5 min. The flow rate was set to 0.35 mL min⁻¹ and the injection volume was set to 10 μ L. The electrospray ionization (ESI) and positive ion mode were used in the tandem quadrupole MS. Lincomycin was detected and quantified using a multiple reaction monitoring mode with a precursor/product transition of 407.2/126.2. The retention time was 2.37 min and the instrument detection limit of lincomycin was 0.2 pg.

The concentration of DOC released from the biochars were determined by our recently developed UV absorption method¹⁶⁰ with a Varian Cary 50 Bio UV-visible spectrophotometer (Varian, USA). We considered the biochar DOC was a mixture of the acid-soluble (AS) and acid-precipitable (AP) fractions and the fraction of AS can be calculated via:

$$f_{AS} = \frac{1.135e^{-2.813}}{e^{-1.797}} \quad (S4.1)$$

where f_{AS} is the proportion of the AS fraction ($0 \leq f_{AS} \leq 1$), and e is the E_2/E_3 ratio. The E_2/E_3 ratio was calculated as the ratio of decadic absorption coefficient (a , cm^{-1}) at 254 nm (a_{254}) to 365 nm (a_{365}), where the a was calculated by UV-vis absorbance (unitless) divided by path length (cm). If calculated f_{AS} value is < 0 or > 1 , it will be assumed to be 0 or 1, respectively. Then, the biochar DOC concentration in solution (in the unit of mg-C L^{-1}) can be calculated via:

$$\text{DOC} = \frac{\alpha_{254}}{0.0232f_{AS} + 0.0642(1-f_{AS})} \quad (\text{S4.2})$$

The DOC determined by the UV absorption method was generally in good agreement with the DOC measured by a total organic carbon (TOC) analyzer.

Mathematical Modeling

The experimental sorption kinetics were fitted to the intraparticle diffusion model (Eq. 4.1) or pseudo-second-order kinetic model (Eq. 4.2):^{73, 74, 161}

$$q_t = K_{id}t^{0.5} + C_{id} \quad (4.1)$$

$$\frac{t}{q_t} = \frac{t}{q_e} + \frac{1}{k_2 q_e^2} \quad (4.2)$$

where q_t ($\mu\text{g g}^{-1}$) is the sorbed lincomycin concentration in the solid phase at time t , K_{id} ($\mu\text{g g}^{-1} \text{day}^{-0.5}$) is the intraparticle diffusion rate constant, t (day) is the reaction time, C_{id} ($\mu\text{g g}^{-1}$) is the intercept constant that reflects the contribution from the rapid initial sorption, q_e ($\mu\text{g g}^{-1}$) is the sorbed lincomycin concentration at equilibrium, and k_2 ($\text{g } \mu\text{g}^{-1} \text{day}^{-1}$) is the pseudo-second-order rate constant.

According to Wu et al.,⁷³ the relative importance of intraparticle diffusion and initial sorption could be further analyzed based on following equations:

$$\left(\frac{q_t}{q_{ref}}\right) = 1 - R_{id} \left[1 - \left(\frac{t}{t_{ref}}\right)^{0.5}\right] \quad (4.3)$$

$$R_{id} = \frac{K_{id}t_{ref}^{0.5}}{q_{ref}} \quad (4.4)$$

where t_{ref} (day) is the longest time used when fitting the intraparticle diffusion model, q_{ref} ($\mu\text{g g}^{-1}$) is the sorbed lincomycin concentration in the solid phase at time t_{ref} , and R_{id} is the intraparticle diffusion factor that represents the relative contribution of the intraparticle diffusion to the total sorption.

The quasi-equilibrium sorption isotherms were fitted to the Freundlich model:¹⁶²

$$q_t = K_F C_t^N \quad (4.5)$$

where q_t ($\mu\text{g g}^{-1}$) is the sorbed lincomycin concentration in the solid phase at time t , C_t ($\mu\text{g L}^{-1}$) is the lincomycin concentration in the solution at time t , K_F ($\mu\text{g}^{1-N} \text{g}^{-1} \text{L}^N$) is the Freundlich sorption coefficient, and N (dimensionless) is the Freundlich nonlinearity factor.

RESULTS AND DISCUSSION

Characterization of Biochars.

The selected physicochemical properties of 17 tested slow-pyrolysis biochars are shown in Table 4.2. The volatile matter content (25.7–55.5%) decreased, whereas the fixed carbon content (0–62.1%) and the ash content (7.7–58.5%) increased with increasing pyrolysis temperature, due to increased carbonization of biomass at higher pyrolysis temperature.^{103, 136} The volatile matter and fixed carbon contents could approximate the labile and recalcitrant fractions of biochars, respectively.¹³⁶ In addition, the biochars produced from PM, CDM, and CDMW had a greater ash content (32.0–55.8%) than that from BM, DM, DDM, and WW (7.70–18.8%), which was attributed to the high ash content in their feedstock.¹⁶³ For biochars from the same feedstocks, the total C content (27.8–85.9%) increased, while total O (11.6–26.6%), H (0.4–4.9%), and N (0.4–2.6%) contents decreased with increasing pyrolysis temperature. Accordingly, the value of atomic ratios of H/C (0.17–0.97) and (O+N)/C (0.13–0.52) decreased at higher pyrolysis

temperature, suggesting that the high-temperature biochars had more condensed aromatic structures and less polar functional groups.^{36, 49, 136}

The SSA and V_{mic} of the tested biochars ranged from 42.8–243 m² g⁻¹ and 0.02–0.12 cm³ g⁻¹, respectively, and generally increased with increasing pyrolysis temperature. The SSA of the biochars was positively correlated with their fixed carbon ($r = 0.90$) and total carbon contents ($r = 0.92$), but negatively correlated with their volatile matter ($r = -0.62$) and ash contents ($r = -0.74$) (Figure 4.2). In agreement with Sun et al.,³⁰ this observation suggests that the SSA of the biochars was mainly contributed by the carbonized fraction in the biochar matrix, other than the uncarbonized or ash fractions. The SEM images of BM300 and BM600 revealed that the biochar pores were irregular in shape, and heterogeneous in pore size distribution from nanometers to micrometers (Figure 4.3). The majority of macroporous structures originated from the feedstock pore structure remained relatively similar for BM300 and BM600. But the abundance of finer nanopores and smoother external surface was greater for BM600 (Figure 4.3), which was in line with the increase of SSA and V_{mic} . Furthermore, the coarse amorphous substance accumulated on the surface of BM300 was presumably formed by the labile carbon compounds (i.e. volatile compounds or DOC) due to the incomplete pyrolysis that is absent at higher pyrolysis temperature. Finally, the zeta potential of tested biochars ranged from -64 to -43 mV at solution pH of 10 and ionic strength of 0.02 M (Table 4.2), indicating that the biochars carried net negative surface charge under the experimental conditions.

Table 4.2. Selected properties of biochar and graphite samples.

Samples	Proximate analysis ^a			Ultimate analysis ^a				Atomic ratio		SSA ^d m ² g ⁻¹	V _{mic} ^e cm ³ g ⁻¹	ZP ^f mV
	VM ^b	Ash	FC ^c	C	O	H	N	H/C	(O+N)/C			
	%	%	%	%	%	%	%					
BM300	55.5	7.7	36.8	60.6	26.6	4.9	1.3	0.97	0.35	125	0.08	-54
BM400	37.0	9.4	53.7	68.5	17.4	3.5	1.2	0.61	0.21	160	0.09	-50
BM500	30.5	10.4	59.2	74.1	17.4	2.6	1.1	0.42	0.19	196	0.10	-58
BM600	30.0	10.6	59.4	76.0	14.3	1.8	0.8	0.28	0.15	237	0.12	-57
DM300	45.4	10.1	44.5	61.5	22.6	4.5	1.6	0.88	0.30	112	0.07	-61
DM400	39.1	11.5	49.5	67.1	16.8	3.3	1.4	0.59	0.21	148	0.08	-58
DM600	30.7	12.6	56.6	75.2	11.6	2.0	1.3	0.32	0.13	221	0.11	-63
PM300	46.8	46.7	6.5	31.9	16.9	2.2	2.3	0.83	0.46	46.8	0.03	-45
PM400	43.8	51.7	4.5	32.1	14.3	0.7	1.2	0.26	0.37	42.8	0.03	-48
PM500	43.2	52.6	4.2	27.8	17.9	0.5	1.1	0.22	0.52	53.1	0.03	-43
PM600	44.2	55.8	0.0	28.7	14.3	0.4	0.9	0.17	0.40	47.0	0.02	-43
RDM500	33.0	32.0	35.0	51.2	n/a ^g	n/a	2.1	n/a	n/a	112	0.06	-52
DDM500	42.7	14.7	42.6	59.4	n/a	n/a	2.6	n/a	n/a	110	0.06	-60
DDM600	39.4	18.8	41.7	62.8	n/a	n/a	2.2	n/a	n/a	183	0.09	-58
CDM500	33.0	50.1	16.9	37.8	n/a	n/a	2.0	n/a	n/a	88.9	0.05	-50
CDMW500	25.7	58.5	15.8	74.0	n/a	n/a	0.6	n/a	n/a	129	0.06	-56
WW500	26.9	10.9	62.1	85.9	n/a	n/a	0.4	n/a	n/a	243	0.12	-64
Graphite	n/a	n/a	n/a	n/a	n/a	n/a	n/a	n/a	n/a	n/a	n/a	-60

^a Data adapted from Enders et al., 2012 and Rajkovich et al., 2012.^{28, 71}; ^b VM: volatile matter; ^c FC: fixed carbon; ^d SSA: specific surface area, measured by the BET-CO₂ method; ^e V_{mic}: micropore volume, calculated using Dubinin-Astakhov method; ^f ZP: zeta potential, sorbent suspension were measured at pH 10 in 0.02 M ionic strength of background solution (6.7 mM NaCl, 2.5 mM Na₂CO₃, 2.5 mM NaHCO₃, and 200 mg L⁻¹ NaN₃); ^g n/a: not available.

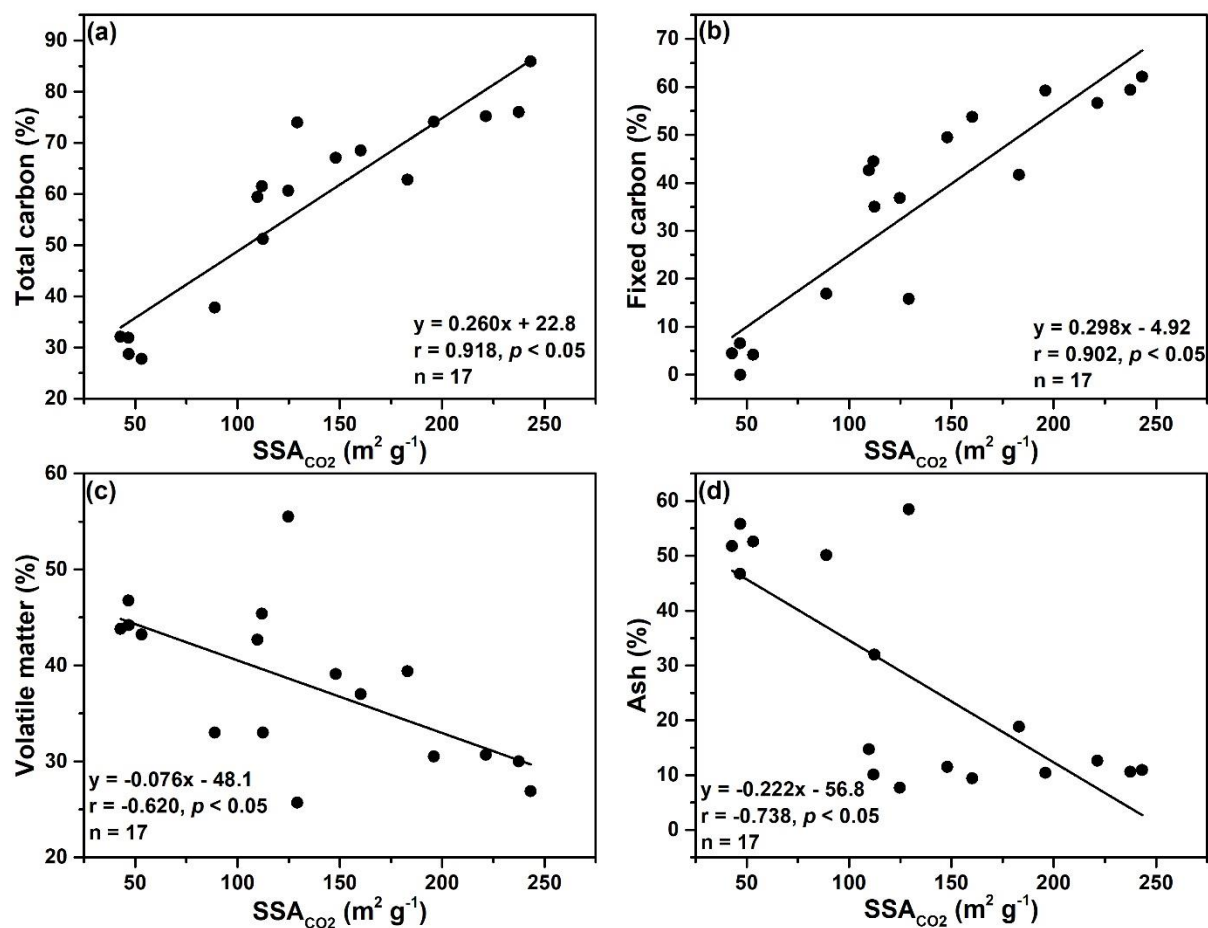


Figure 4.2. The relationship of (a) total carbon, (b) fixed carbon, (c) volatile matter, and (d) ash contents versus CO₂-BET specific surface area for biochars.

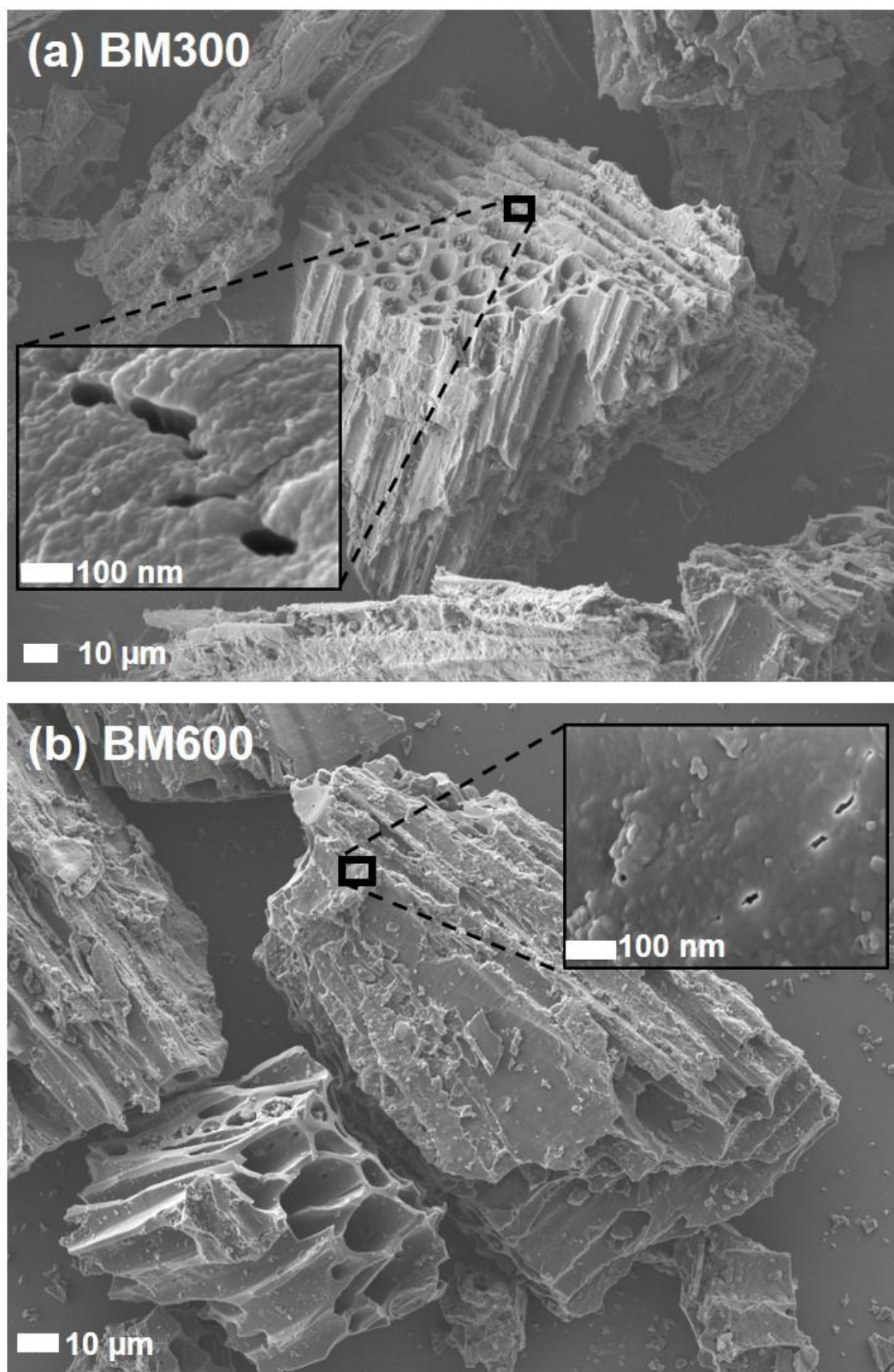


Figure 4.3. Scanning electron microscopy images of raw biochars: (a) BM300 (bull manure biochar produced at 300 °C) and (b) BM600 (bull manure biochar produced at 600 °C).

Long-term Sorption Kinetics

As shown in Figure 4.4, the lincomycin sorption onto the biochars occurred rapidly in the initial sorption phase (within the first day), followed by a slower sorption that gradually increased over the long term (up to 365 days). Approximately 7–34 % of initially applied lincomycin was removed by the biochars after 1 day, whereas up to 84–100 % (with the exception of 54% for PM400) of that was removed by 365 days. The lincomycin sorption kinetics could approach an apparent sorption equilibrium at the equilibration time of 60–365 days, except for BM500, PM400, PM500, and CDM500 that did not reach equilibrium by the end of the experiments (i.e., 365 days). Considering the porous nature of biochars, the fast initial sorption was primarily attributed to the instantaneous or very rapid sorption on the external surface of biochars that provides readily accessible sorption sites for lincomycin. The subsequent long-term slow sorption was mainly caused by the relatively slower intraparticle diffusion into the internal biochar pore structures that provide abundant sorption sites, but require longer time for lincomycin to access.³² As a comparison, the sorption of lincomycin onto the nonporous graphite reached a sorption equilibrium within 1 day and remained unchanged for 30 days due to the lack of pore structures (Figure 4.5). The significant difference in the sorption behaviors between the porous biochars and the nonporous graphite further supported that the sorption of lincomycin to the biochars was controlled by fast surface sorption in the short term and slow intraparticle diffusion in the long term.

The tested biochars had different sorption kinetics, presumably due to the heterogeneity in their pore structures and surface chemistries. Overall, the sorption kinetics decreased in the order: BM300 > BM400 \approx BM600 > BM500 (Figure 4.4a), DM300 \approx DM600 > DM400 (Figure 4.4b), and PM600 > PM300 > PM500 > PM400 (Figure 4.4c) and DDM500 > DDM600 \approx RDW500 > WW500 > CDMW500 > CDM500 (Figure 4.4d). Specifically, although the biochars produced at

higher temperature (i.e. 400–600 °C) generally had faster sorption kinetics in the initial sorption phase, lower-temperature (300 °C) biochars generally exhibited faster sorption kinetics and reached the apparent equilibrium more quickly in the following long-term sorption phase. The sorption kinetics prior to the apparent sorption equilibrium were well fitted by the Weber-Morris intraparticle diffusion model for all tested biochars ($R^2 = 0.940\text{--}0.998$) (Table 4.3). The K_{id} and C_{id} values were in the range of $25.3\text{--}166 \mu\text{g g}^{-1} \text{day}^{-0.5}$ and $39.0\text{--}339 \mu\text{g g}^{-1}$, respectively.

Table 4.3. Fitted parameters of the intraparticle diffusion model for the long-term sorption kinetics of lincomycin by the biochars.^a

Samples	t_{ref}	K_{id}	C_{id}	R_{id}	R^2
	day	$\mu\text{g g}^{-1} \text{day}^{-0.5}$	$\mu\text{g g}^{-1}$		
BM300	30	166	90.6	0.903	0.940
BM400	180	61.7	137	0.852	0.989
BM500	365	43.2	115	0.876	0.998
BM600	180	55.3	180	0.801	0.996
DM300	90	109	53.5	0.946	0.944
DM400	300	50.5	145	0.847	0.975
DM600	90	88.6	205	0.789	0.972
PM300	240	54.1	68.6	0.924	0.984
PM400	365	25.3	39.0	0.928	0.975
PM500	365	35.1	162	0.807	0.993
PM600	180	49.4	262	0.719	0.994
RDM500	180	62.1	162	0.829	0.983
DDM500	180	62.9	209	0.789	0.982
DDM600	180	44.8	339	0.625	0.977
CDM500	365	42.4	124	0.864	0.994
CDMW500	300	47.5	162	0.824	0.987
WW500	240	48.4	211	0.768	0.989

^a t_{ref} : the longest time used when fitting the intraparticle diffusion model; K_{id} : the intraparticle diffusion rate constant; C_{id} : the intercept constant; and R_{id} : the intraparticle diffusion factor.

Interestingly, the C_{id} values showed a positive linear relationship (Figure 4.6a), while the K_{id} values exhibited a U-shaped relationship with increasing pyrolysis temperature from 300 to 600 °C (Figure 4.6b). For example, the average C_{id} values increased monotonically from $70.9 \pm 18.7 \mu\text{g g}^{-1}$, $107 \pm 59 \mu\text{g g}^{-1}$ and $164 \pm 37 \mu\text{g g}^{-1}$ to $247 \pm 71 \mu\text{g g}^{-1}$, whereas the K_{id} values followed the order of 300 °C ($110 \pm 56 \mu\text{g g}^{-1} \text{day}^{-0.5}$) > 600 °C ($59.5 \pm 19.8 \mu\text{g g}^{-1} \text{day}^{-0.5}$) > 500

$^{\circ}\text{C}$ ($48.8 \pm 10.3 \mu\text{g g}^{-1} \text{day}^{-0.5}$) \approx 400°C ($45.8 \pm 18.6 \mu\text{g g}^{-1} \text{day}^{-0.5}$) for the biochars produced at 300, 400, 500, 600 $^{\circ}\text{C}$, respectively. As the C_{id} values represent the initial surface sorption, this positive linear trend was expected because of the greater external surface area of higher-temperature biochars than that of lower-temperature biochars. Furthermore, the observed U-shaped relationship between K_{id} and pyrolysis temperature was unique, which cannot be explained by any measured physicochemical properties of biochars. The greater K_{id} of the higher-temperature biochars might result from more open and less blocked micropores (Figure 4.3 and Table 4.2). However, the greater K_{id} for the lower-temperature (300 $^{\circ}\text{C}$) biochars may be controlled by different mechanisms as elucidated later.

The R_{id} values could reflect the relative contribution of initial sorption and intraparticle diffusion to the total sorption. The R_{id} values closer to one indicate a dominant contribution from the intraparticle diffusion, whereas the R_{id} values closer to zero imply a primary contribution of initial sorption. According to Wu et al.,⁷³ the lincomycin sorption kinetics of BM300, DM300, PM300, and PM400 could be classified as a weak initial sorption and strong intraparticle diffusion ($1.0 > R_{\text{id}} > 0.9$). For the rest of the biochars produced at 400, 500, and 600 $^{\circ}\text{C}$, the lincomycin sorption kinetics could be classified as intermediate initial sorption and intraparticle diffusion ($0.9 > R_{\text{id}} > 0.5$). The R_{id} of all tested biochars ranged from 0.625 to 0.946, showing a negative correlation with pyrolysis temperature (Figure 4.6c). Thus, the relative contribution of initial sorption was more pronounced for the high-temperature biochars, presumably due to their greater SSA. As lincomycin exists as neutral species ($\sim 100\%$, $\text{pK}_a = 7.6$) in aqueous solution under experimental pH of 10, is very hydrophilic, and lacks π -electron donor or acceptor moieties (Table 4.1), lincomycin sorption to biochars was unlikely due to hydrophobic partition, electrostatic and π - π EDA interactions.⁹² Therefore, H-bonding, van der Waals forces, and pore diffusion could

reasonably be considered as possible mechanisms contributing to lincomycin sorption on biochars.⁹² Because lower-temperature biochars contained more oxygenic functional groups and lower SSA and micropore volume than higher-temperature biochars, the contribution of H-bonding may be more important for lincomycin sorption to the low-temperature biochars, whereas the van der Waals interaction may be more important for the high-temperature biochars. However, the different relative contribution of H-bonding and van der Waals interactions in lincomycin sorption still cannot explain why the greater K_{id} values were observed for the low-temperature biochars than for the intermediate-temperature biochars. To further examine possible mechanisms for this observation, we hypothesized that the release of DOC from biochars may play an important role in lincomycin sorption by biochars. As shown in Figure 4.7, the leachable DOC concentrations generally increased with decreasing pyrolysis temperature due to the higher labile carbon fraction. The biochars produced at 300–400 °C generally had greater leachable DOC content than the biochars produced at 500–600 °C with the exception of biochar from DDM feedstock. Thus, the continual and significant release of DOC from lower-temperature biochars probably enhanced their lincomycin sorption during the long-term sorption period by increasing the accessibility of internal pores that were initially blocked by DOC. To further investigate the observed enhancement of lincomycin sorption to the biochars of higher DOC concentration, more experiments were performed as discussed later.

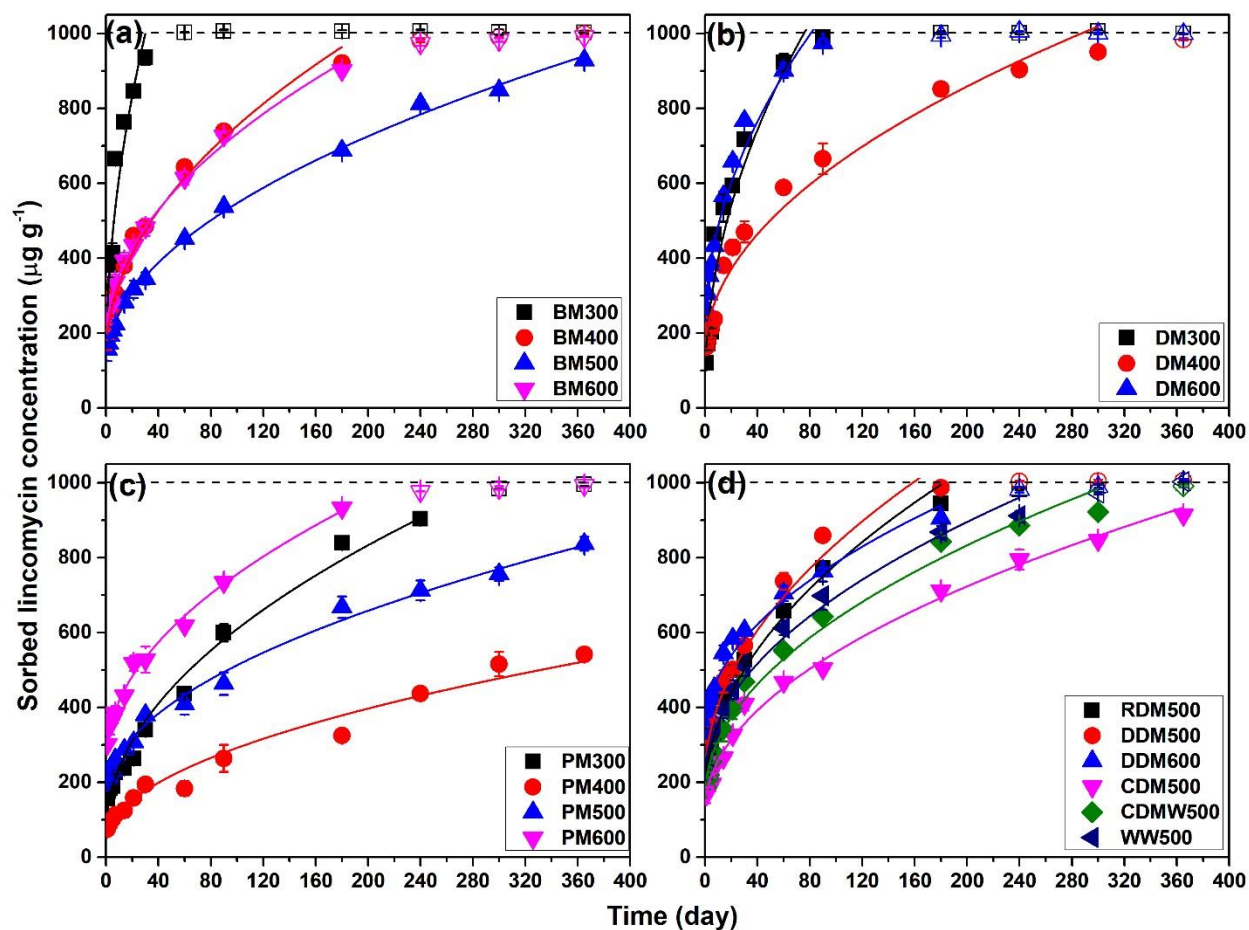


Figure 4.4. Long-term kinetics of lincomycin sorption by biochars. The sorption data were fitted by the intraparticle diffusion model (solid line), and the hollow data were excluded from the fitting because of reaching sorption saturation.

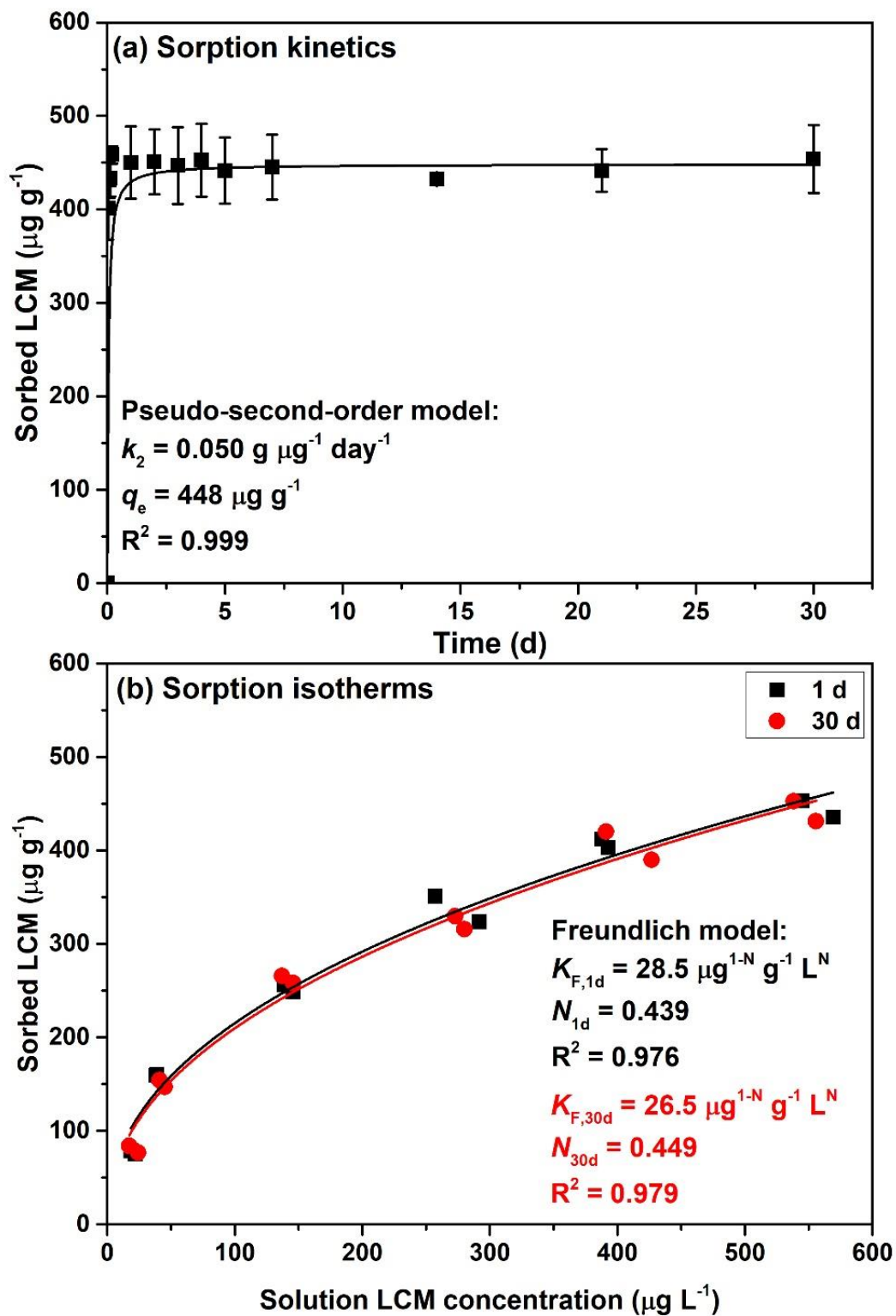


Figure 4.5. Sorption kinetics (a) and isotherms (b) of lincomycin to graphite. The solid lines were fitted by the pseudo-second-order model and the Freundlich model, respectively.

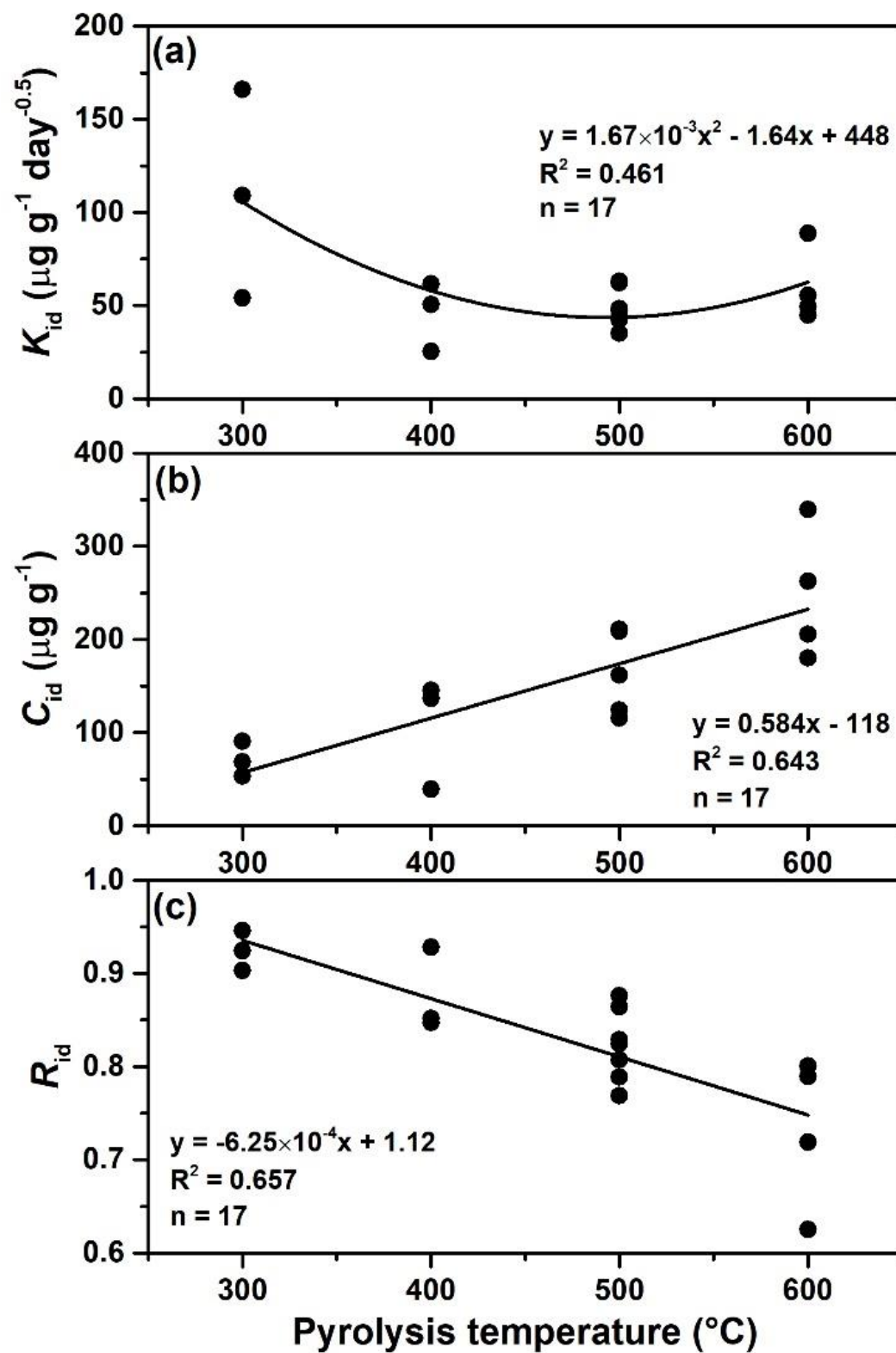


Figure 4.6. The relationship of (a) intraparticle diffusion rate constant (k_{id}), (b) initial sorption (C_{id}), and (c) interparticle diffusion factor (R_{id}) versus pyrolysis temperature for 17 biochars.

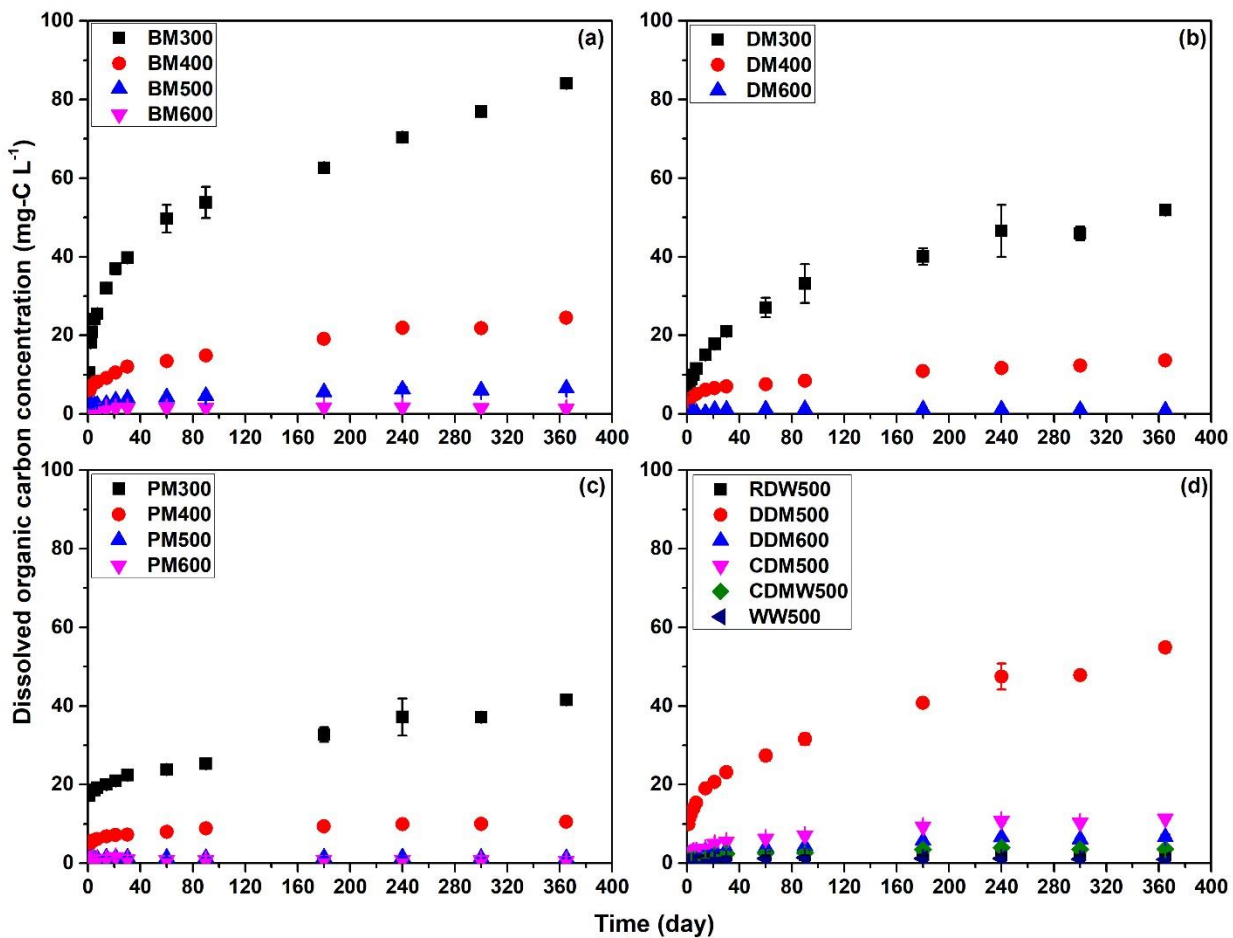


Figure 4.7. Long-term release of dissolved organic carbon from biochars.

Long-term Sorption Isotherms

The quasi-equilibrium isotherms of lincomycin to the 17 biochars with contact time of 1, 7, 30, and 365 days were all nonlinear and exhibited a concave-downward shape (Figure 4.8 and 4.9). All quasi-equilibrium isotherm data could be fitted reasonably well to the Freundlich model (Table 4.4). As expected, for all biochars the K_f values increased, but the N values decreased with increasing equilibration time. For example, the N values decreased from 0.727 at 1 day to 0.424 at 30 days for BM300 and from 0.510 at 1 day to 0.325 at 365 days for BM600 (Figure 4.8a and 4.8d). The lower N values (i.e., more nonlinear) observed at the longer equilibration time indicates a more heterogeneous distribution of the sorption sites in the biochars, which could be explained by the greater contribution of intraparticle pore diffusion allowing lincomycin molecules to interact with more heterogeneous pore space and sorptive sites. As a comparison, the sorption isotherms of lincomycin for the nonporous graphite at 1 day and 30 days were almost identical with similar K_f and N values due to the absence of intraparticle diffusion (Figure 4.5). This result further confirmed that the observed time-dependent lincomycin sorption isotherms were caused by increasing contribution of intraparticle diffusion.

Similar to the kinetic sorption data, there was an equilibration-time-dependent relationship between K_f or N values and pyrolysis temperature (Table 4.4 and Figure 4.10). The K_f values exhibited a positive linear relationship with pyrolysis temperature increasing from 300 to 600 °C for the equilibration time of 1 day, but gradually became the U-shaped relationship as the equilibration time increased to 7 and 30 days (Figure 4.10a). The N values exhibited a negative linear relationship with increasing pyrolysis temperature from 300 to 600 °C for the equilibration time of 1 day, but again gradually became an inverted U-shaped relationship as the equilibration time increased to 7 and 30 days (Figure 4.10b). The positive and negative linear relationship for

K_f and N with pyrolysis temperature at 1 day suggests that the lincomycin sorption to biochars became greater and more nonlinear at higher pyrolysis temperature, presumably due to greater SSA and more heterogeneous surface sorption sites.³⁹ More interestingly, at the longer equilibration time, the lower-temperature (i.e., 300 °C) biochar had greater sorption affinity and nonlinearity, likely resulted from enhanced intraparticle pore diffusion facilitated by the increasing release of DOC.

Table 4.4. Fitted parameters of the Freundlich model for quasi-equilibrium sorption isotherms of lincomycin on the biochars at 1, 7, 30, and 365 days.^a

Samples	1-d			7-d			30-d			365-d		
	K_F	N	R^2	K_F	N	R^2	K_F	N	R^2	K_F	N	R^2
BM300	1.49	0.727	0.945	30.3	0.554	0.974	237	0.424	0.955	n/a	n/a	n/a
BM400	1.64	0.691	0.942	5.54	0.626	0.943	10.4	0.572	0.893	454	0.290	0.920
BM500	4.54	0.556	0.874	7.21	0.524	0.976	12.2	0.514	0.952	73.0	0.483	0.958
BM600	7.57	0.510	0.961	16.4	0.480	0.962	26.9	0.460	0.971	282	0.325	0.924
DM300	0.827	0.690	0.873	22.0	0.513	0.951	65.9	0.459	0.887	n/a	n/a	n/a
DM400	2.51	0.609	0.854	4.10	0.590	0.957	13.6	0.537	0.969	146	0.480	0.957
DM600	10.3	0.483	0.895	38.0	0.397	0.915	104	0.369	0.966	n/a	n/a	n/a
PM300	1.39	0.688	0.922	4.68	0.599	0.946	8.37	0.552	0.959	215	0.407	0.957
PM400	1.21	0.559	0.858	3.22	0.531	0.889	6.44	0.531	0.968	20.5	0.524	0.978
PM500	4.86	0.541	0.939	11.2	0.490	0.952	19.5	0.476	0.966	89.7	0.402	0.929
PM600	12.5	0.493	0.907	18.9	0.479	0.971	45.6	0.414	0.931	312	0.348	0.914
RDM500	6.05	0.519	0.876	14.3	0.479	0.919	29.4	0.456	0.946	359	0.367	0.912
DDM500	6.76	0.554	0.905	12.9	0.513	0.973	38.2	0.413	0.922	n/a	n/a	n/a
DDM600	15.4	0.482	0.917	22.7	0.479	0.957	46.4	0.435	0.970	302	0.340	0.915
CDM500	3.25	0.543	0.791	8.30	0.523	0.954	14.2	0.516	0.962	77.1	0.478	0.915
CDMW500	4.10	0.540	0.834	9.38	0.511	0.947	19.4	0.498	0.935	127	0.434	0.930
WW500	5.66	0.525	0.860	19.8	0.438	0.926	40.2	0.415	0.927	187	0.403	0.915

^a K_F : Freundlich sorption coefficient ($\mu\text{g}^{1-N} \text{g}^{-1} \text{L}^N$); N : Freundlich heterogeneity factor; and n/a: fitted parameters were not available because the concentrations of lincomycin in solution were below detection limit.

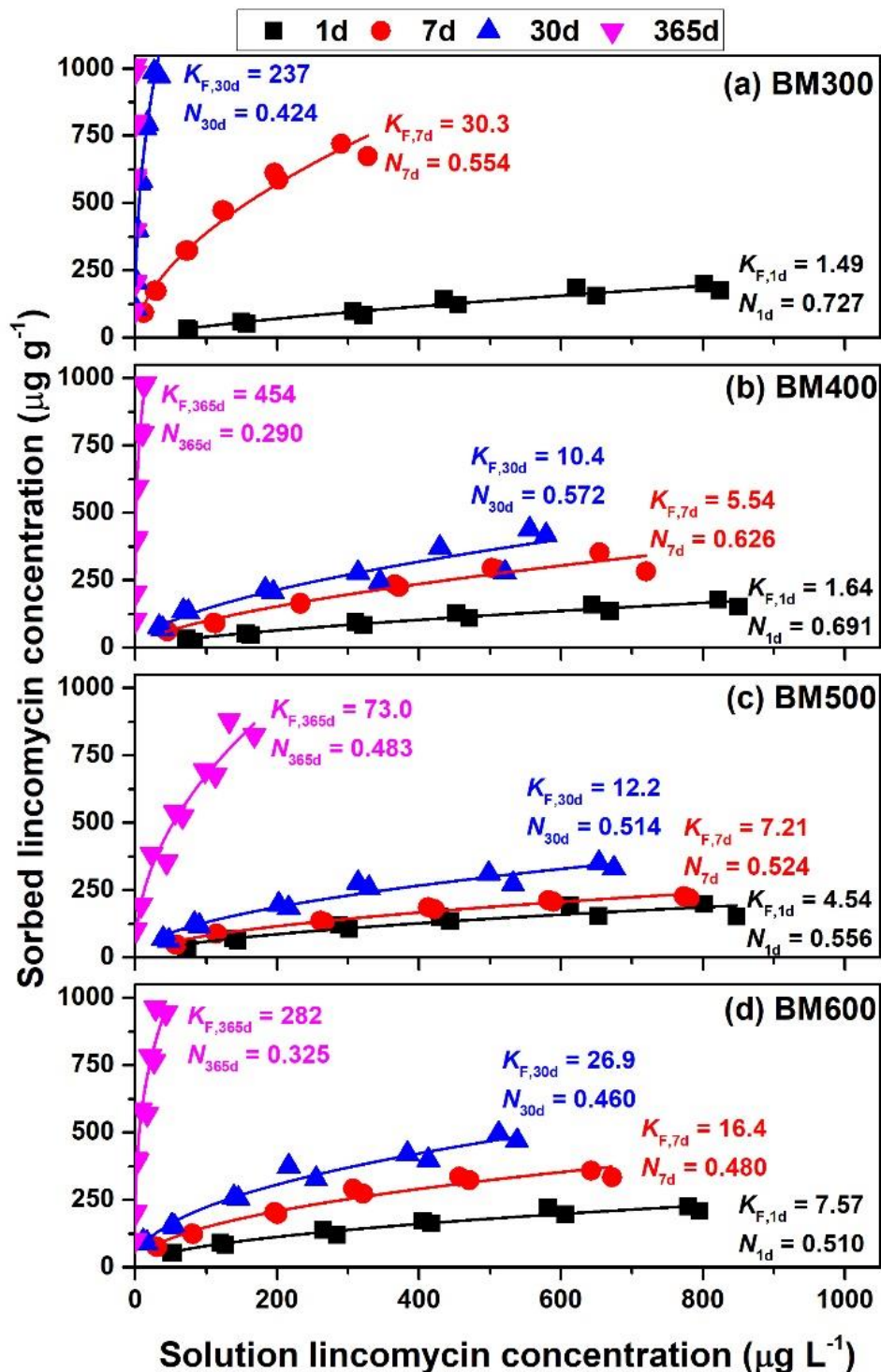


Figure 4.8. Quasi-equilibrium sorption isotherms of lincomycin by bull manure-based biochars produced at different temperature: (a) BM300, (b) BM400, (c) BM500, and (d) BM600. K_F ($\mu\text{g}^{1-N} \text{g}^{-1} \text{L}^N$) is the Freundlich sorption coefficient, and N (dimensionless) is the Freundlich nonlinearity factor.

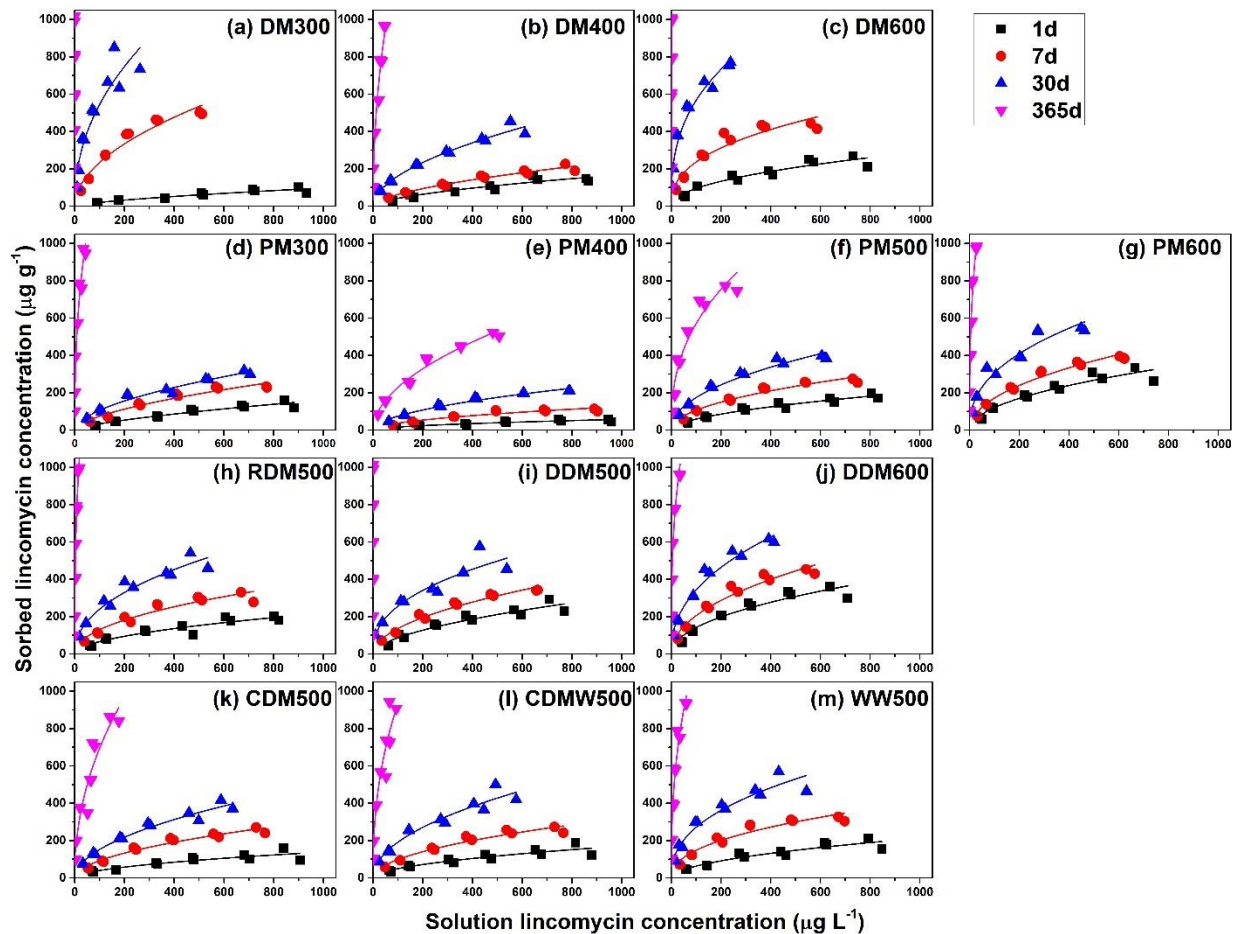


Figure 4.9. Quasi-equilibrium sorption isotherms of lincomycin to biochars: (a) DM300, (b) DM400, (c) DM600, (d) PM300, (e) PM400, (f) PM500, (g) PM600, (h) RDM500, (i) DDM500, (j) DDM600, (k) CDM500, (l) CDMW500, and (m) WW500. The solid lines were fitted with the Freundlich isotherm model.

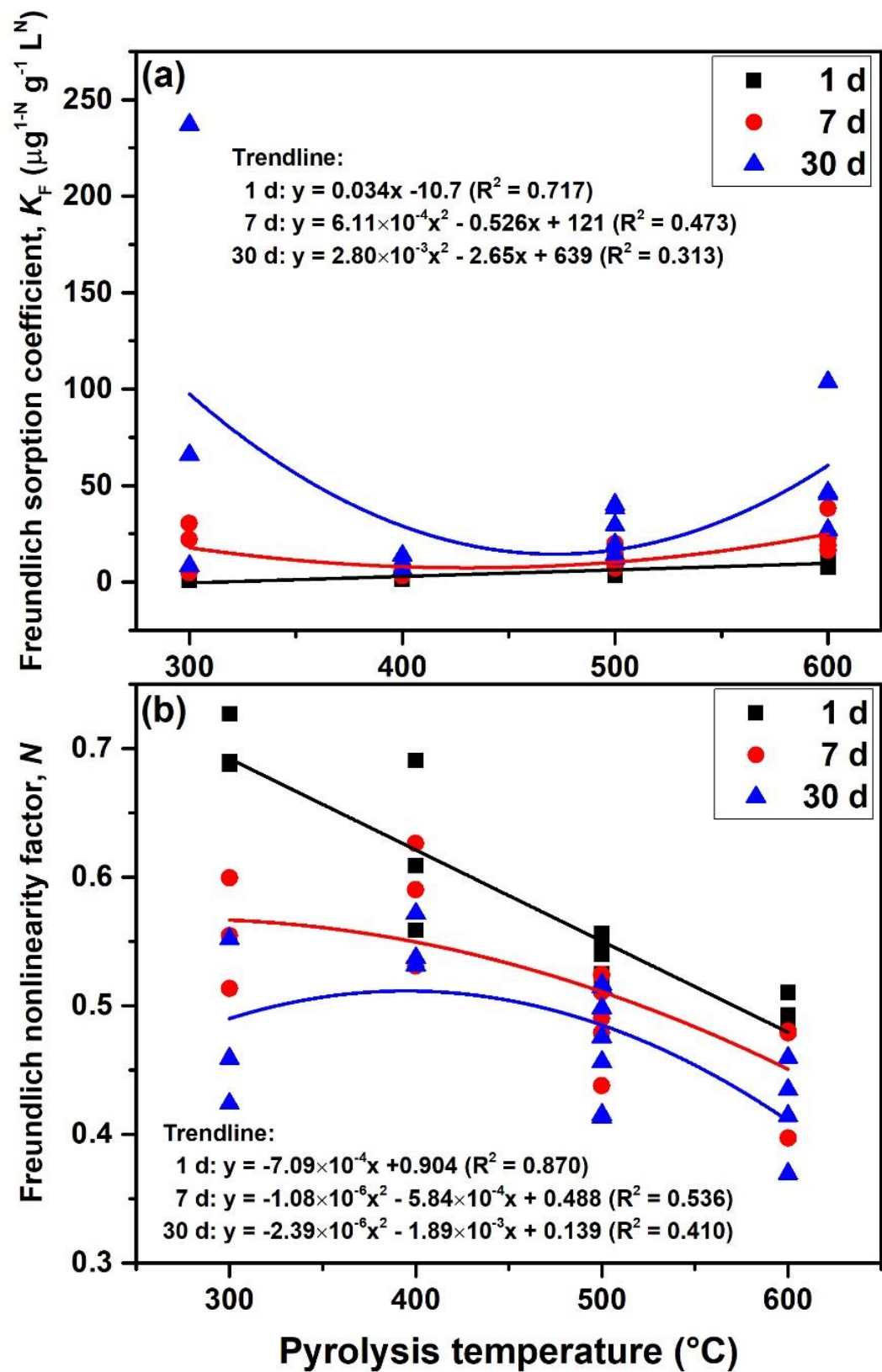


Figure 4.10. The relationship of Freundlich sorption coefficient (K_F) and Freundlich nonlinearity factor (N) versus pyrolysis temperature for biochars.

Effects of DOC on Sorption

We first hypothesized that lincomycin might bind with the DOC in solution. If so, the lincomycin sorption to biochars could be overestimated when the DOC-bound lincomycin was included into the lincomycin sorption to biochars. At the initial lincomycin concentration of 1000 $\mu\text{g/L}$, 15, 6.0, 5.8, and 3.0 % of initially applied lincomycin was bound to DOC-BM300, DOC-DM300, DOC-PM300, and DOC-DDM500 of 186, 93.8, 97.4, and 89.6 mg-C L^{-1} , respectively. The distribution coefficients of lincomycin to DOC-BM300, DOC-DM300, DOC-PM300, and DOC-DDM500 were 955, 686, 631, and 348 L kg-C^{-1} , respectively. Based on the DOC release kinetics (Figure 4.7), the DOC concentrations from 1 day to 365 days in the kinetic sorption experiments were 10.5–84.1, 6.35–51.9, 17.2–41.6, and 10.0–54.9 mg-C L^{-1} for BM300, DM300, PM300, and DDM500, respectively. Even assuming all released DOC could bind with lincomycin in solution, the fraction of the DOC-bound lincomycin was only 0.9–6.8%, 0.4–3.3%, 1.0–2.5%, and 0.3–1.9% of the initially applied amount for DOC-BM300, DOC-DM300, DOC-PM300, and DOC-DDM500, respectively. Therefore, the contribution of lincomycin sorption to DOC in solution could not explain the enhanced lincomycin sorption to biochars over time.

Secondly, we hypothesized that the DOC as co-solute in solution might facilitate the lincomycin sorption to biochars. However, the presence of DOC as co-solute actually inhibited the lincomycin sorption onto WW500 (Figure 4.11). Comparing with lincomycin sorption kinetics without DOC, the fitted K_{id} value decreased from 55.2 to 13.3–29.1 $\mu\text{g g}^{-1} \text{day}^{-0.5}$ and the fitted C_{id} value decreased from 178 to 70.5–85.6 $\mu\text{g g}^{-1}$ in the presence of DOC (Table 4.5). The extent of sorption suppression followed the order of $\text{DOC-BM300} \approx \text{DOC-PM300} > \text{DOC-DM300} > \text{DOC-DDM500}$, which generally (but not completely) agreed with the DOC concentration trend ($\text{DOC-BM300} > \text{DOC-DM300} > \text{DOC-DDM500} > \text{DOC-PM300}$). Thus, the inhibitory effect of

DOC in solution depends on not only the concentration, but also the chemical composition of DOC. The observed slower diffusion rate and lower initial sorption confirmed that the DOC could not enhance the lincomycin sorption by itself. In contrary, the DOC in solution strongly suppressed the lincomycin sorption by blocking the pore entrances (i.e., decreased K_{id}) and/or by competing for the external surface sorption sites (i.e., decreased C_{id}) in biochars.

Table 4.5. Fitted parameters of the intraparticle diffusion model for the sorption kinetics of lincomycin by woodchip waste biochar.^a

Samples	t_{ref}	K_{id}	C_{id}	R_{id}	R^2
	day	$\mu\text{g g}^{-1} \text{day}^{-0.5}$	$\mu\text{g g}^{-1}$		
WW500+DI	60	55.2	178	0.705	0.997
WW500+DOC(BM300)	60	13.3	80.3	0.535	0.678
WW500+DOC(DM300)	60	29.1	70.5	0.767	0.951
WW500+DOC(PM300)	60	15.0	71.1	0.598	0.743
WW500+DOC(DDM500)	60	23.1	85.6	0.648	0.931

^a t_{ref} : the longest time used when fitting the intraparticle diffusion model; K_{id} : the intraparticle diffusion rate constant; C_{id} : the intercept constant; and R_{id} : the intraparticle diffusion factor.

We finally tested the hypothesis in that the long-term release of DOC might gradually increase the accessibility of sorption sites on the external surface and in the biochar pore structure, thus enhancing their sorption ability for lincomycin. Therefore, the sorption kinetics of lincomycin by raw, 40-day-DI-washed, and 1-day-NaOH-washed biochars (selected BM300, DM300, PM300, DDM500, BM600) were analyzed (Figure 4.12, Figure 4.13 and Table 4.6). Apparently, the removal of DOC from the biochars (BM300, DM300, PM300, and DDM500) substantially enhanced the lincomycin sorption kinetics (Figure 4.12), and the DOC removal with NaOH solution was more effective than that with DI water for the enhancement of sorption kinetics (Figure 4.12). In addition, the fitted K_{id} and C_{id} values both increased after the DOC removal for these tested biochars (Table 4.6). For example, the K_{id} values were 160, 166 and 176 $\mu\text{g g}^{-1} \text{day}^{-0.5}$ and the C_{id} values were 87.9, 285 and 527 $\mu\text{g g}^{-1}$ for BM300-Raw, BM300-DI, and BM300-NaOH biochars, respectively. The enhancement of lincomycin sorption kinetics by the DOC removal was

very limited for BM600 (Figure 4.12c). Considering that BM600 was highly carbonized, and had a relatively low DOC content and rigid pore structure, the DOC removal would not substantially alter the surface sorption sites and pore structure of BM600, resulting in minimal enhancement of the sorption kinetics. Furthermore, a close examination of SEM images revealed that the biochar particles of low-temperature biochars (e.g., BM300) were disintegrated, and the biochar particle size appeared to decrease after aging in 0.02 M background solution for 365-d and in 0.1 M NaOH solution for 1-d, presumably because of the DOC release from the biochars (Figure 4.14). We further compared the size of biochar colloids by aging BM300 and BM600 biochars in either 0.1 M NaOH or 0.1 M NaCl solution (Figure 4.15). The size of biochar colloids was much smaller in 0.1 M NaOH than in 0.1 M NaCl for BM300, whereas no obvious difference was observed for BM600. In summary, these results supported that the release of DOC from biochars could enhance the lincomycin sorption on biochars because of increased accessibility of sorption sites initially blocked by DOC on the external surface and in pore structure as well as decreased biochar particle sizes.

Table 4.6. Fitted parameters of the intraparticle diffusion model for the sorption kinetics of lincomycin by raw-, DI-water-washed, and 0.01M-NaOH-washed biochars.^a

Samples	t_{ref}	K_{id}	C_{id}	R_{id}	R^2
	day	$\mu\text{g g}^{-1} \text{day}^{-0.5}$	$\mu\text{g g}^{-1}$		
BM300-Raw	30	160	87.9	0.904	0.968
BM300-DI	15	166	285	0.694	1.000
BM300-NaOH	7	176	527	0.460	0.985
DM300-Raw	60	113	49.8	0.945	0.984
DM300-DI	30	148	99.1	0.894	0.990
DM300-NaOH	10	172	381	0.587	1.000
PM300-Raw	60	51.3	83.1	0.831	0.995
PM300-DI	60	68.1	131	0.811	0.976
DDM500-Raw	60	74.1	164	0.781	0.994
DDM500-DI	60	98.5	191	0.800	0.999
BM600-Raw	60	53.8	174	0.710	0.993
BM600-DI	60	52.2	175	0.705	0.983
BM600-NaOH	60	55.9	203	0.685	0.996

^a t_{ref} : the longest time used when fitting the intraparticle diffusion model; K_{id} : the intraparticle diffusion rate constant; C_{id} : the intercept constant; and R_{id} : the intraparticle diffusion factor.

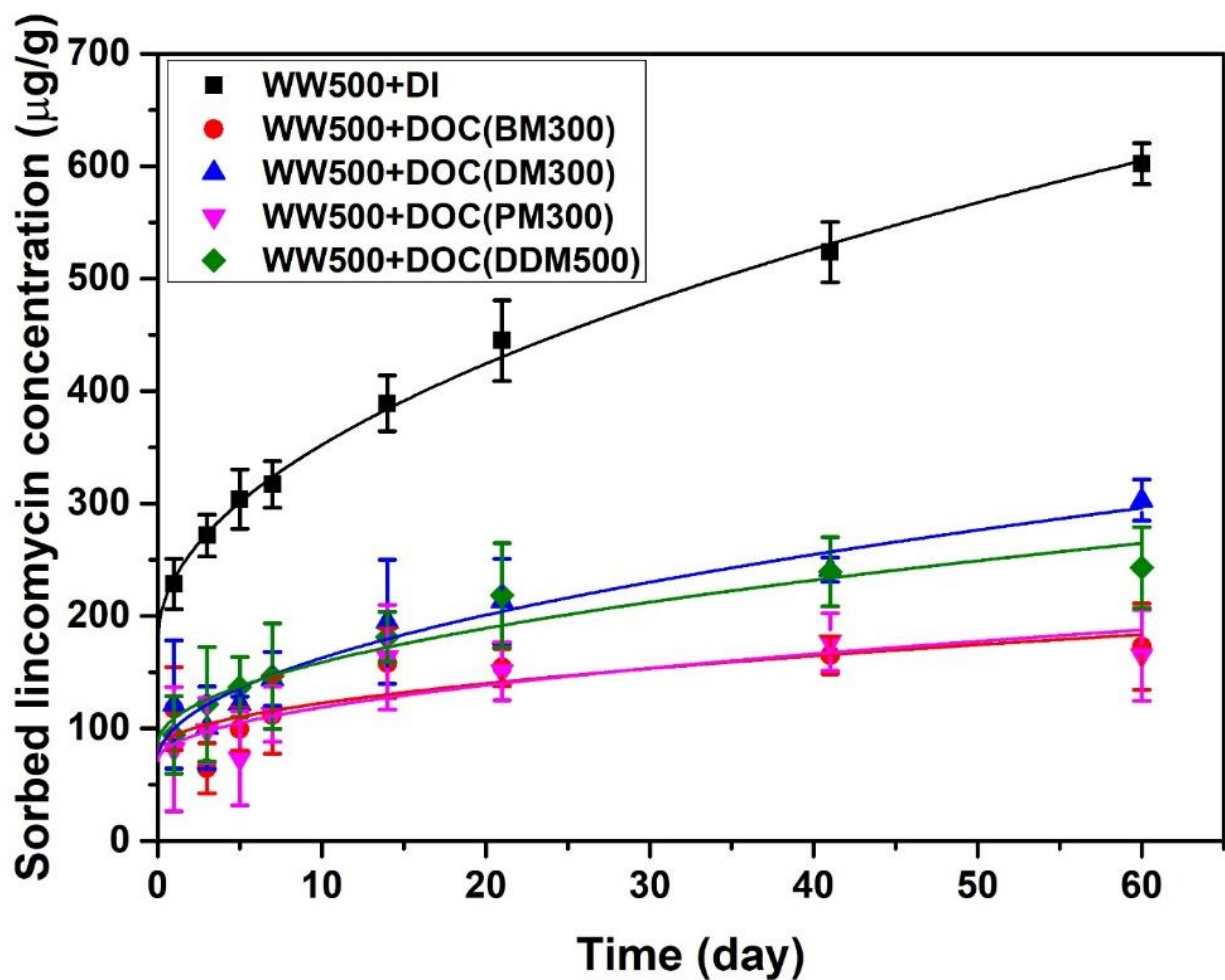


Figure 4.11. The effect of DOC as co-solutes on sorption kinetics of lincomycin by WW500 biochar (WW500+DI was the control of absence DOC).

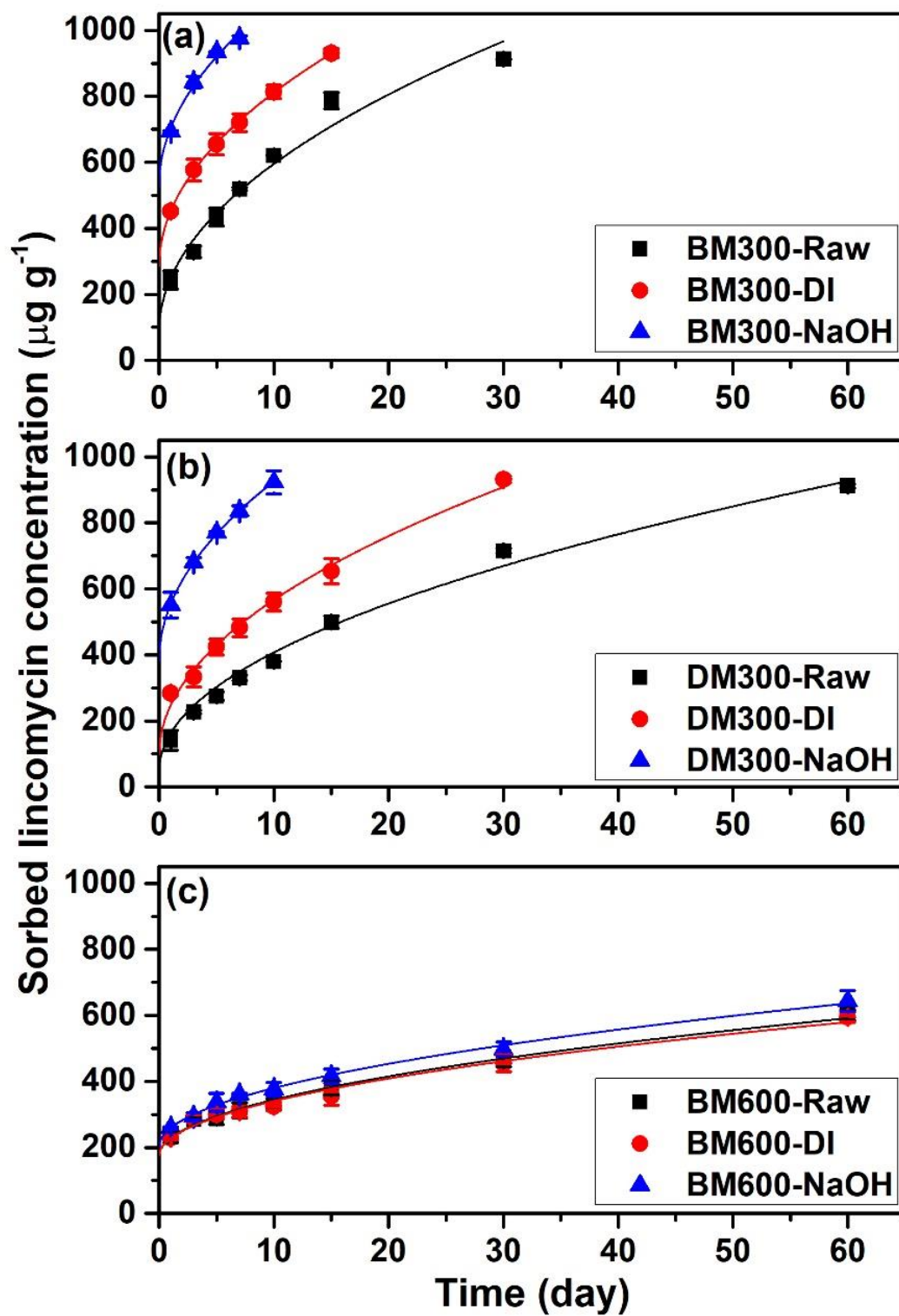


Figure 4.12. Long-term kinetics of lincomycin sorption by raw and DOC-washed biochars. The sorption data were fitted by intraparticle diffusion model (solid line).

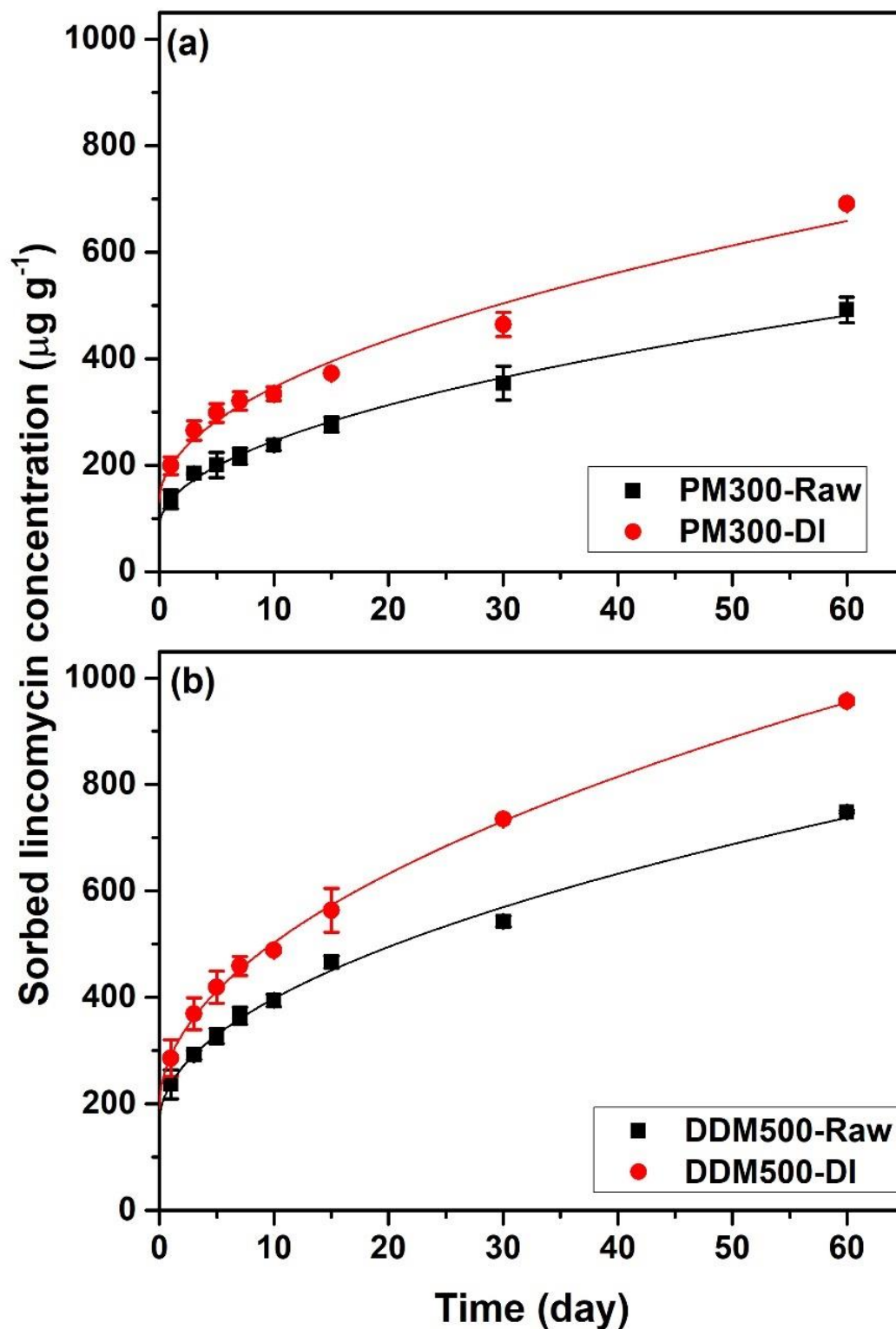


Figure 4.13. Long-term kinetics of lincomycin sorption by raw and DOC-washed biochars. The sorption data were fitted by the intraparticle diffusion model (solid line) and the hollow data were excluded because of approaching sorption saturation.

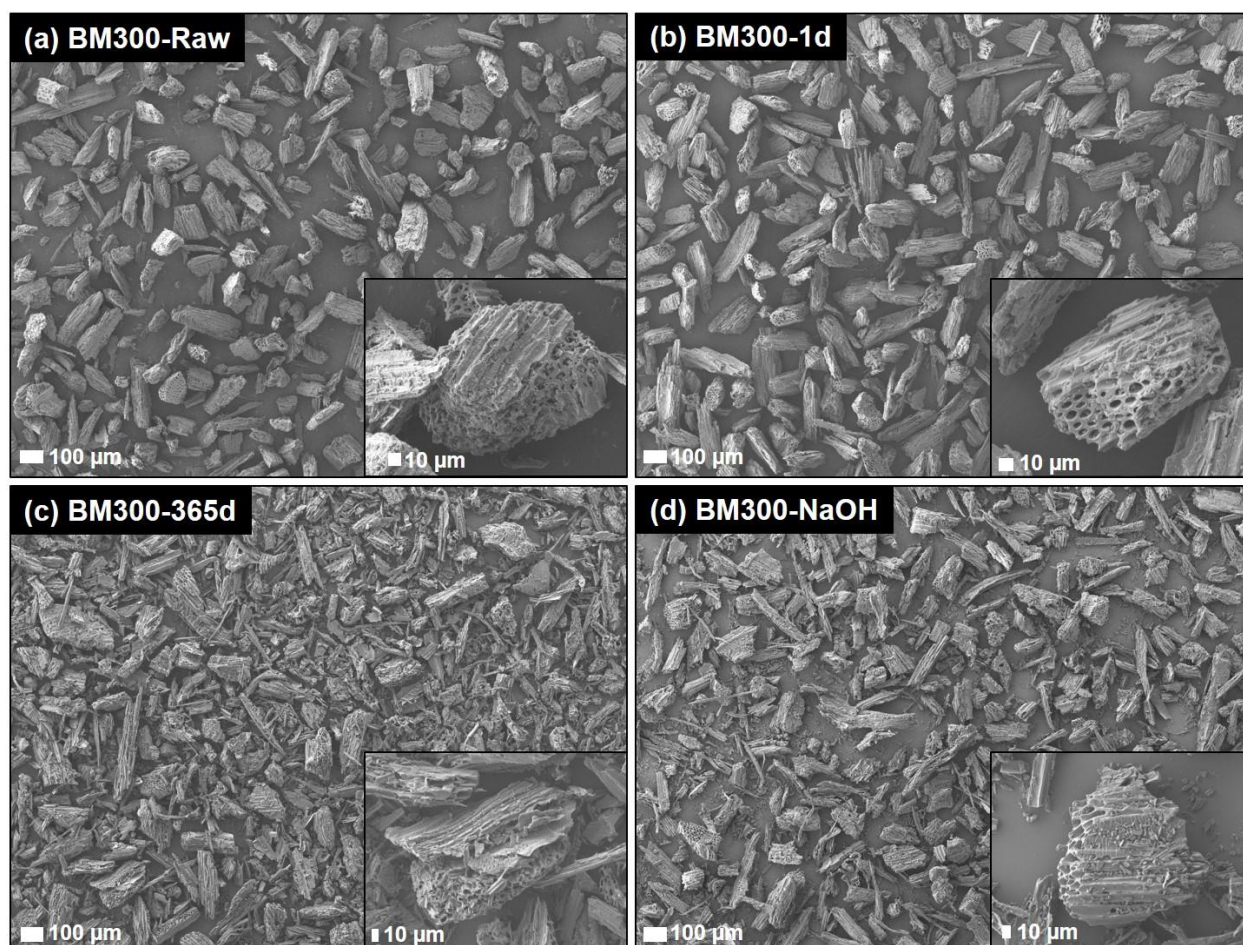


Figure 4.14. Scanning electron microscopy images of bull manure biochar pyrolyzed at 300°C (BM300): (a) raw BM300 without treatment, (b) BM300 after 1-d background solution exposure, (c) BM300 after 365-d background solution exposure, and (d) BM300 after 1-d 0.1M NaOH solution exposure. Background solution contained 1000 µg L⁻¹ lincomycin, 6.7 mM NaCl, 2.5 mM Na₂CO₃, 2.5 mM NaHCO₃, and 200 mg L⁻¹ NaN₃.

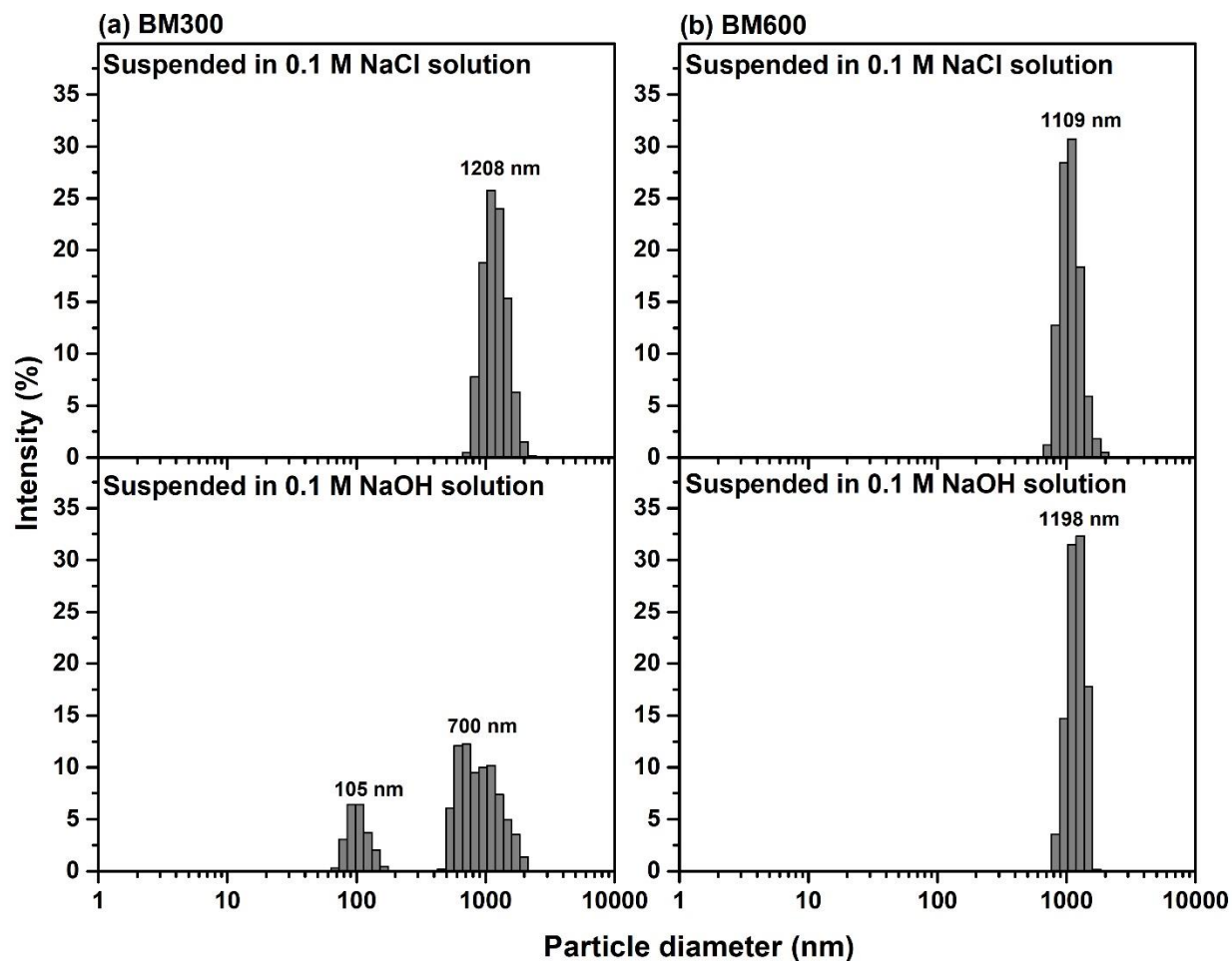


Figure 4.15. Particles size distribution of (a) bull manure biochar pyrolyzed at 300°C (BM300) and (b) bull manure biochar pyrolyzed at 600°C (BM600) suspended in 0.1 M NaCl (upper panel) or in 0.1 M NaOH (lower panel) after one-day exposure.

Desorption Hysteresis

As shown in Figure 4.16a, the extraction recoveries of lincomycin for all tested biochars were generally low. The degree of desorption hysteresis varied among the biochars, with the extraction recoveries ranging from the lowest of 0.02% for BM300 to the highest of 24.7% for PM500. Thus, the long-term sorbed lincomycin on the biochars was highly resistant to desorption. In addition, the extraction recoveries exhibited a negative logarithmic correlation with the K_{id} ($R^2 = 0.721$) (Figure 4.16b), implying that faster pore diffusion would cause stronger desorption hysteresis. This observation was presumably because lincomycin could diffuse deeper into the biochar pores and become trapped in the narrower pores, resulting in lower extraction efficiency. From the standpoint of soil biochar amendment for contaminant immobilization, the observed strong sorption/desorption hysteresis for lincomycin may be desirable because the sorbed lincomycin would tend to remain within the biochars over the long term, thus reducing the mobility and bioavailability of lincomycin in soils.

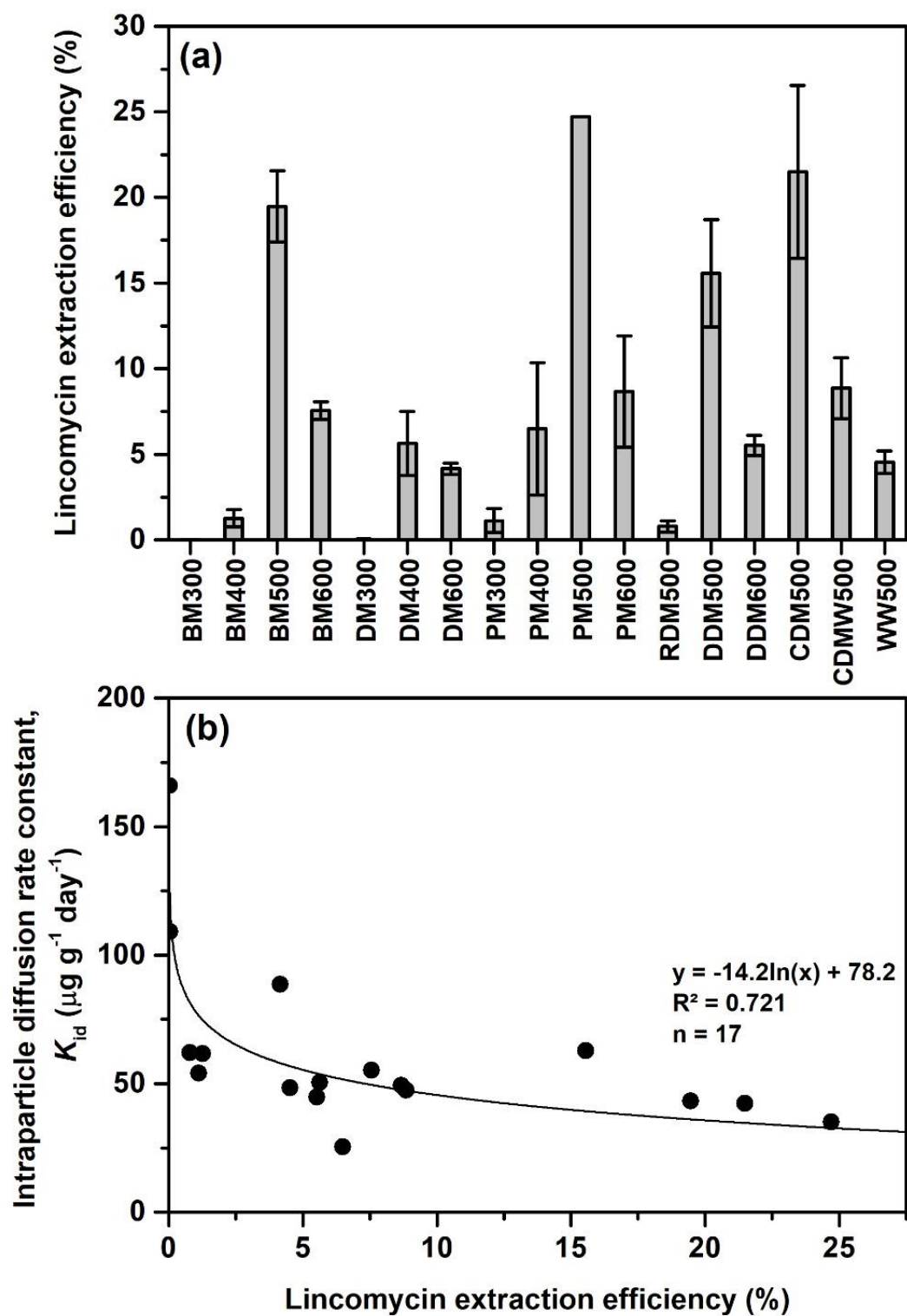


Figure 4.16. (a) Extraction efficiency of 240 d-sorbed lincomycin in the biochars and (b) the relationship of intraparticle diffusion rate constant (K_{id}) versus lincomycin extraction efficiency for biochars.

Implications

We have previously proposed that sequestering manure-borne antibiotics in soils by biochars produced from animal manure may be a novel mitigation strategy for managing animal manures and manure-borne antibiotics.⁹² On one hand, using manure as feedstock to produce biochars could destroy any microbial pathogen and antibiotics via pyrolysis (i.e. 300 to 600 °C). On the other hand, the produced biochars could be applied in soils to reduce the mobility and bioavailability of anthropogenic antibiotics. Under the same tested concentration range (0–1000 $\mu\text{g L}^{-1}$), the observed K_f values of lincomycin on tested biochars at either 1 day (0.827–15.4 $\mu\text{g}^{1-\text{N}}\text{g}^{-1}\text{L}^{\text{N}}$) or 365 days (20.5–454 $\mu\text{g}^{1-\text{N}}\text{g}^{-1}\text{L}^{\text{N}}$) were greater than the previously reported K_f values for whole soils (0.00–0.476 $\mu\text{g}^{1-\text{N}}\text{g}^{-1}\text{L}^{\text{N}}$)⁸⁵. The release of DOC from biochars via aging could even enhance the sorption of antibiotics. Coupled with the strong irreversible sorption, biochars could be promising soil amendments for enhancing both short- and long-term sequestration of antibiotics and reducing the mobility and bioavailability of antibiotics in soils.

CHAPTER V

BLACK CARBON NANOPARTICLES FACILITATED TRANSPORT OF

ANTIBIOTICS IN SATURATED SAND

ABSTRACT

Black carbon (BC) nanoparticles are ubiquitous in nature. However, the impact of BC nanoparticles on the transport of environmental contaminants has not been well studied. This study investigated the possible facilitated transport of three antibiotics (lincomycin, oxytetracycline, and sulfamethoxazole) by BC nanoparticles in saturated sand columns at solution pH of 7, and ionic strength of 0.1, 1, and 10 mM. The transport of BC nanoparticles decreased with increasing ionic strength, in agreement with the XDLVO energy calculations. In the absence of BC nanoparticles, lincomycin transport increased with increasing ionic strength, whereas there was no effect of ionic strength on the transport of sulfamethoxazole and oxytetracycline. Under all tested ionic strength levels, all of the injected sulfamethoxazole was conservatively transported through the column, while all of the injected oxytetracycline was retained. In the presence of BC nanoparticles, the BC nanoparticles facilitated the transport of oxytetracycline with the effluent mass recovery of 1.9–76.7% of the injected mass, but decreased the transport of sulfamethoxazole (4.6–89.6% effluent mass recovery) under all ionic strengths. The lincomycin transport was enhanced at 0.1 mM ionic strength, but decreased at 1 mM and 10 mM ionic strengths, with much earlier breakthroughs under all ionic strengths. The BC-facilitated transport of antibiotics decreased with increasing ionic strength due to enhanced deposition of BC nanoparticles at greater ionic strengths. Overall, our results suggest that the facilitated transport of antibiotics by BC nanoparticles is likely and would occur under rainfall or irrigation with low-salinity water.

INTRODUCTION

Black carbon (BC) is a group of pyrogenic carbonaceous materials produced from thermal decomposition of biomass, organic wastes, and fossil fuel under oxygen-free or -limited conditions, ranging from slightly charred biomass to highly condensed aromatic and elemental carbon. It includes a variety of materials such as biochar, charcoal, carbon black, activated carbon, soot, etc. The common sources of BC are wildfires, vehicle emissions, burning of crop residues, and bioenergy pyrolysis.¹⁶⁴ BC is considered an important part of the Earth's carbon cycle, accounting for 3.8–7.7% of global soil organic carbon (SOC) pool (54–109 Pg), 5–15% of the SOC flux in terrestrial sediments (29–87 Tg yr⁻¹), as well as 19–80 Tg yr⁻¹ of particulate BC and 24.7–28.3 Tg yr⁻¹ of dissolved BC in the global riverine fluxes to oceans,¹⁷ where dissolved BC is often operationally defined as a size fraction less than 0.45 or 0.70 μm .¹⁷ A large portion of dissolved BC may be actually present in the form of nanoparticles with at least one dimension less than 100 nm. For example, carbon black (typically ranging 10–500 nm) is a BC material widely used as filler in rubber, plastic film, and ink pigment, with an annual global production of over 10 million tons (i.e., 9.7 Tg yr⁻¹).¹⁶⁵⁻¹⁶⁷ After the product with the BC is disposed of or degraded, the engineered BC nanoparticles are eventually be released into the environment.

It has been reported that the BC in urban runoff contributed significantly to the BC flux to streams and lakes. For example, in Lake Tahoe, this BC flux typically ranged between 100–400 $\mu\text{g L}^{-1}$ for highway stormwater runoff samples, which likely resulted from vehicle emission and tire wear.^{168, 169} In addition to engineered BC nanoparticles, it is well known that many BCs are not completely inert, but consist of a range of materials that can be transformed, degraded, and mineralized to varying degrees.^{17, 170, 171} This BC can originally contain fine particles, or physically disintegrate and decrease in size to produce nano- and colloidal-particles

over time.^{62, 102, 172, 173} For example, after ultrasonication the mass percentage of micron-sized biochars (0.1–2 μm) was about 4.3–6.5%, and that of nano-sized biochars was about 1.6–2.6%, respectively.⁶² Spokas et al.¹⁰² also reported that the percentage of micron- or submicron-sized biochars ranged from 1.0% to 47% for a variety of biochars, whereas Qu et al.¹⁷² found that the percentage of 0.45–1 μm biochars was about 1.1–1.2% for the rice and bamboo biochars. Due to the prevalence of BC colloids and nanoparticles in nature, a number of recent studies have focused on the aggregation and transport of BC colloids and nanoparticles in soil and water systems.^{63, 173,}

174

The BC nanoparticles tend to aggregate to various degrees in aqueous suspension, depending on BC surface property and solution chemistry.^{175–180} The BC nanoparticles with more oxygenic and hydrophilic surface functional groups are more stable in suspension than pristine BC nanoparticles.¹⁸¹ Aggregation of BC nanoparticles is enhanced at higher ionic strength, lower solution pH and in the presence of multivalent cations (such as Ca^{2+}) due to reduced electrostatic repulsion.^{179, 180} Whereas, natural organic matter and anionic surfactants in solution often inhibit the aggregation of BC nanoparticles.^{176, 177, 181} Aggregation of BC nanoparticles can substantially influence their transport in aquatic systems and their transport in the subsurface such as soils, sediments, and groundwater aquifers.^{175, 182} The subsurface transport of BC nanoparticles is also dependent on properties of BC nanoparticles and porous media, and solution chemistry. Recent work found that the transport of BC colloids through quartz sand decreased with increasing pyrolysis temperature, BC particle size, and iron oxide coating of sand surface, but increased with concentrations of natural organic matter and surfactants.^{62, 63, 173, 177} Higher ionic strength and lower solution pH often increase the retention of BC nanoparticles in porous media,^{183, 184} due to enhanced aggregation of BC nanoparticles as well as increased attraction between the BC

nanoparticles and grain surfaces. Overall, the BC nanoparticles are more mobile in the subsurface than micron-sized and bulk BC particles. As the BC particles interact with many other contaminants in the environment, it becomes important to examine the association of BC nanoparticles with other contaminants and how BC nanoparticles can facilitate contaminant transport.

Amendments of BC to soils (e.g., biochar) is being proposed for many agronomic and environmental benefits, including improved soil characteristics (e.g., improved soil structure, reduced bulk density, and enhanced water and nutrient retention), decreased greenhouse gas emission, and *in-situ* immobilization of contaminants such as excess nutrients, organic pollutants, and trace metals.^{25, 29, 93, 185, 186} However, the possibility of and quantification of contaminant transport that may be facilitated by BC nanoparticles is needed as it is important to determining the overall effectiveness of the BC-based remediation strategy. Hence, in this study, we focused on the interaction of BC nanoparticles with anthropogenic antibiotics transport in porous media. Anthropogenic antibiotics are extensively used in human health care and animal agriculture, resulting in the prevalent presence of antibiotics in soil and water environment.^{15, 187-189} Antibiotics are now considered as emerging contaminants. They vary substantially in their physicochemical properties such as molecular size, pH-dependent charge speciation and hydrophobicity, and consequently their sorption behaviors in the environment.^{9, 188-190} For example, tetracyclines are highly sorptive, but sulfonamides are very mobile in soils and sediments.^{9, 190} Recent studies have revealed that BC has strong sorption affinity to antibiotics.⁴⁰ Considering the high mobility of BC nanoparticles, they could potentially function as a carrier to facilitate the transport of antibiotics in the soil and water systems. Therefore, it is essential to understand how BC nanoparticles may influence the transport of antibiotics in the subsurface, which has not been fully studied.

This study aimed to elucidate the transport of three representative antibiotics, i.e., lincomycin (LCM), oxytetracycline (OTC) and sulfamethoxazole (SMX) in saturated sand at ionic strength of 0.1, 1, or 10 mM KCl and solution pH of 7.0, as influenced by the presence of BC nanoparticles. Sorption of LCM, OTC, and SMX to BC nanoparticles and sand was characterized using batch sorption experiments. Their transport through saturated sand columns with and without BC nanoparticles was measured by solute transport experiments in combination with numerical modeling. These column experiments and model results could give some of the first insights into understanding the transport of common antibiotics facilitated by BC nanoparticles in soils.

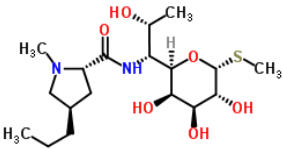
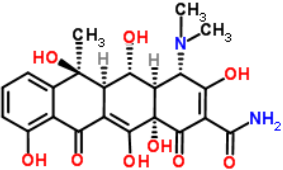
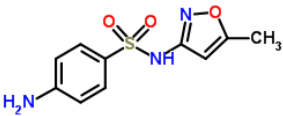
MATERIALS AND METHODS

Chemicals

Lincomycin hydrochloride ($\geq 90\%$), oxytetracycline hydrochloride ($\geq 95\%$), and sulfamethoxazole (analytical standard grade) were purchased from Sigma-Aldrich (St. Louis, MO, USA). The molecular structures and selected physicochemical properties of LCM, OTC, and SMX are listed in Table 5.1. The three antibiotics vary in their molecular weight and pKa, thus their pH-dependent charge speciation and representing mostly cations (LCM, 80%), zwitterion (OTC, 74%), and anion (SMX, 95%) at experimental solution pH of 7.0 (Table 5.1). These antibiotics were dissolved individually in methanol ($\geq 99.9\%$, Sigma-Aldrich) to prepare the stock solutions of 100 mg L^{-1} . The stock solutions were stored in darkness in a refrigerator prior to use. Deionized (DI) water from a Milli-Q water system (Millipore, Billerica, MA, USA) was used to prepare all aqueous solutions and suspensions. Potassium chloride (KCl, 99.0–100.5%, J.T. Baker) was used as background electrolyte to control solution ionic strength. Potassium bromide (KBr, $\geq 99.9\%$, J.T. Baker) was applied as a conservative tracer in column experiments to quantify hydrologic

transport conditions of each experiment. Dilute hydrochloric acid (HCl, Merck) and potassium hydroxide (KOH, J.T. Baker) solutions were used to adjust solution pH.

Table 5.1. Physicochemical properties of lincomycin, oxytetracycline, and sulfamethoxazole.

Antibiotics	Chemical Structure ^a	Molecular weight ^b (g/mol)	Solubility ^b (mg/L)	pK _a ^b	Speciation (at pH 7.0)
Lincomycin		406.54	927	7.6	Cation (80%) Neutral (20%)
Oxytetracycline		460.43	313	3.2; 7.5; 8.9	Zwitterion (74%) Anion (26%)
Sulfamethoxazole		253.28	610	1.6; 5.7	Neutral (5%) anion (95%)

^a Data from ChemSpider (<http://www.chemspider.com/>); ^b Data from TOXNET (<http://www.toxnet.nlm.nih.gov/>)

BC Nanoparticles

Porous carbon nanoparticles were obtained from US Research Nanomaterials Inc. (> 95% carbon, US1075, Houston, Texas, USA), and used as the model BC nanoparticles in this study. These nanoparticles were produced from perennial mountain bamboo and holly trees, and the primary particle size ranged between 60–80 nm. The specific surface area of BC nanoparticles was $727 \pm 24 \text{ m}^2 \text{ g}^{-1}$ determined by the N₂ adsorption at 77K on a Micromeritics ASAP 2020 analyzer (Micromeritics, Norcross, GA, USA). The stock suspension of BC nanoparticles at 20 mg L^{-1} was prepared by mixing 40 mg of the BC nanoparticle powder with 2 L of DI water in a glass bottle, followed by ultrasonication in a water bath sonicator (FS140, Fisher Scientific, Pittsburgh, PA, USA) for 8 h. The prepared stock suspension was ultrasonicated daily for 20 min to maintain the

dispersion of BC nanoparticles. Scanning electron microscopy (SEM, JEOL, JSM-7500F, Tokyo, Japan) images of the BC nanoparticles showed irregular-shaped aggregates formed by primary nanoparticles (Figure 5.1). The hydrodynamic diameter (D_h), zeta potential, and electrophoretic mobility (EPM) of BC nanoparticles suspensions in identical background solution chemistry to that in column transport experiments (i.e., initial antibiotic concentration of 0 or 100 $\mu\text{g L}^{-1}$, BC concentration of 10 mg L^{-1} , ionic strength of 0.1, 1, or 10 mM KCl, and pH of 7.0 ± 0.2) were determined using a Zetasizer Nano-ZS (Malvern Instrument, Westborough, MA, USA). The BC suspension were sonicated for 20 min prior to the D_h , zeta potential, and EPM measurements. Aggregation kinetics of BC nanoparticles at ionic strength of 0.1, 1, or 10 mM and pH of 7.0 was determined by measuring D_h over the first 120 min with time step of 10 s after 20 min sonication.

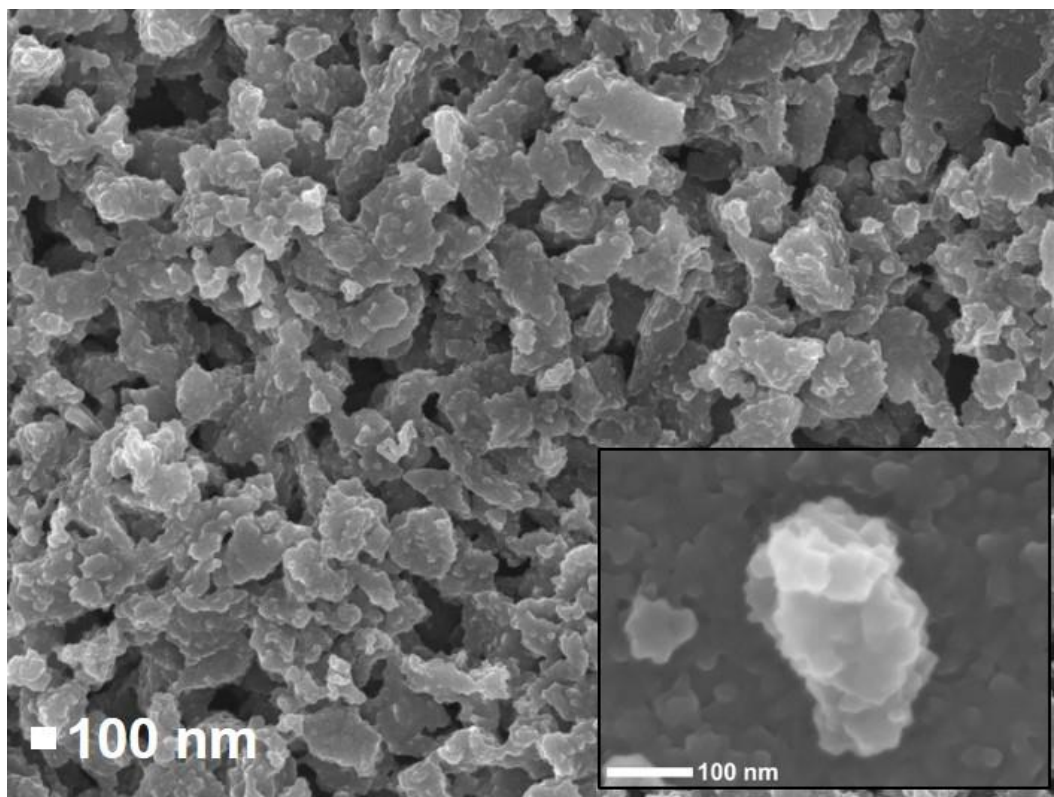


Figure 5.1. Scanning electron microscopy images of BC nanoparticles prepared from stock suspensions.

Porous Medium

Ottawa sand (99.69% silica, Granusil 4020, Unimin Corporation, Le Seueur, MN, USA) used in this study. It was first sieved into size fractions of 250–500 μm . The sand was then washed sequentially with 20 mM KCl solution and DI water to remove fine particles. This washing step was repeated until turbidity was no longer visually observed in the DI water. The cleaned sand was further rinsed with DI water several times, and then oven-dried and stored in a bottle prior to use. To characterize surface potential of sand surface, sand colloid suspension was generated, following the previously established method,¹⁹¹ which is briefly summarized here. First, 20 g of sand grains were ultrasonicated in 20 mL DI water for 30 min to generate sand colloids. This sand colloidal suspension was then passed through a 0.45- μm filter and the filtrates were mixed with KCl solution at ionic strength to 0.1, 1, or 10 mM and solution pH of 7.0. The prepared sand colloidal suspensions were then used to determine the zeta potentials of the sand colloids similar to the sand surface potentials.¹⁹²

Batch Sorption Experiments

The sorption kinetics and isotherms of LCM, OTC, and SMX on the BC nanoparticles and the Ottawa sand were measured in glass vials with polytetrafluoroethylene (PTFE) lined screw-caps and aluminum foil covered. All batch sorption experiments were performed in duplicate at room temperature (23 ± 1 °C) in the dark. The working solutions of the three antibiotics were freshly prepared by diluting the stock solutions with DI water and KCl solutions to desired antibiotic concentrations (100 to 1000 $\mu\text{g L}^{-1}$) and ionic strengths (0.2, 2, and 20 mM). After 20 min ultrasonication, aliquots of the stock suspensions were withdrawn as the working suspensions of BC nanoparticles. The sand and water mixtures were prepared by mixing 20 g sand in 10 mL

DI water. All antibiotic solutions, BC nanoparticle suspensions, and the mixture of sand and water were adjusted to pH of 7.0.

Kinetic sorption experiments were conducted following the similar procedure as sorption isotherm experiments detailed below, except for different initial antibiotic concentration (i.e. $100\ \mu\text{g L}^{-1}$) and different contact times (from 10 min to 8 h). The sorption of all three antibiotics on both the BC nanoparticles and the Ottawa sand occurred rapidly and reached equilibrium within 10 min for the BC nanoparticles and about 60 min for the sand (Figure 5.2). Therefore, the contact time of 2 h was determined for the following sorption isotherm experiments to ensure complete reactions.

For sorption isotherm experiments, 10 mL of BC nanoparticle working suspensions ($20\ \text{mg L}^{-1}$) or sand-water mixtures ($2\ \text{kg L}^{-1}$) was mixed with 10 mL of LCM, OTC, or SMX working solution to reach initial antibiotic concentrations of 50 to $500\ \mu\text{g L}^{-1}$, ionic strength of 0.1, 1, or 10 mM, pH of 7.0 ± 0.2 , and sorbent-water ratio of $10\ \text{mg L}^{-1}$ for BC nanoparticles and $1\ \text{kg L}^{-1}$ for sand, respectively. These mixtures were horizontally shaken at 200 rpm in an incubator shaker (C24, New Brunswick Scientific NJ, USA) for 2 h. After equilibration, 2 mL of suspensions was pipetted into 2 mL microcentrifuge tubes. The tubes were centrifuged at $13793 \times g$ for 10 min, and then the top 1-mL of supernatants were carefully collected. The concentrations of LCM, OTC, or SMX in the supernatants were determined by a Shimadzu Prominence high-performance liquid chromatograph coupled with an Applied Biosystems Sciex 4500 QTrap mass spectrometer (LC-MS/MS) as described in the Analytical Methods section. Since the control experiments free of BC nanoparticles or sand showed a negligible loss of antibiotics during the sorption experiments (data not shown), the difference between the initial and final antibiotic concentrations in solutions was assumed to be sorbed by the BC nanoparticles or the sand.

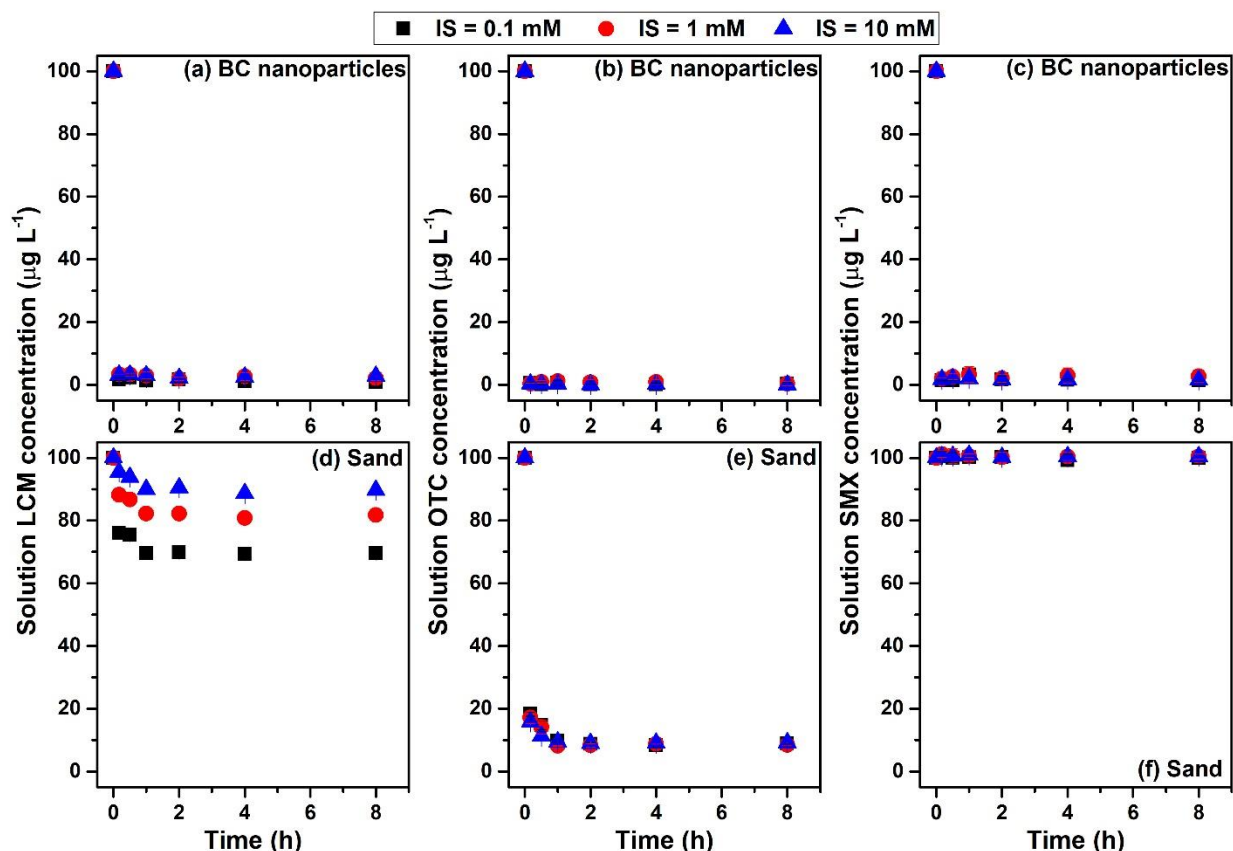


Figure 5.2. Sorption kinetics of LCM (a and d), OTC (b and e), SMX (c and f) on BC nanoparticles and sands under ionic strength (IS) of 0.1, 1 or 10 mM and solution pH of 7.0.

Column Transport Experiments

Packed column experiments were conducted to investigate the transport of each tested antibiotic (LCM, OTC, or SMX) accompanied with and without BC nanoparticles at three different ionic strength (0.1, 1, and 10 mM) under saturated condition. All column experiments were performed in duplicate. The Ottawa sand (61.4 g) was wet-packed into an Omnifit glass column of 2.5-cm inner diameter and 7.3-cm length (Diba Industries, Danbury, CT, USA) and had a porosity of 0.35. The packed sands were supported by stainless steel filter membrane (104-μm mesh opening, Spectra/Mesh, Spectrum laboratories, Houston, TX, USA) and sealed by O-rings and PTFE tubing connectors on both ends of the column. A MasterFlex L/S peristaltic pump (Cole-Parmer Instrument, Vernon Hills, IL, USA) was connected to the inlet at the top of the column to

supply a steady-state downward flow at a flow rate of 1.0 mL min^{-1} and a pore water velocity of 0.58 cm min^{-1} .

During the transport experiments, each column was first flushed with 20 mM KCl solution for 25 min, followed by flushing with DI water for 25 min. After flushing, the background solution free of either antibiotics, BC nanoparticles, or Br^{-1} tracer at ionic strength of 0.1, 1, or 10 mM and pH of 7.0 was injected for at least 120 min to condition the column. Meanwhile, the input solutions and suspensions were freshly prepared following the similar procedure as described above in the batch sorption experiments. Briefly, the antibiotic-only solutions were prepared by mixing 25 mL of LCM, OTC, or SMX working solutions (initial antibiotic concentrations of $200 \mu\text{g L}^{-1}$ and ionic strength of 0.2, 2, or 20 mM) with 25 mL of DI water. The BC nanoparticle suspensions were prepared by mixing 25 mL of BC nanoparticle working suspensions (20 mg L^{-1} in DI water) with 25 mL of KCl solution (initial concentration of 0.2, 2, or 20 mM). Finally, the mixed suspensions of BC nanoparticles with LCM, OTC, or SMX as co-solute were prepared by mixing 25 mL of LCM, OTC, or SMX working solutions with 25 mL of BC nanoparticle working suspension. All input solutions and suspensions (with initial antibiotic concentrations of 0 or $100 \mu\text{g L}^{-1}$, initial BC nanoparticle concentrations of 0 or 10 mg L^{-1} , ionic strength of 0.1, 1, or 10 mM, and pH of 7.0 ± 0.2) were shaken for 120 min to reach equilibrium, followed by 20-min sonication just before injection. The transport experiment was then commenced by instantaneous switching from the background solution to the input solution or suspension as described above. The injection of input solution or suspension continued for 25 min, i.e., about 2 pore volumes (PVs). Afterwards the influent was switched back to the background solution for another 75 min (about 6 PVs) to observe flushing and breakthrough curve tailing behavior in the BC and antibiotics. The effluent samples

were collected from the column outlet with 2 mL intervals by a Retriever 500 fraction collector (Teledyne ISCO, Lincoln, NE, USA).

To determine dissolved antibiotic concentrations, 1 mL of each influent and effluent samples were pipetted into 1.5 mL microcentrifuge tubes and centrifuged at $13793 \times g$ for 10 min. The top 0.75 mL of the supernatants was then carefully collected to be analyzed with the LC-MS/MS. To determine the BC nanoparticles concentrations, 1 mL of each influent and effluent samples were measured for the absorbance at wavelength of 550 nm (the calibration curve showed in Figure 5.3) using a Cary 50 Bio UV-Visible Spectrophotometer (Varian Inc., Palo Alto, CA). For the concentrations of antibiotics associated with BC nanoparticles, the preliminary ultrasonic-assisted solvent extraction of sorbed antibiotics was conducted by sonicating the BC nanoparticles in the mixture of 1-mL 150 mg L^{-1} ethylenediaminetetraacetic acid solution and 5-mL acetonitrile/methanol mixture (65/35 by volume) for 30 min. However, the extraction recoveries of antibiotics sorbed on the BC nanoparticles were generally low, i.e., 38.8 ± 0.3 , 4.4 ± 0.0 , and $32.7 \pm 0.1\%$ for LCM, OTC, and SMX, respectively. Therefore, the BC-associated antibiotic concentrations were calculated by the sorption amounts of antibiotics onto BC nanoparticles and the breakthrough curves (BTCs) of BC nanoparticles in the co-transport experiments. Detailed calculation method is provided in the Analytical Methods section. The bromide tracer experiment followed the same protocols with 50 mg L^{-1} KBr solution as input solution and DI water as background water. The bromide concentrations of effluent samples were determined by the UV absorbance at wavelength of 212 nm. The baseline of effluent background concentrations was subtracted from the effluent sample concentrations. Finally, the BTCs were plotted as normalized effluent concentrations (C/C_0 , where C_0 is initial solute concentration) as a function of PVs.

Effluent mass recoveries (M_R) were calculated from the measured BTCs by dividing the recovered mass in the effluents by the total applied mass.

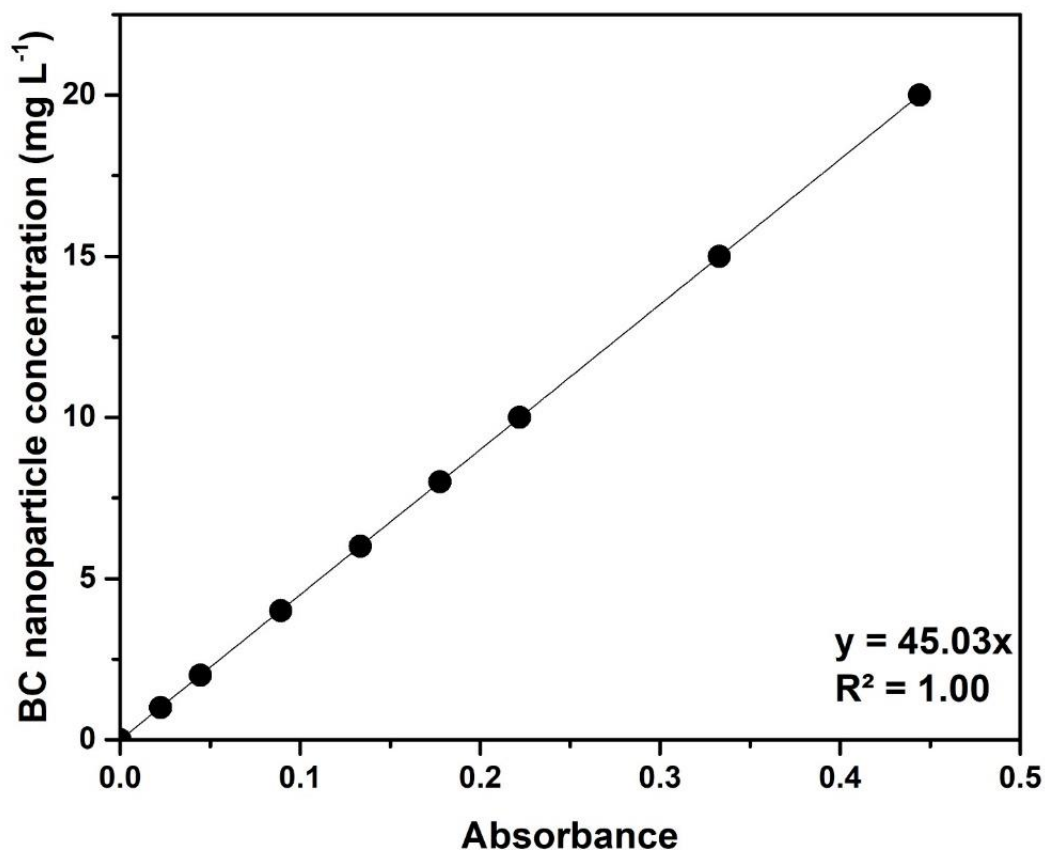


Figure 5.3. Linear regressions between UV-vis absorbance at 550 nm and BC nanoparticle concentrations in suspension.

Analytical Methods

The concentrations of freely dissolved lincomycin (LCM), oxytetracycline (OTC), or sulfamethoxazole (SMX) in solutions were determined by a Shimadzu Prominence high-performance liquid chromatograph coupled with an Applied Biosystems Sciex 4500 QTrap mass spectrometer (LC-MS/MS). The analytical column was a ZORBAX Eclipse Plus C18 column with 50 mm length \times 2.1 mm diameter and 5 μ m particle size (Agilent, Santa Clara, CA, USA). The

mobile phase A consisted of DI water and 0.3% formic acid. The mobile phase B consisted of 65:35 (v/v) acetonitrile/methanol mixture and 0.3% formic acid. The separation was achieved using a gradient condition of 0–40% B in 0–1.0 min, 40–70% B in 1.0–2.0 min, 70–80% B in 2.0–3.0 min, 80–100% B in 3.0–3.5 min, and then 100% B for 7.2 min. The flow rate was 0.35 mL min⁻¹ and the injection volume was 10 µL. The electrospray ionization (ESI) and positive ionization mode were used in the tandem quadrupole MS. Antibiotics were detected and quantified using a multiple reaction monitoring mode with a precursor/product transition of 407.2/126.2 for LCM, 426.1/283.1 for OTC, and 254.0/108.1 for SMX. The retention time was 2.6, 2.8, and 3.7 min for LCM, OTC, and SMX, respectively.

The concentrations of antibiotics associated with BC nanoparticles were alternatively calculated by the sorption amounts of antibiotics onto the BC nanoparticles and the BTCs of the BC nanoparticles from co-transport experiments. Before the co-transport column experiments, the mixed suspensions of antibiotic and BC nanoparticles were prepared by mixing 25 mL of antibiotic working solutions (antibiotic concentrations of 200 µg L⁻¹ and ionic strength of 0.2, 2, or 20 mM KCl) with 25 mL of BC nanoparticle working suspensions (BC concentrations of 20 mg L⁻¹ in DI water) to reach initial antibiotic concentrations ($C_{0, \text{anti}}$) of 100 µg L⁻¹, initial BC nanoparticles concentrations ($C_{0, \text{BC}}$) of 10 mg L⁻¹, ionic strength of 0.1, 1, or 10 mM KCl, and pH of 7.0 ± 0.2 . The mixed suspensions were shaken for 120 min to reach equilibrium. Aliquots of suspensions were withdrawn, centrifuged, and measured for the equilibrium concentration of antibiotics ($C_{e, \text{anti}}$). The antibiotic sorption amount (q_e) on the BC nanoparticles were calculate by the difference between C_0 and C_e and then divided by C_{BC} . After the co-transport experiments, the BC nanoparticle concentrations in each collected effluent sample ($C_{e, \text{BC}}$) were determined by the UV-Vis spectrometer at 550 nm. Simply assuming that constant q_e values (there was no further

sorption/desorption) and homogeneous sorption of antibiotics to the BC nanoparticles, the mass of sorbed antibiotic concentration ($M_{\text{BC-anti}}$) in each effluent could be calculated by sampled effluent volume (0.002 L in this study) times $C_{\text{e, BC}}$ (converted unit form mg L^{-1} to $\mu\text{g L}^{-1}$), and then times q_{e} ($\mu\text{g g}^{-1}$). To calculate the relative concentration (C/C_0) for plotting BTCs, the calculated $M_{\text{BC-anti}}$ were divided by sampled effluent volume (0.002 L) and then divided by $C_{0, \text{anti}}$ ($\mu\text{g L}^{-1}$). Finally, the mass recoveries of total antibiotic (including dissolved and BC-associated fraction) were calculated by integrating $M_{\text{BC-anti}}$ from each effluent samples and then division by the total applied mass.

Mathematical Modeling

The sorption isotherms from the batch experiments were fitted to the Freundlich model:¹⁶²

$$q_{\text{e}} = K_{\text{F}} C_{\text{e}}^N \quad (5.1)$$

where q_{e} ($\mu\text{g g}^{-1}$) is the sorbed antibiotic concentration in the solid phase, C_{e} ($\mu\text{g L}^{-1}$) is the antibiotic concentration in solution, K_{F} ($\mu\text{g}^{1-N} \text{g}^{-1} \text{L}^N$) is the Freundlich sorption coefficient, and N (dimensionless) is the Freundlich nonlinearity factor.

The BTCs were fitted using the CXTFIT 2.0 code in the STANMOD (version 2.08.1130) to simulate one-dimensional transport and co-transport of BC nanoparticles, LCM, OTC, or SMX.^{193, 194} The deterministic equilibrium or nonequilibrium convection-dispersion equation (CDE) was used to fit the experimental BTCs with a zero initial concentration, a pulse-input boundary condition and a zero-concentration-gradient boundary condition at the outlet under the steady flow condition, using the Levenberg-Marquardt optimization algorithm. The transport of the BC nanoparticles or the bromide tracer was described by an equilibrium CDE with a first-order kinetic deposition term as follows:

$$\frac{\partial C_{\text{B}}}{\partial t} = D \frac{\partial^2 C_{\text{B}}}{\partial x^2} - v \frac{\partial C_{\text{B}}}{\partial x} - k_{\text{d}} C_{\text{B}} \quad (5.2)$$

where C_B is the effluent concentration of BC nanoparticles or bromide (mg L^{-1}), t is the elapsed time (min), D is the hydrodynamic dispersion coefficient ($\text{cm}^2 \text{min}^{-1}$), x is the travel distance (cm) in the direction of flow, v is the pore water velocity (cm min^{-1}), and k_d is the first-order deposition rate coefficient (min^{-1}). The hydrodynamic properties of the columns was first characterized by the conservative bromide BTC (Figure 5.4). The k_d of the bromide tracer was equal to zero because bromide is nonreactive to the sand, and the fitted D value was $0.025 \text{ cm}^2 \text{min}^{-1}$ ($R^2 = 1.00$). We then assumed the same D value for all tested column conditions, the k_d values were then estimated by fitting the BTCs of the BC nanoparticles.¹⁹⁵

The transport of LCM, OTC, or SMX and their co-transport with BC nanoparticles were described by a two-site chemical nonequilibrium CDE model. This model assumes that total sorption sites can be divided into equilibrium sorption sites and kinetic sorption sites. Retention on the equilibrium and kinetic sorption sites is assumed to be instantaneous and time-dependent, respectively. The model can be described in the dimensionless forms below:

$$\beta R \frac{\partial C_1}{\partial T} = \frac{1}{P} \frac{\partial^2 C_1}{\partial Z^2} - \frac{\partial C_1}{\partial Z} - \omega(C_1 - C_2) \quad (5.3)$$

$$(1 - \beta)R \frac{\partial C_2}{\partial T} = \omega(C_1 - C_2) \quad (5.4)$$

$$\beta = \frac{\theta + fK_d}{\theta + K_d} \quad (5.5)$$

$$\omega = \frac{\alpha(1-\beta)RL}{v} \quad (5.6)$$

$$R = 1 + \frac{\rho_b K_d}{\theta} \quad (5.7)$$

$$T = \frac{vt}{L} \quad (5.8)$$

$$P = \frac{vL}{D} \quad (5.9)$$

$$Z = \frac{x}{L} \quad (5.10)$$

where β is the partitioning coefficient for the equilibrium and kinetic sorption sites, R is the retardation factor, C_1 and C_2 are the normalized effluent concentrations associated with the equilibrium and kinetic sorption sites, respectively, T is the dimensionless elapsed time, P is the Peclet number, Z is the dimensionless travel distance, ω is the dimensionless mass transfer coefficient, θ is the volumetric water content, f is the fraction of equilibrium sorption sites in total sorption sites, K_d is the distribution coefficient for linear sorption isotherms ($\text{cm}^3 \text{g}^{-1}$), α is the first-order kinetic rate coefficient (min^{-1}), ρ_b is the bulk density (g cm^{-3}) of the sand column, and L is the column length (cm). To fit the BTCs of total LCM, OTC, or SMX (including both the dissolved and BC-associated fraction in the effluents), the same D value ($0.025 \text{ cm}^2 \text{ min}^{-1}$) was applied, and the parameters of R , β , and ω were then estimated.

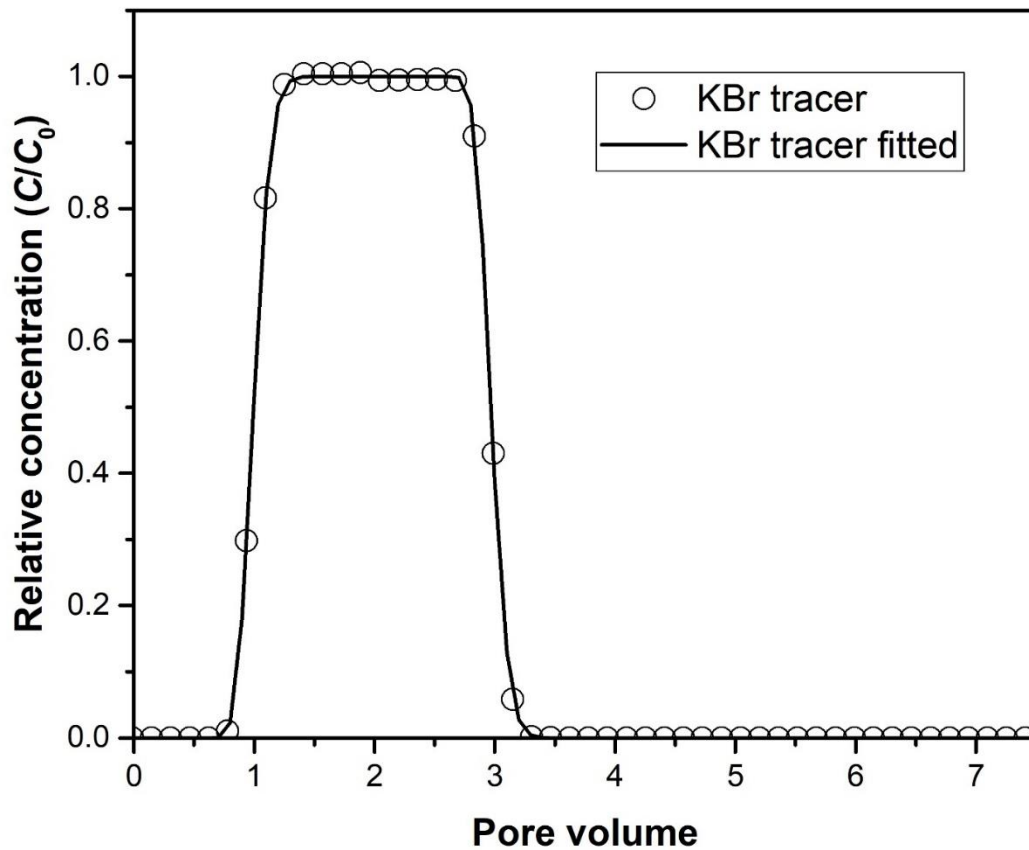


Figure 5.4. Measured and fitted breakthrough curve of the bromide tracer through saturated sand column. Symbols are experimental data and lines are fitted result.

XDLVO and α_{theory} Calculations

The extended Derjaguin-Landau-Verwey-Overbeek (XDLVO) interaction energies were calculated as the sum of Lifshitz-van der Waals (LW), Lewis acid-base (AB), electrical double layer (EL), and Born repulsion (BR) interactions for the BC nanoparticles interacting with sand surfaces using a sphere–plate configuration. The total XDLVO interaction energy (Φ^{XDLVO}) as a function of separation distance (x) was calculated via:

$$\Phi^{XDLVO}(x) = \Phi^{LW}(x) + \Phi^{AB}(x) + \Phi^{EL}(x) + \Phi^{BR}(x) \quad (5.11)$$

The LW interaction energy per unit area ($\Delta G_{x_0}^{LW}$) for a surface (1) interacting with another surface (2) through a medium (3) can be determined as:¹⁹⁶

$$\Delta G_{x_0}^{LW} = -2 \left(\sqrt{\gamma_1^{LW}} - \sqrt{\gamma_3^{LW}} \right) \left(\sqrt{\gamma_2^{LW}} - \sqrt{\gamma_3^{LW}} \right) \quad (5.12)$$

where γ_1^{LW} is the apolar component of LW interaction of surface 1 (e.g., BC), and γ_2^{LW} is the LW component of surface 2 (e.g., quartz sand), and γ_3^{LW} is the LW component of water.

The Hamaker constant (A_{132}) was then calculated as:^{197, 198}

$$A_{132} = -12\pi x_0^2 \Delta G_{x_0}^{LW} \quad (5.13)$$

where x_0 (0.158 nm) is the minimum equilibrium distance at which two condensed-phase surfaces are in contact. The calculated A_{132} for the BC nanoparticles interacting the sand surface through water was 5.2×10^{-21} J. The non-retarded LW interaction energy for the BC nanoparticles interacting with the sand surface was then determined as:¹⁹⁹

$$\Phi^{LW}(x) = -\frac{A_{132}}{6} \left\{ \frac{2a_p(x+a_p)}{x(x+a_p)} - \ln \left(\frac{x+2a_p}{x} \right) \right\} \quad (5.14)$$

where a_p is the particle radius.

The AB interaction energy per unit area at contact ($\Delta G_{x_0}^{AB}$) was calculated as:¹⁹⁶

$$\Delta G_{x_0}^{AB} = 2[(\sqrt{\gamma_1^+} - \sqrt{\gamma_2^+})(\sqrt{\gamma_1^-} - \sqrt{\gamma_2^-}) - (\sqrt{\gamma_1^+} - \sqrt{\gamma_3^+})(\sqrt{\gamma_1^-} - \sqrt{\gamma_3^-}) - (\sqrt{\gamma_2^+} - \sqrt{\gamma_3^+})(\sqrt{\gamma_2^-} - \sqrt{\gamma_3^-})] \quad (5.15)$$

where γ^+ and γ^- are electron-acceptor and electron-donor components of each surface.

The AB interaction energy was calculated as:^{197, 198}

$$\Phi^{AB}(x) = 2\pi a_p \lambda_w \Delta G_{x_0}^{AB} \exp\left(\frac{x_0 - x}{\lambda_w}\right) \quad (5.16)$$

where λ_w is the decay length for AB interactions in water (0.6 nm).¹⁹⁸

An improved equation using linear superposition approximation for the EL interaction of nanoparticles with a planar surface was used:²⁰⁰

$$\Phi^{EL}(x) = \frac{64\pi\epsilon_1\epsilon_0}{\kappa} \left(\frac{kT}{ze}\right)^2 \tanh\left(\frac{ze\psi_1}{4kT}\right) \tanh\left(\frac{ze\psi_2}{4kT}\right) \{(\kappa a_p - 1)\exp(-k\kappa) + (1 + \kappa a_p)\exp[-\kappa(x + 2a_p)]\} \quad (5.17)$$

where ϵ_r is the dielectric constant of the water (80.1 at 293.15 K), ϵ_0 is the vacuum permittivity ($8.854 \times 10^{-12} \text{ C}^2 \text{ N}^{-1} \text{ m}^{-2}$), k is the Boltzmann constant ($1.381 \times 10^{-23} \text{ J K}^{-1}$), T is temperature in Kelvin, e is the elementary charge ($1.602 \times 10^{-19} \text{ C}$), z is the charge number of the electrolyte, ψ_1 and ψ_2 are the surface potential of the BC nanoparticles and sand surface, and κ is the reciprocal electrical double layer thickness (κ^{-1}). The measured zeta potentials were used in place of the surface potentials.¹⁹⁶

The Born repulsion was calculated via:²⁰¹

$$\Phi^{BR}(x) = \frac{A_{132}\sigma^6}{7560} \left[\frac{8a_p + x}{(2a_p + x)^7} + \frac{6a_p - x}{x^7} \right] \quad (5.18)$$

where σ (0.5 nm) is the collision.

The XDLVO energy calculations were conducted at ionic strength of 0.1 mM, 1 mM or 10 mM for BC nanoparticles interacting with sand surface in the absence of antibiotics. It was

believed that the presence of antibiotics would not change the XDLVO energies. Surface energy parameters used in the calculations are provided in Table 5.2.

Table 5.2. Surface energy components and Hamaker constants used in XDLVO calculations.

	γ^{LW} (mJ/m ²)	γ^+ (mJ/m ²)	γ^- (mJ/m ²)	A_{132} (J) ^m	Refs.
BC	45.0	5.67	0.0	—	202
Water	21.8	25.5	25.5	—	202
Quartz (SiO ₂)	36.3	1.1	57.0	4.3×10^{-21}	203

In colloidal filtration theory, attachment efficiency (α) determines whether particle collision with collector surfaces can result in attachment. Theoretical attachment efficiency (α_{theory}) was calculated from a Maxwell model that includes colloid deposition in both the primary and secondary minima.^{204, 205}

$$\alpha_{\text{theory}} = 1 - \int_{\sqrt{\Phi_{2\min}}}^{\sqrt{\Delta\Phi}} \frac{4}{\pi^{1/2}} E^2 \exp(-E^2) dE \quad (5.19)$$

where E^2 is the kinetic energy of particle normalized by kT , and $\Delta\Phi$ is the sum of Φ_{\max} and $\Phi_{2\min}$.

Experimental α_{exp} can be estimated from the column experiments via:^{206, 207}

$$\alpha_{\text{exp}} = \frac{2}{3} \frac{k_d d_c}{(1-\theta)v\eta_0} \quad (5.20)$$

where k_d is the deposition rate coefficient, d_c is the effective collector diameter (375 μm), θ is the volumetric water content, v is the pore water velocity, and η_0 is the single-collector contact efficiency calculated via the Tufenkji and Elimelech equation.²⁰⁶

RESULTS AND DISCUSSION

Characterization of the BC nanoparticles and Sand

As shown in Table 5.3, both BC nanoparticles and sand surface were negatively charged under all experimental conditions. With increasing ionic strength from 0.1 mM to 10 mM, zeta potential became less negative from -54.4 to -35.5 mV for the BC nanoparticles, and from -55.2 to 50.3 mV for the sand, respectively (Table 5.3), due to charge screening at higher ionic

strength.^{180, 208, 209} Thus, at higher ionic strength, electrostatic repulsion among BC nanoparticles could decrease, resulting in large size of aggregates (Table 5.3).^{175, 179, 180} Additionally, the presence of 100 $\mu\text{g L}^{-1}$ of LCM, OTC, or SMX in the BC nanoparticle suspensions had no effect on the size and zeta potential of the BC aggregates (Table 5.3), presumably because the antibiotic concentrations were too low to exert any effect.. As shown by Figure 5.5, BC nanoparticles became more aggregated when ionic strength increased from 0.1 and 1 mM to 10 mM. Further, even the aggregate size of BC nanoparticles at 10 mM ionic strength increased with time from 453 ± 29 nm to 589 ± 47 nm at the end of 120 min. During the first 40 min there was no significant difference in the aggregate sizes at three ionic strength levels ($p < 0.05$, one-way ANOVA with Tukey HSD test to compare the hydrodynamic diameters for 10 min intervals). Therefore, it was reasonable to assume that the BC nanoparticle suspension was stable during the equilibration phase in the batch sorption experiments and the injection phase in the transport columns. However, over 2 hours, the BC nanoparticles could have formed larger aggregates at 10 mM KCl, which may have influenced the sorption and transport of antibiotics.

Table 5.3. Properties for BC nanoparticles and sand colloids.^a

	IS (mM)	pH	D_h (nm)	PDI	EPM ($\mu\text{m cm V}^{-1} \text{s}^{-1}$)	Zeta potential (mV)
BC nanoparticles	0.1	7.1	410 ± 20	0.35	-4.26 ± 0.12	-54.4 ± 1.5
	1	7.0	437 ± 6	0.34	-3.21 ± 0.07	-40.9 ± 0.9
	10	7.0	461 ± 9	0.31	-2.78 ± 0.18	-35.5 ± 2.3
BC nanoparticles + LCM	0.1	7.1	402 ± 8	0.36	-3.86 ± 0.11	-49.2 ± 1.4
	1	7.0	444 ± 20	0.41	-3.23 ± 0.02	-41.3 ± 0.3
	10	7.0	454 ± 15	0.48	-2.83 ± 0.17	-36.1 ± 2.2
BC nanoparticles + OTC	0.1	7.1	396 ± 7	0.38	-3.97 ± 0.12	-50.6 ± 1.5
	1	7.0	444 ± 31	0.44	-3.42 ± 0.11	-43.6 ± 1.4
	10	7.0	468 ± 21	0.50	-2.91 ± 0.20	-37.1 ± 2.5
BC nanoparticles + SMX	0.1	7.1	424 ± 13	0.39	-4.18 ± 0.17	-53.4 ± 2.2
	1	7.0	433 ± 11	0.41	-3.52 ± 0.12	-44.9 ± 1.5
	10	7.0	473 ± 37	0.43	-2.84 ± 0.16	-36.2 ± 2.0
Sand	0.1	7.0	nd	nd	-4.33 ± 0.20	-55.2 ± 2.6
	1	7.0	nd	nd	-4.45 ± 0.21	-56.8 ± 2.7
	10	7.0	nd	nd	-3.94 ± 0.22	-50.3 ± 2.8

^a D_h : hydrodynamic diameter; PDI: polydispersion index; and EPM: electrophoretic mobility

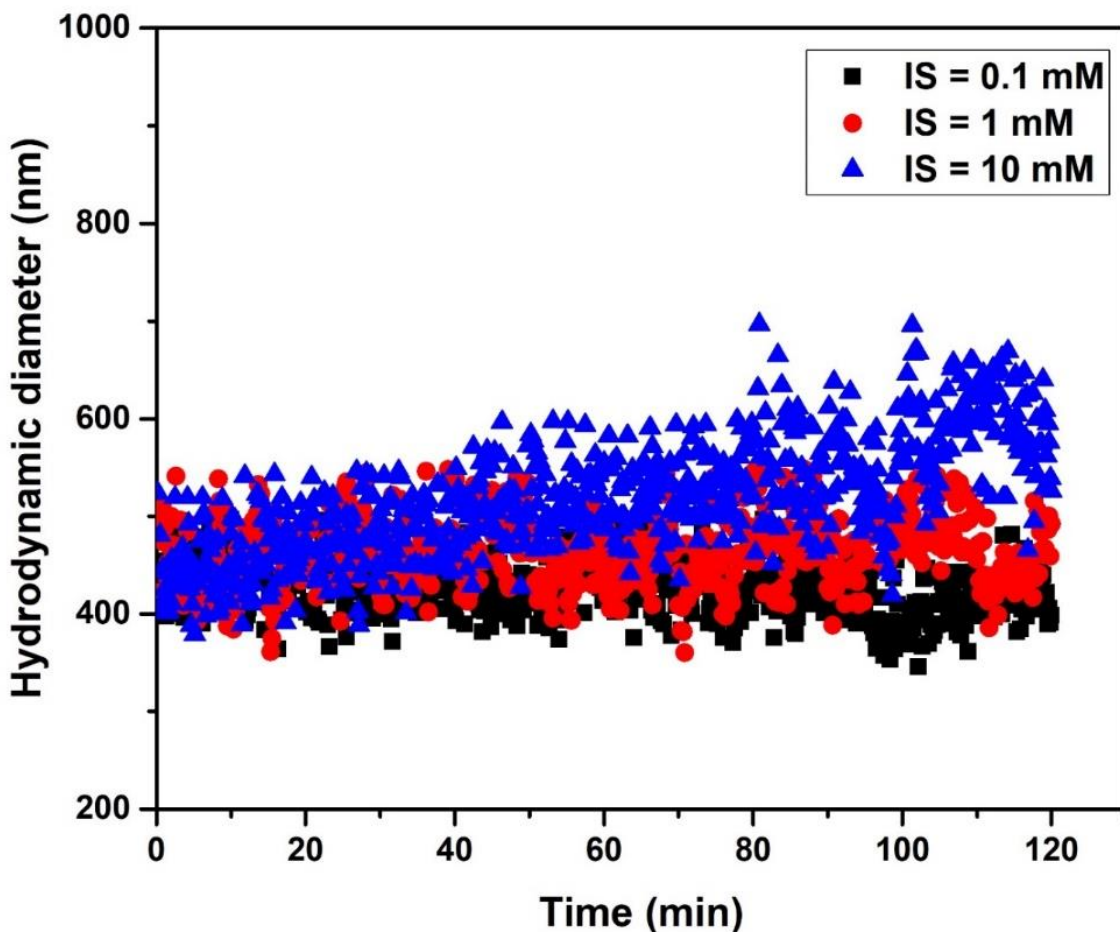


Figure 5.5. Aggregation kinetics of BC nanoparticles dispersed in the KCl solution with ionic strength (IS) of 0.1, 1, or 10 mM at pH 7.0.

Sorption Isotherms

The sorption isotherms of LCM, OTC, and SMX to the BC nanoparticles were all nonlinear with a concave-downward shape at ionic strength of 0.1, 1, and 10 mM and pH 7.0 (Figure 5.6a-c). For the Ottawa sand, the LCM sorption isotherms exhibited a nonlinear concave-upward shape, the OTC sorption isotherms were nearly linear, and no sorption was observed for SMX (Figure 5.6d-f). All sorption isotherms (except for the SMX sorption onto the sand) could be fitted well with the Freundlich model (Table 5.4). The distribution coefficients (K_d , with unit of L Kg^{-1} , calculated from the fitted Freundlich model at $C_e = 100 \mu\text{g L}^{-1}$) decreased in the order from OTC/BC-nanoparticles, SMX/BC-nanoparticles, LCM/BC-nanoparticles, OTC/sand, LCM/sand,

and finally SMX/sand (assumed to be 0) (Table 5.4). The K_d values of LCM, OTC, and SMX were in the order of 10^6 – 10^7 L Kg⁻¹ for BC nanoparticles and 10^{-2} – 10^1 L Kg⁻¹ for sand, indicating much stronger sorption affinity of the three antibiotics to BC nanoparticles than to sand. This observation could be attributed to the greater specific surface area and more sorption sites on the BC nanoparticles. For the sand, the sorption of antibiotics is mainly controlled by electrostatic and van der Waals interactions. Therefore, the negatively charged sand surface could electrostatically attract positive LCM and zwitterionic OTC, but repel negative SMX (thus no observed SMX sorption). On the other hand, BC nanoparticles can interact with antibiotics not only through electrostatic and van der Waals interactions, but also through other more specific sorption mechanisms such as $\pi^+-\pi$ and/or $\pi-\pi$ electron donor–acceptor (EDA) interactions, hydrogen bonding, and pore diffusion, which would greatly enhance the sorption of antibiotics to BC nanoparticles.^{39, 40} Intriguingly, with increasing ionic strength the amount of sorption was decreased for LCM sorption to the BC nanoparticles and the sand, and for OTC sorption to the sand (Figure 5.6). This sorption response is likely due to competition from other cations with the charged antibiotic molecules. Thus, electrostatic interaction seems to play an important role in the sorption of LCM and OTC to sorbents. A small decrease was observed for SMX sorption to the BC nanoparticles with increased ionic strength. Since no electrostatic attraction between SMX and the BC nanoparticles was expected, and thus no competitions from anions in solution, this decrease was presumably due to the reduced accessibility of the sorption sites elicited by aggregation at higher ionic strength. Overall, the BC nanoparticles showed much stronger sorption affinity to LCM, OTC, and SMX than sand. Together these sorption results indicate that the presence of BC nanoparticles can substantially affect the transport of antibiotics through sands.

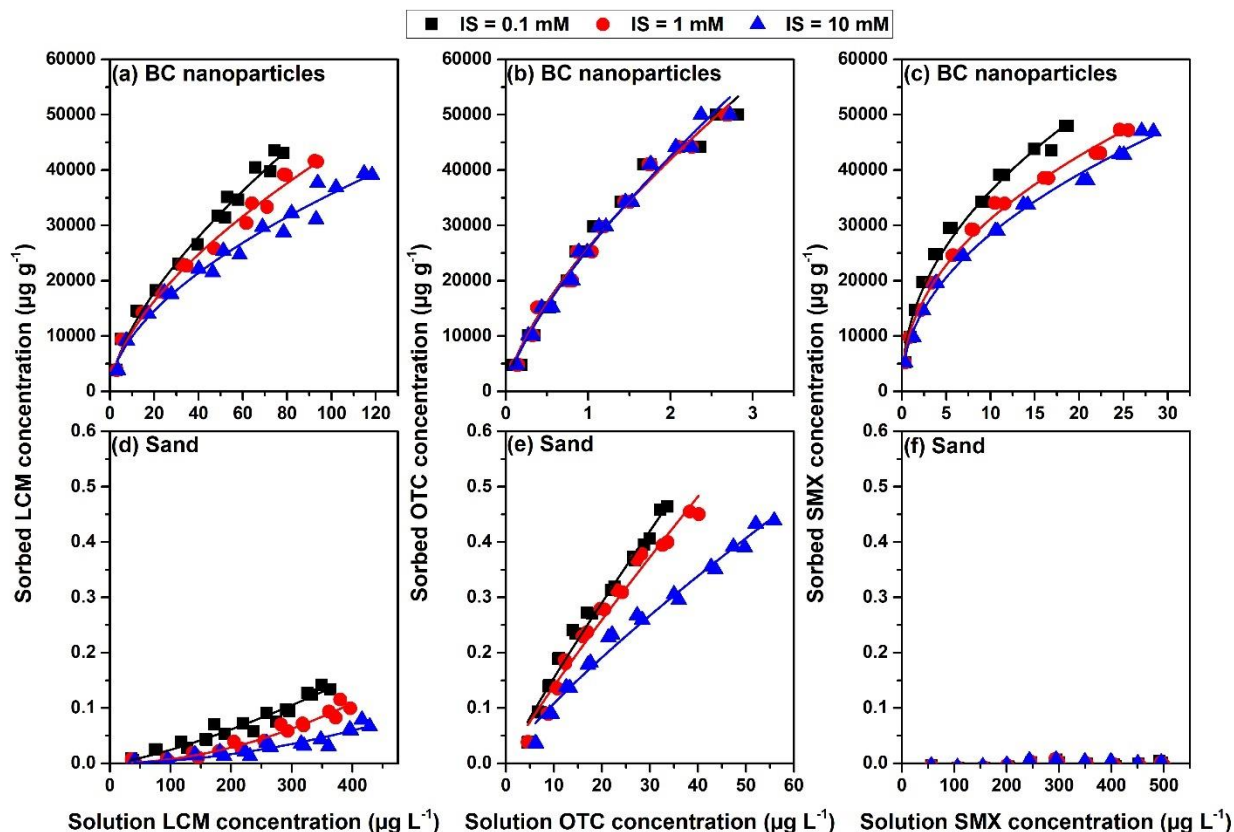


Figure 5.6 Sorption isotherm of LCM (a and d), OTC (b and e), SMX (c and f) on black carbon (BC) nanoparticles and sands under ionic strength (IS) of 0.1, 1 or 10 mM and pH of 7.0.

Table 5.4. Fitted parameters of the Freundlich model for sorption isotherms of LCM, OTC, or SMX on BC nanoparticles and sand under ionic strength (IS) of 0.1, 1, or 10 mM and pH of 7.0.^a

	IS	BC nanoparticles				Sand			
		K_F	N	R^2	K_d	K_F	N	R^2	K_d
LCM	0.1	2.48×10^3	0.66	0.97	5.10×10^5	8.80×10^{-5}	1.2	0.95	0.26
	1	2.47×10^3	0.62	0.97	4.38×10^5	1.53×10^{-5}	1.4	0.87	0.12
	10	2.22×10^3	0.61	0.97	3.69×10^5	4.60×10^{-6}	1.6	0.87	0.06
OTC	0.1	2.53×10^4	0.76	0.97	8.24×10^6	9.75×10^{-3}	1.1	0.94	18.
	1	2.53×10^4	0.78	0.98	8.98×10^6	8.30×10^{-3}	1.1	0.96	15
	10	2.53×10^4	0.78	0.99	9.14×10^6	8.20×10^{-3}	1.0	0.94	9.1
SMX	0.1	1.07×10^4	0.54	0.98	1.29×10^6	nd	nd	nd	nd
	1	9.99×10^3	0.49	0.99	9.76×10^5	nd	nd	nd	nd
	10	9.03×10^3	0.50	0.99	8.89×10^5	nd	nd	nd	nd

^a IS: ionic strength (mM); K_F : Freundlich sorption coefficient ($\mu\text{g}^{1-N} \text{g}^{-1} \text{L}^N$); N : Freundlich nonlinearity factor; K_d : distribution coefficients (L Kg^{-1}), calculated from the fitting parameters of Freundlich isotherm at equilibrium concentration (C_e) = $100 \mu\text{g g}^{-1}$, and nd: parameters were not determined.

Transport of BC nanoparticles

The transport of BC nanoparticles through saturated sand followed classic colloid transport behaviors that had no retardation, which was similar to a conservative tracer (Figure 5.4), and was controlled by the first-order kinetic deposition (Figure 5.7).¹⁸³ In agreement with the zeta potential and aggregate size measurements, there was no difference in the transport of BC nanoparticles with and without antibiotics through saturated sand column (Figure 5.7 and Table 5.3). With increasing ionic strength, the retention of BC nanoparticles was significantly enhanced (Figure 5.7), in agreement with the XDLVO calculations (Figure 5.8). The XDLVO energy profiles showed unfavorable conditions for the deposition of BC nanoparticles, characterized by the formidable energy barriers and shallow secondary minima (Figure 5.8). The energy barrier decreased, and the secondary minimum increased with increasing ionic strength (Figure 5.8b). Also, the estimated α_{theory} value was 0.001, 0.046, and 0.516 for the BC nanoparticles at 0.1, 1, and 10 mM, respectively, suggesting greater deposition of BC nanoparticles at higher ionic strength. Nonetheless, the α_{theory} values were much smaller than the experimental α_{exp} values (Table 5.5). This discrepancy was not surprising because the XDLVO theory neglected the roughness of sand surfaces that could decrease the energy barrier, and increase the depth of secondary minimum.²¹⁰ ²¹¹ Thus, the α_{theory} values estimated from the XDLVO energy calculations may underestimate the actual α_{exp} values. The retention of the BC nanoparticles at the secondary minima may be enhanced by low velocity zones located in the valley, crevices, and pits on rough sand surfaces.^{210, 211} Furthermore, hydrodynamic traps at regions of flow stagnation, low flow vortices, and backward flow in pore space of the sand column may also contribute to the retention of BC nanoparticles,^{208, 210-213} which may actually play a more important role under less favorable conditions. Indeed, the α_{exp} value was about 22 and 5 times of the α_{theory} value at ionic strength of 0.1 and 1 mM, but only

about 1.4 times of the α_{theory} value at ionic strength of 10 mM. Therefore, the surface attachment of the BC nanoparticles at the secondary minima became more important at higher ionic strength (10 mM), resulting in more favorable attachment condition.

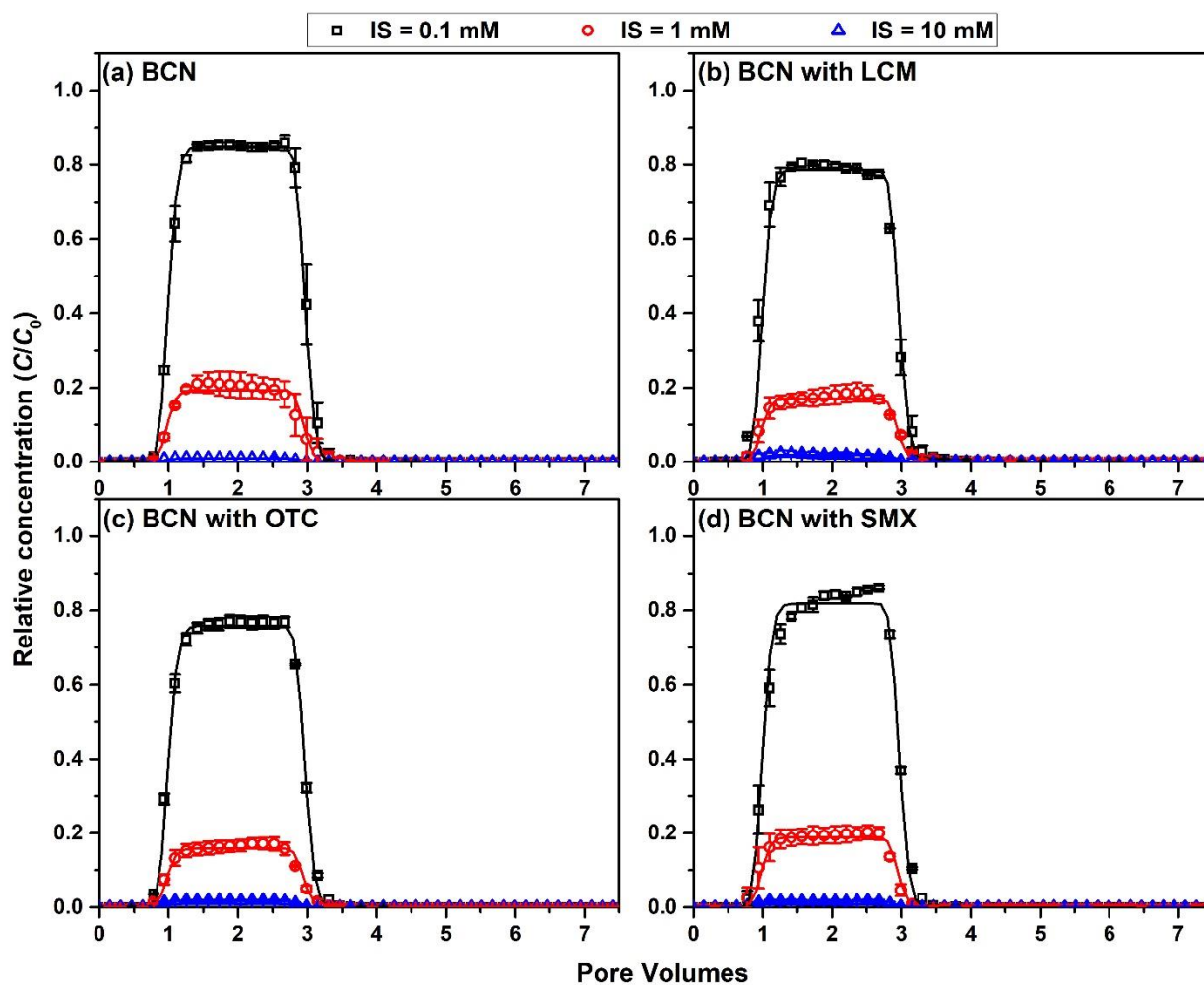


Figure 5.7. Measured and fitted breakthrough curves of black carbon nanoparticles (BCN) without (a) and with (b, c and d) of lincomycin (LCM), oxytetracycline (OTC) or sulfamethoxazole (SMX) in saturated sand columns at solution pH of 7 and ionic strength (IS) of 0.1, 1, or 10 mM KCl.

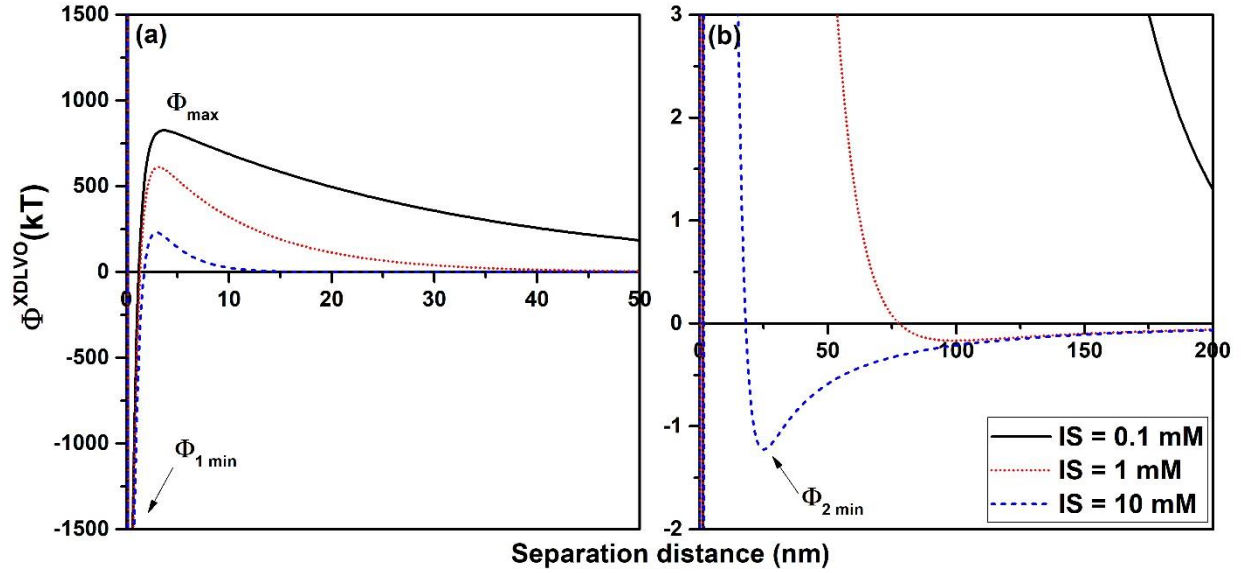


Figure 5.8. XDLVO surface energy profiles for black carbon (BC) nanoparticles interacting with sand surfaces with the energy barrier (a) and the secondary minima (b).

Table 5.5. Fitted transport parameters for breakthrough curves of BC nanoparticles with and without LCM, OTC or SMX in saturated sand column.^a

	IS (mM)	k (min ⁻¹)	R^2	α_{exp}
BC nanoparticles	0.1	0.013	0.998	0.022
	1	0.130	0.986	0.235
	10	0.376	0.962	0.702
BC nanoparticles + LCM	0.1	0.019	0.992	0.032
	1	0.141	0.988	0.256
	10	0.319	0.935	0.589
BC nanoparticles + OTC	0.1	0.022	0.998	0.037
	1	0.147	0.991	0.268
	10	0.324	0.975	0.611
BC nanoparticles + SMX	0.1	0.016	0.996	0.028
	1	0.133	0.988	0.238
	10	0.331	0.971	0.627

^a k : deposition rate coefficient (k) and α_{exp} : experimental attachment efficiency

Transport of Antibiotics

Considering the strong sorption of LCM, OTC, or SMX to the BC nanoparticles and the transport behaviors of the BC nanoparticles as discussed above, it was hypothesized that the co-presence of BC nanoparticles and antibiotics could dramatically change the transport of antibiotics in porous media. To elucidate these complex interactions, we first examined the transport of LCM, OTC, or SMX through the sand column without the BC nanoparticles. As shown in Figure 5.9a, the LCM retention decreased with increasing ionic strength, and the effluent mass recovery increased from $49.4 \pm 2.4\%$ to $97.3 \pm 4.4\%$ when ionic strength increased from 0.1 mM to 10 mM (Table 5.6). This observation was likely due to the competition between K^+ cations and positively charged LCM cations (Table 5.1) for the sorption sites on the sand surface, which was also supported by the LCM sorption isotherms to the sand (Figure 5.6d). The fitted retardation factor of LCM decreased from 26.6 to 1.61 with increasing ionic strength from 0.1 to 10 mM (Table 5.7), suggesting that LCM was more mobile at higher ionic strength. Due to stronger sorption of OTC to the sand, no OTC was transported out of the columns under all experimental conditions (Figure 5.9b and Table 5.6). Conversely, due to minimal sorption of SMX to the sand (Figure 5.6e), about 100% of the initial SMX mass was flushed out of the column (Figure 5.9c and Table 5.6). As a result, the fitted retardation factor was between 0.85–1.05, suggesting a minimal SMX retention. Furthermore, the transport of OTC and SMX was not influenced by ionic strength, in contrast to that of LCM.

Next we examined the transport of LCM, OTC, or SMX in the presence of BC nanoparticles. As shown in Figure 5.9d, the BTCs of LCM (including both the sorbed and dissolved LCM in the effluents) were drastically different from those in the absence of the BC nanoparticles. The LCM BTCs were similar to the BTCs of the BC nanoparticles with no

retardation, and the LCM transport decreased with increasing ionic strength from 0.1 to 10 mM KCl (Figure 5.9d) with the LCM mass recovery decreased from $78.7 \pm 3.3\%$ to $17.8 \pm 2\%$ (Table 5.6). Indeed, the fitted results showed the small value of β (0.0145–0.0957), suggesting the minimal contribution of equilibrium sorption and the predominant contribution of kinetic sorption to the LCM retention. Intriguingly, after the end of the injection phase, the dissolved LCM concentrations in the effluents continued to increase (Figure 5.10a), likely resulted from the desorption of LCM from the retained BC nanoparticles due to replacement of sorbed LCM cations by K^+ . In the presence of the BC nanoparticles, the transport of OTC was substantial (up to $76.7 \pm 2\%$ at 0.1 mM), and decreased to $1.9 \pm 0.2\%$ when increasing ionic strength to 10 mM (Figure 5.9e and Table 5.6). The transported OTC were exclusively associated with the BC nanoparticles (Table 5.6), and the BTCs of OTC resembled those of the BC nanoparticles. Similarly, the OTC transport had very large retardation factors and minimal β values (Table 5.7), further supporting the dominant contribution from the kinetic sorption of the BC-associated OTC due to the deposition of BC nanoparticles. Clearly, the BC nanoparticles could facilitate the transport of a large portion of OTC. Finally, the transport of SMX was reduced by the presence of BC nanoparticles (Figure 5.9f), and the mass recovery ranged between 4.56–89.6% which were much lower than 100% of the mass recovery in the absence of BC nanoparticles (Table 5.6). The transport of SMX decreased with increasing ionic strength, likely again reflecting the contribution from the deposition of the BC nanoparticles. The fitted transport parameters were characterized by the intermediate retardation factors, and lower β values at higher ionic strength. The sizable β value (0.383) at 0.1 mM KCl suggests that SMX equilibrium sorption to the sand and BC nanoparticles still contributed a significant portion of the SMX retention. However, this contribution diminished

at 1 and 10 mM KCl, indicating that the kinetic sorption of BC-associated SMX was the dominant contributor to the SMX retention.

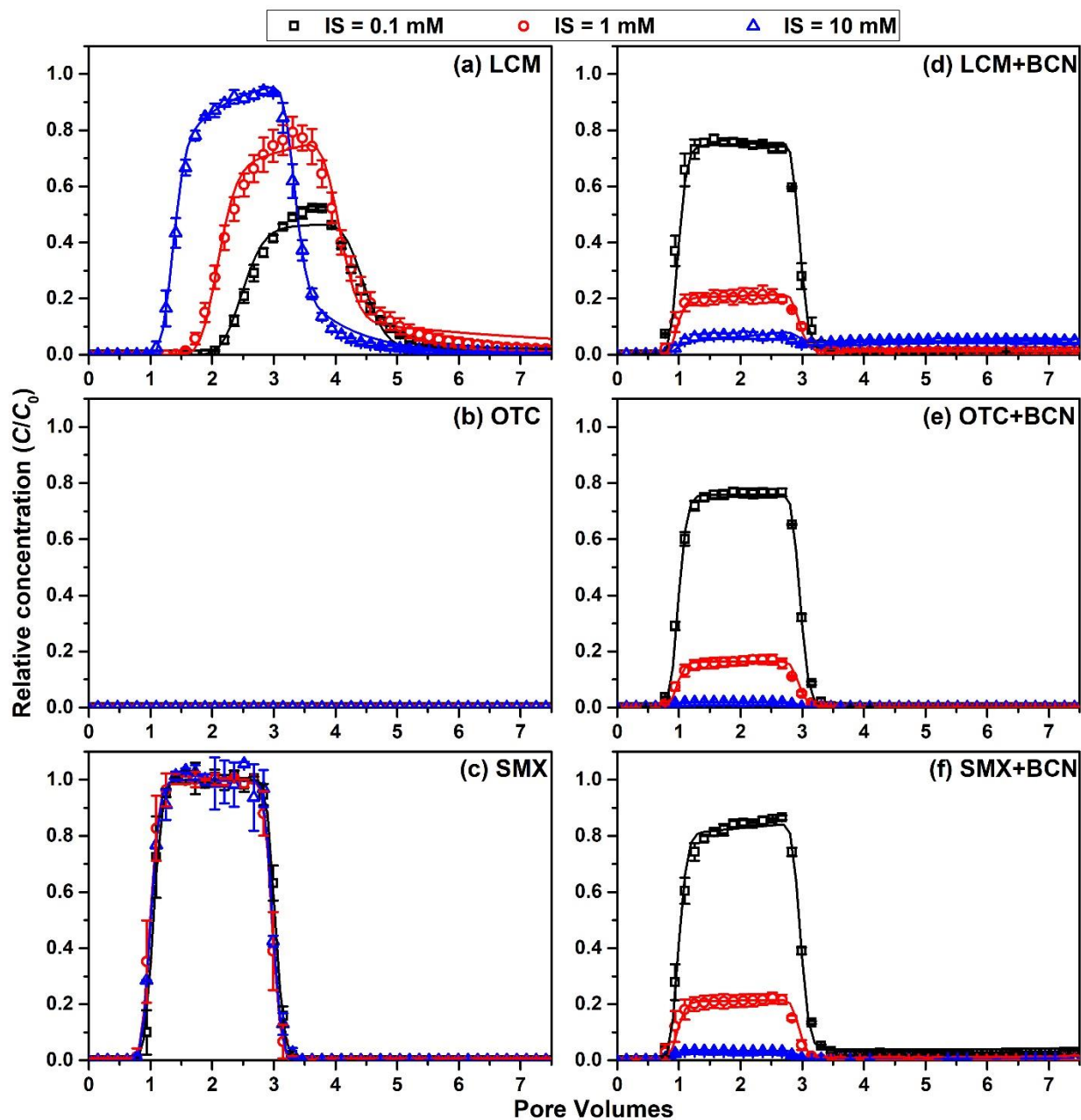


Figure 5.9. Measured and fitted breakthrough curves of lincomycin (LCM), oxytetracycline (OTC) and sulfamethoxazole (SMX) without black carbon nanoparticles (BCN) (a, b and c) and the BCN-associated LCM, OTC and SMX (d, e and f) in saturated sand columns at solution pH of 7 and ionic strengths of 0.1, 1, or 10 mM KCl

Table 5.6. Effluent mass recovery calculations of breakthrough curves for LCM, OTC, and SMX in the antibiotic-only and co-transport experiments.

	IS	Mass recovery (M_R)			
		Dissolved antibiotics	BC-associated antibiotics	Total transported antibiotics	Total retained antibiotics
	mM	%	%	%	%
Antibiotics-only transport experiments					
LCM	0.1	49.4 ± 2.4	n/a	49.4 ± 2.4	50.6 ± 2.4
	1	86.6 ± 10.8	n/a	86.6 ± 10.8	13.4 ± 10.8
	10	97.3 ± 4.4	n/a	97.3 ± 4.4	2.7 ± 4.4
OTC	0.1	0 ± 0	n/a	0 ± 0	100 ± 0
	1	0 ± 0	n/a	0 ± 0	100 ± 0
	10	0 ± 0	n/a	0 ± 0	100 ± 0
SMX	0.1	100.3 ± 4.7	n/a	100 ± 4.7	-0.26 ± 4.7
	1	99.9 ± 7.6	n/a	99.9 ± 7.6	0.08 ± 7.6
	10	100.4 ± 5.3	n/a	100 ± 5.3	-0.43 ± 5.3
Antibiotics and BC nanoparticles co-transport experiments					
LCM	0.1	3.3 ± 0.93	75.4 ± 2.4	78.7 ± 3.3	21.3 ± 3.3
	1	7.55 ± 0.88	16.9 ± 2.2	24.4 ± 3.1	75.6 ± 3.1
	10	15.8 ± 1.3	2.01 ± 0.67	17.8 ± 2	82.2 ± 2
OTC	0.1	0 ± 0	76.7 ± 2	76.7 ± 2	23.3 ± 2
	1	0 ± 0	16.4 ± 2.1	16.4 ± 2.1	83.6 ± 2.1
	10	0 ± 0	1.9 ± 0.24	1.9 ± 0.2	98.1 ± 0.2
SMX	0.1	9.90 ± 0.76	79.7 ± 2.6	89.6 ± 3.3	10.4 ± 3.3
	1	3.91 ± 0.22	18.8 ± 3.9	22.8 ± 4.1	77.2 ± 4.1
	10	2.84 ± 0.09	1.71 ± 0.44	4.6 ± 0.5	95.4 ± 0.5

Table 5.7. Fitted transport parameters of breakthrough curves for LCM, OTC, and SMX in the antibiotic-only and co-transport experiments.^a

	IS (mM)	R	β	ω	R^2
Antibiotics-only transport experiments					
LCM	0.1	26.6	0.095	0.811	0.978
	1	3.66	0.580	0.422	0.984
	10	1.61	0.855	0.311	0.997
OTC	0.1	NF	NF	NF	NF
	1	NF	NF	NF	NF
	10	NF	NF	NF	NF
SMX	0.1	1.05	1.00	8496	0.999
	1	0.85	1.00	8007	0.999
	10	1.01	1.00	7947	0.997
Antibiotics and BCN co-transport experiments ^b					
Total LCM	0.1	10.5	0.0957	0.300	0.991
	1	69.0	0.0145	1.63	0.985
	10	21.8	0.0460	3.25	0.839
Total OTC	0.1	34.3	0.0290	0.28	0.998
	1	1005	0.000995	1.85	0.990
	10	9272	0.000108	4.08	0.975
Total SMX	0.1	2.62	0.383	0.22	0.997
	1	141	0.007	1.59	0.985
	10	141	0.007	3.61	0.934

^a R : the retardation factor; β : the partitioning coefficient of equilibrium sorption and kinetic deposition sites; ω is the mass transfer coefficient, and NF: not fitted. ^bTotal LCM, total OTC, and total SMX included both dissolved fraction and BC-associated fraction.

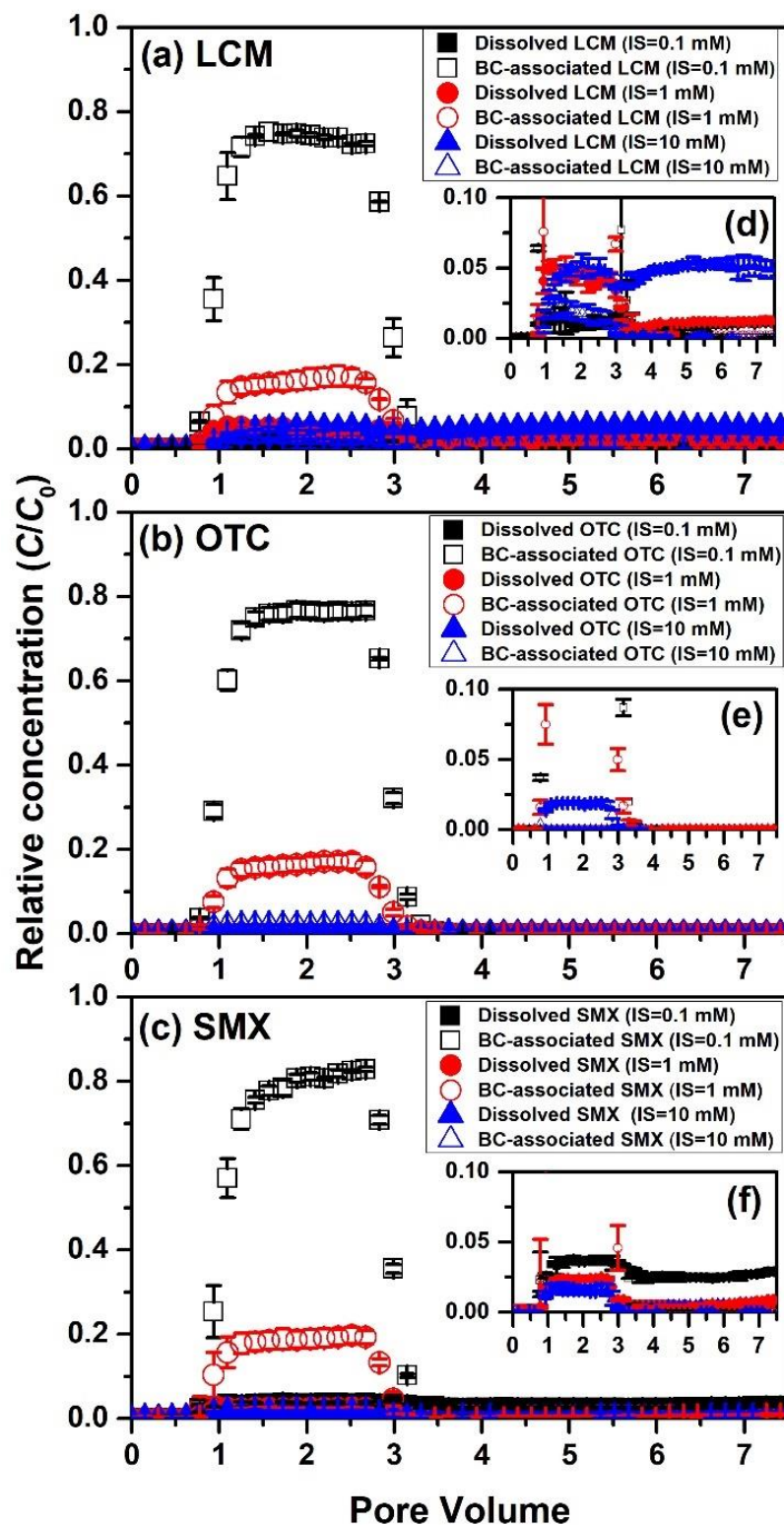


Figure 5.10. Breakthrough curves of LCM (a), OTC (b), and SMX (c) in the presence of black carbon (BC) nanoparticles in saturated sand columns at solution pH of 7 and ionic strengths of 0.1, 1, or 10 mM KCl. The inserts (d, e, and f) showed the x-axis range of 0.0 to 0.1 to better view the released antibiotics in solution.

Implications

This study was limited to only one solution pH level of 7.0 in a model porous media. Future study should be extended to slightly acidic and alkaline pH range in diverse soil types. Overall, the co-presence of BC nanoparticles and antibiotics substantially changed the transport of LCM, OTC or SMX in saturated sand. At all ionic strength levels, the BC nanoparticles facilitated the transport of OTC, but decreased the transport of SMX. It is intriguing that at low ionic strength of 0.1 mM, the BC nanoparticles increased the transport of LCM, but decreased its transport at higher ionic strength of 1 mM and 10 mM. Therefore, the risks for facilitated transport of antibiotics could be much higher for low-salinity pore water, such as when rainfall or irrigation occurs on soils. Still, as soil solution in typical soils range between 1–180 mM,⁸⁶ the transport of antibiotics in most soils would likely experience a net decrease with the addition of BC nanoparticles. However, this is a steady-state perspective. In natural settings, soil moisture and transport in pore water is a dynamic process, so during transient flow conditions such as infiltration and percolation of rainwater and irrigation water of low salinity, the facilitated transport of antibiotics sorbed on the BC nanoparticles could be substantially higher, especially when the BC nanoparticles are released and mobilized.²¹⁴⁻²¹⁶

CHAPTER VI
CONCLUSIONS AND FUTURE WORK

CONCLUSIONS

In this dissertation, the sorption and transport of antibiotics associated with black carbon (BC) in soil and water systems were investigated using batch and column approaches with combination of various spectroscopic analysis and mathematical modeling. This dissertation research demonstrated BC (i.e. biochars) could provide a rapid immobilization of antibiotics by surface adsorption and a lasting sequestration of antibiotics via pore diffusion, and therefore land application of BC as a soil amendment may be used as an effective *in-situ* sequestration strategy to reduce the mobility and bioavailability of antibiotics in soil. The Dissolved organic carbon (DOC) released from BC could be characterized as a mixture of acid-precipitated (AP) fraction with higher molecular weight and aromaticity and an acid-soluble (AS) fraction with lower molecular weight and aromaticity. A quick, easy and robust UV-vis spectrometric method was developed to measure the DOC concentrations in BC produced from diverse feedstocks and pyrolysis conditions. The continuous release of DOC from BC enhanced the lincomycin sorption by decreasing particle size of BC and/or increasing the accessibility of sorption sites initially blocked by DOC. Finally, the facilitated transport of antibiotics by BC nanoparticles in soils was investigated and the results showed that the total transport of antibiotics was enhanced in the presence of BC nanoparticles in low-salinity water, but decreased at high-salinity water, implying that the facilitated transport of antibiotics would occur under rainfall or irrigation.

FUTURE WORK

For the directions of future works, the field study in investigating the application of BC as a soil amendment will be needed for understanding its antibiotics sequestration ability of BC in the real world. The proposed antibiotic sorption mechanisms onto BC (i.e. electrostatic interactions, hydrogen bonding, van der Waals forces, and pore-filling process) need to be validated by direct

evidences in future studies. The role of released DOC from BC plays a critical role in carbon dynamics and contaminant transport in soils and further understand of the chemical compositions of DOC will be important to assess their potential physical, chemical, and biological effects in the environment. Finally, transport and co-transport of antibiotics study should be extended to different antibiotics, BC, solution chemistry in the diverse soil column in the future.

APPENDICES

Appendix A: Sorption Isotherms Data

Figure 2.8							
C_t		Q_t		C_t		Q_t	
$\mu\text{g L}^{-1}$		$\mu\text{g g}^{-1}$		$\mu\text{g L}^{-1}$		$\mu\text{g g}^{-1}$	
AVG	SD	AVG	SD	AVG	SD	AVG	SD
BM600 pH 6.0				BM600 pH9.9			
7.9	1.0	69.9	1.0	33.4	3.8	64.4	3.8
48.5	0.9	192.7	0.9	109.7	9.3	138.7	9.3
155.5	4.2	358.3	4.2	304.3	13.9	212.7	13.9
346.9	13.9	441.7	13.9	528.5	20.8	230.7	20.8
518.7	11.6	492.4	11.6	765.6	18.1	261.1	19.7
DM600 pH 6.5				DM600 pH10.0			
7.4	0.3	70.4	0.3	32.6	1.4	65.1	1.4
36.1	1.2	205.1	1.2	100.0	9.0	148.4	9.0
136.8	3.2	376.9	3.2	304.3	13.9	212.7	13.9
322.3	16.2	466.3	16.2	502.3	25.5	256.9	25.5
466.3	20.8	544.8	20.8	710.5	22.5	316.2	25.4
PM600 pH 7.3				PM600 pH10.4			
34.1	2.7	43.7	2.7	41.9	1.2	55.8	1.2
100.0	8.6	141.2	8.6	117.4	3.9	131.0	3.9
283.1	16.2	230.7	16.2	314.2	18.5	202.9	18.5
453.2	30.1	335.4	30.1	503.9	23.1	255.2	23.1
651.2	27.8	359.9	27.8	711.7	16.5	315.0	19.8
AM600 pH 6.9				AM600 pH10.0			
14.3	1.0	63.5	1.0	36.3	3.1	61.5	3.1
60.0	3.1	181.2	3.1	93.6	4.2	154.8	4.2
170.5	3.7	343.2	3.7	288.0	18.5	229.0	18.5
328.9	6.9	459.7	6.9	479.4	11.6	279.8	11.6
481.0	9.3	530.1	9.3	678.5	18.1	348.2	17.5
Figure 4.8 and 4.9							
C_t	Q_t	C_t	Q_t	C_t	Q_t	C_t	Q_t
$\mu\text{g L}^{-1}$	$\mu\text{g g}^{-1}$	$\mu\text{g L}^{-1}$	$\mu\text{g g}^{-1}$	$\mu\text{g L}^{-1}$	$\mu\text{g g}^{-1}$	$\mu\text{g L}^{-1}$	$\mu\text{g g}^{-1}$
1d		7d		30d		365d	
BM300							
76.3	29.2	12.8	94.3	0.6	107.1	0.0	102.1
73.2	33.4	11.8	92.9	0.8	108.2	0.0	102.0
157.3	52.7	27.7	174.8	0.9	210.8	0.0	207.6
149.7	60.0	30.6	172.9	1.1	205.4	0.0	200.9
321.5	83.4	71.1	323.1	3.2	401.5	0.0	396.3
307.3	99.5	74.7	323.1	1.8	399.3	0.0	398.3
434.8	143.5	126.2	470.2	8.4	584.0	0.0	590.0
455.5	122.4	123.3	473.7	6.0	573.5	0.0	599.6
649.9	155.8	202.1	586.6	17.2	795.3	0.0	790.1
622.0	185.9	196.6	611.7	13.9	779.0	0.0	802.0
824.5	175.9	290.8	719.3	33.9	971.4	0.0	1011.4
801.9	200.5	327.7	674.3	26.9	988.4	0.0	985.3
BM400							
72.4	33.1	45.8	60.3	38.8	69.6	0.0	102.8
83.3	22.6	42.9	64.2	33.3	76.4	0.0	101.6
163.1	46.4	110.4	92.0	74.8	132.8	0.1	201.8
156.0	52.6	113.6	90.7	68.3	137.4	0.1	203.9
310.1	95.3	233.0	162.3	183.3	215.9	1.0	399.3
321.5	84.6	233.0	166.0	194.4	205.8	1.2	408.7

470.4	110.3	372.0	225.4	314.2	277.7	1.2	591.7
452.5	128.4	365.6	234.3	344.8	245.4	3.2	596.5
643.7	160.4	502.5	296.4	429.3	371.1	3.7	804.3
668.7	136.1	509.4	290.9	521.0	279.4	10.6	796.4
850.5	151.6	654.7	353.1	578.8	418.7	12.0	975.9
821.3	179.1	719.6	283.3	555.4	440.1	14.4	980.8
<hr/>							
BM500							
73.4	32.7	56.9	48.5	47.4	62.9	1.0	103.5
71.8	34.4	58.6	47.7	39.3	70.8	1.0	103.3
144.6	64.3	114.2	88.6	90.1	117.6	8.6	195.9
138.0	71.4	115.2	88.2	83.8	124.6	8.6	196.1
301.6	105.7	260.6	135.8	216.6	183.1	23.3	385.8
287.4	120.1	266.6	131.7	202.5	197.3	44.2	355.9
443.7	136.0	413.0	186.0	329.4	258.3	66.9	524.8
428.9	150.8	421.8	178.3	314.2	277.7	55.7	540.0
653.1	154.4	589.2	206.5	532.4	272.8	113.2	677.3
612.8	193.6	582.0	213.4	498.3	310.9	98.5	694.4
801.9	198.7	773.3	228.1	653.3	351.8	132.5	879.9
847.2	152.7	781.1	220.4	674.7	331.9	168.1	827.2
<hr/>							
BM600							
53.3	53.3	29.5	76.4	10.9	98.1	0.0	101.7
51.5	53.8	31.3	74.9	16.6	92.0	0.0	101.2
126.7	83.4	81.8	122.8	52.1	157.1	0.6	205.2
120.2	90.4	80.2	125.5	55.1	151.3	0.6	205.7
264.8	139.4	196.4	205.3	145.3	255.8	1.5	402.3
284.6	120.1	200.2	198.3	139.1	260.1	3.0	394.9
405.4	171.8	321.5	274.5	254.8	328.7	8.1	585.6
417.2	162.6	307.1	292.0	216.6	375.2	16.9	569.6
582.1	220.9	457.2	337.4	413.1	398.9	20.9	783.9
606.6	196.1	470.7	323.2	383.9	421.2	26.6	765.6
779.4	226.6	672.0	334.3	538.1	470.0	28.5	963.2
795.5	209.0	642.4	358.3	512.5	496.6	43.5	944.8
<hr/>							
PM300							
81.4	24.7	61.3	44.9	52.7	57.9	0.8	100.2
87.0	19.0	57.9	48.6	47.8	62.1	0.7	102.5
162.3	47.3	133.9	69.3	109.2	99.2	0.8	201.6
165.3	44.6	133.0	71.0	99.5	110.0	0.9	203.5
335.9	70.9	264.6	133.4	214.2	186.7	2.6	393.3
330.1	74.2	256.6	142.2	210.5	188.8	3.0	394.9
479.3	100.8	406.5	194.7	368.1	216.7	10.9	573.5
467.4	110.2	415.2	183.3	394.4	193.9	12.4	574.8
681.2	123.8	567.8	231.6	526.7	273.8	27.5	759.1
671.8	133.5	577.2	223.7	538.1	269.8	18.8	786.0
844.0	158.5	773.3	228.4	680.8	318.8	34.5	970.5
883.1	118.7	770.8	233.3	705.6	299.1	43.1	946.4
<hr/>							
PM400							
92.1	14.0	81.3	24.4	65.4	44.6	19.6	82.4
95.5	10.3	80.4	25.6	62.3	46.8	19.4	84.7
185.8	23.5	166.8	36.8	128.1	78.9	51.3	154.7
189.7	19.7	158.5	46.3	125.2	83.3	46.8	159.2
370.5	34.9	323.6	73.4	262.1	135.2	140.0	260.0
376.3	29.4	327.7	70.8	271.9	126.2	149.3	250.8
536.4	43.0	493.4	106.7	418.5	167.9	213.9	385.5
530.3	49.1	495.7	101.7	410.4	175.6	216.3	374.0
747.5	58.4	686.9	108.9	605.3	200.5	352.2	449.6

757.0	48.6	694.4	102.1	605.3	197.3	353.2	444.7
959.1	43.8	903.3	100.7	791.0	210.1	482.0	523.8
945.8	56.5	889.8	113.8	787.8	210.2	507.5	503.3
PM500							
64.7	41.8	48.6	57.8	29.7	80.4	4.8	97.4
67.9	38.6	49.2	56.1	32.5	78.0	4.8	99.1
134.8	73.5	102.6	102.8	68.5	138.0	13.9	187.5
143.2	67.0	98.6	107.3	72.7	135.9	10.6	195.8
284.6	119.7	231.0	168.2	158.1	238.1	21.2	380.6
298.7	106.4	238.9	158.1	166.0	227.7	33.8	362.1
461.4	115.5	369.8	227.2	294.1	297.3	63.3	533.0
431.9	145.5	378.4	220.9	276.8	306.3	66.4	526.6
656.2	149.9	541.9	253.9	451.1	355.2	136.3	670.2
637.5	170.2	537.2	258.2	423.9	384.5	113.6	694.0
805.1	196.3	750.2	253.1	623.2	382.7	264.2	745.8
831.0	171.0	729.7	274.5	605.3	397.3	216.8	772.2
PM600							
49.1	57.7	29.8	76.3	12.1	97.9	0.0	103.4
42.5	63.8	31.5	73.4	14.6	95.1	0.0	101.1
84.9	123.1	68.0	137.5	31.1	176.9	0.2	205.0
95.0	115.8	66.1	140.3	27.9	177.9	0.2	204.7
231.5	176.2	177.5	217.6	105.5	297.3	1.9	404.4
221.7	187.2	165.0	229.7	69.2	333.5	5.5	401.8
361.8	217.7	286.7	309.0	208.4	386.5	6.1	583.2
341.6	237.4	288.7	315.5	201.1	392.8	8.2	581.1
533.4	275.9	448.3	348.0	274.3	534.9	8.8	787.2
494.2	309.7	432.8	365.8	274.3	530.2	10.1	801.9
665.5	334.2	603.6	395.4	448.4	547.1	26.8	973.3
741.1	263.5	622.9	382.9	462.1	531.5	28.4	984.0
DM300							
89.4	16.7	25.5	81.5	8.7	101.5	0.0	103.7
93.4	12.8	25.0	81.7	10.3	98.0	0.0	102.4
176.5	32.6	56.6	145.1	15.7	192.1	0.0	204.2
177.8	31.2	56.8	146.3	11.7	197.3	0.0	206.8
361.8	43.3	123.7	275.5	31.9	364.8	0.0	409.4
364.7	40.8	123.7	271.1	36.9	356.8	0.0	406.3
509.3	68.5	216.3	388.3	77.9	505.1	0.0	589.2
518.3	61.6	207.6	385.3	71.0	515.8	0.0	600.4
715.8	89.7	335.0	458.3	179.0	633.4	0.0	800.0
725.3	81.4	327.1	463.3	132.1	664.1	0.0	812.2
932.6	68.9	502.5	502.3	159.0	849.0	0.0	991.4
899.6	101.5	511.7	494.3	262.1	732.2	0.0	1019.1
DM400							
79.3	26.7	60.8	45.3	26.5	82.8	0.0	104.3
78.2	28.0	63.0	43.6	32.5	76.8	0.0	101.5
148.6	60.0	130.1	75.2	69.8	139.6	1.1	202.3
164.2	45.8	135.6	67.2	74.8	131.8	1.2	203.8
301.6	105.2	292.8	105.6	180.4	220.0	7.8	392.0
330.1	76.2	278.6	118.0	173.7	223.9	7.9	394.8
470.4	109.6	448.3	153.3	294.4	293.7	21.9	566.7
491.3	86.2	435.0	164.0	308.1	282.4	22.5	568.3
643.7	163.2	622.9	173.4	437.4	361.7	26.5	783.3
662.4	141.7	608.4	190.8	452.5	348.6	35.9	777.7
866.8	133.8	773.3	225.9	611.3	387.0	48.7	964.7
857.0	147.7	812.5	188.8	552.5	454.8	45.5	965.5

DM600							
48.6	57.5	16.3	89.5	3.3	105.6	0.0	104.2
56.2	50.5	19.8	87.5	3.3	104.6	0.0	101.4
102.8	105.9	51.2	151.9	8.0	202.1	0.0	208.1
105.2	104.9	49.7	157.1	8.9	200.1	0.0	203.9
245.2	163.1	122.0	275.4	26.1	375.8	0.0	405.8
267.6	137.5	132.5	267.3	22.3	380.1	0.0	405.8
408.4	168.7	211.7	392.5	62.3	535.8	0.0	588.5
390.8	189.3	238.9	353.7	71.0	526.2	0.0	604.2
554.6	249.9	363.5	434.4	132.3	666.5	2.1	798.8
572.9	236.4	378.4	422.6	165.8	630.1	2.4	791.6
731.6	268.7	586.8	414.1	233.2	755.2	2.3	996.5
789.0	210.4	560.7	443.9	238.0	770.4	2.8	1007.3
RDM500							
60.2	45.8	39.1	66.4	19.1	91.7	0.0	101.2
67.3	39.3	38.3	68.8	19.1	90.3	0.0	101.1
124.8	83.3	93.7	110.8	45.2	165.5	0.5	201.7
129.4	79.1	90.9	113.9	45.2	162.8	0.6	203.9
287.4	119.1	200.2	197.6	143.3	255.3	1.4	401.9
281.7	125.4	225.2	170.4	117.2	284.0	1.6	406.7
431.9	149.0	331.9	265.5	200.2	385.9	1.7	584.7
476.3	101.9	334.0	262.5	235.6	357.0	4.5	593.6
628.2	178.5	511.7	288.6	386.5	422.8	6.2	791.8
606.6	198.5	495.7	304.9	368.1	435.4	10.3	777.0
801.9	200.5	719.6	278.4	464.9	540.8	12.4	976.7
821.3	180.5	669.5	330.5	535.3	460.0	18.9	997.4
DDM500							
61.5	44.4	34.8	71.8	9.4	99.5	0.0	104.2
61.8	43.7	34.6	70.8	9.4	100.0	0.0	101.7
124.3	86.9	92.1	113.6	37.5	168.2	0.0	203.7
105.7	104.9	89.5	115.6	37.5	169.2	0.0	202.4
256.4	151.3	185.0	212.0	111.8	284.4	0.0	405.3
248.0	159.7	209.8	189.5	123.9	278.9	0.0	395.8
399.6	182.6	338.2	262.9	259.7	330.0	0.0	600.4
373.4	206.9	327.7	275.8	238.0	348.4	0.0	595.9
594.3	207.7	484.3	312.4	362.9	434.1	0.0	794.0
566.8	235.7	473.0	319.8	362.9	436.7	0.0	801.0
709.5	292.1	662.1	342.6	538.1	455.5	0.9	992.9
769.8	229.4	657.1	340.2	429.3	575.9	0.6	1015.9
DDM600							
40.2	65.1	24.5	83.0	10.7	98.9	0.4	104.2
43.8	61.7	25.7	80.9	9.2	99.2	0.4	101.5
78.5	130.6	59.6	144.9	19.0	187.6	0.4	203.3
86.5	122.0	56.9	147.6	30.3	175.1	0.4	205.8
204.3	205.0	139.8	258.0	88.0	308.8	3.1	398.6
197.7	208.0	150.2	245.4	88.0	313.1	3.1	398.6
310.1	274.0	240.8	363.8	153.8	433.7	2.3	586.9
321.5	256.8	268.6	332.2	132.9	451.2	5.2	597.4
482.3	317.3	372.0	427.4	245.2	550.5	15.8	778.3
470.4	331.9	395.6	396.7	281.7	524.1	10.4	778.9
709.5	297.6	541.9	453.7	413.1	597.5	32.6	961.5
637.5	359.7	577.2	430.0	391.8	615.2	35.4	958.8
CDM500							
75.0	30.6	51.2	55.4	32.1	76.8	3.5	100.6
69.4	36.6	54.9	51.6	33.9	75.7	3.7	100.6

166.3	43.0	116.0	86.6	81.5	125.8	5.6	201.1
165.0	44.4	109.5	93.0	74.4	133.6	5.6	197.3
333.0	73.4	246.7	150.9	181.7	216.5	21.1	375.5
327.3	78.4	236.9	161.9	189.8	210.0	51.3	347.1
473.3	107.0	397.8	201.7	294.1	293.2	61.1	527.3
479.3	98.6	384.8	212.1	304.1	281.1	66.0	525.0
681.2	122.7	558.3	236.4	498.3	307.0	70.9	724.4
703.2	100.6	579.6	219.6	459.4	348.2	79.9	706.7
906.1	94.8	765.6	239.7	587.6	416.1	140.0	865.8
840.7	159.9	729.7	270.8	635.2	371.1	176.6	840.6

CDMW500

73.4	32.3	47.8	57.3	24.5	85.7	0.7	103.9
65.7	39.6	47.8	58.6	20.9	87.4	0.5	103.4
151.1	57.7	108.8	94.2	69.0	137.8	3.1	197.8
143.5	65.7	109.5	94.0	62.3	146.0	3.1	199.3
304.4	99.3	246.7	150.3	143.3	254.0	14.7	391.0
324.4	81.6	236.9	160.9	144.2	257.9	9.4	390.0
476.3	103.1	397.8	203.5	289.2	293.8	30.3	566.9
452.5	124.4	374.1	222.4	271.9	315.0	52.6	542.4
653.1	150.6	558.3	238.7	405.1	398.0	52.6	737.2
678.0	127.6	537.2	257.6	445.6	365.8	67.3	726.2
814.8	188.5	765.6	241.5	492.7	500.8	65.5	944.1
879.9	122.9	729.7	273.2	575.8	419.0	93.1	907.2

WW500

61.8	44.0	35.3	71.0	15.0	94.4	0.0	103.8
57.0	48.2	33.8	71.9	17.6	90.8	0.0	102.6
142.1	67.8	83.4	122.2	30.3	176.0	2.5	205.0
145.6	63.4	80.2	124.7	44.3	162.4	2.5	204.0
293.1	112.9	183.1	216.0	96.5	299.2	5.0	398.3
273.3	133.3	205.9	190.0	104.0	297.3	11.1	390.2
440.7	139.1	317.4	284.9	202.5	391.4	16.4	577.3
461.4	119.8	317.4	281.0	216.6	369.6	10.4	588.4
615.9	189.3	482.0	311.2	357.7	445.7	34.8	752.9
625.1	178.9	488.8	306.0	337.1	469.8	23.3	789.5
792.3	210.1	672.0	326.9	432.0	569.6	56.2	940.5
847.2	153.1	696.9	304.1	543.9	464.7	60.6	933.7

Figure 4.8 and 4.9

C_t	Q_t	C_t	Q_t	C_t	Q_t	C_t	Q_t	C_t	Q_t	C_t	Q_t
$\mu\text{g L}^{-1}$	$\mu\text{g g}^{-1}$	$\mu\text{g L}^{-1}$	$\mu\text{g g}^{-1}$	$\mu\text{g L}^{-1}$	$\mu\text{g g}^{-1}$	$\mu\text{g L}^{-1}$	$\mu\text{g g}^{-1}$	$\mu\text{g L}^{-1}$	$\mu\text{g g}^{-1}$	$\mu\text{g L}^{-1}$	$\mu\text{g g}^{-1}$
BC						Sand					
IS = 0.1 mM		IS = 1 mM		IS = 10 mM		IS = 0.1 mM		IS = 1 mM		IS = 10 mM	
LCM											
2.9	3866	3.1	3843	3.5	3809	35.4	0.0	36.0	0.0	43.4	0.0
3.0	3859	3.1	3850	3.6	3796	38.5	0.0	41.0	0.0	40.0	0.0
4.9	9425	5.3	9385	7.4	9178	76.8	0.0	95.9	0.0	95.3	0.0
5.1	9408	5.5	9365	7.7	9142	75.2	0.0	93.5	0.0	96.5	0.0
13.1	14405	14.9	14230	16.7	14052	118.1	0.0	146.0	0.0	141.7	0.0
12.0	14520	14.7	14242	17.4	13975	127.6	0.0	136.8	0.0	139.8	0.0
20.9	18242	23.3	18006	24.6	17873	157.7	0.0	180.0	0.0	188.6	0.0
21.2	18214	24.3	17904	27.7	17566	159.5	0.0	179.7	0.0	181.5	0.0
32.7	22861	32.4	22887	40.1	22119	189.4	0.1	217.3	0.0	231.2	0.0
31.2	23012	34.8	22650	46.4	21487	172.3	0.1	204.9	0.0	222.7	0.0
39.7	26567	47.1	25832	51.2	25420	220.0	0.1	254.4	0.0	264.7	0.0
39.8	26563	47.1	25834	58.5	24687	236.8	0.1	256.0	0.0	258.6	0.0
48.8	31698	61.8	30403	68.9	29691	258.3	0.1	282.3	0.1	315.7	0.0

52.1	31373	61.5	30426	78.4	28742	274.4	0.1	293.2	0.1	320.4	0.0
58.0	34604	71.0	33304	81.9	32211	296.0	0.1	318.1	0.1	360.6	0.0
52.9	35119	64.1	33994	93.1	31096	290.9	0.1	319.6	0.1	347.9	0.0
65.9	40458	79.5	39092	102.1	36833	325.9	0.1	361.6	0.1	397.5	0.1
72.5	39790	78.6	39183	93.7	37668	333.1	0.1	372.5	0.1	395.6	0.1
74.2	43462	93.6	41527	114.8	39405	349.2	0.1	396.6	0.1	415.6	0.1
78.5	43040	92.4	41640	118.3	39048	363.5	0.1	379.8	0.1	428.7	0.1
OTC											
0.1	4805	0.1	4801	0.1	4800	4.5	0.0	4.6	0.0	6.3	0.0
0.2	4794	0.2	4799	0.1	4801	4.7	0.0	4.6	0.0	6.1	0.0
0.3	10134	0.3	10130	0.3	10129	6.8	0.1	8.9	0.1	9.5	0.1
0.3	10127	0.3	10129	0.3	10134	7.2	0.1	8.7	0.1	9.1	0.1
0.5	15156	0.4	15165	0.4	15160	8.9	0.1	10.8	0.1	13.3	0.1
0.5	15149	0.4	15162	0.6	15147	9.1	0.1	10.5	0.1	12.6	0.1
0.8	19967	0.8	19970	0.8	19964	11.0	0.2	12.3	0.2	17.1	0.2
0.7	19971	0.8	19965	0.8	19970	10.9	0.2	12.4	0.2	17.6	0.2
0.9	25237	1.0	25217	1.0	25223	14.5	0.2	17.0	0.2	22.1	0.2
1.0	25226	0.9	25236	0.9	25233	13.9	0.2	16.0	0.2	21.4	0.2
1.2	29729	1.1	29731	1.2	29724	18.0	0.3	19.8	0.3	28.4	0.3
1.1	29739	1.2	29727	1.1	29733	16.9	0.3	20.5	0.3	27.3	0.3
1.5	34250	1.4	34254	1.5	34253	22.6	0.3	24.3	0.3	36.0	0.3
1.4	34258	1.5	34247	1.5	34245	21.9	0.3	23.1	0.3	35.0	0.3
1.8	41003	1.8	41003	1.8	41004	26.6	0.4	27.3	0.4	43.6	0.4
1.7	41012	1.7	41006	1.8	41003	26.9	0.4	28.3	0.4	42.8	0.4
2.1	44151	2.3	44136	2.3	44137	28.8	0.4	33.7	0.4	49.8	0.4
2.4	44126	2.1	44152	2.1	44156	30.0	0.4	32.6	0.4	47.4	0.4
2.6	49991	2.7	49976	2.4	50010	33.7	0.5	40.2	0.5	55.9	0.4
2.8	49965	2.7	49980	2.7	49975	32.2	0.5	38.3	0.5	52.1	0.4
SMX											
0.3	5155	0.3	5153	0.3	5149	56.3	0.0	56.3	0.0	55.9	0.0
0.4	5145	0.3	5149	0.4	5145	56.3	0.0	56.3	0.0	55.9	0.0
0.9	9780	0.8	9788	1.3	9746	107.9	0.0	111.4	0.0	106.1	0.0
1.0	9774	0.9	9783	1.3	9744	108.6	0.0	106.7	0.0	106.2	0.0
1.5	14715	2.2	14647	2.4	14625	157.6	0.0	156.4	0.0	154.6	0.0
1.6	14701	2.1	14652	2.3	14630	157.6	0.0	156.4	0.0	154.6	0.0
2.4	19714	3.3	19617	3.8	19567	205.3	0.0	205.6	0.0	200.1	0.0
2.5	19698	3.4	19609	3.9	19556	203.5	0.0	200.3	0.0	201.1	0.0
3.7	24784	5.7	24580	6.6	24491	247.3	0.0	245.8	0.0	243.4	0.0
4.0	24756	5.8	24575	6.9	24459	247.3	0.0	245.8	0.0	243.4	0.0
5.3	29514	7.8	29261	10.5	28990	295.1	0.0	298.6	0.0	294.4	0.0
5.6	29483	8.1	29237	10.8	28966	299.7	0.0	293.2	0.0	294.4	0.0
9.0	34213	10.5	34057	13.7	33736	354.1	0.0	353.1	0.0	349.3	0.0
9.3	34175	11.6	33946	14.2	33688	354.1	0.0	353.1	0.0	349.3	0.0
11.0	39090	16.0	38587	20.4	38145	404.6	0.0	408.8	0.0	399.0	0.0
11.5	39039	16.5	38536	20.9	38099	408.2	0.0	403.3	0.0	400.2	0.0
16.9	43588	21.9	43092	24.6	42820	452.0	0.0	453.4	0.0	450.3	0.0
14.9	43785	22.4	43035	25.0	42773	452.0	0.0	453.4	0.0	450.3	0.0
18.8	47892	24.6	47311	28.4	46928	492.4	0.0	500.1	0.0	497.6	0.0
18.4	47925	25.6	47210	27.1	47062	496.2	0.0	494.9	0.0	495.1	0.0

Appendix B: Sorption Kinetics Data

Figure 2.1

Time	C_t		C_t		C_t		C_t		C_t	
day	$\mu\text{g L}^{-1}$		$\mu\text{g L}^{-1}$		$\mu\text{g L}^{-1}$		$\mu\text{g L}^{-1}$		$\mu\text{g L}^{-1}$	
	AVG	SD	AVG	SD	AVG	SD	AVG	SD	AVG	SD
	Control		BM600		DM600		PM600		AM600	
0.04			822.2	14.7	820.7	0.0	773.2	12.6	840.0	14.7
0.13			810.3	2.1	804.3	2.1	753.9	2.1	816.2	10.5
0.21	1001.8	4.2	802.9	4.2	798.4	2.1	743.5	4.2	791.0	16.8
1	1000.4	2.1	788.0	8.4	740.5	8.4	733.1	10.5	706.3	10.5
2	1000.4	2.1	758.3	12.6	707.8	12.6	707.8	0.0	666.2	8.4
3	1006.3	14.7	750.9	6.3	669.2	8.4	700.4	10.5	645.5	4.2
5	1012.2	10.5	734.5	12.6	638.0	18.9	679.6	2.1	617.2	10.5
7	1006.0	4.2	712.2	6.1	615.9	43.2	674.4	14.7	591.4	19.6
15	1005.7	1.9	682.3	43.1	499.0	54.4	611.3	24.9	503.0	14.9
30	999.1	2.8	521.3	20.4	331.0	13.2	569.3	36.8	451.3	32.9
60	1002.7	21.3	467.5	28.7	219.3	60.9	471.9	26.4	394.0	19.8
90	998.4	6.3	420.0	33.0	123.5	51.1	381.8	54.2	285.8	11.3
180	1006.2	23.9	71.8	2.2	10.9	1.9	81.8	34.4	44.5	8.1

Figure 2.5

Time	Q_t		Q_t		Q_t		Q_t	
day	$\mu\text{g g}^{-1}$		$\mu\text{g g}^{-1}$		$\mu\text{g g}^{-1}$		$\mu\text{g g}^{-1}$	
	AVG	SD	AVG	SD	AVG	SD	AVG	SD
	BM600		DM600		PM600		AM600	
0.04	182.1	14.7	183.5	0.0	231.1	12.6	164.2	14.7
0.13	193.9	2.1	199.9	2.1	250.4	2.1	188.0	10.5
0.21	201.4	4.2	205.8	2.1	260.8	4.2	213.2	16.8
1	216.2	8.4	263.7	8.4	271.1	10.5	297.9	10.5
2	245.9	12.6	296.4	12.6	296.4	0.0	338.0	8.4
3	253.3	6.3	335.0	8.4	303.8	10.5	358.8	4.2
5	269.7	12.6	366.2	18.9	324.6	2.1	387.0	10.5
7	290.2	6.1	386.5	43.2	327.9	14.7	411.0	19.6
15	320.1	43.1	503.4	54.4	391.1	24.9	499.3	14.9
30	481.0	20.4	671.4	13.2	433.1	36.8	551.0	32.9
60	534.9	28.7	783.0	60.9	530.5	26.4	608.4	19.8
90	582.3	33.0	878.9	51.1	620.6	54.2	716.5	11.3
180	930.6	2.2	991.5	1.9	920.6	34.4	957.9	8.1

Figure 4.1

Time	C_t		C_t		C_t		C_t		C_t	
day	$\mu\text{g L}^{-1}$		$\mu\text{g L}^{-1}$		$\mu\text{g L}^{-1}$		$\mu\text{g L}^{-1}$		$\mu\text{g L}^{-1}$	
	AVG	SD	AVG	SD	AVG	SD	AVG	SD	AVG	SD
	Control		BM300		BM400		BM500		BM600	
0	1002.8	9.5	1002.8	9.5	1002.8	9.5	1002.8	9.5	1002.8	9.5
1	1008.3	10.3	807.0	19.9	821.1	28.5	847.5	31.6	777.1	5.6
2	1004.8	19.3	691.1	38.2	801.0	22.6	831.2	25.7	733.7	11.1
3	1010.2	13.6	622.3	0.0	789.1	33.8	811.1	25.6	737.6	0.0
5	1010.8	9.1	588.7	26.3	737.7	22.2	797.3	27.9	722.0	22.1
7	1005.4	5.7	340.1	18.3	696.7	2.4	780.9	5.3	666.4	21.3
14	1009.7	15.8	240.1	5.5	624.9	9.3	720.6	12.1	611.8	18.5
21	1010.4	20.5	157.2	6.3	542.5	11.2	688.3	23.9	569.6	13.6
30	1000.5	12.9	70.3	14.9	518.5	1.6	658.8	17.6	519.8	22.9
60	999.5	14.6	1.2	0.8	359.1	1.7	551.8	5.3	390.7	19.0

90	1004.5	6.8	1.2	0.1	265.2	5.1	466.4	1.0	275.7	3.7
180	1007.6	21.1	0.5	0.0	79.4	1.7	316.5	9.3	103.8	2.8
240	997.2	22.2	0.0	0.0	43.4	1.9	189.9	12.1	75.6	2.7
300	994.7	22.8	0.0	0.0	14.8	0.3	157.1	1.3	41.8	0.1
365	975.2	8.5	0.0	0.0	2.9	0.0	80.7	3.2	14.2	0.1
	DM300		DM400		DM600		PM300		PM400	
0	1002.8	9.5	1002.8	9.5	1002.8	9.5	1002.8	9.5	1002.8	9.5
1	884.2	14.5	840.5	14.8	741.6	27.8	848.0	16.8	928.6	4.9
2	833.2	17.2	822.6	6.3	700.6	8.2	827.7	2.4	918.2	9.8
3	815.0	2.8	797.4	16.7	652.6	5.4	821.0	2.4	909.6	17.1
5	801.0	11.3	791.5	8.3	620.4	2.7	814.2	2.4	902.7	22.0
7	539.3	11.2	766.5	10.3	569.6	0.0	778.1	6.4	890.6	14.6
14	467.8	36.8	624.3	6.9	437.2	10.7	766.6	8.6	879.3	17.4
21	413.2	2.1	574.9	18.5	347.2	16.3	741.1	12.8	845.3	0.0
30	287.6	14.1	534.7	30.7	237.8	12.2	665.9	6.8	810.2	7.1
60	84.9	22.5	416.3	6.9	104.8	18.6	565.6	3.6	820.5	20.6
90	14.3	5.2	341.3	40.3	33.8	8.3	402.0	24.1	741.4	36.2
180	0.7	0.0	153.9	18.5	7.7	1.3	165.0	9.6	678.1	16.7
240	0.0	0.0	100.1	11.5	3.6	0.6	100.5	6.4	566.6	13.4
300	0.0	0.0	52.0	4.7	4.8	3.0	42.2	2.5	488.7	30.2
365	0.0	0.0	18.5	3.1	5.7	0.1	6.2	1.3	465.2	5.9
	PM500		PM600		RDM500		DDM500		DDM600	
0	1002.8	9.5	1002.8	9.5	1002.8	9.5	1002.8	9.5	1002.8	9.5
1	800.9	21.2	702.8	6.1	802.0	16.5	729.9	20.1	658.4	9.8
2	787.6	21.1	657.3	18.0	777.2	14.3	722.8	22.1	618.7	7.7
3	772.7	23.4	646.1	29.8	768.5	6.1	707.2	12.0	599.8	11.4
5	772.7	28.0	634.8	5.9	724.2	4.0	676.5	23.6	577.1	1.9
7	743.0	9.3	619.4	19.7	679.2	3.9	647.4	1.9	551.9	0.0
14	716.7	10.8	571.0	9.7	578.4	0.0	533.7	29.6	456.2	18.9
21	697.6	12.5	487.7	21.2	508.2	13.0	500.2	4.8	422.0	1.5
30	624.2	11.3	474.7	36.7	476.1	8.6	438.2	10.7	396.3	10.5
60	597.3	27.0	387.0	0.0	345.8	13.7	264.5	20.1	302.6	20.3
90	539.4	28.2	274.0	10.1	230.9	10.4	145.8	10.6	240.1	2.0
180	335.7	26.5	74.9	4.5	63.0	0.5	17.5	2.0	102.7	3.3
240	292.5	24.4	48.5	1.3	36.9	3.2	4.7	0.1	59.6	0.8
300	246.7	13.8	33.9	1.2	16.3	0.0	1.3	0.1	31.0	0.1
365	170.9	17.4	9.4	3.8	4.1	2.0	0.0	0.0	13.1	2.7
	CDM500		CDMW500		WW500					
0	1002.8	9.5	1002.8	9.5	1002.8	9.5				
1	837.3	22.9	817.1	5.7	769.1	0.0				
2	827.1	14.3	795.0	8.5	753.3	5.6				
3	819.1	2.8	785.0	5.6	716.1	2.8				
5	809.0	17.0	747.4	2.8	685.2	2.7				
7	763.7	14.8	725.7	24.2	668.1	9.5				
14	737.7	2.4	661.5	33.1	613.5	20.8				
21	676.5	2.4	608.6	27.7	556.9	22.6				
30	595.2	13.6	537.1	14.8	492.3	29.0				
60	536.7	8.9	450.8	3.5	390.7	22.4				
90	499.7	0.0	361.1	0.0	305.9	35.0				
180	291.6	5.8	164.5	13.3	138.0	17.7				
240	211.2	22.9	120.9	3.0	94.5	13.4				
300	152.8	3.2	81.5	5.9	63.7	0.3				
365	93.5	1.3	36.5	6.3	23.9	0.2				

Figure 4.4

Time	Q_t	Q_t	Q_t	Q_t	Q_t
------	-------	-------	-------	-------	-------

day	$\mu\text{g g}^{-1}$		$\mu\text{g g}^{-1}$		$\mu\text{g g}^{-1}$		$\mu\text{g g}^{-1}$		$\mu\text{g g}^{-1}$	
	AVG	SD	AVG	SD	AVG	SD	AVG	SD	AVG	SD
	BM300		BM400		BM500		BM600		DM300	
1	196.4	19.8	183.7	28.6	156.3	31.3	227.6	5.4	119.5	14.3
2	311.7	37.5	202.9	21.9	172.2	25.2	270.1	12.7	171.3	17.1
3	380.5	1.0	214.9	32.5	193.1	26.4	267.2	1.2	189.4	3.2
5	414.5	25.9	266.0	22.2	206.6	27.5	281.2	21.0	202.9	10.2
7	665.1	17.7	307.1	3.2	223.3	6.7	336.4	20.4	463.8	10.8
14	763.4	2.2	379.5	9.3	282.7	12.1	392.5	21.6	534.2	36.7
21	846.3	7.1	460.3	10.4	317.0	23.1	434.9	12.9	594.2	1.6
30	936.0	19.9	485.1	1.4	346.0	16.4	482.1	22.4	716.8	10.9
60	1002.7	0.8	644.1	2.8	452.2	6.1	614.0	17.9	923.1	23.4
90	1006.6	3.7	738.8	3.8	537.6	2.8	727.4	7.6	989.7	3.5
180	1006.0	3.5	921.1	1.7	687.9	11.1	902.4	1.2	1002.1	3.5
240	1006.5	3.6	980.8	4.6	812.6	11.3	974.1	7.4	1001.5	3.5
300	1004.0	7.1	989.8	0.6	848.5	2.0	982.4	4.6	1006.5	3.6
365	1003.3	4.4	999.2	4.4	929.1	3.2	991.6	0.8	1000.2	0.0
	DM400		DM600		PM300		PM400		PM500	
1	163.1	14.8	262.8	27.6	155.5	17.1	75.1	4.8	203.9	21.2
2	181.4	6.0	303.8	10.4	176.3	3.6	85.9	10.0	216.0	20.9
3	206.6	17.4	352.7	5.4	183.2	1.4	94.5	17.7	232.3	24.1
5	213.1	7.4	384.0	3.3	190.1	1.5	101.2	22.0	231.0	26.6
7	237.3	11.4	432.2	0.0	226.9	5.8	113.5	14.6	261.8	10.0
14	380.9	7.3	565.8	13.2	237.7	8.2	124.9	18.2	287.5	13.1
21	428.8	19.6	658.3	12.8	263.4	14.4	158.6	0.8	307.5	12.6
30	470.1	27.9	767.6	8.8	340.2	6.9	194.2	8.1	380.0	11.6
60	589.5	9.6	900.8	19.4	437.5	5.5	183.6	20.0	408.7	27.8
90	665.6	41.1	974.4	10.9	599.4	23.5	263.7	36.1	463.7	30.1
180	852.2	15.5	994.4	5.7	839.5	14.8	325.2	15.8	667.8	28.3
240	903.9	17.8	1005.4	0.6	904.0	4.0	437.3	11.1	712.9	26.4
300	950.8	9.7	1000.4	3.0	984.5	0.1	516.3	32.5	756.4	17.8
365	984.9	3.0	998.9	1.0	995.9	3.9	541.8	6.5	837.3	19.0
	PM600		RDM500		DDM500		DDM600		CDM500	
1	302.3	6.1	202.7	16.2	274.9	19.9	345.1	8.5	167.6	22.9
2	346.5	19.5	226.3	13.3	280.5	23.0	387.2	8.4	176.3	14.4
3	359.1	30.9	235.9	7.6	297.9	12.5	404.9	13.9	185.8	2.5
5	368.7	5.3	279.8	3.5	327.5	22.4	427.2	0.8	195.2	18.1
7	385.2	18.7	326.0	4.0	355.5	2.2	451.8	2.0	240.4	15.0
14	431.9	8.1	426.9	1.9	469.6	29.6	545.7	19.8	265.9	2.9
21	518.2	20.4	498.9	13.1	502.2	6.2	584.2	1.5	326.9	2.1
30	528.2	35.2	528.1	5.4	566.1	14.2	605.8	11.0	409.1	16.9
60	618.9	0.5	658.6	17.7	737.2	22.0	704.9	20.4	468.2	6.0
90	734.6	10.2	772.6	7.0	859.9	15.9	764.3	5.4	504.3	3.6
180	933.2	3.7	945.1	0.3	987.1	8.1	905.2	0.9	711.9	2.7
240	977.5	0.5	983.1	2.0	1004.3	1.7	981.8	7.2	795.3	26.5
300	986.1	4.7	990.8	4.4	1005.2	3.4	989.1	5.2	847.0	3.2
365	994.0	6.4	998.0	0.6	1005.9	4.5	1002.8	7.1	914.4	1.1
	CDMW500		WW500							
1	186.6	5.5	233.9	0.4						
2	208.9	7.4	251.9	5.2						
3	220.0	6.1	287.3	3.5						
5	255.7	2.1	319.0	0.2						
7	278.5	26.5	337.8	9.2						
14	341.8	32.7	392.0	20.2						
21	394.8	26.3	447.7	25.0						

30	468.9	13.7	511.3	26.7
60	552.2	5.9	612.4	19.1
90	642.4	0.6	698.6	38.1
180	842.6	16.4	868.7	15.4
240	886.3	1.5	912.3	12.7
300	922.4	4.2	972.5	3.0
365	991.7	3.8	1003.2	1.1

Figure 4.11

Time	Q_t		Q_t		Q_t		Q_t		Q_t	
day	$\mu\text{g g}^{-1}$		$\mu\text{g g}^{-1}$		$\mu\text{g g}^{-1}$		$\mu\text{g g}^{-1}$		$\mu\text{g g}^{-1}$	
	AVG	SD	AVG	SD	AVG	SD	AVG	SD	AVG	SD
	WW500+DI		WW500+DO C(BM300)		WW500+DO C(DM300)		WW500+DO C(PM300)		WW500+DO C(DDM500)	
1	228.3	22.3	117.5	36.8	121.2	56.9	81.4	55.4	94.2	34.3
3	271.5	18.8	64.6	22.4	100.5	36.8	98.2	28.6	121.4	51.2
5	303.7	26.5	99.3	19.0	122.2	6.1	73.1	41.9	136.7	26.7
7	317.1	20.7	111.5	34.1	143.9	24.1	112.5	24.5	146.4	47.1
14	388.9	24.8	157.9	30.9	194.9	55.1	163.3	46.5	181.1	22.3
21	444.8	35.7	154.3	16.6	212.9	37.9	150.7	25.7	218.3	46.5
41	523.5	26.8	165.0	16.9	241.2	10.8	176.8	25.5	239.2	30.8
60	602.1	18.3	172.7	38.3	303.0	18.4	164.9	40.3	242.9	36.1

Figure 4.12 and 4.13

Time	Q_t		Q_t		Q_t		Q_t		Q_t	
day	$\mu\text{g g}^{-1}$		$\mu\text{g g}^{-1}$		$\mu\text{g g}^{-1}$		$\mu\text{g g}^{-1}$		$\mu\text{g g}^{-1}$	
	AVG	SD	AVG	SD	AVG	SD	AVG	SD	AVG	SD
	BM300Raw		BM300DI		BM300NaOH		DM300Raw		DM300DI	
1	243.8	27.5	451.8	7.1	692.7	2.5	141.3	30.1	284.4	2.1
3	328.5	17.4	576.4	32.8	843.0	17.7	226.9	5.7	332.7	30.5
5	434.6	26.8	654.5	32.1	934.2	0.7	275.2	12.7	423.7	24.5
7	518.8	4.7	720.0	26.4	975.9	7.6	330.0	7.9	482.2	26.4
10	620.1	0.6	813.5	20.0			380.0	0.5	559.9	26.9
15	786.2	25.2	930.5	13.7			499.4	18.8	653.2	37.7
30	912.2	0.8					714.8	7.5	931.2	9.7
60							911.5	5.8		
	DM300NaOH		BM600Raw		BM600DI		BM600NaOH		PM300Raw	
1	550.7	39.4	231.8	17.9	228.1	3.6	259.2	2.7	135.6	17.7
3	680.6	13.7	285.9	6.9	288.4	11.4	293.2	11.8	184.0	1.8
5	770.2	3.3	289.2	20.0	300.4	14.2	336.2	26.9	200.4	23.6
7	835.8	15.1	312.8	23.3	309.0	16.7	360.8	3.4	217.0	15.1
10	923.0	35.2	330.9	16.7	324.9	11.7	376.4	20.4	237.5	9.9
15			379.4	20.2	355.0	26.8	415.5	21.1	276.2	14.4
30			462.7	17.8	455.0	25.4	497.3	22.0	353.8	32.3
60			600.9	16.4	594.3	15.0	643.5	31.0	491.6	24.1
	PM300DI		DDM500Raw		DDM500DI					
1	199.0	16.9	236.5	27.5	286.3	34.3				
3	265.0	17.9	292.0	8.4	369.1	30.3				
5	298.0	17.5	327.5	14.2	419.3	29.9				
7	320.5	17.2	365.6	16.1	459.2	17.9				
10	333.9	13.1	394.3	11.9	488.3	1.8				
15	372.4	2.7	466.4	11.5	563.7	41.6				
30	464.0	22.8	542.6	10.4	734.8	1.3				
60	691.0	3.3	748.2	2.8	956.8	5.9				

Figure 5.2

Time	C_t		C_t		C_t		C_t		C_t		C_t	
h	$\mu\text{g L}^{-1}$		$\mu\text{g L}^{-1}$		$\mu\text{g L}^{-1}$		$\mu\text{g L}^{-1}$		$\mu\text{g L}^{-1}$		$\mu\text{g L}^{-1}$	
	BC				Sand							
	IS = 0.1 mM		IS = 1 mM		IS = 10 mM		IS = 0.1 mM		IS = 1 mM		IS = 10 mM	
	AVG	SD	AVG	SD	AVG	SD	AVG	SD	AVG	SD	AVG	SD
LCM												
0	100.0	0.0	100.0	0.0	100.0	0.0	100.0	0.0	100.0	0.0	100.0	0.0
0.2	1.7	0.4	3.3	0.0	3.1	0.1	76.1	0.1	88.2	0.0	95.4	0.5
0.5	2.4	0.8	3.3	0.4	3.2	0.2	75.4	0.1	86.8	1.0	93.9	0.7
1	1.3	0.2	2.9	1.1	2.9	0.3	69.6	0.1	82.2	0.1	90.0	0.0
2	1.7	0.7	1.9	0.5	2.1	0.2	69.8	0.4	82.2	0.3	90.5	0.3
4	1.1	0.2	2.6	1.3	2.4	0.3	69.3	0.6	80.8	0.8	88.7	0.2
8	0.8	0.0	2.1	0.8	2.8	0.3	69.5	0.3	81.8	0.4	89.7	0.2
OTC												
0	100.0	0.0	100.0	0.0	100.0	0.0	100.0	0.0	100.0	0.0	100.0	0.0
0.2	0.5	0.2	0.4	0.1	0.3	0.0	18.3	0.7	17.2	2.0	15.9	1.5
0.5	0.1	0.2	0.9	0.5	0.2	0.0	14.7	1.5	14.2	2.2	11.3	1.6
1	0.6	0.8	1.2	1.1	0.3	0.1	9.8	0.4	8.2	0.2	9.4	0.2
2	0.1	0.1	0.8	0.9	0.1	0.0	8.7	0.4	8.4	0.5	9.0	0.7
4	0.2	0.3	0.9	0.8	0.1	0.0	8.3	0.7	8.8	0.1	9.1	0.1
8	0.3	0.5	0.4	0.6	0.0	0.0	8.9	0.5	8.5	0.3	9.1	0.2
SMX												
0	100.0	0.0	100.0	0.0	100.0	0.0	100.0	0.0	100.0	0.0	100.0	0.0
0.2	1.4	0.1	2.0	0.3	1.7	0.1	100.6	1.5	101.3	1.0	100.5	1.5
0.5	1.4	0.0	2.6	1.0	2.1	0.3	100.0	1.6	100.5	2.4	100.5	0.8
1	3.2	2.5	3.3	2.5	2.0	0.4	100.1	1.7	100.6	0.6	100.9	1.0
2	1.7	1.1	2.1	1.2	1.5	0.2	100.3	1.8	100.2	1.6	100.1	1.4
4	1.6	0.3	3.0	2.4	1.7	0.4	99.2	1.8	100.5	1.3	100.4	0.9
8	1.5	0.4	2.7	2.0	1.6	0.4	99.9	1.8	100.4	0.8	100.5	1.1

Appendix C: Column Breakthrough Experiments Data

Figure 5.4

Tracer experiments								
PV	C/C_0		PV	C/C_0		PV	C/C_0	
	AVG	SD		AVG	SD		AVG	SD
0.15	0.00	0.00	2.83	0.91	0.01	5.52	0.00	0.00
0.31	0.00	0.00	2.99	0.43	0.03	5.67	0.00	0.00
0.46	0.00	0.00	3.15	0.06	0.02	5.83	0.00	0.00
0.62	0.00	0.00	3.31	0.00	0.00	5.99	0.00	0.00
0.78	0.01	0.00	3.46	0.00	0.00	6.15	0.00	0.00
0.94	0.30	0.01	3.62	0.00	0.00	6.31	0.00	0.00
1.09	0.82	0.04	3.78	0.00	0.00	6.46	0.00	0.00
1.25	0.99	0.01	3.94	0.00	0.00	6.62	0.00	0.00
1.41	1.00	0.01	4.10	0.00	0.00	6.78	0.00	0.00
1.57	1.00	0.00	4.25	0.00	0.00	6.94	0.00	0.00
1.73	1.00	0.01	4.41	0.00	0.00	7.10	0.00	0.00
1.88	1.01	0.01	4.57	0.00	0.00	7.25	0.00	0.00
2.04	0.99	0.00	4.73	0.00	0.00	7.41	0.00	0.00
2.20	0.99	0.00	4.89	0.00	0.00			
2.36	1.00	0.00	5.04	0.00	0.00			
2.52	1.00	0.01	5.20	0.00	0.00			
2.67	0.99	0.00	5.36	0.00	0.00			

Figure 5.7

BC only experiments							LCM-BC co-transport experiments						
PV	IS=0.1 mM		IS=1 mM		IS=10 mM		IS=0.1 mM		IS=1 mM		IS=10 mM		
	C/C_0		C/C_0		C/C_0		C/C_0		C/C_0		C/C_0		
	AVG	SD	AVG	SD	AVG	SD	AVG	SD	AVG	SD	AVG	SD	
0.15	0.00	0.00	0.00	0.00	0.00	0.00	0.00	0.00	0.00	0.00	0.00	0.00	
0.31	0.00	0.00	0.00	0.00	0.00	0.00	0.00	0.00	0.00	0.00	0.00	0.00	
0.46	0.00	0.00	0.00	0.00	0.00	0.00	0.00	0.00	0.00	0.00	0.00	0.00	
0.62	0.00	0.00	0.00	0.00	0.00	0.00	0.00	0.00	0.00	0.00	0.00	0.00	
0.78	0.02	0.01	0.01	0.00	0.00	0.00	0.07	0.00	0.02	0.01	0.00	0.00	
0.94	0.25	0.01	0.07	0.01	0.01	0.00	0.38	0.06	0.08	0.03	0.02	0.01	
1.09	0.64	0.05	0.15	0.01	0.01	0.00	0.69	0.06	0.15	0.03	0.02	0.01	
1.25	0.82	0.01	0.20	0.01	0.01	0.00	0.77	0.02	0.16	0.02	0.02	0.01	
1.41	0.85	0.01	0.21	0.02	0.01	0.00	0.79	0.00	0.17	0.02	0.02	0.01	
1.57	0.85	0.01	0.21	0.03	0.01	0.00	0.80	0.00	0.17	0.02	0.02	0.00	
1.73	0.86	0.01	0.21	0.03	0.01	0.00	0.80	0.00	0.17	0.02	0.02	0.01	
1.88	0.86	0.01	0.21	0.03	0.01	0.00	0.80	0.01	0.18	0.02	0.02	0.01	
2.04	0.85	0.00	0.21	0.04	0.01	0.00	0.80	0.01	0.18	0.03	0.02	0.01	
2.20	0.85	0.00	0.20	0.03	0.01	0.00	0.79	0.01	0.19	0.02	0.02	0.01	
2.36	0.85	0.01	0.20	0.03	0.01	0.00	0.79	0.00	0.19	0.03	0.02	0.01	
2.52	0.85	0.01	0.20	0.03	0.01	0.00	0.77	0.00	0.18	0.02	0.02	0.01	
2.67	0.86	0.02	0.18	0.04	0.01	0.00	0.78	0.01	0.17	0.01	0.02	0.00	
2.83	0.79	0.05	0.13	0.06	0.01	0.00	0.63	0.00	0.13	0.00	0.01	0.00	
2.99	0.42	0.11	0.06	0.06	0.00	0.00	0.28	0.05	0.07	0.01	0.00	0.00	
3.15	0.11	0.05	0.03	0.03	0.00	0.00	0.08	0.04	0.03	0.00	0.00	0.01	
3.31	0.02	0.02	0.01	0.02	0.00	0.00	0.03	0.02	0.01	0.00	0.00	0.00	
3.46	0.00	0.00	0.01	0.01	0.00	0.00	0.01	0.01	0.01	0.01	0.00	0.00	
3.62	0.01	0.00	0.00	0.00	0.00	0.00	0.01	0.00	0.00	0.00	0.00	0.00	
3.78	0.00	0.00	0.00	0.00	0.00	0.00	0.00	0.00	0.00	0.00	0.00	0.00	
3.94	0.00	0.00	0.00	0.00	0.00	0.00	0.00	0.00	0.00	0.00	0.00	0.00	
4.10	0.00	0.00	0.00	0.00	0.00	0.00	0.00	0.00	0.00	0.00	0.00	0.00	
4.25	0.00	0.00	0.00	0.00	0.00	0.00	0.00	0.00	0.00	0.00	0.00	0.00	

4.41	0.00	0.00	0.00	0.00	0.00	0.00	0.00	0.00	0.00	0.00	0.00	0.00
4.57	0.00	0.00	0.00	0.00	0.00	0.00	0.00	0.00	0.00	0.00	0.00	0.00
4.73	0.00	0.00	0.00	0.00	0.00	0.00	0.00	0.00	0.00	0.00	0.00	0.00
4.89	0.00	0.00	0.00	0.00	0.00	0.00	0.00	0.00	0.00	0.00	0.00	0.00
5.04	0.00	0.00	0.00	0.00	0.00	0.00	0.00	0.00	0.00	0.00	0.00	0.00
5.20	0.00	0.00	0.00	0.00	0.00	0.00	0.00	0.00	0.00	0.00	0.00	0.00
5.36	0.00	0.00	0.00	0.00	0.00	0.00	0.00	0.00	0.00	0.00	0.00	0.00
5.52	0.00	0.00	0.00	0.00	0.00	0.00	0.00	0.00	0.00	0.00	0.00	0.00
5.67	0.00	0.00	0.00	0.00	0.00	0.00	0.00	0.00	0.00	0.00	0.00	0.00
5.83	0.00	0.00	0.00	0.00	0.00	0.00	0.00	0.00	0.00	0.00	0.00	0.00
5.99	0.00	0.00	0.00	0.00	0.00	0.00	0.00	0.00	0.00	0.00	0.00	0.00
6.15	0.00	0.00	0.00	0.00	0.00	0.00	0.00	0.00	0.00	0.00	0.00	0.00
6.31	0.00	0.00	0.00	0.00	0.00	0.00	0.00	0.00	0.00	0.00	0.00	0.00
6.46	0.00	0.00	0.00	0.00	0.00	0.00	0.00	0.00	0.00	0.00	0.00	0.00
6.62	0.00	0.00	0.00	0.00	0.00	0.00	0.00	0.00	0.00	0.00	0.00	0.00
6.78	0.00	0.00	0.00	0.00	0.00	0.00	0.00	0.00	0.00	0.00	0.00	0.00
6.94	0.00	0.00	0.00	0.00	0.00	0.00	0.00	0.00	0.00	0.00	0.00	0.00
7.10	0.00	0.00	0.00	0.00	0.00	0.00	0.00	0.00	0.00	0.00	0.00	0.00
7.25	0.00	0.00	0.00	0.00	0.00	0.00	0.00	0.00	0.00	0.00	0.00	0.00
7.41	0.00	0.00	0.00	0.00	0.00	0.00	0.00	0.00	0.00	0.00	0.00	0.00

OTC-BC co-transport experiments							SMX-BC co-transport experiments					
PV	IS=0.1 mM		IS=1 mM		IS=10 mM		IS=0.1 mM		IS=1 mM		IS=10 mM	
	C/C_0		C/C_0		C/C_0		C/C_0		C/C_0		C/C_0	
	AVG	SD	AVG	SD	AVG	SD	AVG	SD	AVG	SD	AVG	SD
0.15	0.00	0.00	0.00	0.00	0.00	0.00	0.00	0.00	0.00	0.01	0.00	0.00
0.31	0.00	0.00	0.00	0.00	0.00	0.00	0.00	0.01	0.00	0.00	0.00	0.00
0.46	0.00	0.00	0.00	0.00	0.00	0.00	0.00	0.01	0.00	0.00	0.00	0.00
0.62	0.00	0.00	0.00	0.00	0.00	0.00	0.00	0.01	0.00	0.00	0.00	0.00
0.78	0.04	0.00	0.02	0.01	0.00	0.00	0.02	0.02	0.03	0.03	0.00	0.00
0.94	0.29	0.02	0.08	0.01	0.01	0.00	0.26	0.07	0.11	0.06	0.01	0.00
1.09	0.60	0.02	0.13	0.02	0.02	0.00	0.59	0.05	0.16	0.04	0.02	0.00
1.25	0.72	0.02	0.15	0.02	0.02	0.00	0.74	0.03	0.18	0.03	0.02	0.00
1.41	0.75	0.01	0.16	0.02	0.02	0.00	0.78	0.01	0.19	0.02	0.02	0.00
1.57	0.76	0.02	0.16	0.02	0.02	0.00	0.81	0.01	0.19	0.02	0.02	0.00
1.73	0.76	0.02	0.16	0.02	0.02	0.00	0.82	0.02	0.19	0.03	0.02	0.00
1.88	0.77	0.02	0.17	0.02	0.02	0.00	0.84	0.01	0.19	0.02	0.02	0.00
2.04	0.77	0.02	0.17	0.02	0.02	0.00	0.84	0.01	0.20	0.02	0.02	0.00
2.20	0.77	0.02	0.17	0.01	0.02	0.00	0.84	0.00	0.20	0.02	0.02	0.00
2.36	0.77	0.02	0.17	0.02	0.02	0.00	0.85	0.01	0.20	0.02	0.02	0.00
2.52	0.77	0.02	0.17	0.02	0.02	0.00	0.86	0.00	0.20	0.02	0.02	0.00
2.67	0.77	0.01	0.16	0.02	0.02	0.00	0.86	0.01	0.20	0.02	0.02	0.00
2.83	0.66	0.00	0.11	0.00	0.01	0.00	0.74	0.01	0.14	0.01	0.01	0.01
2.99	0.32	0.01	0.05	0.01	0.00	0.00	0.37	0.01	0.05	0.02	0.00	0.00
3.15	0.09	0.01	0.02	0.01	0.00	0.00	0.11	0.00	0.01	0.00	0.00	0.00
3.31	0.02	0.00	0.01	0.00	0.00	0.00	0.03	0.00	0.00	0.00	0.00	0.00
3.46	0.00	0.00	0.00	0.00	0.00	0.00	0.01	0.00	0.00	0.00	0.00	0.00
3.62	0.00	0.00	0.00	0.00	0.00	0.00	0.00	0.00	0.00	0.01	0.00	0.00
3.78	0.00	0.00	0.00	0.00	0.00	0.00	0.00	0.00	0.00	0.00	0.00	0.00
3.94	0.00	0.00	0.00	0.00	0.00	0.00	0.00	0.00	0.00	0.00	0.00	0.00
4.10	0.00	0.00	0.00	0.00	0.00	0.00	0.00	0.00	0.00	0.00	0.00	0.00
4.25	0.00	0.00	0.00	0.00	0.00	0.00	0.00	0.00	0.00	0.01	0.00	0.00
4.41	0.00	0.00	0.00	0.00	0.00	0.00	0.00	0.00	0.00	0.01	0.00	0.00
4.57	0.00	0.00	0.00	0.00	0.00	0.00	0.00	0.00	0.00	0.01	0.00	0.00
4.73	0.00	0.00	0.00	0.00	0.00	0.00	0.00	0.00	0.00	0.01	0.00	0.00
4.89	0.00	0.00	0.00	0.00	0.00	0.00	0.00	0.00	0.00	0.01	0.00	0.00
5.04	0.00	0.00	0.00	0.00	0.00	0.00	0.00	0.00	0.00	0.01	0.00	0.00

5.20	0.00	0.00	0.00	0.00	0.00	0.00	0.00	0.00	0.00	0.01	0.00	0.00
5.36	0.00	0.00	0.00	0.00	0.00	0.00	0.00	0.00	0.00	0.01	0.00	0.00
5.52	0.00	0.00	0.00	0.00	0.00	0.00	0.00	0.00	0.00	0.01	0.00	0.00
5.67	0.00	0.00	0.00	0.00	0.00	0.00	0.00	0.00	0.00	0.01	0.00	0.00
5.83	0.00	0.00	0.00	0.00	0.00	0.00	0.00	0.00	0.00	0.01	0.00	0.00
5.99	0.00	0.00	0.00	0.00	0.00	0.00	0.00	0.00	0.00	0.01	0.00	0.00
6.15	0.00	0.00	0.00	0.00	0.00	0.00	0.00	0.00	0.00	0.01	0.00	0.00
6.31	0.00	0.00	0.00	0.00	0.00	0.00	0.00	0.00	0.00	0.01	0.00	0.00
6.46	0.00	0.00	0.00	0.00	0.00	0.00	0.00	0.00	0.00	0.00	0.00	0.00
6.62	0.00	0.00	0.00	0.00	0.00	0.00	0.00	0.00	0.00	0.01	0.00	0.00
6.78	0.00	0.00	0.00	0.00	0.00	0.00	0.00	0.00	0.00	0.01	0.00	0.00
6.94	0.00	0.00	0.00	0.00	0.00	0.00	0.00	0.00	0.00	0.00	0.00	0.00
7.10	0.00	0.00	0.00	0.00	0.00	0.00	0.00	0.00	0.00	0.00	0.00	0.00
7.25	0.00	0.00	0.00	0.00	0.00	0.00	0.00	0.00	0.00	0.01	0.00	0.00
7.41	0.00	0.00	0.00	0.00	0.00	0.00	0.00	0.00	0.00	0.01	0.00	0.00

Figure 5.9

PV	LCM only experiments						LCM-BC co-transport experiments					
	IS=0.1 mM		IS=1 mM		IS=10 mM		IS=0.1 mM		IS=1 mM		IS=10 mM	
	C/C_0		C/C_0		C/C_0		C/C_0		C/C_0		C/C_0	
	AVG	SD	AVG	SD	AVG	SD	AVG	SD	AVG	SD	AVG	SD
0.15	0.00	0.00	0.00	0.00	0.00	0.00	0.00	0.00	0.00	0.00	0.00	0.00
0.31	0.00	0.00	0.00	0.00	0.00	0.00	0.00	0.00	0.00	0.00	0.00	0.00
0.46	0.00	0.00	0.00	0.00	0.00	0.00	0.00	0.00	0.00	0.00	0.00	0.00
0.62	0.00	0.00	0.00	0.00	0.00	0.00	0.00	0.00	0.00	0.00	0.00	0.00
0.78	0.00	0.00	0.00	0.00	0.00	0.00	0.07	0.00	0.02	0.02	0.00	0.00
0.94	0.00	0.00	0.00	0.00	0.00	0.00	0.37	0.05	0.12	0.04	0.02	0.01
1.09	0.00	0.00	0.00	0.00	0.03	0.02	0.66	0.06	0.19	0.03	0.05	0.01
1.25	0.00	0.00	0.00	0.00	0.17	0.06	0.73	0.04	0.20	0.02	0.06	0.01
1.41	0.00	0.00	0.00	0.00	0.43	0.05	0.76	0.01	0.20	0.02	0.07	0.01
1.57	0.00	0.00	0.01	0.01	0.67	0.03	0.77	0.02	0.21	0.03	0.07	0.01
1.73	0.00	0.00	0.06	0.02	0.78	0.02	0.76	0.01	0.21	0.02	0.07	0.01
1.88	0.00	0.00	0.15	0.03	0.85	0.01	0.76	0.01	0.21	0.03	0.07	0.01
2.04	0.01	0.00	0.28	0.04	0.87	0.02	0.75	0.01	0.21	0.03	0.07	0.01
2.20	0.05	0.01	0.42	0.04	0.90	0.01	0.75	0.01	0.21	0.03	0.07	0.01
2.36	0.12	0.02	0.52	0.04	0.92	0.02	0.75	0.01	0.22	0.03	0.06	0.01
2.52	0.21	0.02	0.61	0.04	0.91	0.02	0.73	0.01	0.21	0.02	0.07	0.01
2.67	0.29	0.03	0.66	0.05	0.92	0.01	0.73	0.01	0.20	0.01	0.06	0.00
2.83	0.36	0.02	0.71	0.06	0.94	0.02	0.60	0.00	0.16	0.00	0.05	0.01
2.99	0.42	0.01	0.75	0.06	0.93	0.00	0.28	0.05	0.10	0.01	0.04	0.00
3.15	0.46	0.01	0.77	0.05	0.84	0.05	0.09	0.04	0.04	0.01	0.04	0.01
3.31	0.49	0.01	0.79	0.06	0.62	0.06	0.03	0.02	0.02	0.00	0.04	0.01
3.46	0.51	0.02	0.77	0.05	0.37	0.04	0.02	0.01	0.02	0.01	0.04	0.01
3.62	0.52	0.01	0.74	0.06	0.22	0.02	0.01	0.00	0.01	0.00	0.04	0.00
3.78	0.52	0.01	0.65	0.05	0.14	0.01	0.01	0.00	0.01	0.00	0.05	0.00
3.94	0.46	0.01	0.52	0.06	0.09	0.01	0.01	0.00	0.01	0.00	0.05	0.00
4.10	0.39	0.01	0.40	0.04	0.07	0.01	0.01	0.00	0.01	0.00	0.05	0.00
4.25	0.30	0.01	0.31	0.04	0.05	0.01	0.01	0.00	0.01	0.00	0.05	0.00
4.41	0.23	0.02	0.23	0.04	0.04	0.01	0.01	0.00	0.01	0.00	0.05	0.00
4.57	0.17	0.02	0.18	0.04	0.04	0.01	0.01	0.00	0.01	0.00	0.05	0.00
4.73	0.12	0.01	0.14	0.03	0.03	0.00	0.01	0.00	0.01	0.00	0.05	0.00
4.89	0.10	0.01	0.12	0.03	0.03	0.01	0.01	0.00	0.01	0.00	0.05	0.00
5.04	0.07	0.01	0.10	0.03	0.02	0.00	0.01	0.01	0.01	0.00	0.05	0.00
5.20	0.05	0.01	0.08	0.03	0.02	0.00	0.01	0.00	0.01	0.00	0.05	0.01
5.36	0.04	0.01	0.07	0.02	0.02	0.00	0.01	0.00	0.01	0.00	0.05	0.01
5.52	0.03	0.00	0.06	0.02	0.02	0.00	0.01	0.01	0.01	0.00	0.05	0.00
5.67	0.03	0.00	0.06	0.02	0.02	0.00	0.01	0.00	0.01	0.00	0.05	0.00

5.83	0.02	0.00	0.05	0.02	0.01	0.00	0.01	0.00	0.01	0.00	0.05	0.00
5.99	0.02	0.00	0.04	0.02	0.01	0.00	0.01	0.00	0.01	0.00	0.05	0.00
6.15	0.02	0.00	0.04	0.02	0.01	0.00	0.01	0.00	0.01	0.00	0.05	0.00
6.31	0.01	0.00	0.04	0.02	0.01	0.00	0.01	0.00	0.01	0.00	0.05	0.01
6.46	0.01	0.00	0.03	0.01	0.01	0.00	0.01	0.00	0.01	0.00	0.05	0.01
6.62	0.01	0.00	0.03	0.01	0.01	0.00	0.01	0.00	0.01	0.00	0.05	0.01
6.78	0.01	0.00	0.03	0.01	0.01	0.00	0.01	0.00	0.01	0.00	0.05	0.01
6.94	0.01	0.00	0.03	0.01	0.01	0.00	0.01	0.00	0.01	0.00	0.05	0.01
7.10	0.01	0.00	0.02	0.01	0.01	0.00	0.01	0.00	0.01	0.00	0.05	0.01
7.25	0.01	0.00	0.02	0.01	0.01	0.00	0.01	0.00	0.02	0.00	0.05	0.01
7.41	0.01	0.00	0.02	0.01	0.01	0.00	0.01	0.00	0.01	0.00	0.05	0.01

PV	OTC only experiments						OTC-BC co-transport experiments					
	IS=0.1 mM		IS=1 mM		IS=10 mM		IS=0.1 mM		IS=1 mM		IS=10 mM	
	C/C_0		C/C_0		C/C_0		C/C_0		C/C_0		C/C_0	
	AVG	SD	AVG	SD	AVG	SD	AVG	SD	AVG	SD	AVG	SD
0.15	0.00	0.00	0.00	0.00	0.00	0.00	0.00	0.00	0.00	0.00	0.00	0.00
0.31	0.00	0.00	0.00	0.00	0.00	0.00	0.00	0.00	0.00	0.00	0.00	0.00
0.46	0.00	0.00	0.00	0.00	0.00	0.00	0.00	0.00	0.00	0.00	0.00	0.00
0.62	0.00	0.00	0.00	0.00	0.00	0.00	0.00	0.00	0.00	0.00	0.00	0.00
0.78	0.00	0.00	0.00	0.00	0.00	0.00	0.04	0.00	0.02	0.01	0.00	0.00
0.94	0.00	0.00	0.00	0.00	0.00	0.00	0.29	0.02	0.08	0.01	0.01	0.00
1.09	0.00	0.00	0.00	0.00	0.00	0.00	0.60	0.02	0.13	0.02	0.02	0.00
1.25	0.00	0.00	0.00	0.00	0.00	0.00	0.72	0.02	0.15	0.02	0.02	0.00
1.41	0.00	0.00	0.00	0.00	0.00	0.00	0.75	0.01	0.16	0.02	0.02	0.00
1.57	0.00	0.00	0.00	0.00	0.00	0.00	0.76	0.02	0.16	0.02	0.02	0.00
1.73	0.00	0.00	0.00	0.00	0.00	0.00	0.76	0.02	0.16	0.02	0.02	0.00
1.88	0.00	0.00	0.00	0.00	0.00	0.00	0.77	0.02	0.16	0.02	0.02	0.00
2.04	0.00	0.00	0.00	0.00	0.00	0.00	0.77	0.02	0.17	0.02	0.02	0.00
2.20	0.00	0.00	0.00	0.00	0.00	0.00	0.76	0.02	0.17	0.01	0.02	0.00
2.36	0.00	0.00	0.00	0.00	0.00	0.00	0.77	0.02	0.17	0.02	0.02	0.00
2.52	0.00	0.00	0.00	0.00	0.00	0.00	0.76	0.02	0.17	0.02	0.02	0.00
2.67	0.00	0.00	0.00	0.00	0.00	0.00	0.77	0.01	0.16	0.02	0.02	0.00
2.83	0.00	0.00	0.00	0.00	0.00	0.00	0.65	0.00	0.11	0.00	0.01	0.00
2.99	0.00	0.00	0.00	0.00	0.00	0.00	0.32	0.01	0.05	0.01	0.00	0.00
3.15	0.00	0.00	0.00	0.00	0.00	0.00	0.09	0.01	0.02	0.01	0.00	0.00
3.31	0.00	0.00	0.00	0.00	0.00	0.00	0.02	0.00	0.01	0.00	0.00	0.00
3.46	0.00	0.00	0.00	0.00	0.00	0.00	0.00	0.00	0.00	0.00	0.00	0.00
3.62	0.00	0.00	0.00	0.00	0.00	0.00	0.00	0.00	0.00	0.00	0.00	0.00
3.78	0.00	0.00	0.00	0.00	0.00	0.00	0.00	0.00	0.00	0.00	0.00	0.00
3.94	0.00	0.00	0.00	0.00	0.00	0.00	0.00	0.00	0.00	0.00	0.00	0.00
4.10	0.00	0.00	0.00	0.00	0.00	0.00	0.00	0.00	0.00	0.00	0.00	0.00
4.25	0.00	0.00	0.00	0.00	0.00	0.00	0.00	0.00	0.00	0.00	0.00	0.00
4.41	0.00	0.00	0.00	0.00	0.00	0.00	0.00	0.00	0.00	0.00	0.00	0.00
4.57	0.00	0.00	0.00	0.00	0.00	0.00	0.00	0.00	0.00	0.00	0.00	0.00
4.73	0.00	0.00	0.00	0.00	0.00	0.00	0.00	0.00	0.00	0.00	0.00	0.00
4.89	0.00	0.00	0.00	0.00	0.00	0.00	0.00	0.00	0.00	0.00	0.00	0.00
5.04	0.00	0.00	0.00	0.00	0.00	0.00	0.00	0.00	0.00	0.00	0.00	0.00
5.20	0.00	0.00	0.00	0.00	0.00	0.00	0.00	0.00	0.00	0.00	0.00	0.00
5.36	0.00	0.00	0.00	0.00	0.00	0.00	0.00	0.00	0.00	0.00	0.00	0.00
5.52	0.00	0.00	0.00	0.00	0.00	0.00	0.00	0.00	0.00	0.00	0.00	0.00
5.67	0.00	0.00	0.00	0.00	0.00	0.00	0.00	0.00	0.00	0.00	0.00	0.00
5.83	0.00	0.00	0.00	0.00	0.00	0.00	0.00	0.00	0.00	0.00	0.00	0.00
5.99	0.00	0.00	0.00	0.00	0.00	0.00	0.00	0.00	0.00	0.00	0.00	0.00
6.15	0.00	0.00	0.00	0.00	0.00	0.00	0.00	0.00	0.00	0.00	0.00	0.00
6.31	0.00	0.00	0.00	0.00	0.00	0.00	0.00	0.00	0.00	0.00	0.00	0.00
6.46	0.00	0.00	0.00	0.00	0.00	0.00	0.00	0.00	0.00	0.00	0.00	0.00

6.62	0.00	0.00	0.00	0.00	0.00	0.00	0.00	0.00	0.00	0.00	0.00	0.00
6.78	0.00	0.00	0.00	0.00	0.00	0.00	0.00	0.00	0.00	0.00	0.00	0.00
6.94	0.00	0.00	0.00	0.00	0.00	0.00	0.00	0.00	0.00	0.00	0.00	0.00
7.10	0.00	0.00	0.00	0.00	0.00	0.00	0.00	0.00	0.00	0.00	0.00	0.00
7.25	0.00	0.00	0.00	0.00	0.00	0.00	0.00	0.00	0.00	0.00	0.00	0.00
7.41	0.00	0.00	0.00	0.00	0.00	0.00	0.00	0.00	0.00	0.00	0.00	0.00

PV	SMX only experiments						SMX-BC co-transport experiments					
	IS=0.1 mM		IS=1 mM		IS=10 mM		IS=0.1 mM		IS=1 mM		IS=10 mM	
	C/C_0		C/C_0		C/C_0		C/C_0		C/C_0		C/C_0	
	AVG	SD	AVG	SD	AVG	SD	AVG	SD	AVG	SD	AVG	SD
0.15	0.00	0.00	0.00	0.01	0.00	0.00	0.00	0.00	0.00	0.01	0.00	0.00
0.31	0.00	0.00	0.00	0.01	0.00	0.00	0.00	0.01	0.00	0.00	0.00	0.00
0.46	0.00	0.00	0.00	0.01	0.00	0.00	0.00	0.01	0.00	0.00	0.00	0.00
0.62	0.00	0.00	0.00	0.01	0.00	0.00	0.00	0.01	0.00	0.00	0.00	0.00
0.78	0.00	0.00	0.01	0.03	0.01	0.01	0.04	0.02	0.03	0.03	0.01	0.00
0.94	0.10	0.08	0.35	0.15	0.29	0.00	0.28	0.06	0.12	0.06	0.02	0.00
1.09	0.72	0.15	0.83	0.12	0.77	0.00	0.60	0.05	0.18	0.04	0.03	0.00
1.25	0.95	0.02	0.96	0.06	0.91	0.05	0.74	0.03	0.20	0.03	0.03	0.00
1.41	1.00	0.01	1.00	0.02	1.01	0.02	0.79	0.01	0.21	0.02	0.03	0.01
1.57	1.01	0.02	1.00	0.01	1.03	0.01	0.81	0.01	0.21	0.02	0.03	0.00
1.73	1.01	0.06	1.00	0.03	1.03	0.03	0.82	0.02	0.21	0.03	0.03	0.00
1.88	0.99	0.01	1.00	0.00	1.00	0.02	0.84	0.01	0.21	0.02	0.03	0.00
2.04	1.01	0.03	1.00	0.02	0.99	0.09	0.85	0.01	0.21	0.02	0.03	0.00
2.20	0.99	0.03	0.99	0.01	0.99	0.08	0.84	0.01	0.22	0.02	0.03	0.00
2.36	1.02	0.02	1.01	0.00	0.98	0.08	0.86	0.01	0.22	0.02	0.03	0.00
2.52	0.98	0.03	0.99	0.01	1.06	0.01	0.86	0.00	0.22	0.02	0.03	0.00
2.67	1.00	0.01	1.00	0.00	0.94	0.12	0.87	0.01	0.22	0.02	0.03	0.00
2.83	0.95	0.04	0.88	0.08	0.97	0.07	0.74	0.02	0.15	0.01	0.02	0.01
2.99	0.63	0.06	0.39	0.14	0.43	0.02	0.39	0.01	0.06	0.02	0.01	0.00
3.15	0.16	0.03	0.07	0.06	0.13	0.04	0.14	0.01	0.02	0.00	0.00	0.00
3.31	0.02	0.00	0.00	0.01	0.03	0.02	0.05	0.00	0.01	0.00	0.00	0.00
3.46	0.00	0.00	0.00	0.00	0.00	0.00	0.03	0.01	0.01	0.00	0.00	0.00
3.62	0.00	0.00	0.00	0.00	0.00	0.00	0.03	0.01	0.01	0.01	0.00	0.00
3.78	0.00	0.00	0.00	0.01	0.00	0.00	0.03	0.01	0.01	0.00	0.00	0.00
3.94	0.00	0.00	0.00	0.01	0.00	0.00	0.03	0.01	0.01	0.00	0.00	0.00
4.10	0.00	0.00	0.00	0.01	0.00	0.00	0.03	0.00	0.01	0.00	0.00	0.00
4.25	0.00	0.00	0.00	0.01	0.00	0.00	0.03	0.00	0.01	0.01	0.00	0.00
4.41	0.00	0.00	0.00	0.01	0.00	0.00	0.03	0.01	0.01	0.01	0.01	0.00
4.57	0.00	0.00	0.00	0.01	0.00	0.00	0.03	0.00	0.01	0.01	0.01	0.00
4.73	0.00	0.00	0.00	0.01	0.00	0.00	0.03	0.01	0.01	0.01	0.01	0.00
4.89	0.00	0.00	0.00	0.01	0.00	0.00	0.03	0.00	0.01	0.01	0.01	0.00
5.04	0.00	0.00	0.00	0.01	0.00	0.00	0.03	0.00	0.01	0.01	0.01	0.00
5.20	0.00	0.00	0.00	0.01	0.00	0.00	0.03	0.00	0.01	0.01	0.01	0.00
5.36	0.00	0.00	0.00	0.01	0.00	0.00	0.03	0.00	0.01	0.00	0.01	0.00
5.52	0.00	0.00	0.00	0.01	0.00	0.00	0.03	0.00	0.01	0.01	0.01	0.00
5.67	0.00	0.00	0.00	0.01	0.00	0.00	0.02	0.00	0.01	0.01	0.01	0.00
5.83	0.00	0.00	0.00	0.01	0.00	0.00	0.03	0.00	0.01	0.01	0.01	0.00
5.99	0.00	0.00	0.00	0.01	0.00	0.00	0.03	0.00	0.01	0.01	0.01	0.00
6.15	0.00	0.00	0.00	0.01	0.00	0.00	0.03	0.00	0.01	0.01	0.01	0.00
6.31	0.00	0.00	0.00	0.01	0.00	0.00	0.03	0.00	0.01	0.01	0.01	0.00
6.46	0.00	0.00	0.00	0.01	0.00	0.00	0.03	0.01	0.01	0.01	0.01	0.00
6.62	0.00	0.00	0.00	0.01	0.00	0.00	0.03	0.00	0.01	0.01	0.01	0.00
6.78	0.00	0.00	0.00	0.01	0.00	0.00	0.03	0.00	0.01	0.01	0.01	0.00
6.94	0.00	0.00	0.00	0.01	0.00	0.00	0.03	0.00	0.01	0.01	0.01	0.00
7.10	0.00	0.00	0.00	0.01	0.00	0.00	0.03	0.00	0.01	0.01	0.01	0.00
7.25	0.00	0.00	0.00	0.01	0.00	0.00	0.03	0.01	0.01	0.01	0.01	0.00

7.41	0.00	0.00	0.00	0.01	0.00	0.00	0.03	0.01	0.01	0.01	0.01	0.00
LCM-BC co-transport experiments												
PV	Dissolved LCM		BC-associated LCM		Dissolved LCM		BC-associated LCM		Dissolved LCM		BC-associated LCM	
	IS=0.1 mM		IS=0.1 mM		IS=1 mM		IS=1 mM		IS=10 mM		IS=10 mM	
	C/C_0		C/C_0		C/C_0		C/C_0		C/C_0		C/C_0	
	AVG	SD	AVG	SD	AVG	SD	AVG	SD	AVG	SD	AVG	SD
0.15	0.00	0.00	0.00	0.00	0.00	0.00	0.00	0.00	0.00	0.00	0.00	0.00
0.31	0.00	0.00	0.00	0.00	0.00	0.00	0.00	0.00	0.00	0.00	0.00	0.00
0.46	0.00	0.00	0.00	0.00	0.00	0.00	0.00	0.00	0.00	0.00	0.00	0.00
0.62	0.00	0.00	0.00	0.00	0.00	0.00	0.00	0.00	0.00	0.00	0.00	0.00
0.78	0.01	0.00	0.06	0.00	0.01	0.01	0.01	0.01	0.00	0.00	0.00	0.00
0.94	0.02	0.00	0.36	0.05	0.04	0.01	0.08	0.03	0.01	0.01	0.01	0.01
1.09	0.01	0.00	0.65	0.06	0.05	0.00	0.13	0.03	0.03	0.00	0.02	0.01
1.25	0.02	0.01	0.72	0.02	0.05	0.01	0.15	0.02	0.04	0.00	0.02	0.01
1.41	0.01	0.01	0.74	0.00	0.05	0.01	0.15	0.02	0.05	0.00	0.02	0.01
1.57	0.02	0.02	0.75	0.00	0.05	0.01	0.16	0.02	0.05	0.01	0.02	0.00
1.73	0.01	0.01	0.75	0.00	0.05	0.00	0.16	0.02	0.05	0.00	0.02	0.01
1.88	0.01	0.00	0.75	0.01	0.04	0.01	0.16	0.02	0.05	0.01	0.02	0.01
2.04	0.01	0.00	0.74	0.01	0.05	0.00	0.17	0.02	0.05	0.01	0.02	0.01
2.20	0.01	0.00	0.74	0.01	0.04	0.01	0.17	0.02	0.05	0.01	0.02	0.01
2.36	0.01	0.00	0.74	0.00	0.04	0.01	0.17	0.02	0.05	0.00	0.02	0.01
2.52	0.01	0.00	0.72	0.00	0.04	0.00	0.17	0.02	0.05	0.01	0.02	0.01
2.67	0.01	0.00	0.72	0.01	0.04	0.00	0.16	0.01	0.05	0.00	0.02	0.00
2.83	0.01	0.00	0.59	0.00	0.04	0.00	0.12	0.00	0.04	0.00	0.01	0.00
2.99	0.02	0.00	0.26	0.05	0.03	0.01	0.07	0.01	0.04	0.00	0.00	0.00
3.15	0.01	0.01	0.08	0.04	0.02	0.00	0.03	0.00	0.04	0.00	0.00	0.01
3.31	0.01	0.00	0.03	0.01	0.01	0.00	0.01	0.00	0.04	0.01	0.00	0.00
3.46	0.00	0.00	0.01	0.01	0.01	0.00	0.01	0.01	0.04	0.01	0.00	0.00
3.62	0.00	0.00	0.01	0.00	0.01	0.00	0.00	0.00	0.04	0.00	0.00	0.00
3.78	0.00	0.00	0.00	0.00	0.01	0.00	0.00	0.00	0.05	0.00	0.00	0.00
3.94	0.00	0.00	0.00	0.00	0.01	0.00	0.00	0.00	0.05	0.00	0.00	0.00
4.10	0.01	0.00	0.00	0.00	0.01	0.00	0.00	0.00	0.05	0.00	0.00	0.00
4.25	0.01	0.00	0.00	0.00	0.01	0.00	0.00	0.00	0.05	0.00	0.00	0.00
4.41	0.01	0.00	0.00	0.00	0.01	0.00	0.00	0.00	0.05	0.00	0.00	0.00
4.57	0.01	0.00	0.00	0.00	0.01	0.00	0.00	0.00	0.05	0.00	0.00	0.00
4.73	0.01	0.00	0.00	0.00	0.01	0.00	0.00	0.00	0.05	0.00	0.00	0.00
4.89	0.01	0.00	0.00	0.00	0.01	0.00	0.00	0.00	0.05	0.00	0.00	0.00
5.04	0.01	0.00	0.00	0.00	0.01	0.00	0.00	0.00	0.05	0.00	0.00	0.00
5.20	0.01	0.00	0.00	0.00	0.01	0.00	0.00	0.00	0.05	0.00	0.00	0.00
5.36	0.01	0.00	0.00	0.00	0.01	0.00	0.00	0.00	0.05	0.00	0.00	0.00
5.52	0.01	0.00	0.00	0.00	0.01	0.00	0.00	0.00	0.05	0.00	0.00	0.00
5.67	0.01	0.00	0.00	0.00	0.01	0.00	0.00	0.00	0.05	0.00	0.00	0.00
5.83	0.01	0.00	0.00	0.00	0.01	0.00	0.00	0.00	0.05	0.00	0.00	0.00
5.99	0.01	0.00	0.00	0.00	0.01	0.00	0.00	0.00	0.05	0.00	0.00	0.00
6.15	0.01	0.00	0.00	0.00	0.01	0.00	0.00	0.00	0.05	0.00	0.00	0.00
6.31	0.01	0.00	0.00	0.00	0.01	0.00	0.00	0.00	0.05	0.01	0.00	0.00
6.46	0.01	0.00	0.00	0.00	0.01	0.00	0.00	0.00	0.05	0.01	0.00	0.00
6.62	0.01	0.00	0.00	0.00	0.01	0.00	0.00	0.00	0.05	0.01	0.00	0.00
6.78	0.01	0.00	0.00	0.00	0.01	0.00	0.00	0.00	0.05	0.01	0.00	0.00
6.94	0.01	0.00	0.00	0.00	0.01	0.00	0.00	0.00	0.05	0.01	0.00	0.00
7.10	0.01	0.00	0.00	0.00	0.01	0.00	0.00	0.00	0.05	0.01	0.00	0.00
7.25	0.01	0.00	0.00	0.00	0.01	0.00	0.00	0.00	0.05	0.01	0.00	0.00
7.41	0.01	0.00	0.00	0.00	0.01	0.00	0.00	0.00	0.05	0.01	0.00	0.00

OTC-BC co-transport experiments

PV	Dissolved OTC IS=0.1 mM		BC-associated OTC IS=0.1 mM		Dissolved OTC IS=1 mM		BC-associated OTC IS=1 mM		Dissolved OTC IS=10 mM		BC-associated OTC IS=10 mM	
	C/C_0		C/C_0		C/C_0		C/C_0		C/C_0		C/C_0	
	AVG	SD	AVG	SD	AVG	SD	AVG	SD	AVG	SD	AVG	SD
0.15	0.00	0.00	0.00	0.00	0.00	0.00	0.00	0.00	0.00	0.00	0.00	0.00
0.31	0.00	0.00	0.00	0.00	0.00	0.00	0.00	0.00	0.00	0.00	0.00	0.00
0.46	0.00	0.00	0.00	0.00	0.00	0.00	0.00	0.00	0.00	0.00	0.00	0.00
0.62	0.00	0.00	0.00	0.00	0.00	0.00	0.00	0.00	0.00	0.00	0.00	0.00
0.78	0.00	0.00	0.04	0.00	0.00	0.00	0.02	0.01	0.00	0.00	0.00	0.00
0.94	0.00	0.00	0.29	0.02	0.00	0.00	0.08	0.01	0.00	0.00	0.01	0.00
1.09	0.00	0.00	0.60	0.02	0.00	0.00	0.13	0.02	0.00	0.00	0.02	0.00
1.25	0.00	0.00	0.72	0.02	0.00	0.00	0.15	0.02	0.00	0.00	0.02	0.00
1.41	0.00	0.00	0.75	0.01	0.00	0.00	0.16	0.02	0.00	0.00	0.02	0.00
1.57	0.00	0.00	0.76	0.02	0.00	0.00	0.16	0.02	0.00	0.00	0.02	0.00
1.73	0.00	0.00	0.76	0.02	0.00	0.00	0.16	0.02	0.00	0.00	0.02	0.00
1.88	0.00	0.00	0.77	0.02	0.00	0.00	0.16	0.02	0.00	0.00	0.02	0.00
2.04	0.00	0.00	0.77	0.02	0.00	0.00	0.17	0.02	0.00	0.00	0.02	0.00
2.20	0.00	0.00	0.76	0.02	0.00	0.00	0.17	0.01	0.00	0.00	0.02	0.00
2.36	0.00	0.00	0.77	0.02	0.00	0.00	0.17	0.02	0.00	0.00	0.02	0.00
2.52	0.00	0.00	0.76	0.02	0.00	0.00	0.17	0.02	0.00	0.00	0.02	0.00
2.67	0.00	0.00	0.77	0.01	0.00	0.00	0.16	0.02	0.00	0.00	0.02	0.00
2.83	0.00	0.00	0.65	0.00	0.00	0.00	0.11	0.00	0.00	0.00	0.01	0.00
2.99	0.00	0.00	0.32	0.01	0.00	0.00	0.05	0.01	0.00	0.00	0.00	0.00
3.15	0.00	0.00	0.09	0.01	0.00	0.00	0.02	0.01	0.00	0.00	0.00	0.00
3.31	0.00	0.00	0.02	0.00	0.00	0.00	0.01	0.00	0.00	0.00	0.00	0.00
3.46	0.00	0.00	0.00	0.00	0.00	0.00	0.00	0.00	0.00	0.00	0.00	0.00
3.62	0.00	0.00	0.00	0.00	0.00	0.00	0.00	0.00	0.00	0.00	0.00	0.00
3.78	0.00	0.00	0.00	0.00	0.00	0.00	0.00	0.00	0.00	0.00	0.00	0.00
3.94	0.00	0.00	0.00	0.00	0.00	0.00	0.00	0.00	0.00	0.00	0.00	0.00
4.10	0.00	0.00	0.00	0.00	0.00	0.00	0.00	0.00	0.00	0.00	0.00	0.00
4.25	0.00	0.00	0.00	0.00	0.00	0.00	0.00	0.00	0.00	0.00	0.00	0.00
4.41	0.00	0.00	0.00	0.00	0.00	0.00	0.00	0.00	0.00	0.00	0.00	0.00
4.57	0.00	0.00	0.00	0.00	0.00	0.00	0.00	0.00	0.00	0.00	0.00	0.00
4.73	0.00	0.00	0.00	0.00	0.00	0.00	0.00	0.00	0.00	0.00	0.00	0.00
4.89	0.00	0.00	0.00	0.00	0.00	0.00	0.00	0.00	0.00	0.00	0.00	0.00
5.04	0.00	0.00	0.00	0.00	0.00	0.00	0.00	0.00	0.00	0.00	0.00	0.00
5.20	0.00	0.00	0.00	0.00	0.00	0.00	0.00	0.00	0.00	0.00	0.00	0.00
5.36	0.00	0.00	0.00	0.00	0.00	0.00	0.00	0.00	0.00	0.00	0.00	0.00
5.52	0.00	0.00	0.00	0.00	0.00	0.00	0.00	0.00	0.00	0.00	0.00	0.00
5.67	0.00	0.00	0.00	0.00	0.00	0.00	0.00	0.00	0.00	0.00	0.00	0.00
5.83	0.00	0.00	0.00	0.00	0.00	0.00	0.00	0.00	0.00	0.00	0.00	0.00
5.99	0.00	0.00	0.00	0.00	0.00	0.00	0.00	0.00	0.00	0.00	0.00	0.00
6.15	0.00	0.00	0.00	0.00	0.00	0.00	0.00	0.00	0.00	0.00	0.00	0.00
6.31	0.00	0.00	0.00	0.00	0.00	0.00	0.00	0.00	0.00	0.00	0.00	0.00
6.46	0.00	0.00	0.00	0.00	0.00	0.00	0.00	0.00	0.00	0.00	0.00	0.00
6.62	0.00	0.00	0.00	0.00	0.00	0.00	0.00	0.00	0.00	0.00	0.00	0.00
6.78	0.00	0.00	0.00	0.00	0.00	0.00	0.00	0.00	0.00	0.00	0.00	0.00
6.94	0.00	0.00	0.00	0.00	0.00	0.00	0.00	0.00	0.00	0.00	0.00	0.00
7.10	0.00	0.00	0.00	0.00	0.00	0.00	0.00	0.00	0.00	0.00	0.00	0.00
7.25	0.00	0.00	0.00	0.00	0.00	0.00	0.00	0.00	0.00	0.00	0.00	0.00
7.41	0.00	0.00	0.00	0.00	0.00	0.00	0.00	0.00	0.00	0.00	0.00	0.00
SMX-BC co-transport experiments												
	Dissolved SMX IS=0.1 mM		BC-associated SMX IS=0.1 mM		Dissolved SMX IS=1 mM		BC-associated SMX IS=1 mM		Dissolved SMX IS=10 mM		BC-associated SMX IS=10 mM	
	C/C_0		C/C_0		C/C_0		C/C_0		C/C_0		C/C_0	
	AVG	SD	AVG	SD	AVG	SD	AVG	SD	AVG	SD	AVG	SD

PV	C/C_0		C/C_0		C/C_0		C/C_0		C/C_0		C/C_0	
	AVG	SD	AVG	SD	AVG	SD	AVG	SD	AVG	SD	AVG	SD
0.15	0.00	0.00	0.00	0.00	0.00	0.00	0.00	0.01	0.00	0.00	0.00	0.00
0.31	0.00	0.00	0.00	0.01	0.00	0.00	0.00	0.00	0.00	0.00	0.00	0.00
0.46	0.00	0.00	0.00	0.01	0.00	0.00	0.00	0.00	0.00	0.00	0.00	0.00
0.62	0.00	0.00	0.00	0.01	0.00	0.00	0.00	0.00	0.00	0.00	0.00	0.00
0.78	0.01	0.00	0.02	0.02	0.00	0.00	0.03	0.03	0.00	0.00	0.00	0.00
0.94	0.03	0.00	0.25	0.06	0.02	0.00	0.10	0.05	0.01	0.00	0.01	0.00
1.09	0.03	0.00	0.57	0.05	0.02	0.00	0.16	0.04	0.02	0.00	0.02	0.00
1.25	0.03	0.01	0.71	0.03	0.02	0.00	0.18	0.02	0.02	0.00	0.02	0.00
1.41	0.04	0.00	0.76	0.01	0.02	0.00	0.18	0.02	0.02	0.00	0.02	0.00
1.57	0.04	0.00	0.78	0.01	0.02	0.00	0.19	0.02	0.02	0.00	0.02	0.00
1.73	0.04	0.00	0.78	0.02	0.02	0.00	0.19	0.02	0.02	0.00	0.02	0.00
1.88	0.04	0.00	0.81	0.01	0.02	0.00	0.19	0.02	0.02	0.00	0.02	0.00
2.04	0.04	0.00	0.81	0.01	0.02	0.00	0.19	0.02	0.02	0.00	0.02	0.00
2.20	0.04	0.00	0.81	0.00	0.02	0.00	0.19	0.02	0.02	0.00	0.02	0.00
2.36	0.04	0.00	0.82	0.01	0.02	0.00	0.19	0.02	0.02	0.00	0.02	0.00
2.52	0.04	0.00	0.82	0.00	0.03	0.00	0.20	0.02	0.02	0.00	0.02	0.00
2.67	0.04	0.00	0.83	0.01	0.02	0.00	0.19	0.02	0.02	0.00	0.02	0.00
2.83	0.04	0.01	0.71	0.01	0.02	0.00	0.13	0.01	0.01	0.00	0.01	0.01
2.99	0.04	0.00	0.36	0.01	0.01	0.00	0.05	0.02	0.01	0.00	0.00	0.00
3.15	0.03	0.00	0.10	0.00	0.01	0.00	0.01	0.00	0.00	0.00	0.00	0.00
3.31	0.03	0.00	0.02	0.00	0.01	0.00	0.00	0.00	0.00	0.00	0.00	0.00
3.46	0.03	0.00	0.00	0.00	0.01	0.00	0.00	0.00	0.00	0.00	0.00	0.00
3.62	0.03	0.00	0.00	0.00	0.01	0.00	0.00	0.01	0.00	0.00	0.00	0.00
3.78	0.02	0.00	0.00	0.00	0.01	0.00	0.00	0.00	0.00	0.00	0.00	0.00
3.94	0.03	0.00	0.00	0.00	0.01	0.00	0.00	0.00	0.00	0.00	0.00	0.00
4.10	0.03	0.00	0.00	0.00	0.01	0.00	0.00	0.00	0.00	0.00	0.00	0.00
4.25	0.03	0.00	0.00	0.00	0.01	0.00	0.00	0.01	0.00	0.00	0.00	0.00
4.41	0.03	0.00	0.00	0.00	0.01	0.00	0.00	0.01	0.01	0.00	0.00	0.00
4.57	0.03	0.00	0.00	0.00	0.01	0.00	0.00	0.01	0.01	0.00	0.00	0.00
4.73	0.03	0.00	0.00	0.00	0.01	0.00	0.00	0.01	0.01	0.00	0.00	0.00
4.89	0.03	0.00	0.00	0.00	0.01	0.00	0.00	0.01	0.01	0.00	0.00	0.00
5.04	0.03	0.00	0.00	0.00	0.01	0.00	0.00	0.01	0.01	0.00	0.00	0.00
5.20	0.03	0.00	0.00	0.00	0.01	0.00	0.00	0.01	0.01	0.00	0.00	0.00
5.36	0.03	0.00	0.00	0.00	0.01	0.00	0.00	0.00	0.01	0.00	0.00	0.00
5.52	0.03	0.00	0.00	0.00	0.01	0.00	0.00	0.01	0.01	0.00	0.00	0.00
5.67	0.02	0.00	0.00	0.00	0.01	0.00	0.00	0.01	0.01	0.00	0.00	0.00
5.83	0.03	0.00	0.00	0.00	0.01	0.00	0.00	0.01	0.01	0.00	0.00	0.00
5.99	0.03	0.00	0.00	0.00	0.01	0.00	0.00	0.01	0.01	0.00	0.00	0.00
6.15	0.03	0.00	0.00	0.00	0.01	0.00	0.00	0.01	0.01	0.00	0.00	0.00
6.31	0.03	0.00	0.00	0.00	0.01	0.00	0.00	0.01	0.01	0.00	0.00	0.00
6.46	0.03	0.00	0.00	0.00	0.01	0.00	0.00	0.00	0.01	0.00	0.00	0.00
6.62	0.03	0.00	0.00	0.00	0.01	0.00	0.00	0.01	0.01	0.00	0.00	0.00
6.78	0.03	0.00	0.00	0.00	0.01	0.00	0.00	0.01	0.01	0.00	0.00	0.00
6.94	0.03	0.00	0.00	0.00	0.01	0.00	0.00	0.00	0.01	0.00	0.00	0.00
7.10	0.03	0.00	0.00	0.00	0.01	0.00	0.00	0.00	0.01	0.00	0.00	0.00
7.25	0.03	0.00	0.00	0.00	0.01	0.00	0.00	0.01	0.01	0.00	0.00	0.00
7.41	0.03	0.00	0.00	0.00	0.01	0.00	0.00	0.01	0.01	0.00	0.00	0.00

REFERENCES

REFERENCES

- (1) Martinez, J. L. Environmental pollution by antibiotics and by antibiotic resistance determinants. *Environ. Pollut.* **2009**, *157* (11), 2893-2902.
- (2) Sarmah, A. K.; Meyer, M. T.; Boxall, A. B. A. A global perspective on the use, sales, exposure pathways, occurrence, fate and effects of veterinary antibiotics (vas) in the environment. *Chemosphere* **2006**, *65* (5), 725-759.
- (3) Kumar, K.; Gupta, S. C.; Chander, Y.; Singh, A. K. Antibiotic use in agriculture and its impact on the terrestrial environment. *Advances in Agronomy, Vol 87* **2005**, 87 1-54.
- (4) Kummerer, K. Antibiotics in the aquatic environment--a review--part i. *Chemosphere* **2009**, *75* (4), 417-34.
- (5) Kolpin, D. W.; Furlong, E. T.; Meyer, M. T.; Thurman, E. M.; Zaugg, S. D.; Barber, L. B.; Buxton, H. T. Pharmaceuticals, hormones, and other organic wastewater contaminants in us streams, 1999-2000: A national reconnaissance. *Environ. Sci. Technol.* **2002**, *36* (6), 1202-1211.
- (6) Ankley, G. T.; Brooks, B. W.; Huggett, D. B.; Sumpter, J. P. Repeating history: Pharmaceuticals in the environment. *Environ. Sci. Technol.* **2007**, *41* (24), 8211-7.
- (7) Rivera-Utrilla, J.; Sanchez-Polo, M.; Ferro-Garcia, M. A.; Prados-Joya, G.; Ocampo-Perez, R. Pharmaceuticals as emerging contaminants and their removal from water. A review. *Chemosphere* **2013**, *93* (7), 1268-87.
- (8) Homem, V.; Santos, L. Degradation and removal methods of antibiotics from aqueous matrices--a review. *J. Environ. Manage.* **2011**, *92* (10), 2304-47.
- (9) Li, S.; Shi, W.; Liu, W.; Li, H.; Zhang, W.; Hu, J.; Ke, Y.; Sun, W.; Ni, J. A duodecennial national synthesis of antibiotics in china's major rivers and seas (2005–2016). *Sci. Total Environ.* **2018**, *615* (Supplement C), 906-917.
- (10) Mellon, M. G.; Benbrook, C.; Benbrook, K. L.; Union of Concerned, S. Hogging it: Estimates of antimicrobial abuse in livestock. **2001**, (Book, Whole).
- (11) Kummerer, K.; Henninger, A. Promoting resistance by the emission of antibiotics from hospitals and households into effluent. *Clinical Microbiology and Infection* **2003**, *9* (12), 1203-1214.
- (12) Kuchta, S. L.; Cessna, A. J. Fate of lincomycin in snowmelt runoff from manure-amended pasture. *Chemosphere* **2009**, *76* (4), 439-46.

- (13) Zhu, Y. G.; Johnson, T. A.; Su, J. Q.; Qiao, M.; Guo, G. X.; Stedtfeld, R. D.; Hashsham, S. A.; Tiedje, J. M. Diverse and abundant antibiotic resistance genes in chinese swine farms. *P Natl Acad Sci USA* **2013**, *110* (9), 3435-3440.
- (14) Jjemba, P. K. The potential impact of veterinary and human therapeutic agents in manure and biosolids on plants grown on arable land: A review. *Agr Ecosyst Environ* **2002**, *93* (1-3), 267-278.
- (15) Zhang, Q.-Q.; Ying, G.-G.; Pan, C.-G.; Liu, Y.-S.; Zhao, J.-L. Comprehensive evaluation of antibiotics emission and fate in the river basins of china: Source analysis, multimedia modeling, and linkage to bacterial resistance. *Environ. Sci. Technol.* **2015**, *49* (11), 6772-6782.
- (16) Zhu, Y.-G.; Zhao, Y.; Li, B.; Huang, C.-L.; Zhang, S.-Y.; Yu, S.; Chen, Y.-S.; Zhang, T.; Gillings, M. R.; Su, J.-Q. Continental-scale pollution of estuaries with antibiotic resistance genes. *Nat. Microbiol.* **2017**, *2* 16270.
- (17) Bird, M. I.; Wynn, J. G.; Saiz, G.; Wurster, C. M.; McBeath, A. The pyrogenic carbon cycle. *Annu. Rev. Earth Planet. Sci.* **2015**, *43* (1), 273-298.
- (18) Schmidt, M. W. I.; Noack, A. G. Black carbon in soils and sediments: Analysis, distribution, implications, and current challenges. *Global Biogeochem. Cycles* **2000**, *14* (3), 777-793.
- (19) Czimczik, C. I.; Masiello, C. A. Controls on black carbon storage in soils. *Global Biogeochem. Cycles* **2007**, *21* (3), GB3005.
- (20) Preston, C. M.; Schmidt, M. W. I. Black (pyrogenic) carbon: A synthesis of current knowledge and uncertainties with special consideration of boreal regions. *Biogeosciences* **2006**, *3* (4), 397-420.
- (21) Laird, D. A. The charcoal vision: A win–win–win scenario for simultaneously producing bioenergy, permanently sequestering carbon, while improving soil and water quality. *Agron. J.* **2008**, *100* (1), 178-181.
- (22) Lehmann, J.; Gaunt, J.; Rondon, M. Bio-char sequestration in terrestrial ecosystems – a review. *Mitig. adapt. strategies glob. chang.* **2006**, *11* (2), 395-419.
- (23) Jeffery, S.; Verheijen, F. G. A.; van der Velde, M.; Bastos, A. C. A quantitative review of the effects of biochar application to soils on crop productivity using meta-analysis. *Agric., Ecosyst. Environ.* **2011**, *144* (1), 175-187.
- (24) Lehmann, J.; Joseph, S. *Biochar for environmental management: Science and technology*. Earthscan: Sterling, VA; London, 2009.
- (25) Kookana, R. S. The role of biochar in modifying the environmental fate, bioavailability, and efficacy of pesticides in soils: A review. *Soil Res.* **2010**, *48* (7), 627-637.

- (26) Lehmann, J.; Rillig, M. C.; Thies, J.; Masiello, C. A.; Hockaday, W. C.; Crowley, D. Biochar effects on soil biota - a review. *Soil Biol. Biochem.* **2011**, *43* (9), 1812-1836.
- (27) Morales, V. L.; Pérez-Reche, F. J.; Hapca, S. M.; Hanley, K. L.; Lehmann, J.; Zhang, W. Reverse engineering of biochar. *Bioresour. Technol.* **2015**, *183* (0), 163-174.
- (28) Enders, A.; Hanley, K.; Whitman, T.; Joseph, S.; Lehmann, J. Characterization of biochars to evaluate recalcitrance and agronomic performance. *Bioresour. Technol.* **2012**, *114* 644-53.
- (29) Ahmad, M.; Rajapaksha, A. U.; Lim, J. E.; Zhang, M.; Bolan, N.; Mohan, D.; Vithanage, M.; Lee, S. S.; Ok, Y. S. Biochar as a sorbent for contaminant management in soil and water: A review. *Chemosphere* **2014**, *99* 19-33.
- (30) Sun, K.; Kang, M.; Zhang, Z.; Jin, J.; Wang, Z.; Pan, Z.; Xu, D.; Wu, F.; Xing, B. Impact of deashing treatment on biochar structural properties and potential sorption mechanisms of phenanthrene. *Environ. Sci. Technol.* **2013**, *47* (20), 11473-81.
- (31) Tolls, J. Sorption of veterinary pharmaceuticals in soils: A review. *Environ. Sci. Technol.* **2001**, *35* (17), 3397-406.
- (32) Pignatello, J. J.; Xing, B. S. Mechanisms of slow sorption of organic chemicals to natural particles. *Environ. Sci. Technol.* **1996**, *30* (1), 1-11.
- (33) Beesley, L.; Moreno-Jimenez, E.; Gomez-Eyles, J. L.; Harris, E.; Robinson, B.; Sizmur, T. A review of biochars' potential role in the remediation, revegetation and restoration of contaminated soils. *Environ. Pollut.* **2011**, *159* (12), 3269-82.
- (34) Beesley, L.; Moreno-Jimenez, E.; Gomez-Eyles, J. L. Effects of biochar and greenwaste compost amendments on mobility, bioavailability and toxicity of inorganic and organic contaminants in a multi-element polluted soil. *Environ. Pollut.* **2010**, *158* (6), 2282-7.
- (35) Tan, X.; Liu, Y.; Zeng, G.; Wang, X.; Hu, X.; Gu, Y.; Yang, Z. Application of biochar for the removal of pollutants from aqueous solutions. *Chemosphere* **2015**, *125* 70-85.
- (36) Chun, Y.; Sheng, G.; Chiou, C. T.; Xing, B. Compositions and sorptive properties of crop residue-derived chars. *Environ. Sci. Technol.* **2004**, *38* (17), 4649-55.
- (37) Zhu, D.; Kwon, S.; Pignatello, J. J. Adsorption of single-ring organic compounds to wood charcoals prepared under different thermochemical conditions. *Environ Sci Technol* **2005**, *39* (11), 3990-3998.
- (38) Chen, Z.; Chen, B.; Chiou, C. T. Fast and slow rates of naphthalene sorption to biochars produced at different temperatures. *Environ. Sci. Technol.* **2012**, *46* (20), 11104-11.
- (39) Lian, F.; Xing, B. Black carbon (biochar) in water/soil environments: Molecular structure, sorption, stability, and potential risk. *Environ. Sci. Technol.* **2017**, *51* (23), 13517-13532.

- (40) Kah, M.; Sigmund, G.; Xiao, F.; Hofmann, T. Sorption of ionizable and ionic organic compounds to biochar, activated carbon and other carbonaceous materials. *Water Res.* **2017**, *124* 673-692.
- (41) Ji, L.; Wan, Y.; Zheng, S.; Zhu, D. Adsorption of tetracycline and sulfamethoxazole on crop residue-derived ashes: Implication for the relative importance of black carbon to soil sorption. *Environ. Sci. Technol.* **2011**, *45* (13), 5580-6.
- (42) Teixido, M.; Pignatello, J. J.; Beltran, J. L.; Granados, M.; Peccia, J. Speciation of the ionizable antibiotic sulfamethazine on black carbon (biochar). *Environ. Sci. Technol.* **2011**, *45* (23), 10020-7.
- (43) Liao, P.; Zhan, Z. Y.; Dai, J.; Wu, X. H.; Zhang, W. B.; Wang, K.; Yuan, S. H. Adsorption of tetracycline and chloramphenicol in aqueous solutions by bamboo charcoal: A batch and fixed-bed column study. *Chemical Engineering Journal* **2013**, *228* 496-505.
- (44) Jia, M. Y.; Wang, F.; Bian, Y. R.; Jin, X.; Song, Y.; Kengara, F. O.; Xu, R. K.; Jiang, X. Effects of pH and metal ions on oxytetracycline sorption to maize-straw-derived biochar. *Bioresource Technol* **2013**, *136* 87-93.
- (45) Wu, M.; Pan, B.; Zhang, D.; Xiao, D.; Li, H.; Wang, C.; Ning, P. The sorption of organic contaminants on biochars derived from sediments with high organic carbon content. *Chemosphere* **2013**, *90* (2), 782-8.
- (46) Essandoh, M.; Kunwar, B.; Pittman, C. U.; Mohan, D.; Mlsna, T. Sorptive removal of salicylic acid and ibuprofen from aqueous solutions using pine wood fast pyrolysis biochar. *Chemical Engineering Journal* **2015**, *265* 219-227.
- (47) Rajapaksha, A. U.; Vithanage, M.; Ahmad, M.; Seo, D.-C.; Cho, J.-S.; Lee, S.-E.; Lee, S. S.; Ok, Y. S. Enhanced sulfamethazine removal by steam-activated invasive plant-derived biochar. *J Hazard Mater* **2015**, *290* 43-50.
- (48) Nguyen, T. H.; Cho, H.-H.; Poster, D. L.; Ball, W. P. Evidence for a pore-filling mechanism in the adsorption of aromatic hydrocarbons to a natural wood char. *Environ. Sci. Technol.* **2007**, *41* (4), 1212-1217.
- (49) Chen, B.; Zhou, D.; Zhu, L. Transitional adsorption and partition of nonpolar and polar aromatic contaminants by biochars of pine needles with different pyrolytic temperatures. *Environ. Sci. Technol.* **2008**, *42* (14), 5137-43.
- (50) Nguyen, B. T.; Lehmann, J.; Hockaday, W. C.; Joseph, S.; Masiello, C. A. Temperature sensitivity of black carbon decomposition and oxidation. *Environ. Sci. Technol.* **2010**, *44* (9), 3324-3331.
- (51) Lin, Y.; Munroe, P.; Joseph, S.; Henderson, R.; Ziolkowski, A. Water extractable organic carbon in untreated and chemical treated biochars. *Chemosphere* **2012**, *87* (2), 151-7.

- (52) Uchimiya, M.; Ohno, T.; He, Z. Q. Pyrolysis temperature-dependent release of dissolved organic carbon from plant, manure, and biorefinery wastes. *J. Anal. Appl. Pyrolysis* **2013**, *104* 84-94.
- (53) Jamieson, T.; Sager, E.; Gueguen, C. Characterization of biochar-derived dissolved organic matter using UV-visible absorption and excitation-emission fluorescence spectroscopies. *Chemosphere* **2014**, *103* 197-204.
- (54) Qu, X. L.; Fu, H. Y.; Mao, J. D.; Ran, Y.; Zhang, D. N.; Zhu, D. Q. Chemical and structural properties of dissolved black carbon released from biochars. *Carbon* **2016**, *96* 759-767.
- (55) Smith, C. R.; Hatcher, P. G.; Kumar, S.; Lee, J. W. Investigation into the sources of biochar water-soluble organic compounds and their potential toxicity on aquatic microorganisms. *ACS Sustainable Chem. Eng.* **2016**, *4* (5), 2550-2558.
- (56) Fu, H.; Liu, H.; Mao, J.; Chu, W.; Li, Q.; Alvarez, P. J.; Qu, X.; Zhu, D. Photochemistry of dissolved black carbon released from biochar: Reactive oxygen species generation and phototransformation. *Environ. Sci. Technol.* **2016**, *50* (3), 1218-26.
- (57) Uchimiya, M.; Lima, I. M.; Klasson, K. T.; Wartelle, L. H. Contaminant immobilization and nutrient release by biochar soil amendment: Roles of natural organic matter. *Chemosphere* **2010**, *80* (8), 935-40.
- (58) Bruun, E. W.; Ambus, P.; Egsgaard, H.; Hauggaard-Nielsen, H. Effects of slow and fast pyrolysis biochar on soil C and N turnover dynamics. *Soil Biol. Biochem.* **2012**, *46* 73-79.
- (59) Deenik, J. L.; McClellan, T.; Uehara, G.; Antal, M. J.; Campbell, S. Charcoal volatile matter content influences plant growth and soil nitrogen transformations all rights reserved. No part of this periodical may be reproduced or transmitted in any form or by any means, electronic or mechanical, including photocopying, recording, or any information storage and retrieval system, without permission in writing from the publisher. Permission for printing and for reprinting the material contained herein has been obtained by the publisher. *Soil Sci. Soc. Am. J.* **2010**, *74* (4), 1259-1270.
- (60) Norwood, M. J.; Louchouart, P.; Kuo, L. J.; Harvey, O. R. Characterization and biodegradation of water-soluble biomarkers and organic carbon extracted from low temperature chars. *Org. Geochem.* **2013**, *56* 111-119.
- (61) Major, J.; Lehmann, J.; Rondon, M.; Goodale, C. Fate of soil-applied black carbon: Downward migration, leaching and soil respiration. *Global Change Biol.* **2010**, *16* (4), 1366-1379.
- (62) Wang, D.; Zhang, W.; Hao, X.; Zhou, D. Transport of biochar particles in saturated granular media: Effects of pyrolysis temperature and particle size. *Environ. Sci. Technol.* **2013**, *47* (2), 821-828.

- (63) Zhang, W.; Niu, J.; Morales, V. L.; Chen, X.; Hay, A. G.; Lehmann, J.; Steenhuis, T. S. Transport and retention of biochar particles in porous media: Effect of pH, ionic strength, and particle size. *Ecohydrology* **2010**, *3* (4), 497-508.
- (64) Reeves, P. T. Antibiotics: Groups and properties. In *Chemical analysis of antibiotic residues in food*, John Wiley & Sons, Inc.: 2011; pp 1-60.
- (65) Loftin, K. A.; Adams, C. D.; Meyer, M. T.; Surampalli, R. Effects of ionic strength, temperature, and pH on degradation of selected antibiotics. *J. Environ. Qual.* **2008**, *37* (2), 378-386.
- (66) Watanabe, N.; Bergamaschi, B. A.; Loftin, K. A.; Meyer, M. T.; Harter, T. Use and environmental occurrence of antibiotics in freestall dairy farms with manured forage fields. *Environ. Sci. Technol.* **2010**, *44* (17), 6591-6600.
- (67) Andreozzi, R.; Canterino, M.; Giudice, R. L.; Marotta, R.; Pinto, G.; Pollio, A. Lincomycin solar photodegradation, algal toxicity and removal from wastewaters by means of ozonation. *Water Res.* **2006**, *40* (3), 630-638.
- (68) Lissemore, L.; Hao, C.; Yang, P.; Sibley, P. K.; Mabury, S.; Solomon, K. R. An exposure assessment for selected pharmaceuticals within a watershed in southern ontario. *Chemosphere* **2006**, *64* (5), 717-729.
- (69) Morales, V. L.; Perez-Reche, F. J.; Hapca, S. M.; Hanley, K. L.; Lehmann, J.; Zhang, W. Reverse engineering of biochar. *Bioresour. Technol.* **2015**, *183* 163-74.
- (70) Rhodes, A. H.; Carlin, A.; Semple, K. T. Impact of black carbon in the extraction and mineralization of phenanthrene in soil. *Environ. Sci. Technol.* **2008**, *42* (3), 740-5.
- (71) Rajkovich, S.; Enders, A.; Hanley, K.; Hyland, C.; Zimmerman, A. R.; Lehmann, J. Corn growth and nitrogen nutrition after additions of biochars with varying properties to a temperate soil. *Biol. Fertil. Soils* **2011**, *48* (3), 271-284.
- (72) Calza, P.; Medana, C.; Padovano, E.; Dal Bello, F.; Baiocchi, C. Identification of the unknown transformation products derived from lincomycin using lc-hrms technique. *J. Mass Spectrom.* **2012**, *47* (6), 751-759.
- (73) Wu, F. C.; Tseng, R. L.; Juang, R. S. Initial behavior of intraparticle diffusion model used in the description of adsorption kinetics. *Chemical Engineering Journal* **2009**, *153* (1-3), 1-8.
- (74) Ho, Y. S.; McKay, G. Pseudo-second order model for sorption processes. *Process Biochem.* **1999**, *34* (5), 451-465.
- (75) Kasozi, G. N.; Zimmerman, A. R.; Nkedi-Kizza, P.; Gao, B. Catechol and humic acid sorption onto a range of laboratory-produced black carbons (biochars). *Environ. Sci. Technol.* **2010**, *44* (16), 6189-95.

- (76) Mukherjee, A.; Zimmerman, A. R. Organic carbon and nutrient release from a range of laboratory-produced biochars and biochar-soil mixtures. *Geoderma* **2013**, *193* 122-130.
- (77) Xiao, X.; Chen, B.; Zhu, L. Transformation, morphology, and dissolution of silicon and carbon in rice straw-derived biochars under different pyrolytic temperatures. *Environ. Sci. Technol.* **2014**, *48* (6), 3411-9.
- (78) Wu, H.; Che, X.; Ding, Z.; Hu, X.; Creamer, A. E.; Chen, H.; Gao, B. Release of soluble elements from biochars derived from various biomass feedstocks. *Environ. Sci. Pollut. Res. Int.* **2016**, *23* (2), 1905-15.
- (79) Raposo, F.; De La Rubia, M. A.; Borja, R. Methylene blue number as useful indicator to evaluate the adsorptive capacity of granular activated carbon in batch mode: Influence of adsorbate/adsorbent mass ratio and particle size. *J. Hazard. Mater.* **2009**, *165* (1-3), 291-9.
- (80) Zheng, W.; Guo, M.; Chow, T.; Bennett, D. N.; Rajagopalan, N. Sorption properties of greenwaste biochar for two triazine pesticides. *J. Hazard. Mater.* **2010**, *181* (1-3), 121-6.
- (81) Chai, Y.; Currie, R. J.; Davis, J. W.; Wilken, M.; Martin, G. D.; Fishman, V. N.; Ghosh, U. Effectiveness of activated carbon and biochar in reducing the availability of polychlorinated dibenzo-p-dioxins/dibenzofurans in soils. *Environ. Sci. Technol.* **2012**, *46* (2), 1035-43.
- (82) Zhang, W.; Faulkner, J. W.; Giri, S. K.; Geohring, L. D.; Steenhuis, T. S. Evaluation of two langmuir models for phosphorus sorption of phosphorus-enriched soils in new york for environmental applications. *Soil Sci.* **2009**, *174* (10), 523-530.
- (83) Ji, L. L.; Chen, W.; Duan, L.; Zhu, D. Q. Mechanisms for strong adsorption of tetracycline to carbon nanotubes: A comparative study using activated carbon and graphite as adsorbents. *Environ. Sci. Technol.* **2009**, *43* (7), 2322-2327.
- (84) Wang, C. P.; Ding, Y. J.; Teppen, B. J.; Boyd, S. A.; Song, C. Y.; Li, H. Role of interlayer hydration in lincomycin sorption by smectite clays. *Environ. Sci. Technol.* **2009**, *43* (16), 6171-6176.
- (85) Wang, C. P.; Teppen, B. J.; Boyd, S. A.; Li, H. Sorption of lincomycin at low concentrations from water by soils. *Soil Sci. Soc. Am. J.* **2012**, *76* (4), 1222-1228.
- (86) Harter, R. D.; Naidu, R. An assessment of environmental and solution parameter impact on trace-metal sorption by soils. *Soil Sci. Soc. Am. J.* **2001**, *65* (3), 597-612.
- (87) Ding, Y.; Teppen, B. J.; Boyd, S. A.; Li, H. Measurement of associations of pharmaceuticals with dissolved humic substances using solid phase extraction. *Chemosphere* **2013**, *91* (3), 314-9.

- (88) Laird, D. A. The charcoal vision: A win-win-win scenario for simultaneously producing bioenergy, permanently sequestering carbon, while improving soil and water quality. *Agron. J.* **2008**, *100* (1), 178-181.
- (89) Lehmann, J.; Gaunt, J.; Rondon, M. Bio-char sequestration in terrestrial ecosystems – a review. *Mitig. Adapt. Strat. Gl.* **2006**, *11* (2), 403-427.
- (90) Jeffery, S.; Verheijen, F. G. A.; van der Velde, M.; Bastos, A. C. A quantitative review of the effects of biochar application to soils on crop productivity using meta-analysis. *Agr. Ecosyst. Environ.* **2011**, *144* (1), 175-187.
- (91) Kookana, R. S. The role of biochar in modifying the environmental fate, bioavailability, and efficacy of pesticides in soils: A review. *Aust. J. Soil Res.* **2010**, *48* (6-7), 627-637.
- (92) Liu, C. H.; Chuang, Y. H.; Li, H.; Teppen, B. J.; Boyd, S. A.; Gonzalez, J. M.; Johnston, C. T.; Lehmann, J.; Zhang, W. Sorption of lincomycin by manure-derived biochars from water. *J. Environ. Qual.* **2016**, *45* (2), 519-27.
- (93) Lehmann, J. Bio-energy in the black. *Front. Ecol. Environ.* **2007**, *5* (7), 381-387.
- (94) Bird, M. I.; Wynn, J. G.; Saiz, G.; Wurster, C. M.; McBeath, A. The pyrogenic carbon cycle. *Annu Rev Earth Pl Sc* **2015**, *43* (1), 273-298.
- (95) Jaffe, R.; Ding, Y.; Niggemann, J.; Vahatalo, A. V.; Stubbins, A.; Spencer, R. G.; Campbell, J.; Dittmar, T. Global charcoal mobilization from soils via dissolution and riverine transport to the oceans. *Science* **2013**, *340* (6130), 345-7.
- (96) Wang, B.; Zhang, W.; Li, H.; Fu, H.; Qu, X.; Zhu, D. Micropore clogging by leachable pyrogenic organic carbon: A new perspective on sorption irreversibility and kinetics of hydrophobic organic contaminants to black carbon. *Environ. Pollut.* **2017**, *220* (Pt B), 1349-1358.
- (97) Deenik, J. L.; McClellan, T.; Uehara, G.; Antal, M. J.; Campbell, S. Charcoal volatile matter content influences plant growth and soil nitrogen transformations. *Soil Sci. Soc. Am. J.* **2010**, *74* (4), 1259-1270.
- (98) Hockaday, W. C.; Grannas, A. M.; Kim, S.; Hatcher, P. G. Direct molecular evidence for the degradation and mobility of black carbon in soils from ultrahigh-resolution mass spectral analysis of dissolved organic matter from a fire-impacted forest soil. *Org. Geochem.* **2006**, *37* (4), 501-510.
- (99) Dittmar, T.; de Rezende, C. E.; Manecki, M.; Niggemann, J.; Ovalle, A. R. C.; Stubbins, A.; Bernardes, M. C. Continuous flux of dissolved black carbon from a vanished tropical forest biome. *Nat. Geosci.* **2012**, *5* (9), 618-622.

- (100) Wang, D.; Zhang, W.; Hao, X.; Zhou, D. Transport of biochar particles in saturated granular media: Effects of pyrolysis temperature and particle size. *Environ. Sci. Technol.* **2013**, *47* (2), 821-8.
- (101) Wang, D.; Zhang, W.; Zhou, D. Antagonistic effects of humic acid and iron oxyhydroxide grain-coating on biochar nanoparticle transport in saturated sand. *Environ. Sci. Technol.* **2013**, *47* (10), 5154-61.
- (102) Spokas, K. A.; Novak, J. M.; Masiello, C. A.; Johnson, M. G.; Colosky, E. C.; Ippolito, J. A.; Trigo, C. Physical disintegration of biochar: An overlooked process. *Environ. Sci. Technol. Lett.* **2014**, *1* (8), 326-332.
- (103) Antal, M. J.; Gronli, M. The art, science, and technology of charcoal production. *Ind. Eng. Chem. Res.* **2003**, *42* (8), 1619-1640.
- (104) Spokas, K. A.; Novak, J. M.; Stewart, C. E.; Cantrell, K. B.; Uchimiya, M.; Dusaire, M. G.; Ro, K. S. Qualitative analysis of volatile organic compounds on biochar. *Chemosphere* **2011**, *85* (5), 869-82.
- (105) Buss, W.; Masek, O.; Graham, M.; Wust, D. Inherent organic compounds in biochar--their content, composition and potential toxic effects. *J. Environ. Manage.* **2015**, *156* 150-7.
- (106) Swift, R. S. Organic matter characterization. In *Methods of soil analysis part 3—chemical methods*, Sparks, D. L.; Page, A. L.; Helmke, P. A.; Loeppert, R. H., Eds. Soil Science Society of America, American Society of Agronomy: Madison, WI, 1996; pp 1011-1069.
- (107) International Humic Substances Society. What are humic substances. <http://humic-substances.org/what-are-humic-substances-2/> (Last accessed on July 24, 2017).
- (108) Lehmann, J.; Kleber, M. The contentious nature of soil organic matter. *Nature* **2015**, *528* (7580), 60-8.
- (109) Kleber, M.; Nico, P. S.; Plante, A.; Filley, T.; Kramer, M.; Swanston, C.; Sollins, P. Old and stable soil organic matter is not necessarily chemically recalcitrant: Implications for modeling concepts and temperature sensitivity. *Global Change Biol.* **2011**, *17* (2), 1097-1107.
- (110) Schmidt, M. W.; Torn, M. S.; Abiven, S.; Dittmar, T.; Guggenberger, G.; Janssens, I. A.; Kleber, M.; Kogel-Knabner, I.; Lehmann, J.; Manning, D. A.; Nannipieri, P.; Rasse, D. P.; Weiner, S.; Trumbore, S. E. Persistence of soil organic matter as an ecosystem property. *Nature* **2011**, *478* (7367), 49-56.
- (111) Chen, Z.; Xiao, X.; Chen, B.; Zhu, L. Quantification of chemical states, dissociation constants and contents of oxygen-containing groups on the surface of biochars produced at different temperatures. *Environ. Sci. Technol.* **2015**, *49* (1), 309-17.

- (112) Rajapaksha, A. U.; Chen, S. S.; Tsang, D. C.; Zhang, M.; Vithanage, M.; Mandal, S.; Gao, B.; Bolan, N. S.; Ok, Y. S. Engineered/designer biochar for contaminant removal/immobilization from soil and water: Potential and implication of biochar modification. *Chemosphere* **2016**, *148* 276-91.
- (113) Liu, P.; Ptacek, C. J.; Blowes, D. W.; Berti, W. R.; Landis, R. C. Aqueous leaching of organic acids and dissolved organic carbon from various biochars prepared at different temperatures. *J. Environ. Qual.* **2015**, *44* (2), 684-95.
- (114) Yao, Y.; Gao, B.; Zhang, M.; Inyang, M.; Zimmerman, A. R. Effect of biochar amendment on sorption and leaching of nitrate, ammonium, and phosphate in a sandy soil. *Chemosphere* **2012**, *89* (11), 1467-71.
- (115) Boateng, A. A. Characterization and thermal conversion of charcoal derived from fluidized-bed fast pyrolysis oil production of switchgrass. *Ind. Eng. Chem. Res.* **2007**, *46* (26), 8857-8862.
- (116) Boateng, A. A.; Mullen, C. A.; Goldberg, N. M.; Hicks, K. B.; Devine, T. E.; Lima, I. M.; McMurtrey, J. E. Sustainable production of bioenergy and biochar from the straw of high-biomass soybean lines via fast pyrolysis. *Environ. Prog. Sustainable Energy* **2010**, *29* (2), 175-183.
- (117) Boateng, A. A.; Daugaard, D. E.; Goldberg, N. M.; Hicks, K. B. Bench-scale fluidized-bed pyrolysis of switchgrass for bio-oil production. *Ind. Eng. Chem. Res.* **2007**, *46* (7), 1891-1897.
- (118) Yao, Y.; Gao, B.; Inyang, M.; Zimmerman, A. R.; Cao, X.; Pullammanappallil, P.; Yang, L. Biochar derived from anaerobically digested sugar beet tailings: Characterization and phosphate removal potential. *Bioresour. Technol.* **2011**, *102* (10), 6273-8.
- (119) Brewer, C. E.; Chuang, V. J.; Masiello, C. A.; Gonnermann, H.; Gao, X. D.; Dugan, B.; Driver, L. E.; Panzacchi, P.; Zygourakis, K.; Davies, C. A. New approaches to measuring biochar density and porosity. *Biomass Bioenerg* **2014**, *66* 176-185.
- (120) Helms, J. R.; Stubbins, A.; Ritchie, J. D.; Minor, E. C.; Kieber, D. J.; Mopper, K. Absorption spectral slopes and slope ratios as indicators of molecular weight, source, and photobleaching of chromophoric dissolved organic matter. *Limnol. Oceanogr.* **2008**, *53* (3), 955-969.
- (121) Johnson, R. L.; Schmidt-Rohr, K. Quantitative solid-state ^{13}C NMR with signal enhancement by multiple cross polarization. *J. Magn. Reson.* **2014**, *239* 44-9.
- (122) Mao, J. D.; Schmidt-Rohr, K. Accurate quantification of aromaticity and nonprotonated aromatic carbon fraction in natural organic matter by ^{13}C solid-state nuclear magnetic resonance. *Environ. Sci. Technol.* **2004**, *38* (9), 2680-2684.

- (123) Mao, J. D.; Hu, W. G.; Schmidt-Rohr, K.; Davies, G.; Ghabbour, E. A.; Xing, B. S. Quantitative characterization of humic substances by solid-state carbon-13 nuclear magnetic resonance. *Soil Sci. Soc. Am. J.* **2000**, *64* (3), 873-884.
- (124) Cao, X.; Pignatello, J. J.; Li, Y.; Lattao, C.; Chappell, M. A.; Chen, N.; Miller, L. F.; Mao, J. Characterization of wood chars produced at different temperatures using advanced solid-state ^{13}C NMR spectroscopic techniques. *Energ Fuel* **2012**, *26* (9), 5983-5991.
- (125) Mao, J. D.; Kong, X. Q.; Schmidt-Rohr, K.; Pignatello, J. J.; Perdue, E. M. Advanced solid-state NMR characterization of marine dissolved organic matter isolated using the coupled reverse osmosis/electrodialysis method. *Environ. Sci. Technol.* **2012**, *46* (11), 5806-5814.
- (126) Brewer, C. E.; Schmidt-Rohr, K.; Satrio, J. A.; Brown, R. C. Characterization of biochar from fast pyrolysis and gasification systems. *Environ. Prog. Sustainable Energy* **2009**, *28* (3), 386-396.
- (127) Mao, J. D.; Johnson, R. L.; Lehmann, J.; Olk, D. C.; Neves, E. G.; Thompson, M. L.; Schmidt-Rohr, K. Abundant and stable char residues in soils: Implications for soil fertility and carbon sequestration. *Environ. Sci. Technol.* **2012**, *46* (17), 9571-6.
- (128) Pastorova, I.; Arisz, P. W.; Boon, J. J. Preservation of d-glucose-oligosaccharides in cellulose chars. *Carbohydr. Res.* **1993**, *248* 151-165.
- (129) Bruun, E. W.; Hauggaard-Nielsen, H.; Ibrahim, N.; Egsgaard, H.; Ambus, P.; Jensen, P. A.; Dam-Johansen, K. Influence of fast pyrolysis temperature on biochar labile fraction and short-term carbon loss in a loamy soil. *Biomass Bioenerg* **2011**, *35* (3), 1182-1189.
- (130) Kumar, P.; Barrett, D. M.; Delwiche, M. J.; Stroeve, P. Methods for pretreatment of lignocellulosic biomass for efficient hydrolysis and biofuel production. *Ind. Eng. Chem. Res.* **2009**, *48* (8), 3713-3729.
- (131) He, Z. Q.; Mao, J. D.; Honeycutt, C. W.; Ohno, T.; Hunt, J. F.; Cade-Menun, B. J. Characterization of plant-derived water extractable organic matter by multiple spectroscopic techniques. *Biol. Fertil. Soils* **2009**, *45* (6), 609-616.
- (132) Minor, E. C.; Swenson, M. M.; Mattson, B. M.; Oyler, A. R. Structural characterization of dissolved organic matter: A review of current techniques for isolation and analysis. *Environ. Sci. Process. Impact* **2014**, *16* (9), 2064-79.
- (133) Fichot, C. G.; Benner, R. The spectral slope coefficient of chromophoric dissolved organic matter (s₂₇₅₋₂₉₅) as a tracer of terrigenous dissolved organic carbon in river-influenced ocean margins. *Limnol. Oceanogr.* **2012**, *57* (5), 1453-1466.
- (134) Brewer, C. E.; Hu, Y. Y.; Schmidt-Rohr, K.; Loynachan, T. E.; Laird, D. A.; Brown, R. C. Extent of pyrolysis impacts on fast pyrolysis biochar properties. *J. Environ. Qual.* **2012**, *41* (4), 1115-1122.

- (135) Harvey, O. R.; Herbert, B. E.; Kuo, L.-J.; Louchouart, P. Generalized two-dimensional perturbation correlation infrared spectroscopy reveals mechanisms for the development of surface charge and recalcitrance in plant-derived biochars. *Environ. Sci. Technol.* **2012**, *46* (19), 10641-10650.
- (136) Keiluweit, M.; Nico, P. S.; Johnson, M. G.; Kleber, M. Dynamic molecular structure of plant biomass-derived black carbon (biochar). *Environ. Sci. Technol.* **2010**, *44* (4), 1247-53.
- (137) Xiao, B.; Sun, X. F.; Sun, R. C. Chemical, structural, and thermal characterizations of alkali-soluble lignins and hemicelluloses, and cellulose from maize stems, rye straw, and rice straw. *Polym. Degrad. Stab.* **2001**, *74* (2), 307-319.
- (138) Cole, D. P.; Smith, E. A.; Lee, Y. J. High-resolution mass spectrometric characterization of molecules on biochar from pyrolysis and gasification of switchgrass. *Energ Fuel* **2012**, *26* (6), 3803-3809.
- (139) Bridgwater, A. V. Review of fast pyrolysis of biomass and product upgrading. *Biomass Bioenerg* **2012**, *38* 68-94.
- (140) Yang, H. P.; Yan, R.; Chen, H. P.; Lee, D. H.; Zheng, C. G. Characteristics of hemicellulose, cellulose and lignin pyrolysis. *Fuel* **2007**, *86* (12-13), 1781-1788.
- (141) Zhao, L.; Cao, X.; Masek, O.; Zimmerman, A. Heterogeneity of biochar properties as a function of feedstock sources and production temperatures. *J. Hazard. Mater.* **2013**, *256-257* 1-9.
- (142) Budai, A.; Zimmerman, A. R.; Cowie, A. L.; Webber, J. B. W.; Singh, B. P.; Glaser, B.; Masiello, C. A.; Andersson, D.; Shields, F.; Lehmann, J.; Camps Arbestain, M.; Williams, M.; Sohi, S.; Joseph, S. *Biochar carbon stability test method: An assessment of methods to determine biochar carbon stability*; International Biochar Initiative: 2013; http://www.biochar-international.org/sites/default/files/IBI_Report_Biochar_Stability_Test_Method_Final.pdf.
- (143) Camps-Arbestain, M.; Amonette, J. E.; Singh, B.; Wang, T.; Schmidt, H. P. A biochar classification system and associated test methods. In *Biochar for environmental management: Science and technology and implementation, 2nd edition*, Lehmann, J.; Joseph, S., Eds. Routledge: 2015; pp 165-194.
- (144) Zhang, Q. Q.; Ying, G. G.; Pan, C. G.; Liu, Y. S.; Zhao, J. L. Comprehensive evaluation of antibiotics emission and fate in the river basins of china: Source analysis, multimedia modeling, and linkage to bacterial resistance. *Environ. Sci. Technol.* **2015**, *49* (11), 6772-82.
- (145) Van Boeckel, T. P.; Glennon, E. E.; Chen, D.; Gilbert, M.; Robinson, T. P.; Grenfell, B. T.; Levin, S. A.; Bonhoeffer, S.; Laxminarayan, R. Reducing antimicrobial use in food animals. *Science* **2017**, *357* (6358), 1350-1352.

- (146) Zhu, Y. G.; Johnson, T. A.; Su, J. Q.; Qiao, M.; Guo, G. X.; Stedtfeld, R. D.; Hashsham, S. A.; Tiedje, J. M. Diverse and abundant antibiotic resistance genes in chinese swine farms. *P Natl Acad Sci USA* **2013**, *110* (9), 3435-40.
- (147) Heuer, H.; Schmitt, H.; Smalla, K. Antibiotic resistance gene spread due to manure application on agricultural fields. *Curr. Opin. Microbiol.* **2011**, *14* (3), 236-43.
- (148) Chee-Sanford, J. C.; Mackie, R. I.; Koike, S.; Krapac, I. G.; Lin, Y. F.; Yannarell, A. C.; Maxwell, S.; Aminov, R. I. Fate and transport of antibiotic residues and antibiotic resistance genes following land application of manure waste. *J. Environ. Qual.* **2009**, *38* (3), 1086-1108.
- (149) Lehmann, J.; Joseph, S. *Biochar for environmental management: Science, technology and implementation*. Routledge: 2015.
- (150) Ahmed, M. B.; Zhou, J. L.; Ngo, H. H.; Guo, W. Adsorptive removal of antibiotics from water and wastewater: Progress and challenges. *Sci. Total Environ.* **2015**, *532* 112-26.
- (151) Peiris, C.; Gunatilake, S. R.; Mlsna, T. E.; Mohan, D.; Vithanage, M. Biochar based removal of antibiotic sulfonamides and tetracyclines in aquatic environments: A critical review. *Bioresour. Technol.* **2017**, *246* 150-159.
- (152) Shang, J. G.; Kong, X. R.; He, L. L.; Li, W. H.; Liao, Q. J. H. Low-cost biochar derived from herbal residue: Characterization and application for ciprofloxacin adsorption. *Int. J. Environ. Sci. Technol.* **2016**, *13* (10), 2449-2458.
- (153) Feng, D.; Yu, H. M.; Deng, H.; Li, F. Z.; Ge, C. J. Adsorption characteristics of norfloxacin by biochar prepared by cassava dreg: Kinetics, isotherms, and thermodynamic analysis. *Bioresources* **2015**, *10* (4), 6751-6768.
- (154) Wang, H.; Chu, Y.; Fang, C.; Huang, F.; Song, Y.; Xue, X. Sorption of tetracycline on biochar derived from rice straw under different temperatures. *PLoS One* **2017**, *12* (8), e0182776.
- (155) Huang, H.; Tang, J. C.; Gao, K.; He, R. Z.; Zhao, H.; Werner, D. Characterization of koh modified biochars from different pyrolysis temperatures and enhanced adsorption of antibiotics. *RSC Adv.* **2017**, *7* (24), 14640-14648.
- (156) Zheng, H.; Wang, Z. Y.; Zhao, J.; Herbert, S.; Xing, B. S. Sorption of antibiotic sulfamethoxazole varies with biochars produced at different temperatures. *Environ. Pollut.* **2013**, *181* 60-67.
- (157) Pan, B.; Huang, P.; Wu, M.; Wang, Z.; Wang, P.; Jiao, X.; Xing, B. Physicochemical and sorption properties of thermally-treated sediments with high organic matter content. *Bioresour. Technol.* **2012**, *103* (1), 367-73.

- (158) Lian, F.; Sun, B.; Song, Z.; Zhu, L.; Qi, X.; Xing, B. Physicochemical properties of herb-residue biochar and its sorption to ionizable antibiotic sulfamethoxazole. *Chemical Engineering Journal* **2014**, *248* 128-134.
- (159) Zimmerman, A. R.; Gao, B. *The stability of biochar in the environment introduction*. 2013; Vol. 1, p 1-40.
- (160) Liu, C. H.; Chu, W.; Li, H.; Boyd, S. A.; Teppen, B. J.; Mao, J.; Lehmann, J.; W., Z. Quantification and characterization of dissolved organic carbon from biochars *Under review*.
- (161) Weber, W. J.; Morris, J. C. Kinetics of adsorption on carbon from solution. *Journal of the Sanitary Engineering Division* **1963**, *89* (2), 31-60.
- (162) Xing, B. S.; Pignatello, J. J. Time-dependent isotherm shape of organic compounds in soil organic matter: Implications for sorption mechanism. *Environ. Toxicol. Chem.* **1996**, *15* (8), 1282-1288.
- (163) Bernal, M. P.; Alburquerque, J. A.; Moral, R. Composting of animal manures and chemical criteria for compost maturity assessment. A review. *Bioresour. Technol.* **2009**, *100* (22), 5444-53.
- (164) Laird, D. A.; Chappell, M. A.; Martens, D. A.; Wershaw, R. L.; Thompson, M. Distinguishing black carbon from biogenic humic substances in soil clay fractions. *Geoderma* **2008**, *143* (1-2), 115-122.
- (165) Continental Carbon. Rubber grade carbon blacks.
http://www.continentalcarbon.com/pdfs/What_Is_Carbon_Black.pdf (Accessed on April 9, 2018).
- (166) Ozawa, M.; Ozawa, E. Carbon blacks as the source materials for carbon nanotechnology. *Carbon Nanotechnology* **2006**, 127-151.
- (167) International Carbon Black Association. What is carbon black? <http://www.carbon-black.org/index.php/what-is-carbon-black> (Accessed on April 9, 2018).
- (168) Bisiaux, M. M.; Edwards, R.; Heyvaert, A. C.; Thomas, J. M.; Fitzgerald, B.; Susfalk, R. B.; Schladow, S. G.; Thaw, M. Stormwater and fire as sources of black carbon nanoparticles to lake tahoe. *Environ. Sci. Technol.* **2011**, *45* (6), 2065-2071.
- (169) Kole, P. J.; Löhr, A. J.; Van Belleghem, F. G. A. J.; Ragas, A. M. J. Wear and tear of tyres: A stealthy source of microplastics in the environment. *Int. J. Environ. Res. Public Health* **2017**, *14* (10), 1265.
- (170) Joseph, S. D.; Camps-Arbestain, M.; Lin, Y.; Munroe, P.; Chia, C. H.; Hook, J.; van Zwieten, L.; Kimber, S.; Cowie, A.; Singh, B. P.; Lehmann, J.; Foidl, N.; Smernik, R. J.;

Amonette, J. E. An investigation into the reactions of biochar in soil. *Soil Res.* **2010**, 48 (7), 501-515.

(171) Atkinson, C.; Fitzgerald, J.; Hipps, N. Potential mechanisms for achieving agricultural benefits from biochar application to temperate soils: A review. *Plant and Soil* **2010**, 337 (1), 1-18.

(172) Qu, X.; Fu, H.; Mao, J.; Ran, Y.; Zhang, D.; Zhu, D. Chemical and structural properties of dissolved black carbon released from biochars. *Carbon* **2016**, 96 759-767.

(173) Wang, D.; Zhang, W.; Zhou, D.-M. Antagonistic effects of humic acid and iron oxyhydroxide grain-coating on biochar nanoparticle transport in saturated sand. *Environ. Sci. Technol.* **2013**, 47 (10), 5154-5161.

(174) Wang, D.; Bradford, S. A.; Paradelo, M.; Peijnenburg, W. J. G. M.; Zhou, D. Facilitated transport of copper with hydroxyapatite nanoparticles in saturated sand. *Soil Sci. Soc. Am. J.* **2012**, 76 (2), 375-388.

(175) Xu, F.; Wei, C.; Zeng, Q.; Li, X.; Alvarez, P. J. J.; Li, Q.; Qu, X.; Zhu, D. Aggregation behavior of dissolved black carbon: Implications for vertical mass flux and fractionation in aquatic systems. *Environ. Sci. Technol.* **2017**, 51 (23), 13723-13732.

(176) Zhang, W.; Rattanaudompol, U.; Li, H.; Bouchard, D. Effect of humic and fulvic acids on aggregation of aqu/nc₆₀ nanoparticles. *Water Res.* **2013**, 47 (5), 1793-1802.

(177) Bouchard, D.; Zhang, W.; Powell, T.; Rattanaudompol, U. Aggregation kinetics and transport of single-walled carbon nanotubes at low surfactant concentrations. *Environ. Sci. Technol.* **2012**, 46 (8), 4458-4465.

(178) Isaacson, C. W.; Bouchard, D. C. Effects of humic acid and sunlight on the generation and aggregation state of aqu/c₆₀ nanoparticles. *Environ. Sci. Technol.* **2010**, 44 (23), 8971-8976.

(179) Bouchard, D.; Ma, X.; Isaacson, C. Colloidal properties of aqueous fullerenes: Isoelectric points and aggregation kinetics of c₆₀ and c₆₀ derivatives. *Environ. Sci. Technol.* **2009**, 43 (17), 6597-6603.

(180) Chen, C.; Huang, W. Aggregation kinetics of diesel soot nanoparticles in wet environments. *Environ. Sci. Technol.* **2017**, 51 (4), 2077-2086.

(181) Qu, X.; Hwang, Y. S.; Alvarez, P. J. J.; Bouchard, D.; Li, Q. UV irradiation and humic acid mediate aggregation of aqueous fullerene (nc₆₀) nanoparticles. *Environ. Sci. Technol.* **2010**, 44 (20), 7821-7826.

(182) Petosa, A. R.; Jaisi, D. P.; Quevedo, I. R.; Elimelech, M.; Tufenkji, N. Aggregation and deposition of engineered nanomaterials in aquatic environments: Role of physicochemical interactions. *Environ. Sci. Technol.* **2010**, 44 (17), 6532-6549.

- (183) Zhang, W.; Isaacson, C. W.; Rattanaudompol, U.; Powell, T. B.; Bouchard, D. Fullerene nanoparticles exhibit greater retention in freshwater sediment than in model porous media. *Water Res.* **2012**, *46* (9), 2992-3004.
- (184) Hu, Z.; Zhao, J.; Gao, H.; Nourafkan, E.; Wen, D. Transport and deposition of carbon nanoparticles in saturated porous media. *Energies* **2017**, *10* (8), 1151.
- (185) Liu, C.-H.; Chuang, Y.-H.; Li, H.; Teppen, B. J.; Boyd, S. A.; Gonzalez, J. M.; Johnston, C. T.; Lehmann, J.; Zhang, W. Sorption of lincomycin by manure-derived biochars from water. *J. Environ. Qual.* **2016**, *45* (2), 519-527.
- (186) Beesley, L.; Moreno-Jiménez, E.; Gomez-Eyles, J. L.; Harris, E.; Robinson, B.; Sizmur, T. A review of biochars' potential role in the remediation, revegetation and restoration of contaminated soils. *Environ. Pollut.* **2011**, *159* (12), 3269-3282.
- (187) Williams-Nguyen, J.; Sallach, J. B.; Bartelt-Hunt, S.; Boxall, A. B.; Durso, L. M.; McLain, J. E.; Singer, R. S.; Snow, D. D.; Zilles, J. L. Antibiotics and antibiotic resistance in agroecosystems: State of the science. *J. Environ. Qual.* **2016**, *45* (2), 394-406.
- (188) Lee, L. S.; Carmosini, N.; Sassman, S. A.; Dion, H. M.; Sepúlveda, M. S. Agricultural contributions of antimicrobials and hormones on soil and water quality. In *Advances in agronomy*, Donald, L. S., Ed. Academic Press: 2007; Vol. Volume 93, pp 1-68.
- (189) Kumar, K.; C. Gupta, S.; Chander, Y.; Singh, A. K. Antibiotic use in agriculture and its impact on the terrestrial environment. In *Advances in agronomy*, Donald, L. S., Ed. Academic Press: San Diego, CA, 2005; Vol. 87, pp 1-54.
- (190) Tolls, J. Sorption of veterinary pharmaceuticals in soils: A review. *Environ. Sci. Technol.* **2001**, *35* (17), 3397-3406.
- (191) Zhang, W.; Isaacson, C. W.; Rattanaudompol, U. S.; Powell, T. B.; Bouchard, D. Fullerene nanoparticles exhibit greater retention in freshwater sediment than in model porous media. *Water Res.* **2012**, *46* (9), 2992-3004.
- (192) Johnson, P. R. A comparison of streaming and microelectrophoresis methods for obtaining the ζ potential of granular porous media surfaces. *J. Colloid Interface Sci.* **1999**, *209* (1), 264-267.
- (193) Toride, N.; Leij, F.; Van Genuchten, M. T. *The cxtfit code for estimating transport parameters from laboratory or field tracer experiments*. version: 1995; Vol. 2.
- (194) Šimůnek, J.; Van Genuchten, M. T.; Šejna, M.; Toride, N.; Leij, F. The stanmod computer software for evaluating solute transport in porous media using analytical solutions of convection–dispersion equation. Versions 1.0 and 2.0. *International Ground Water Modeling Center, Golden, CO.* **1999**, -.

- (195) Simunek, J.; van Genuchten, M. T.; Sejna, M. Development and applications of the hydrus and stanmod software packages and related codes. *Vadose Zone J.* **2008**, 7 (2), 587-600.
- (196) van Oss, C. J. *Interfacial forces in aqueous media*. 2nd ed.; CRC Taylor & Francis: Boca Raton, FL, 2006.
- (197) van Oss, C. J. Long-range and short-range mechanisms of hydrophobic attraction and hydrophilic repulsion in specific and aspecific interactions. *J. Mol. Recognit.* **2003**, 16 177-190.
- (198) Hoek, E. M. V.; Agarwal, G. K. Extended dlvo interactions between spherical particles and rough surfaces. *J. Colloid Interface Sci.* **2006**, 298 (1), 50-58.
- (199) Norde, W.; Lyklema, J. Protein adsorption and bacterial adhesion to solid surfaces: A colloid-chemical approach. *Colloids and Surfaces* **1989**, 38 (1), 1-13.
- (200) Lin, S.; Wiesner, M. R. Exact analytical expressions for the potential of electrical double layer interactions for a sphere-plate system. *Langmuir* **2010**, 26 (22), 16638-16641.
- (201) Ruckenstein, E.; Prieve, D. C. Adsorption and desorption of particles and their chromatographic separation. *AIChE J.* **1976**, 22 (2), 276-283.
- (202) González-Martín, M. L.; Jańczuk, B.; Labajos-Broncano, L.; Bruque, J. M. Determination of the carbon black surface free energy components from the heat of immersion measurements. *Langmuir* **1997**, 13 (22), 5991-5994.
- (203) Giese, R. F.; van Oss, C. J. *Colloid and surface properties of clays and related minerals*. Marcel Dekker, Inc.: New York, NY, 2002; Vol. 105.
- (204) Hahn, M. W.; O'Melia, C. R. Deposition and reentrainment of brownian particles in porous media under unfavorable chemical conditions: Some concepts and applications. *Environ. Sci. Technol.* **2004**, 38 (1), 210-220.
- (205) Shen, C.; Li, B.; Huang, Y.; Jin, Y. Kinetics of coupled primary- and secondary-minimum deposition of colloids under unfavorable chemical conditions. *Environ. Sci. Technol.* **2007**, 41 (20), 6976-6982.
- (206) Tufenkji, N.; Elimelech, M. Correlation equation for predicting single-collector efficiency in physicochemical filtration in saturated porous media. *Environ. Sci. Technol.* **2004**, 38 (2), 529-536.
- (207) Yao, K.-M.; Habibian, M. T.; O'Melia, C. R. Water and waste water filtration: Concepts and applications. *Environ. Sci. Technol.* **1971**, 5 (11), 1105-1112.
- (208) Zhang, W.; Morales, V. L.; Cakmak, M. E.; Salvucci, A. E.; Geohring, L. D.; Hay, A. G.; Parlange, J.-Y.; Steenhuis, T. S. Colloid transport and retention in unsaturated porous media: Effect of colloid input concentration. *Environ. Sci. Technol.* **2010**, 44 (13), 4965-4972.

- (209) Xu, R.; Wu, C.; Xu, H. Particle size and zeta potential of carbon black in liquid media. *Carbon* **2007**, *45* (14), 2806-2809.
- (210) Shen, C.; Li, B.; Wang, C.; Huang, Y.; Jin, Y. Surface roughness effect on deposition of nano- and micro-sized colloids in saturated columns at different solution ionic strengths. *Vadose Zone J.* **2011**, *10* (3), 1071-1081.
- (211) Shen, C.; Wang, F.; Li, B.; Jin, Y.; Wang, L.-P.; Huang, Y. Application of dlvo energy map to evaluate interactions between spherical colloids and rough surfaces. *Langmuir* **2012**, *28* (41), 14681-14692.
- (212) Bradford, S. A.; Torkzaban, S. Colloid transport and retention in unsaturated porous media: A review of interface-, collector-, and pore-scale processes and models. *Vadose Zone J.* **2008**, *7* (2), 667-681.
- (213) Li, X.; Li, Z.; Zhang, D. Role of low flow and backward flow zones on colloid transport in pore structures derived from real porous media. *Environ. Sci. Technol.* **2010**, *44* (13), 4936-4942.
- (214) Zhou, D.; Wang, D.; Cang, L.; Hao, X.; Chu, L. Transport and re-entrainment of soil colloids in saturated packed column: Effects of ph and ionic strength. *J. Soils Sediments* **2011**, *11* (3), 491-503.
- (215) Zhuang, J.; Tyner, J. S.; Perfect, E. Colloid transport and remobilization in porous media during infiltration and drainage. *J. Hydrol.* **2009**, *377* (1-2), 112-119.
- (216) Lenhart, J. J.; Saiers, J. E. Colloid mobilization in water-saturated porous media under transient chemical conditions. *Environ. Sci. Technol.* **2003**, *37* (12), 2780-2787.